Short-and-long term behaviour of plain and prestressed concrete subjected to temperature gradients and thermal cycling.

Labib, G A

SHORT-AND-LONG TERM BEHAVIOUR OF PLAIN AND PRESTRESSED CONCRETE SUBJECTED TO TEMPERATURE GRADIENTS AND THERMAL CYCLING

BY

GIUMA ASHUR LABIB, B.Sc (C. Eng.), D.I.C.

A THESIS SUBMITTED FOR THE DEGREE OF

DOCTOR OF PHILOSOPHY

IN THE FACULTY OF ENGINEERING OF THE UNIVERSITY OF LONDON

KING'S COLLEGE

LONDON

AUGUST 1980

I wish to dedicate this work to my beloved wife

Hawa in appreciation of her support and

encouragement during the course of my studies.

ABSTRACT

Short-and-long term behaviour of plain and prestressed concrete subjected to temperature gradients and thermal cycling

by

Giuma Ashur Labib, B.Sc.(C,Eng.), D.I.C.

Recent research studies have shown that the elastic, creep and shrinkage properties of the concrete and hence the serviceability of structures can be affected significantly by exposure to elevated temperatures. Observations of external boundary actions in experiments confirm that significant redistribution of stresses with time occur in structures subjected to spatial temperature variations. Direct measurements of the time-varying stresses in experiments is difficult and has not been attempted previously. Part of the experimental work reported here is concerned with the evaluation of a direct stress measurement technique.

The time variations of stresses over a uniform moment zone of a 3-span continuous prestressed concrete beam was being monitored directly by the use of embedded elastic inclusions. It is shown that the 'steady state' theory and the 'rate of creep' method of analyses based on the 'specific thermal creep' concept are able to predict the non-homogeneous creep behaviour of the test structure. Close agreement was obtained between recorded and predicted stresses.

The second part of the experimental work extends the knowledge of the effects of sustained and cyclically varying temperature gradients on the moisture movement in concrete; and investigates its influence on shrinkage and creep. The creep tests were carried out in specially designed rigs which allowed movement of moisture in a direction orthogonal to the applied uniaxial stress. It is shown that the creep rate increases with temperature and with the continuing migration of water from the concrete.

Finally, a theoretical study has been made on the influence of sustained and cyclically varying non-linear temperatures, of the kind caused by solar heating in bridges, on the behaviour of a 3-span continuous beam. The example highlights the importance of non-linear heating and differential creep on the structural behaviour and calls for the long-term effects of solar heating to be taken account of more seriously in the design of road and bridge structures.

ACKNOWLEDGEMENTS

The research work reported herein was carried out under the supervision of Dr. G.L. England, D.Sc.(Eng.) London, C.Eng., M.I.C.E., M.I.Struct.E., FINucE, M.A.S.C.E., to whom the author is greatly indebted for his help and guidance.

The author acknowledges the help of the retired Chief Technician, Mr. A.W. Blake, and his successor, Mr. R. Earl. Sincere thanks are extended to all the workshop staff and laboratory technicians, in particular to Mr. C.S. Blakey, for the many technical advices, and to Mr. M.D. Collins, Mr. R. Hunt who prepared the photographs for the thesis, and Mr. V.E. Nisbett and Mr. B. Heslip for their assistance in the laboratory.

The author wishes to thank Alfatah University, Tripoli, who sponsored his studies in this country.

CONTENTS

Basic notations

ε	=	strain in general
ε_a	=	axial strain
ε_c	=	creep strain
ε_{se}	=	specific elastic strain
C	=	specific creep strain
c	=	specific thermal creep strain
S	=	unrestrained shrinkage strain
σ	=	stress
θ	=	section curvature
η	=	slope of the elastic line
γ	=	linear displacement or deflection
d_{01}	=	discontinuity at the release of the structure due to the applied mechanical loading
d_{0t}	=	discontinuity at the release of a structure due to the applied temperature loading
M	=	bending moment, in general, positive when sagging
M_1	=	bending moment due to unit action applied at the release of the structure
P	=	applied transverse loading
R	=	support reaction
N	=	axial force on the section
f	=	prestress
b,D	=	section dimensions
L	=	span between supports
T	=	temperature, generally in degree Celsius
T_1 and T_2	=	the hot and cold face temperatures respectively of a section
$\phi(T)$	=	creep-temperature normalization function

α = the uniform temperature of a section

β = temperature gradient across a section

$\bar{\alpha}_c$ = coefficient of thermal expansion of concrete

$\bar{\alpha}_a$ = coefficient of thermal expansion of aluminium

E_c = Young's modulus for concrete

E_a = Young's modulus for aluminium

E_T = Young's modulus of the concrete as a function of temperature

I_c = second moment of area of the cross section of a concrete member

I_a = second moment of area of the cross section of the aluminium

t = time as variable

p, q, ψ = constants or coefficients

CHAPTER I

INTRODUCTION.

1.1 General

Interest in the effects of elevated temperatures on the properties and behaviour of concrete was stimulated by the need to generate an understanding of the fire resistance of concrete; and more recently by the advancement of the prestressed concrete pressure vessel industry, and the use of concrete in offshore oil storage vessel structures. Concrete in these and many other installations can be subjected to considerable temperature gradients.

Lined chimney walls, for example, are normally subjected to gradients in excess of 125°C/m (1,2). The walls of oil storage cells are usually subjected to cyclic temperature gradients with the inside face alternating between 50°C and 5°C while the outside may be at a steady 5°C (3). In the case of nuclear pressure vessels, however, elaborate and costly cooling systems are normally provided in order to lower the temperature from around 400°C to about 70°C (4).

Temperature differentials are also created in structures by direct exposure to solar radiation particularly in tropical climate countries. In West Africa, for example, temperature gradients of about 66°C/m are commonly adopted in the design of exposed structures (5). Similar effects are also experienced in non-tropical regions; within the British Isles, for example, prolonged exposure to direct sunlight can raise the surface temperature of concrete to up to 65°C (6). Further supplementary evidence on the solar temperature effects on some bridge structures in the U.K. are reported by Emerson (7).

Temperature gradients build up in mass concrete structures between the core and the exterior due to the exothermic process of hydration of

the cement paste. The core temperature may rise to 40°C (7,9) or even more.

Thermal gradients caused by climatic changes, industrial processes or other conditions can significantly affect material and structural behaviour, which can consequently affect the serviceability of structures. Careful consideration must therefore be given in design for short and long term effects of temperature.

1.2 Material behaviour

The future behaviour of any structure is usually dictated by the ability or otherwise of the material to remain serviceable. In the design of concrete structures therefore, consideration needs to be given to their deformation with time under environmental conditions.

In recent years, however, there has been a growing awareness of the influential role of temperature on the creep and shrinkage of concrete, and their cumulative effects on the state of service stresses and deformations in structures over many years. In an attempt to generate a better understanding of the long-range material behaviour, experiments have been staged on laboratory samples under simulated environments. The quest has been to gain sufficient experimental evidence from which a realistic model of the material behaviour can be constructed.

To date, various theories for material behaviour have been advanced though no generally accepted one has been agreed. This is largely attributed to the inherent peculiarity of concrete and the multiplicity of the influencing variables. In general, the physical nature of concrete has been described (10,11,12,13) as being heterogeneous, complex multiphase material. Ross, Illston and England (14)

have shown that the deformations of concrete are functions of the structure and state of the cement paste and the influencing variables are multiply inter-dependent.

Exposing concrete to higher than normal temperature levels can induce harmful effects on many of its structural properties thus modifying the material behaviour and possibly affecting the serviceability of the structure. The subject of temperature influence on the structural properties of concrete has been dealt with in some detail in Chapter 2.

1.3 Structural behaviour

Concrete exhibits, in addition to elastic, time-dependent deformations, widely known as creep and shrinkage. Their precise mechanisms, however, are still a matter for debate, which justifies the continuity of research on these aspects of material behaviour.

In the simplest context, creep is defined as a sustained stress movement in excess of shrinkage or swelling strain, immediate loading strain and strain due to temperature changes; while shrinkage is identified with deformations observed in the absence of other effects caused by loading, coefficient of thermal expansion or ingress of moisture.

The creep and shrinkage phenomena in concrete are two processes which can occur independently of each other. However, both characteristics are often described as in-elastic strains which develop at a decreasing rate with time.

The long-term effects of creep and shrinkage deformations on some concrete structural members are well known. For example, loss of prestress force in prestressed concrete construction; gradual transfer

of load from concrete to steel in reinforced concrete columns where the events may cause the steel to reach its yield limit. Also, in reinforced concrete flexural members, the progress of creep and shrinkage will shift the neutral axes towards the tensile reinforcement. This leads to an increase in the steel stress and curvature which will ultimately cause a progressive increase of deflection.

In the absence of steel reinforcement and imposed displacements in a structure and provided the structure is maintained at uniform temperature, the state of stress in general is little affected by creep, although displacements may alter significantly with time (15,16,17). Nonetheless, shrinkage stresses may well develop wherever restraint to free deformations exist. This situation may arise due to aggregate restraint from within the concrete or where there is a difference in the strain behaviour of two materials, such as composite steel/concrete structures.

1.4 Effects of sustained and cyclic temperatures

Several experimental investigations have shown that the creep and creep rates of concrete are enhanced by the rise in the environmental temperatures (see Chapter 3). Some evidence exists in which the creep/temperature relationship is shown to be almost linear for test temperatures below 100°C (17). Hence, if a structural member is maintained in a non-isothermal state, different parts of its section will creep at varying rates; and, in presence of movement constraint on the member, creep will alleviate the high temperature stresses initially induced, causing them to redistribute over the section at a decreasing rate. The process of stress redistribution must occur in order that the total strain rates, i.e. elastic and creep, may remain compatible at all

times. Results concluded from external action measurements on some simple statically indeterminate structures (16,17) as well as actual stress measurements in a continuous beam test reported in Chapter 6 have confirmed this behaviour. Some of the observations reported by Ross et al. (16) and Krishnamoorty (17) illustrating the time variation in the bending moments of prestressed concrete beam and portal frame structures carrying sustained loading and temperature cross falls are given in Fig. 1.1. It shows the ability of creep to change not only the magnitude but also the sense of the initial thermo-elastic design parameters. The examples further indicate the inability of the elastic theory to give reliable estimate of stresses and stress redistribution with time due to creep. Therefore, alternative techniques which recognise the differential thermal creep effects have to be employed in the design of redundant concrete structures, subjected to spatial variation in temperature.

Under the condition of cyclically varying temperature cross falls on structures, re-distribution of stress also occurs and at rates governed by the current state of temperature and the period of the temperature cycling. It is shown in some analyses (18,19) that when temperature cycles are frequent and when reversal of temperature cross falls takes place the structures will suffer less severe stressing than when temperatures are sustained. Such behaviour is illustrated by the example given in Fig. 1.2.

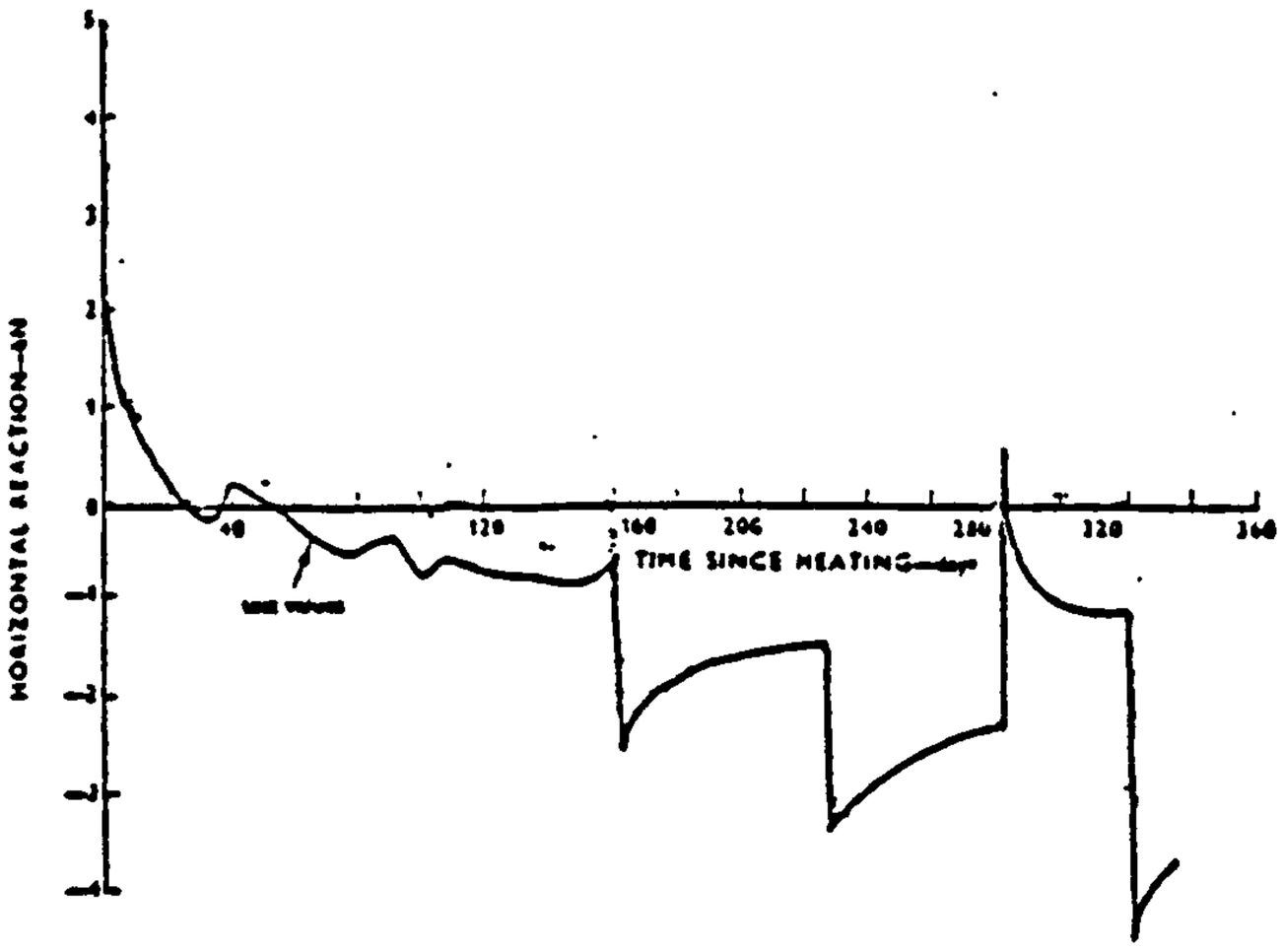

Variation in horizontal reaction with time for portal A.

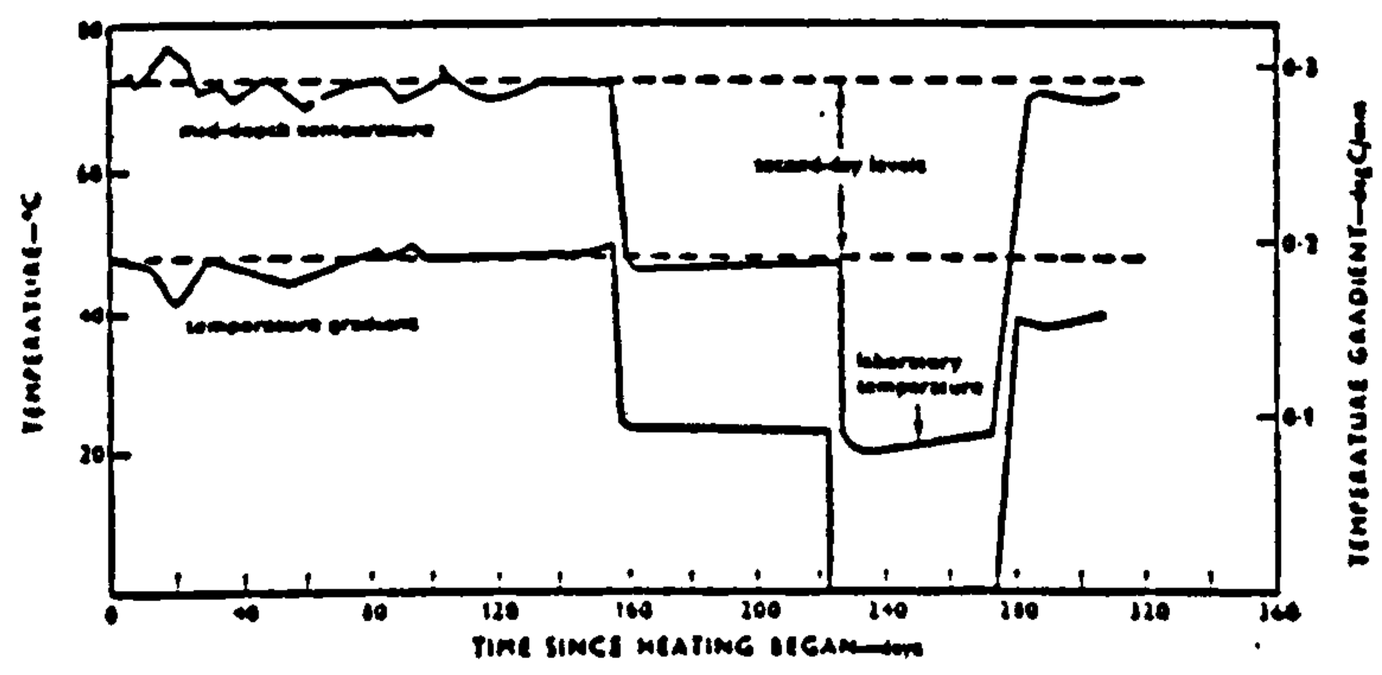

Variation in mid-depth temperature and temperature gradient of a typical section with time for portal A.

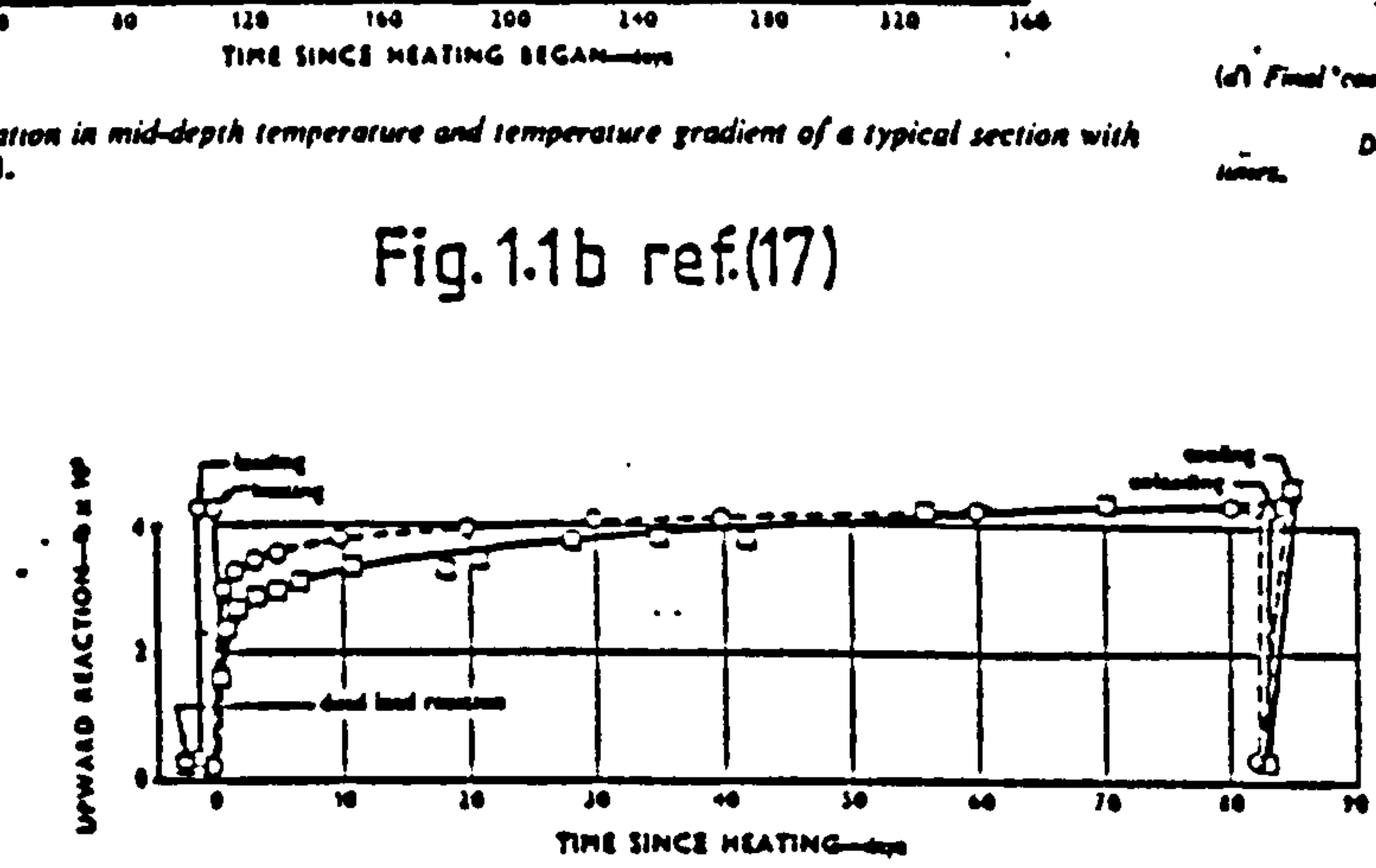

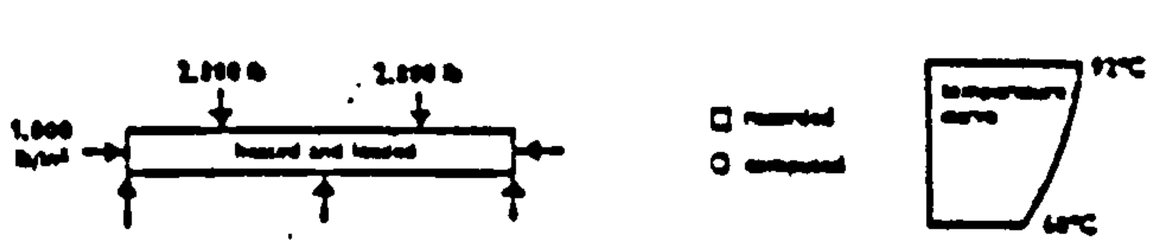

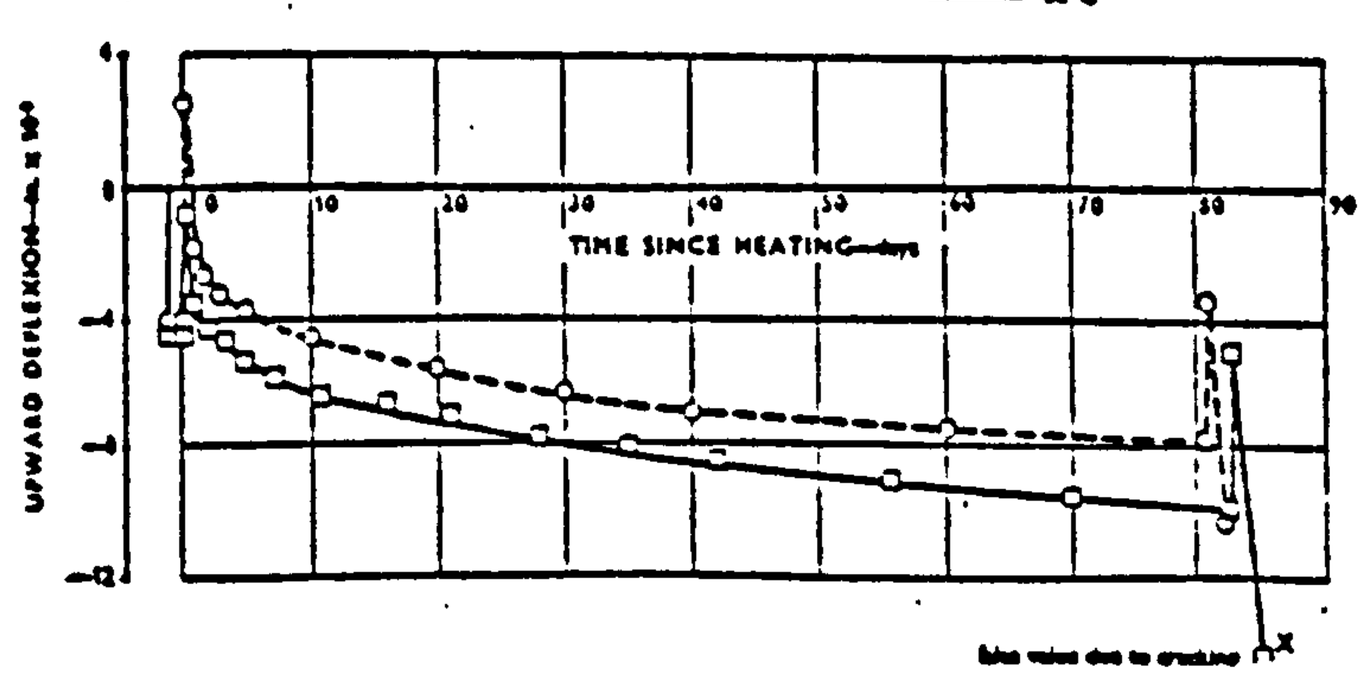

Fig.1.1a ref.(16)

The variation of centre support reaction with time for continuous beam E, first heated at 91 days.

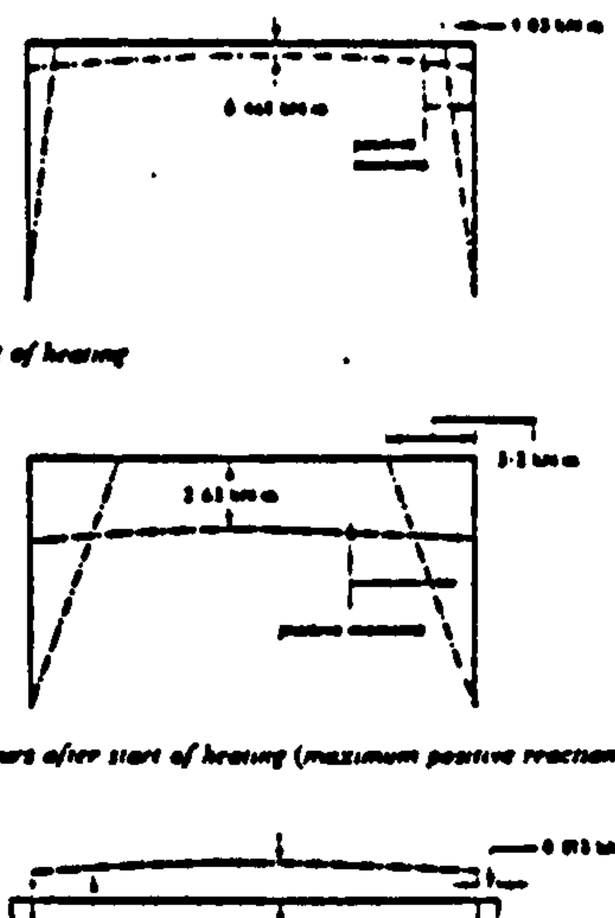

(a) *At start of heating*

(b) *Two hours after start of heating (maximum positive reaction)*

(c) *First stable state*

(d) *Final 'cooled' state*

Distribution of moment for portal A at significant times.

Fig. 1.1b ref.(17)

1.5 Experimental testing

Experimental evidence cited in the above section has allowed considerable insight to be gained in relation to possible states of stress within these structures. However, since the external actions represent an integrated response of all internal stresses throughout the entire volume of the structure, it has not been possible from the experiments to determine explicitly the actual internal stress distributions. Instead, they have been inferred from comparisons made between experimental observations of strains and external actions with theoretical predictions for which specific stress/strain relationships have been adopted. There is therefore an eminent need for a bridging mechanism enabling the actual stresses in structures to be measured directly in order to reinforce or amend these deductions.

The need to determine the internal stresses in structures is also desirable, even those developing under short-term loading at normal temperature conditions. This is because of the uncertainties and variability of the elastic modulus of concrete even within the same member of the structure (20), Fig. 1.3.

Some of the current techniques used for both strain and stress measurements in concrete are discussed in Sections 1.6 and 1.7.

1.6 Strain measurements

The use of strain devices to study the deformational behaviour of model or prototype concrete structures is an accepted part of present day engineering technology. There exists a large amount of instrumentation from which a choice can be made to suit a particular application. However, in selecting the appropriate device for short-term measurements,

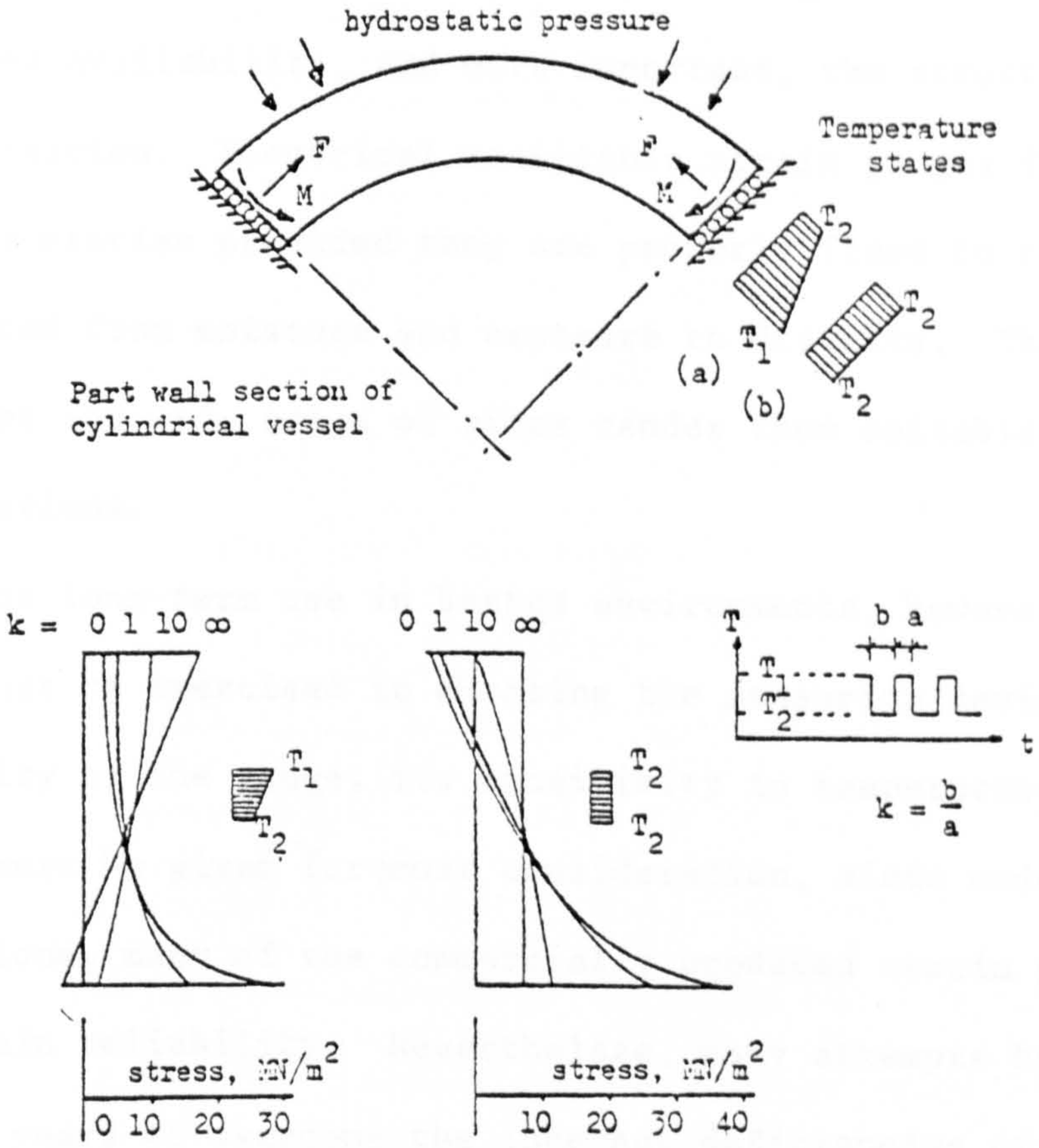

Fig 1.2 ref.(19)

Influence of cyclic temperatures and creep on the steady-state-cyclic stresses in the wall of a cylindrical containment structure. The ratio of the 'hold' times at the two temperature states defines the parameter k = b/a.

Fig 1.3 ref.(20)

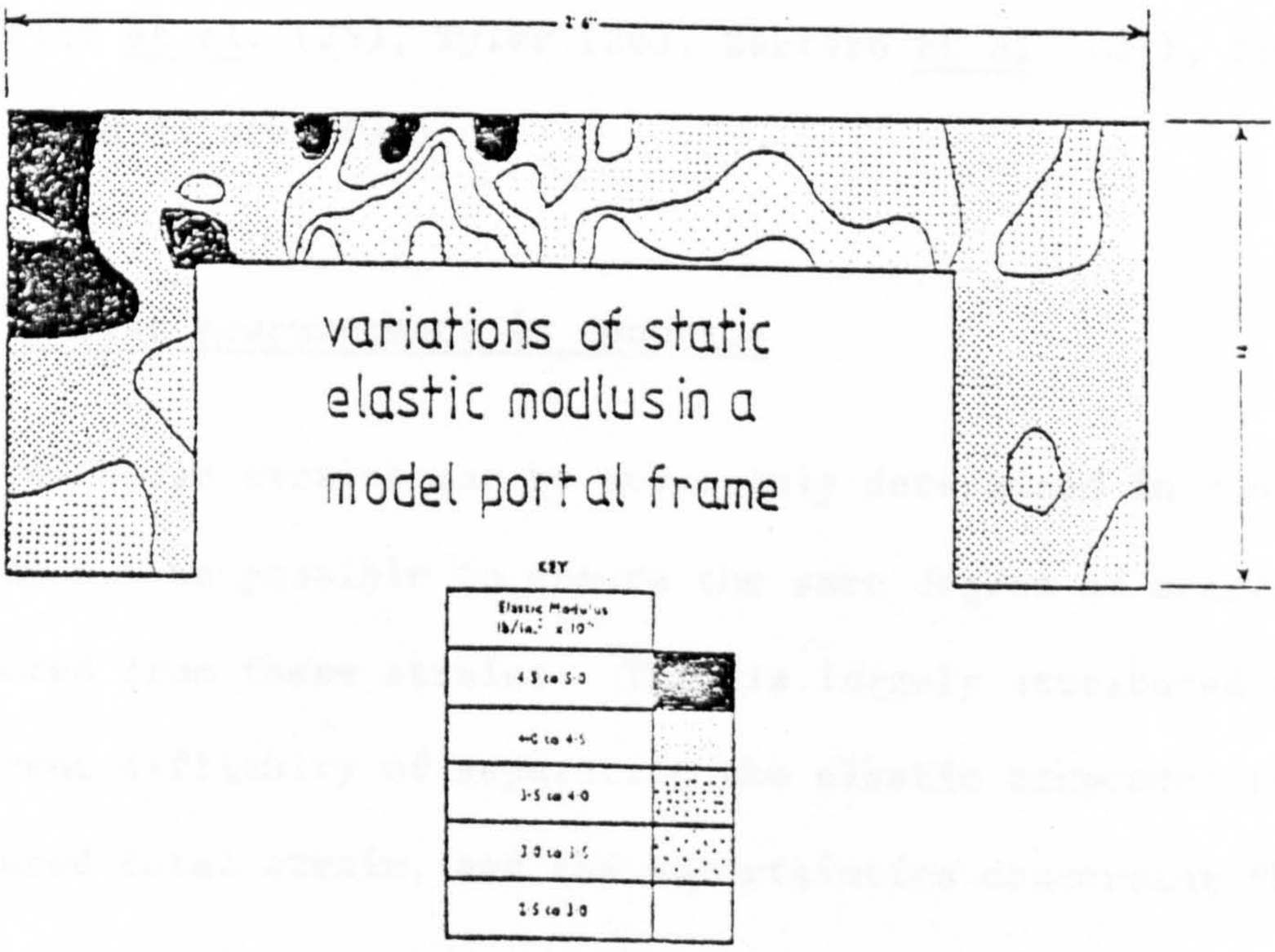

the choice is usually influenced by the degree of accuracy required, cost and availability, and more important, the structure under investigation. Electrical resistance strain gauges for example can be very precise provided they are properly fixed to the concrete and protected from moisture and exposure to draughts. Their relatively low cost and wide range of sizes render them suitable for most applications.

For long-term use in heated environments, however, considerable care must be exercised in choosing the measuring device. The long-term stability of the gauge, its sensitivity to temperature, moisture and creep must be given foremost consideration, since under such operating conditions, many of the commercially produced strain gauges have uncertain reliability. Nevertheless, many attempts have been made in recent years to overcome the inherent deficiencies of certain techniques, by way of providing some kind of protection against the adverse effects of the environment or by way of modifying the existing design. However, for a wider and more detailed account of these and other relevant matters, the reader is referred to the works by Elvery (20), Czaika (21), Browne (22), Hornby (23), Cullington et al. (24), McKillen et al. (25), Tyler (26), Bertero et al. (27), Irving et al (29), and Potocki (30).

1.7 Stress measurements in concrete

Although strains can be accurately determined in concrete structures it may not be possible to ensure the same degree of accuracy of stresses computed from these strains. This is largely attributed to the inherent difficulty of separating the elastic component from the measured total strain, and the uncertainties concerning the value of the

elasticity modulus of the material in the structure. It may therefore be expedient to determine the stresses directly with a stress meter rather than to translate them from strains.

For a stress meter to indicate very nearly the true state of stress in the material at all times without any analysis, it has to have identical physical properties to those of the concrete it replaces (31), i.e., it should have elastic and creep modulus, Poisson's ratio, thermal and moisture movement characteristics of the concrete. However, since complete matching of such properties is not feasible, stress gauges are liable to be inaccurate to some degree. Loh (31) discussed the problems resulting from the mismatch of some of the physical properties between the gauge and concrete and derived expressions for the errors likely to be introduced in the measurements.

Various types of stress meter designed to measure compressive stresses in concrete already exist. Among these are the Carlson stress meter, Glotzle stress meter and Photo-elastic stress plug. Although several tests were made to assess the performance of these gauges in site and laboratory works, very few attempts were actually made to test them in heated structures. A detailed account of the theory, design and proving tests of these gauges is beyond the scope of this work. However, for these and other relevant information the reader's attention is drawn to the references given in the following list:-

1. Carlson Stress meter; 32, 33.
2. Glotzle Stress meter; 26, 34, 35.
3. Photo-elastic Stress plug; 26, 36-39.

It has not been established yet that any of these or other existing devices are capable of conveying an accurate picture of the stress and/or stress redistribution due to creep in heated structures. Even

in the less severe testing environments, they seem to suffer from sensitivity to the creep and shrinkage occurring within the structure and slowness in response to stress changes. These are in addition to the difficulties normally encountered during installation. Their relatively large sizes also impose additional limitation on the number which can be used within a given section in the structure. Hence it is not possible to install across a section in a laboratory size test structure, such as the continuous beams referred to earlier, a sufficient number of gauges in order to define clearly the stress profile. Therefore, there is a need to introduce some other methods by which stresses in similar structures can be ascertained.

1.8 Objective for long term experiments

Part 1 of the experimental program was designed to investigate the long-term behaviour of a prestressed concrete continuous beam structure, under a combination of sustained loading and temperature cross fall, using a direct stress measuring technique.

The method used was based on the concept of correlating concrete stresses to the deformations observed in an elastic material incorporated within the stress field of a structural member. This is often referred to as the elastic inclusion technique. Previous attempts to apply this technique have been centred around its use in short-term experiments at room temperature conditions. Stanculescu (40) has successfully applied it to determine the non-linear stress distribution in un-reinforced concrete beams close to and at ultimate load. It was decided to take this idea a step further by developing a similar technique suitable for the experimental beam, involving creep.

The inclusion was designed to fit in between two identical concrete prisms which when stressed axially altogether formed a rigid beam structure. The beam was then tested as a 3-span continuous beam with the elastic inclusion in a constant moment zone. Provision was made for surface heating to create the desired temperature gradient. Details of this experiment are given in Chapter 5. Experimental results along with theoretical predictions of the beam behaviour may be seen in Chapter 6.

Part 2 of the experimental program deals with the effect of thermal gradients on the creep behaviour of plain concrete from the standpoint of moisture movement. Since it is possible that moisture transfer caused by temperature gradients can affect the creep behaviour of concrete, some creep experiments designed to include this aspect have been staged and are expounded in Chapter 7. The experimental results are displayed in Chapter 8.

Finally, a theoretical study, presented in Chapter 9, investigates the long-term effects of sustained and cyclically varying non-linear heating on the behaviour of a 3-span continuous prestressed concrete beam. The example has been intended to illustrate the possible effects of solar radiation heating caused in bridge and viaduct structures on their long-term behaviour.

CHAPTER II

EFFECT OF THERMAL EXPOSURE ON THE MECHANICAL PROPERTIES OF CONCRETE

Chapter 2-Synopsis

The effects of elevated temperatures on some of the engineering properties of the concrete namely, compressive and tensile strengths, modulus of elasticity and Poisson's ratio, thermal conductivity and expansion are discussed. Test results from some 23 pertinent references are reviewed and compiled in tabular and/or graphical forms.

It is concluded that heat exposure of concrete generally results in strength loss, and reductions in elasticity modulus and thermal conductivity of the material. The moisture condition of the concrete, the severity and duration of exposure being the main influencing variables.

2.1 Introduction

Strength, elasticity and thermal properties associated with the hardened concrete constitute an essential part of the data required for the analysis of the structure. Whether it is compressive, tensile or bond, etc., the strength is needed to establish limits to the load stresses and thereby permit safe design to be carried out. The elastic modulus, Poisson's ratio and the coefficient of thermal expansion are also required to compute the actual stresses and movements in structures. The extent of progress of deterioration in these material properties depends essentially on a number of intrinsic and environmental parameters, experienced by the concrete from the time of casting.

Under normal temperature conditions, the ageing properties of concrete are well known, and in many cases the property changes are beneficial to the structure (41). Exposing concrete structural members to above normal temperatures, by accident or design, has been shown to cause marked changes in its basic properties. Such changes are functions of several variables. For a particular concrete, the most important of these variables are the severity and duration of thermal exposure and the hygrothermic state of the medium (4, 42-53).

2.2 Review of studies on the effects of thermal exposure on the engineering properties of concrete

Earlier works relating to the effects of temperature on concrete have been reviewed by several investigators (4, 46, 47, 54). Some of the earlier and more recent data are reviewed here and compiled in tabular form. Entries in the tables include the source of information, the test variables, and the variation in the property with respect to the unheated value as reference.

2.2.1 Compressive strength

In Table 2.1 data on the effects of temperatures up to 600°C on the compressive strength of several concretes are listed. Most of these indicate that on heating concrete the compressive strength is reduced with no apparent long-term recovery, particularly when the specimens are not allowed to lose moisture during heating. It is apparent also that the loss in strength is greater the higher the temperature of exposure. In general, limestone concrete appears to be the worst affected of all concretes even at relatively low temperatures.

2.2.2 Tensile strength

The tensile strength of concrete has been determined by some investigators by direct tensile and/or cylinder splitting tests. Others, however, viewed it through flexural strength tests on beam specimens. The evidence shown in Table 2.2 indicates that the extent and rate of deterioration in the tensile strength, as a result of heat exposure, are considerably greater than that observed in the compressive strength. Both direct tensile and flexural strengths of concrete are shown to lose as much as 30 to 40% of their initial unheated values when the concrete is heated to temperatures between 60° and 100°C. Again limestone concrete seems to offer less resistance to reduction in its tensile or flexural strength than gravel concrete subjected to raised temperatures.

2.2.3 Modulus of elasticity

With reference to Table 2.3 and Fig. 2.1 it appears that the elastic modulus of concrete is affected by exposure to elevated temperatures in much the same way as the compressive strength. There is no

evidence of recovery with age, except in one of the cases reported by Hannant (42). He observed a complete recovery of the initial loss at the end of 430 days of heating at 75°C for sealed limestone concrete specimens. In general, a reduction in the modulus is experienced by most conventional concretes whenever they are subjected to elevated temperatures, regardless of whether the specimens are sealed or unsealed, or whether they are tested hot or after being cooled.

2.2.4 Poisson's ratio

Experimental data on the effects of temperature on this property, particularly under sustained loading, are very scarce. Results concerning the effects of temperature on the elastic Poisson's ratio are given in Table 2.4, and some of the literature data compiled by Browne and Blundell (68) are shown in Fig. 2.2. These indicate that the property is reduced with increasing test temperature, the extent of influence, however, seeming to depend on the moisture state of the test specimen.

2.3 Thermal characteristics of concrete

The principal material characteristics of relevant interest are: thermal diffusivity, specific heat, thermal conductivity and coefficient of thermal expansion. The first three quantities are related to each other by the equation

$$D = \frac{K}{\rho . c}$$

where D is the thermal diffusivity, K is the thermal conductivity, c is the specific heat and ρ is the material density.

Table 2.1 Comp. Strength vs. Temperature

Ref.	Mix		Specimen	Curing	Temp. Envt.	Heating duration	f_{c28} MN/M^2	% change	Remarks
	Aggt.	W/C							
4	Gravel	0.42	Sld. Cyl.	Fog Room for 150 to 260 d.	autoclave 79 to 260°C	20 to 28 hrs			Progressive decrease in strength with temp. Max. Loss being 52% @ 260°C
	G. or, L.S.	.42/.4	Cyl.	Fog Room for 28 d.	oven @ 79, 121, 190°C	91 to 109 d.			Both concretes showed increase in their strengths
4	"	"	"	" " "	oven @ 190°C	82d.			
42	Th.G. L.S.	0.46 0.46	Cube Cube	Under water for 80-85 days	Water @ 93°C	3 d. 3 d.	53 64	-20 -38	Loss recovered after 18 months No recovery
43	Gravel	0.5	Cyl.	Std. Curing	drying @ 80°C	6 m.			Loss recovered after a year
44		0.4	Sld. Cyl.	Water @ 20°C for 28 d.	90°C	1-2 wks	44	-12	Partial recovery
45	L.S.	0.425	Sld. Cyl.	@ 21°C for 90d	149°C	2 wks	45	-65	
	"	"	" "	" " "	"	25 days	45	-71	
45	"	"	" "	" " "	14 cycl. 21-149-21°C		"	-48	
49	L.S.	0.47	Cube	Under water @ 19°C for 31-89d	Water @ 65°C	2 to 334d	50	-18	
51	Qtz.			@ 98% R.H. for 12 to 18 mths.	100°C		35		cont. Fall with temp. up to 44% @ 400°C
	L.S.				100°C		42		cont. Fall with temp. up to 63% @ 400°C
55	Quartz	0.6		air dried	150°C	84 d.	49	-15	
	"	"		" "	600°C	"		-60	

Table 2.2 Tensile Strength vs. Temperature

Ref.	Mix: Aggt.	Mix: W/C	Specimen size and type	Curing before heating	Temp. Envt.	Time after heating	Condition at test	Change in value after htg as % of ref.	Remarks
4	Gravel L.S.		75x64x250 mm beams sealed " " "	fog room for 195 to 206 days " " "	autoclave @ 79, 121, 190, 260°C " " "	24 to 48 hrs	cold	-30 @ 79°C -50 @ 260°C -15 @ 79°C -64 @ 260°C	In general gravel concrete showed a lesser degree of flexural strength loss than L.S. concrete especially at higher temperature
43	Gravel " " " "	0.5 " "	100mm cyl. unsealed sealed sealed	standard curing	60°C 60°C 80°C	3 mths 3 mths		-30 to -40 -10 +20	Direct tensile " " Splitting test, The increase dropped thereafter to the 28 day value at 12 months
48	Th.Val. Gravel	0.56	50x75x838 mm beam	moist curing for 7 days then in air @ 20°C 50% R.H.	cycling up to 400°C	40 to 60 hrs	hot	-75 to -100 @ 400°C	Gradual decline in flexural strength with temperature
50	Crushed shale " "	.44 "	76x76x838 beam (unsld) " " "	4 wks @ 22°C 100% R.H. then in air till the test " " "	furnace heating 100°C 250°C	6 hrs "	hot "	-30 to -40 0 to -10	Flexural strength Heating to 250 has less effect than 100°C
52	L.S.	.4	Cyl.	Water curing for 28 to 56 days. Pre-drying for 28 days in oven to 200°C	6 th cycles up to 200°C			+80	Splitting test

Table 2.3 Modulus of Elasticity vs. Temperature

Ref.	Mix		Specimen	Curing	Temp. °C	Heating duration	Condition at test	$E_{20}^{°C}$ MM/M^2	% change	Remarks
	Aggt.	W/C								
4	Gravel	.42	100 mm unsealed cyl.	24°C @ 100% R.H. for 28 to 200 days	190	82 days	hot		-20	
	" "	"	sealed	" " for 150 to 260 d.	79-260	20 to 28 hrs	hot		-50 to -70	
42	L.S.	.47	105 mm cyl.	6 mths under water @ 20°C in sealed saturated condn.	75	up to 430 days	hot	42	-23	The loss observed on fist heating then completely recovered at the end of 430 days
	" "	"	" " "	" " "	50	" "	"	"	-8	The loss remained throughout the test
	" "	"	" " "	6 mths under water @ 20°C unsealed	75	" "	"	38	-20	The loss remained almost the same
43	Sagami Gravel	.50	100 mm unsealed cyl.	standard curing	20	3 months			-30 to -40	
48	Th.Val. Gravel	.56	50x75x838 mm beams	moist cured for 7 days then in air @ 20°C 50% R.H. for 28 days	95 125 200	15 hrs " "	hot " "	43 44.5 44.3	-19 -29 -38	
51	Quartz Rounded L.S.			98% R.H. for 18 months " " "	110 250 100 200			35 42	-20 -40 -10 -50	
53	Elgin gravel	.64	35 mm cyl. 610 mm long	moist cured for 3 days @ 24°C then in air 50% R.H. and 24°C for 20 days	147 315.5	15 min. "	hot "	34.3	-15 -41	
	L.S. "	.60 "		" " "	147 315.5	"	"	36.9 "	-22 -38	

Table 2.4 Poisson's Ratio vs. Temperature

Ref.	Mix		Specimen	Curing	Temp. Envt.	Heating duration	Condition at test	Ref. value unheated at 20°C	% change	Remarks
	Aggt.	W/C								
44		0.4 & 0.5	150 mm. dia. sld. cylinder	Water curing @ 20°C for 28 days	Sld.storage @40,70 & 90°C	1 to 13 wks	hot	0.15 to 0.2	No change	
51	Quartz			12 to 18 mths @ 98% R.H.	105°C 255°C 400°C			0.28	-18% -46% -64%	Predried specimens
45	L.S.	0.425	150mm dia. sld. cylinder	21°C for 90 days	149°C	0 to 25 days	hot	0.22	-18%	
					Temp.cycl. 21-149-21°C	10 days	hot		-32%	Five temp. cycles were applied

Fig.2·1 mod. of elasticity of concrete vs. temperature

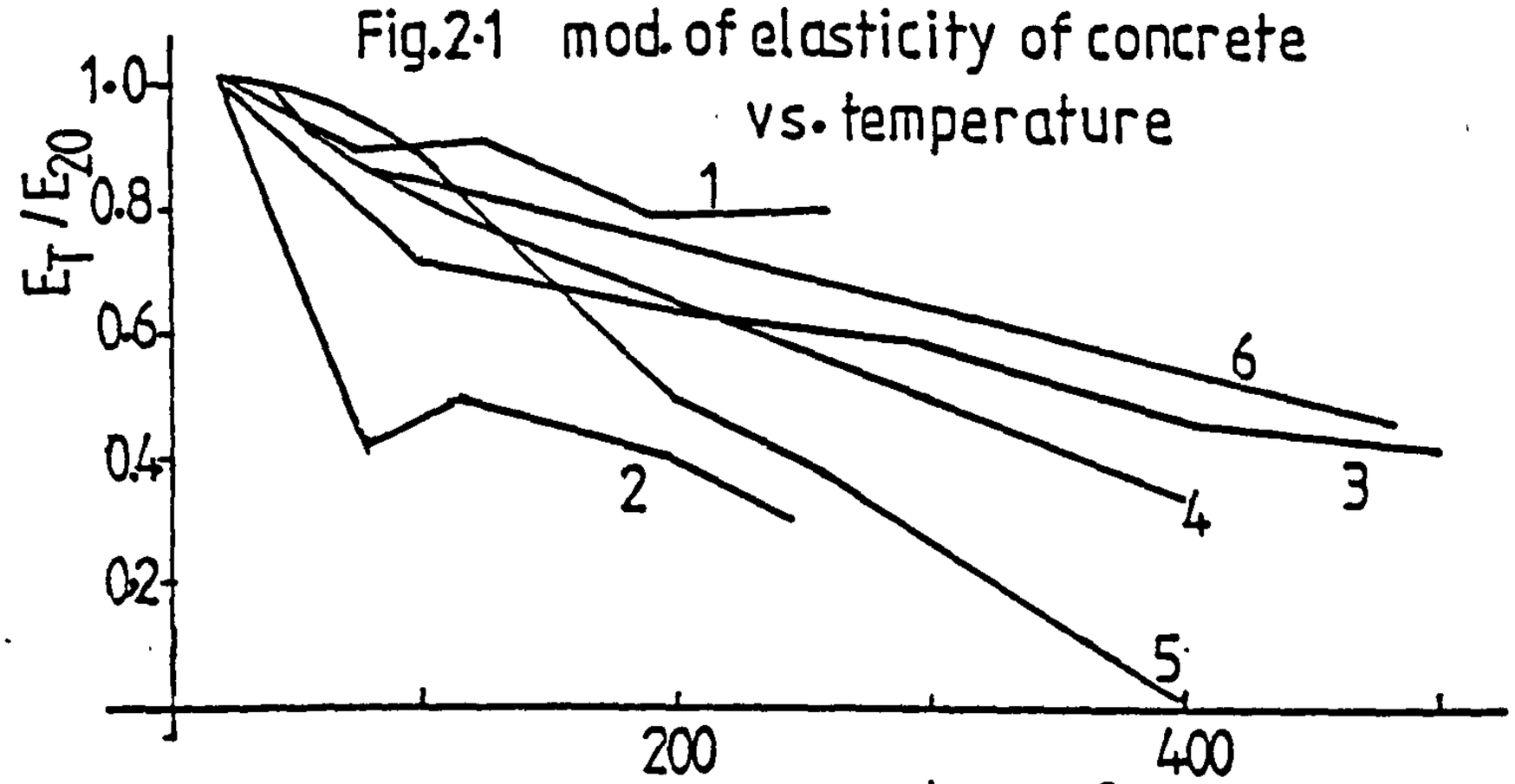

Key

1-grvl. conc. htd. at atm. pressure w/c = 0.42 ref (4)
2-" " " " s.steam " " " " "
3-" " htd. at atm. " " 0 45 " (43)
4-qrtz. " " " " " " " (51)
5-l.s. " " " " " " " "
6-Elgin sand & lime stone conc " 0·6 " (53)

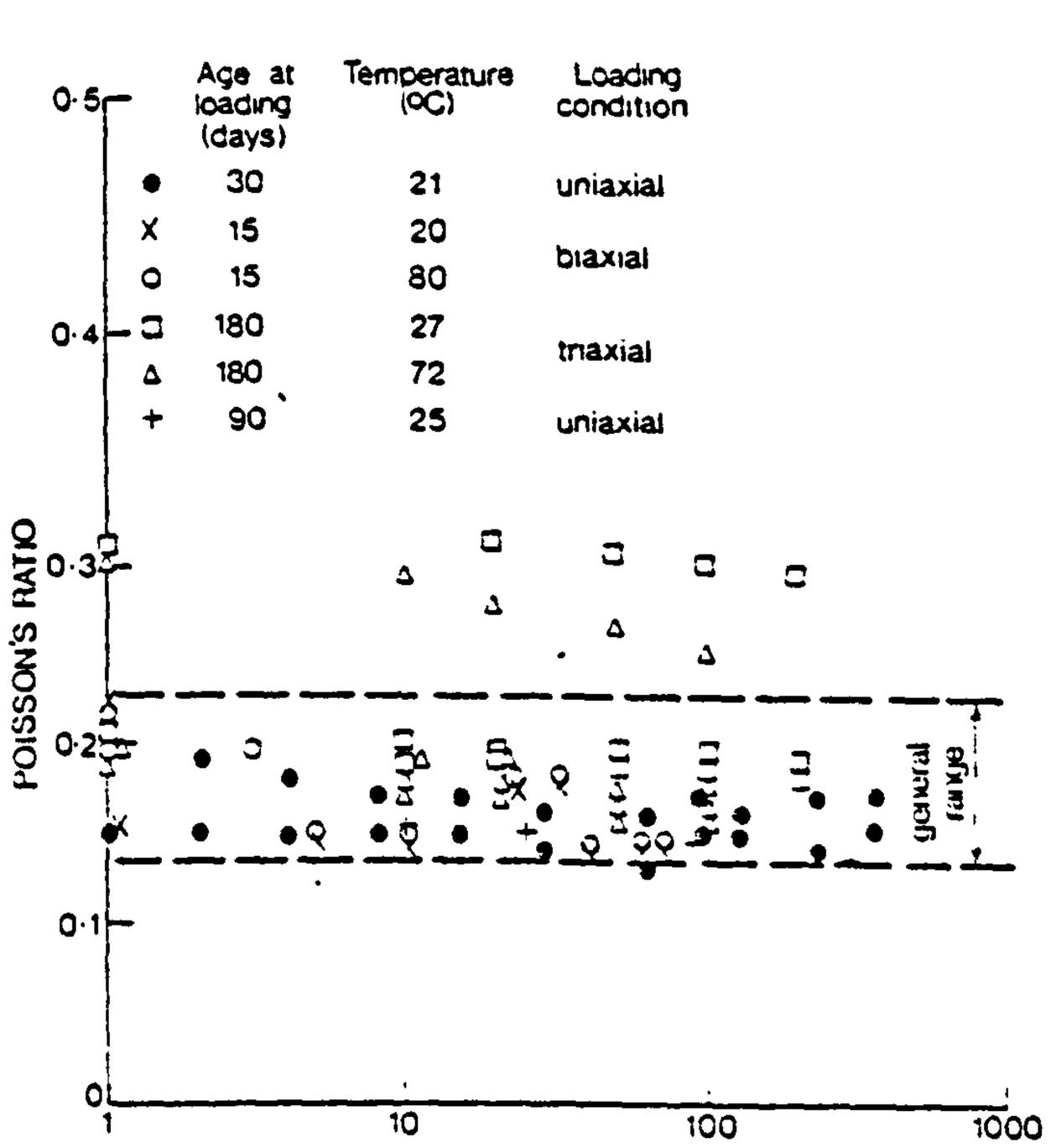

Fig.2·2 Poisson's ratio for sealed concrete under uniaxial and multiaxial sustained loading conditions (68)

It is generally considered that the intrinsic properties of the individual components of the concrete mix, particularly the aggregates, are influential factors on these quantities. A more detailed account of this theory supported by quantitative data on the various properties is given by Browne (8), Neville (41) and Zoldners (46).

The interest in this thesis is mainly associated with the influence of these thermal properties on structural behaviour and performance. The coefficients of thermal conductivity and expansion of concrete are of importance in the thermal analysis of structures. The conductivity governs the flow of heat through concrete, and therefore its variations with time will affect the prescribed temperature gradient on the member. Also variations with time in the expansion coefficient of the material can lead to false predictions of the dimensional changes and thermal stresses in statically indeterminate structures.

2.3.1 Thermal conductivity

This measures the ability of the material to conduct heat and is defined as the ratio of the flux of heat to temperature gradient. For a given composition the water contained in the material becomes an important factor of the thermal conductivity in relation to temperature. The effect of moisture content on thermal conductivity values of normal and high density concretes made with different types of rock was investigated by Campbell-Allen and Thorne (57). Their results (Fig. 2.3) indicate an approximately linear relationship between the two.

2.3.1.1 Influence of temperature

Of the many factors likely to affect the conductivity of a given concrete, temperature is particularly influential when viewed from the standpoint of moisture content. Data reported by Harada et al. (42), [43] Crispino (52) and Marechal (58) on the effects of temperature exposure on the thermal conductivity values of several concretes are shown in Fig. 2.4. Conductivity values for limestone concrete (52) indicated an initial rise followed by a rapid decline with rising temperatures. Partial recovery was subsequently observed when measurements were taken at decreasing temperatures. Similar behaviour was observed with the pre-dried quartzite concrete specimens (58) at increasing temperatures. After being re-humidified these specimens showed no recovery in their initial conductivity values. This was attributed to the destruction of a large number of conductive bonds. On the other hand, silica aggregate concrete (43) indicated a progressive decline in its conductivity with rise in temperature.

2.3.2 Thermal expansion

Dimensional changes of unrestrained concrete are made of two components: true expansion or contraction based on kinetic molecular movements, and an apparent expansion or contraction caused by hygro-thermal volume changes associated with the moisture movement. The observed changes in the size of a concrete member are essentially the result of combined behaviour of the hardened cement paste and the aggregates.

At a particular age, the coefficient of thermal expansion of hardened cement paste varies according to its hygral state. It increases

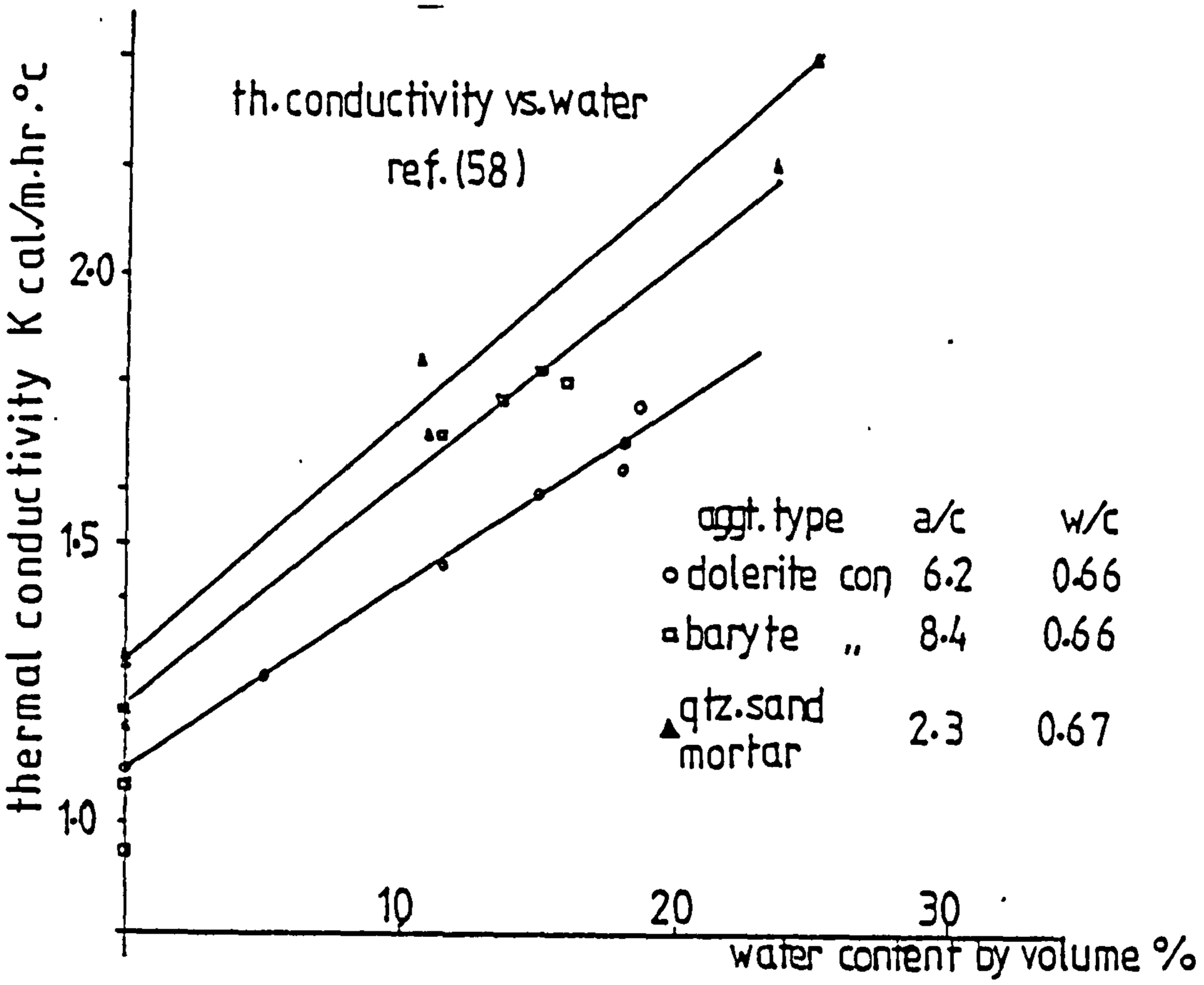
th. conductivity vs. water
ref. (58)
thermal conductivity K cal/m.hr.°c
2·0
1·5
1·0
10
20
30
water content by volume %
aggt. type a/c w/c
dolerite con 6.2 0.66
baryte „ 8.4 0.66
qtz. sand mortar 2.3 0.67

Fig 2.3

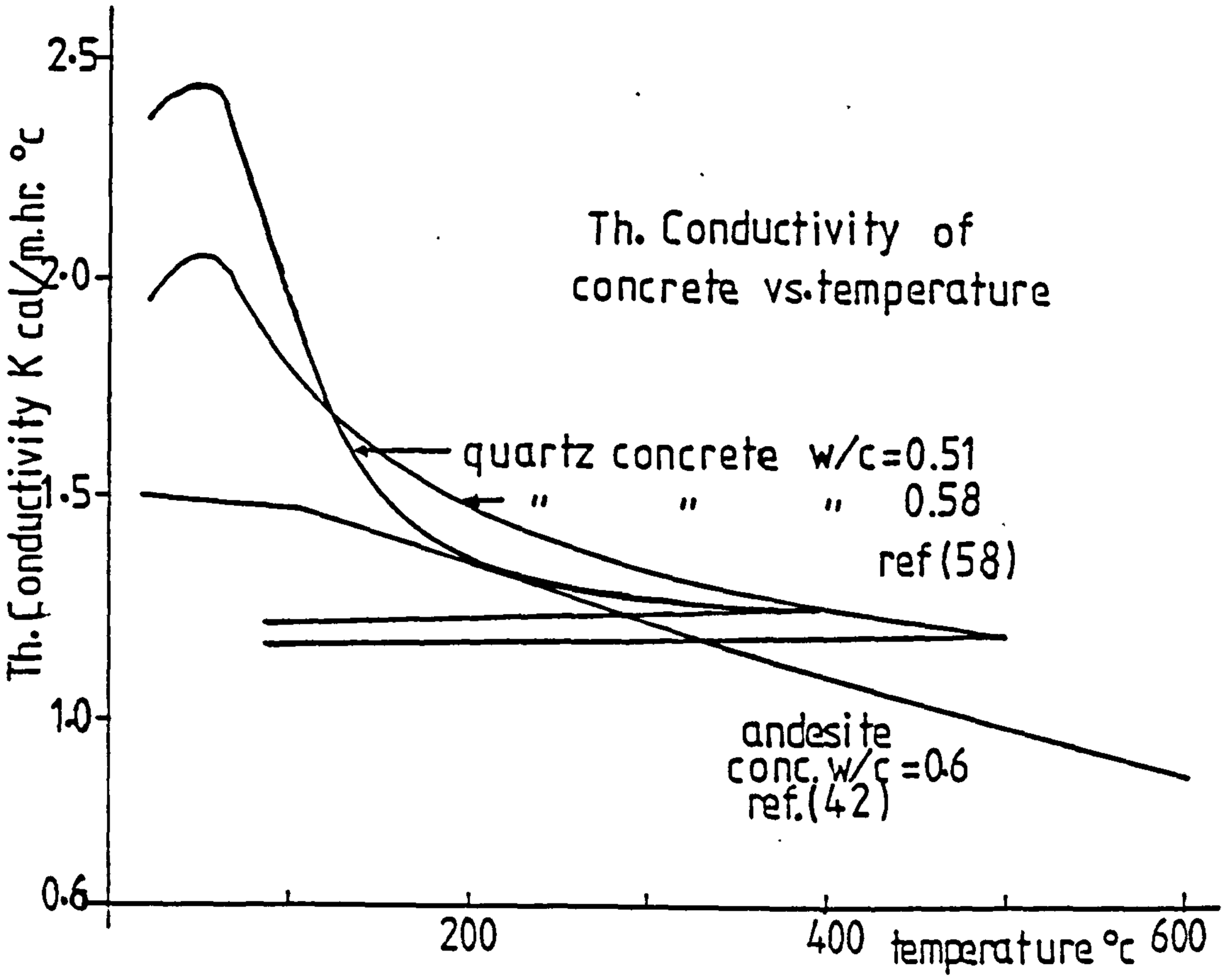
Th. Conductivity of
concrete vs. temperature
Th. Conductivity K cal/m.hr. °c
2·5
2·0
1·5
1·0
0·6
quartz concrete w/c=0.51
" " " 0.58
ref (58)
andesite
conc. w/c = 0.6
ref. (42)
200
400
temperature °c
600

Fig. 2·4

from the dry state with rise in humidity to a peak at about 70% relative humidity and then decreases steeply to 100% relative humidity and water saturation (59). Such effect is still detectable but to a lesser degree in concrete in which the coarse aggregates inhibit the larger thermal movement. This is illustrated in Fig. 2.5 by the results reported by Chapman and England (60) of an experiment on a laminated block of limestone concrete tested under a temperature cross fall. They obtained a maximum value for the coefficient of expansion of about $6.1 \times 10^{-6}/^{o}C$ when the evaporable water content per weight of mix water was 0.55.

2.3.2.1 Influence of temperature

Data from other studies (43, 55) concerning the influence of elevated temperatures on the expansion behaviour of Portland cement paste, aggregates and concretes are presented graphically in Fig. 2.6. The work by Harada et al. (43) shows that the initial expansion of hardened cement paste reverses to contraction or shrinkage at temperatures around $100^{o}C$. Such behaviour is overshadowed in concrete by the aggregate expansion, where for instance the expansion curve of sandstone concrete appears to coincide roughly with that of the sandstone rock itself in temperatures up to $500^{o}C$. On the other hand, the plotted results indicate that above about $150^{o}C$ the coefficient of thermal expansion of these concretes appears to increase with rise in temperature, with the sandstone showing abrupt change at about $500^{o}C$. Observations reported by Weigler and Fischer (55) on quartz aggregate concrete indicate a considerable increase in the coefficient of expansion above $100^{o}C$. Under conditions of temperature cycling, Bertero and Polivka (45) observed that the coefficient of thermal expansion of

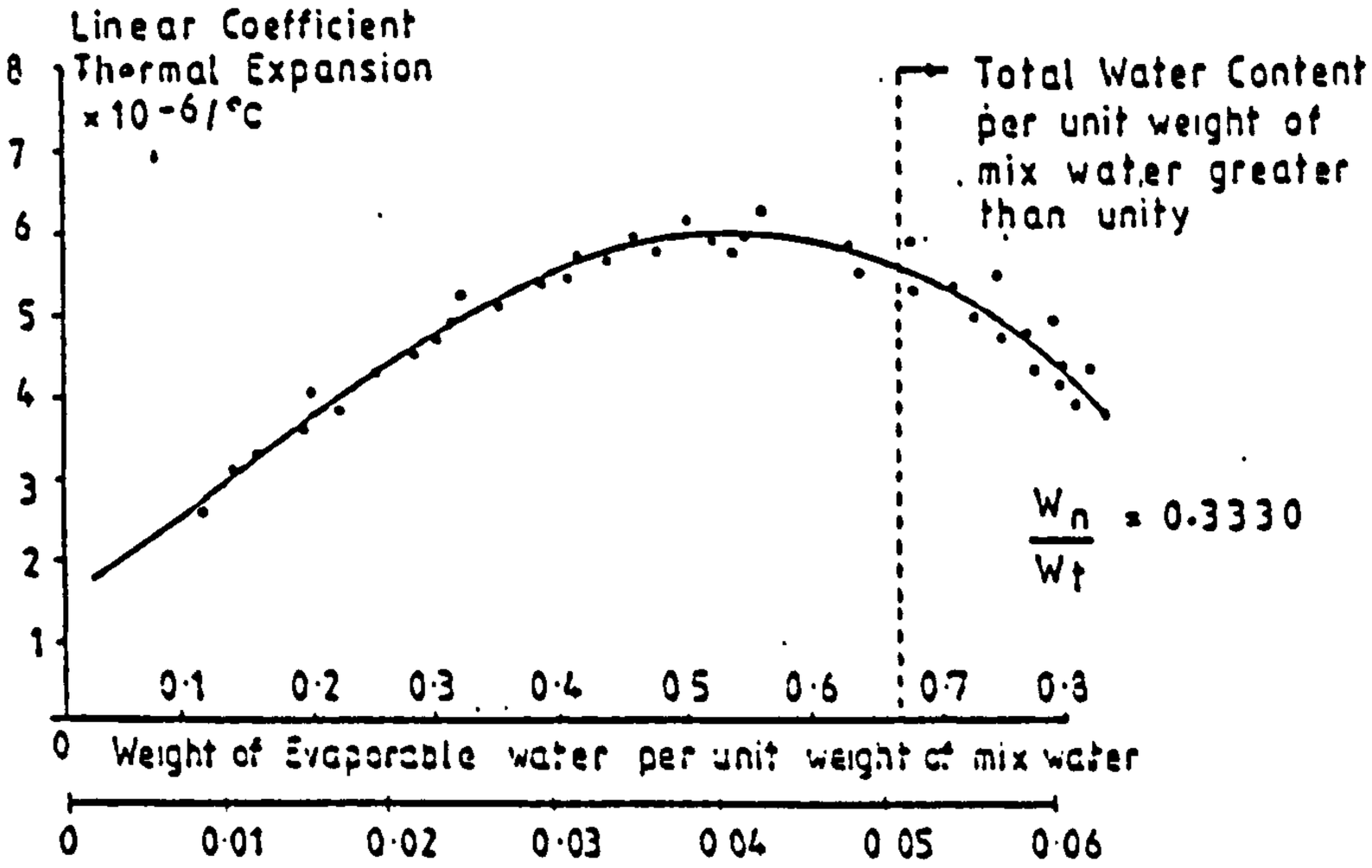

VARIATION OF LINEAR COEFFICIENT OF THERMAL EXPANSION WITH EVAPORABLE WATER CONTENT LIMESTONE CONCRETE

Fig. 2·5 ref. (60)

Variations with temperatures of the thermal expansion of cement, aggregates, and concretes

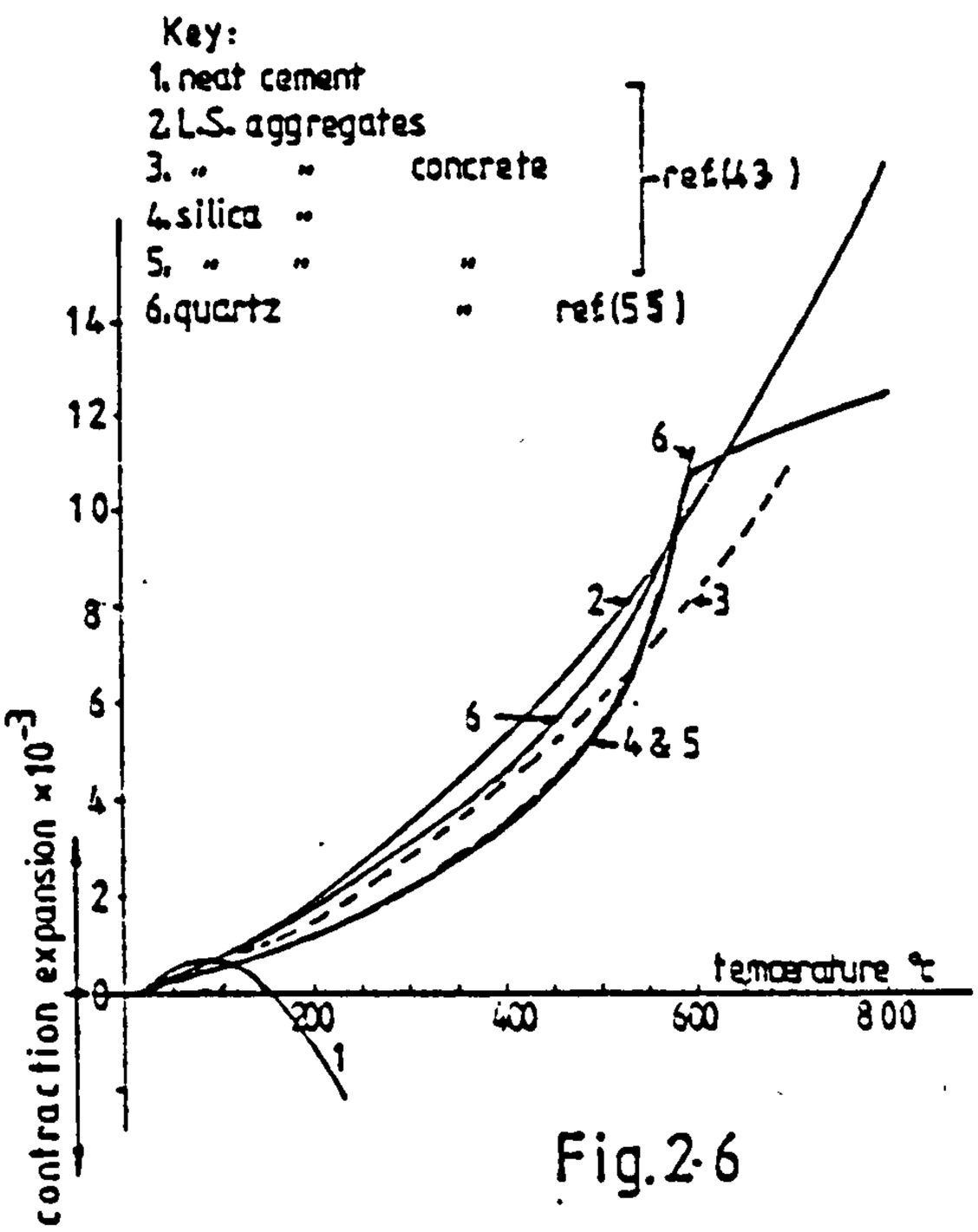

Fig. 2·6

sealed limestone specimens temperature cycled between 21°C and 149°C increases with the decrease in the rate of first heating, and decreases with the increase of the temperature cycles.

2.4 Concluding remarks

Although numerous studies have been devoted to investigating the material behaviour at elevated temperatures, the results appear to be inconsistent and often contradictory, thus rendering it difficult to formulate a general conclusion. The reasons may, however, be attributed to the inherent difficulty of performing and controlling concrete experiments dealing with temperature, the lack of a systematic approach for carrying out such experiments, and more evidently the multiplicity of the influencing parameters on the results. The review shows nonetheless that most of the literature results tend to agree on a general trend of behaviour which can be summarised as follows:-

1. Exposing concrete to elevated temperatures can be expected to induce serious changes in its structural properties, such as loss in compressive and tensile strengths, reductions in the elastic modulus and thermal conductivity.
2. The extent of property deterioration due to heating essentially depends on a number of intrinsic and test parameters. For a given composition, the most important of these are the severity and duration of heating and the moisture condition of the test specimen.
3. When the free moisture is contained in the concrete during heating, deterioration in many of its structural properties can be expected in increasing degrees of severity at all levels of heating.

CHAPTER III

MOISTURE TRANSFER AND THERMAL CREEP PHENOMENON IN CONCRETE

Chapter 3 - Synopsis

The properties and deformational behaviour of concrete are sensitive to its moisture content; a parameter which in itself can be considerably influenced by non-uniform heating.

This chapter discusses and summarises available literature data on the aspect of temperature-gradient-activated drying and the concomitant shrinkage in concrete. It also presents a review of literature on the influence of temperature and moisture content on the creep behaviour of the concrete.

3.1 Moisture transfer in concrete

3.1.1 Introduction

The transfer of free moisture in concrete, whether it is induced by drying from an exposed face or by a temperature gradient, can change many of the basic properties of the material and hence the structure behaviour. Elastic, creep, shrinkage and thermal properties of concrete are all sensitive to moisture change. Changes in the thermal conductivity of concrete, for instance, could significantly affect the prescribed temperature gradient on the structure and the corresponding stresses. In nuclear reactor pressure vessels the moisture content in the walls of the vessel has a particular importance, in that it provides an economical barrier to radiation by attenuating the neutron flux present in the structure.

3.1.2 The hygral state in concrete

A macroscopic view into the structure of concrete reveals a conglomerate of naturally occurring fine and coarse aggregates, cement, and water in various degrees of fixation. For reasons of workability at casting, the amount of water originally added to the concrete is usually in excess of the quantity required for the hydration process of the cement paste. In time, the concrete is bonded to a firm and solid mass by the hydration products. In such a state, the concrete normally contains, in addition to some unhydrated cement, a certain quantity of free water. The state of water in a hardened concrete matrix has been arbitrarily classified according to its degree of fixity into:

1. Evaporable water; this consists of water that is tightly held in the gel pore structure, this being evaporable over the range from 40 to 0% relative humidity; water held in larger cavities of the system, known as capillary water, which is more easily evaporable and will migrate out of the cement paste at a relative humidity of 40 to 50% and above (6). In heated conditions this is defined as the moisture which can be driven off at 105°C (40,60,61).
2. Non-evaporable water, known also as the water of hydration, which is chemically or physically combined with the cement gel structure. It cannot evaporate at 0% relative humidity, it is however regarded as being approximately equal to the amount of moisture held at 100°C but lost at 1000°C (61).

3.1.3 Influence of temperature gradient on moisture transfer in concrete

Several experimental studies have been devoted to investigating the temperature gradient-activated moisture movement in concrete, although most of these were mainly concerned with moisture movement within simulated thick wall structures. Sealed and partially sealed samples of different concretes, shapes, and sizes were subjected to various temperature histories. Measurements were in many cases made of temperatures, weight changes, evaporable and non-evaporable water contents, electrical resistance, shrinkage and pore pressure. Whilst it is not intended here to introduce a comprehensive survey of the various attempts, the reader is referred to the following references - (60,62, 63,64,65,66,67,78). Some of the observations reported in these references, in relation to a concrete block drying under temperature gradient, are summarized as follows:-

1. At temperatures above 100°C a significant pressure develops in the pores of concrete as a result of the entrained air and the rapid increase of saturated vapour pressure with increase in temperature. This pressure becomes a dominating factor in thick sections affecting the moisture movement.
2. Water migrates down the temperature gradient creating a drying front until eventually there is insufficient water available to maintain the saturation vapour pressure.
3. A constant temperature gradient causes more water to migrate into the cooler zones thus producing areas of higher than normal water content.
4. The pressure in the hot regions continues to fall with time (Fig. 3.1) as the drying front moves along the specimen progressively into the cooler regions.
5. For concrete which is exposed to atmospheric drying and which is far removed from zones of high temperatures, the variation of water content will depend more on diffusion and other processes than on pore pressure gradients due to the non-uniform temperature states.
6. Evaporation drying is a more slowly moving mass transfer process than the migration caused by higher pressure in the hot regions.
7. When moisture paths are long and when gradients of temperature and pressure are shallow, evaporation drying becomes the influential mechanism of drying at a free face.
8. After a long time and depending upon the length of the moisture path, the two drying zones will eventually meet and drying will then continue throughout the entire section (Fig. 3.2a).

9. Shrinkage will tend to occur whenever pore pressures are sufficient to cause significant quantities of moisture to migrate, even deep in a concrete mass.

3.1.4 The process of drying shrinkage

Dimensional changes normally take place in concrete whenever changes of moisture contents occur. Removal of the evaporable water contents from the pores of concrete gives rise to drying shrinkage, and water gain causes swelling (Fig. 3.2). The transfer of moisture is a slow moving process and so is the attendant shrinkage. Drying penetrates gradually inwards compressing the interior and creating tensile stresses in the outer skin. Due to this non-uniform state of stress, cracking often results. Also, because shrinkage is primarily a property of the cement paste, a state of differential shrinkage is created in the hardened concrete matrix which then produces micro-cracks at the cement paste-aggregate interface. These are thought to be responsible for the higher deformation behaviour of concrete when load is initially applied (68).

3.1.5 Shape and size effects on shrinkage

The shrinkage behaviour of real structures is often inferred from deformation measurements on unloaded scaled down models in the form of laboratory or site samples. Since drying shrinkage is closely related to the moisture loss, it is therefore essentially a specimen size and shape-dependent material property. Proper consideration has to be given to this effect when correlating the shrinkage of a model specimen to that of a life size structure, or to other samples having different geometries.

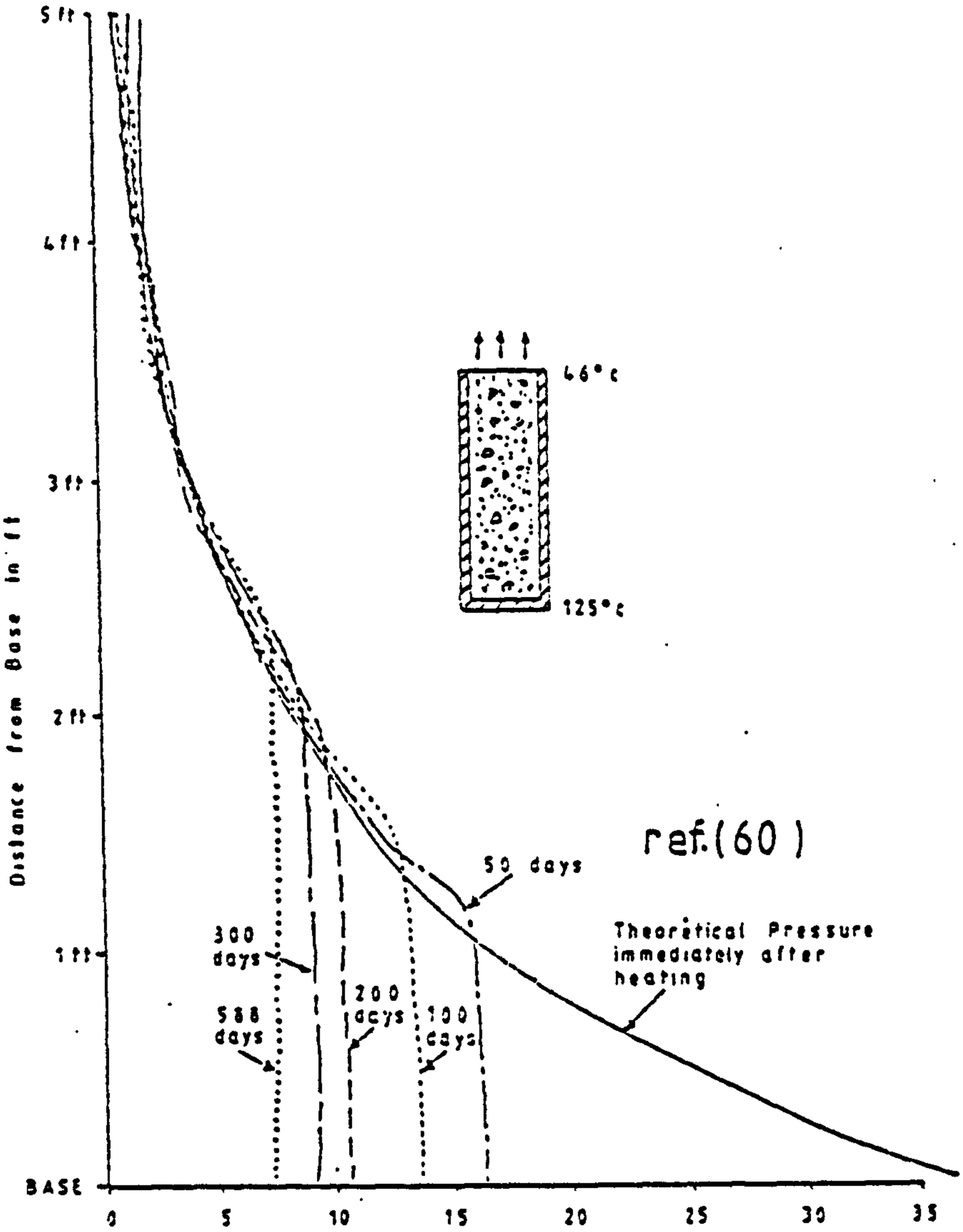

Fig.3·1 GAUGE PORE PRESSURE DISTRIBUTIONS AT VARIOUS AGES OF HEATING

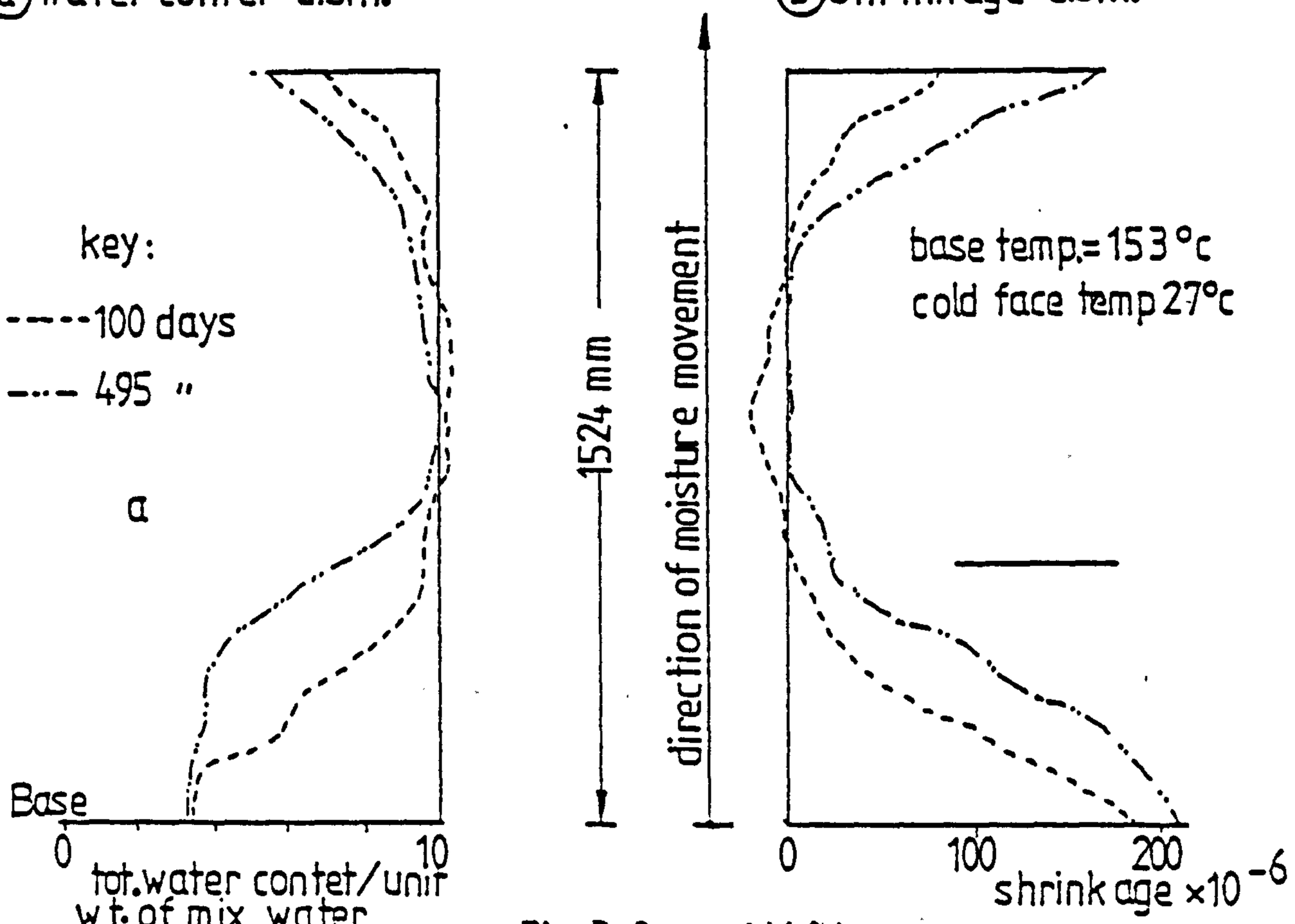

Fig.3·2 ref.(60)

Ross (69) suggested that a suitable parameter for use in comparing the shrinkage of members of differing size and shape is the ratio of the exposed (drying) surface area S to the volume of the member V. Hansen and Matlock (70) investigated the significance of this parameter both theoretically and experimentally and concluded in support of the argument.

Hobbs (71) obtained approximate fit for his and other data (70) using an exponential form of the ratio and concluded that ultimate shrinkage is broadly independent of specimen size. This was in agreement with an earlier conclusion derived from an analytical study by Campbell-Allen and Rogers (72) who suggested the elimination of the size effect on the final shrinkage from the codes of practice.

3.1.6 Elementary theory of diffusion

One of the theoretical approaches used to describe the drying process and its subsequent deformation in concrete is by use of Fick's law of diffusion. The basic equation used in terms of shrinkage is:

$$\frac{\partial S}{\partial t} = \kappa . \left(\frac{\partial^2 S}{\partial x^2} + \frac{\partial^2 S}{\partial y^2} + \frac{\partial^2 S}{\partial z^2} \right)$$

where S = unrestrained shrinkage strain, t = time, x, y and z are rectangular coordinates, and κ = shrinkage diffusivity or diffusion coefficient.

Hansen and Mattock (70), Becker and Macinnis (73) among others have shown that the linear diffusion theory, which is based on an average constant diffusion coefficient 'K' adequately describes the shrinkage (or drying) of concrete at ordinary temperature conditions. Work by Hughes et al. (74) has also shown that elementary diffusion

theory, although requiring a temperature-dependent diffusion coefficient, can describe the drying process of concrete at temperatures in the range of 50-95°C provided that some care is taken with surface drying. Yuan et al. (75) concluded a satisfactory agreement between theory and experiments in which mortar specimens were allowed to dry at temperatures up to 60°C in carbon dioxide free environments. However, investigations by Lowe et al. (76) into the drying of concrete at temperatures of 30°C showed that the rate of moisture diffusion was a function of the concentration of evaporable water causing drying to become increasingly difficult. For problems where drying is considered to be too slow to predict with the linear diffusion theory Bazant and Najjar (77) postulated the diffusion coefficient to be a function of pore relative humidity (relative vapour pressure) which makes the diffusion problem of drying non-linear.

When drying of concrete is being activated by a temperature gradient the problem becomes more complex to solve by the simple diffusion theory, and perhaps other approaches (77-78) could be more appropriate. In general, the applicability of any method and its ability to predict acceptable results rests on whether it recognises all possible mechanisms capable of producing mass movement of water in the problem under consideration.

3.2 Thermal creep pheomenon in concrete

3.2.1 Definition of thermal creep

The term 'thermal creep' refers to the age, temperature and time-dependent strain occurring after the instantaneous application of a fixed load to a concrete specimen or structure at time zero, in excess of the strain observed in an unloaded and heated companion specimen or

structure. In other words, it is the strain in excess of shrinkage and temperature strains and immediate elastic strain, which changes in time according to the dependence of the elastic modulus on the prevailing temperature and time under load.

Creep, in general, is reckoned to embrace two independent components (Fig3.3):

1. Recoverable creep, or delayed elastic strain, which appears as a time-dependent recovery after removal of the load. It has a limiting magnitude that is proportional to the stress, and it is shown (79) that the limiting value is approached gradually at a rate which declines with the age of the material. It has also been shown by Nasser and Neville (80), Arthanari and Yu (81), Nasser (82), Illston and Sanders (79) that the delayed elastic component is little affected by temperature. In relation to the other strain components, the delayed elastic strain is usually small, and in many analyses of concrete structures it is completely neglected.

2. Irrecoverable creep strain, or flow, which is the major component of total creep strain, and unlike the delayed elastic strain has no limiting value; instead it continues indefinitely at an ever decreasing rate, and for a given temperature history its rate per unit stress can be considered as independent of the time at which the stress was applied.

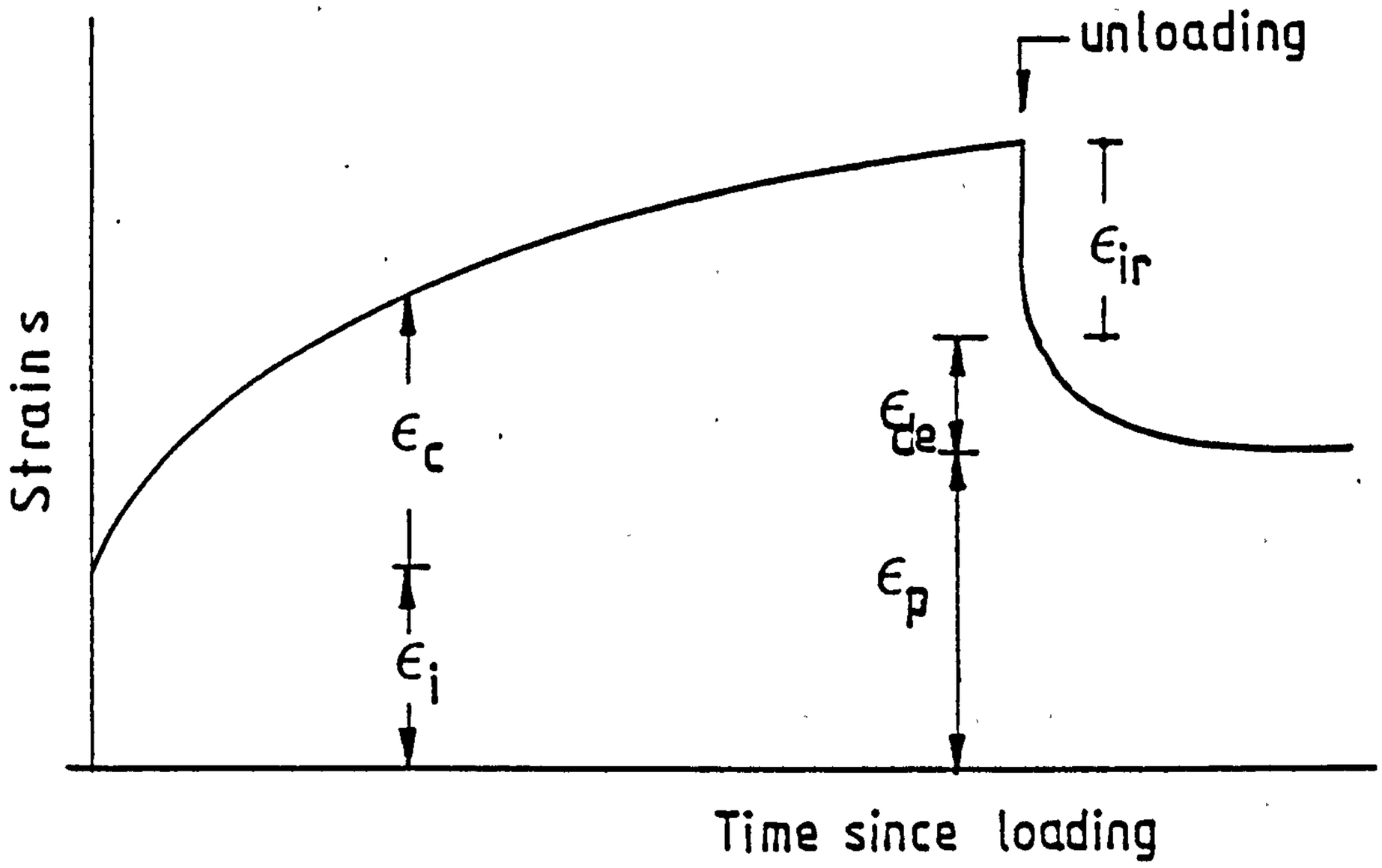

ϵ_i = instantaneous strain on loading.
ϵ_{ir} = " " recovery upon unloading.
ϵ_c = creep strain.
ϵ_{de} = delayed elastic (creep recovery) strain.
ϵ_p = residual deformation (irrecoverable creep)

Fig 3.3 Total strain curve of concrete

3.2.2 Influence of sustained and cyclic temperatures on creep

Although the influence of temperature on the creep behaviour of concrete has long been realised, it is only since the introduction of concrete in the pressure vessel industry in the late 'fifties that the matter has been taken more seriously. In the early times of developing interest in the subject, conflicting results were often reported due largely to what was then considered to be a unique and complex testing environment. Fortunately, the gap in the differences of opinion seems nowadays to be significantly narrowed and the diverse lines of thought have converged towards a more unified picture on the general thermal creep behaviour of concrete. Geymayer (84), Mukaddam and Bresler (85) reviewed literature data reported over the years 1934 to 1969 on the effects of temperature on the creep of concrete. Some of the results compiled by Geymayer (84) are shown in Fig. 3.4 Based on the information given in these reviews and in the references (8,9,12,16,80,81,83,86,87) the following summary is believed to be warranted.

1. Creep at elevated temperatures follows the same general trend of creep at room temperatures.
2. For temperatures up to 80°C, the creep of concrete and the creep rate are several times greater than those at room temperature.
3. The creep of a specimen allowed to lose moisture during the test is higher than that when the moisture is contained.
4. Within the temperature range stated in 2, and for a stress/strength ratio of up to 0.5, the creep is a fairly linear function of applied stress.

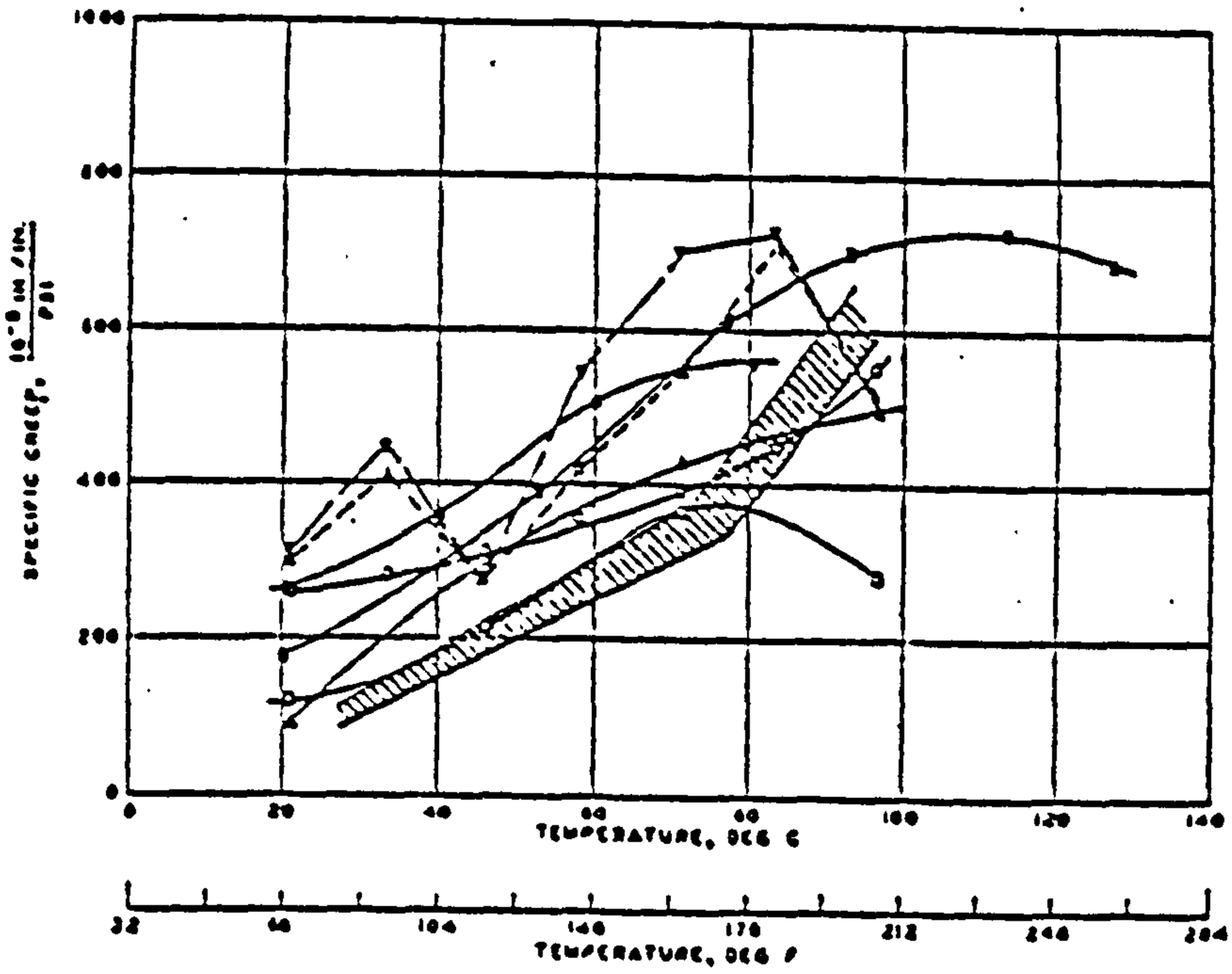

LEGEND

- ● Hasser and Neville: Siliceous, uncrushed concrete loaded to f/f'_c of 0.45. Creep measured on 6 x 18 in. cylinders after 90 days of loading stored in water
- ■ Hasser and Neville: Limestone dolomite normal-type concrete loaded at 10 days to f/f'_c of 0.35. Creep determined on 6 x 18 in. sealed cylinders after 90 days of loading
- ▲ Same as above, but f/f'_c 0.60
- ▼ Same as above, but f/f'_c 0.70
- ◆ England and Ross: Limestone concrete loaded at 10 days to f/f'_c of 0.30. Creep determined on 4 x 8 in. sealed cylinders after 90 days of loading
- Hansen: Limestone concrete loaded at 3 months to f/f'_c of 0.20 to 0.70. Creep determined on 6 x 12 in. sealed cylinders after 100 days of loading
- ● Abrams and Tu: Limestone gravel concrete loaded at 10 days to f/f'_c of 0.20; creep determined on 6 x 12 in. sealed cylinders after 90 days of loading
- ▲ Hasser and Neville: Siliceous dolomite normal-type concrete loaded after 1 year water storage to f/f'_c of 0.35. Creep determined on 6 x 18 in. cylinders after 90 days of loading underwater

INFLUENCE OF TEMPERATURE ON CREEP

SEALED OR WATER-STORED SPECIMENS AFTER 60, 90, 90, OR 100 DAYS OF LOADING

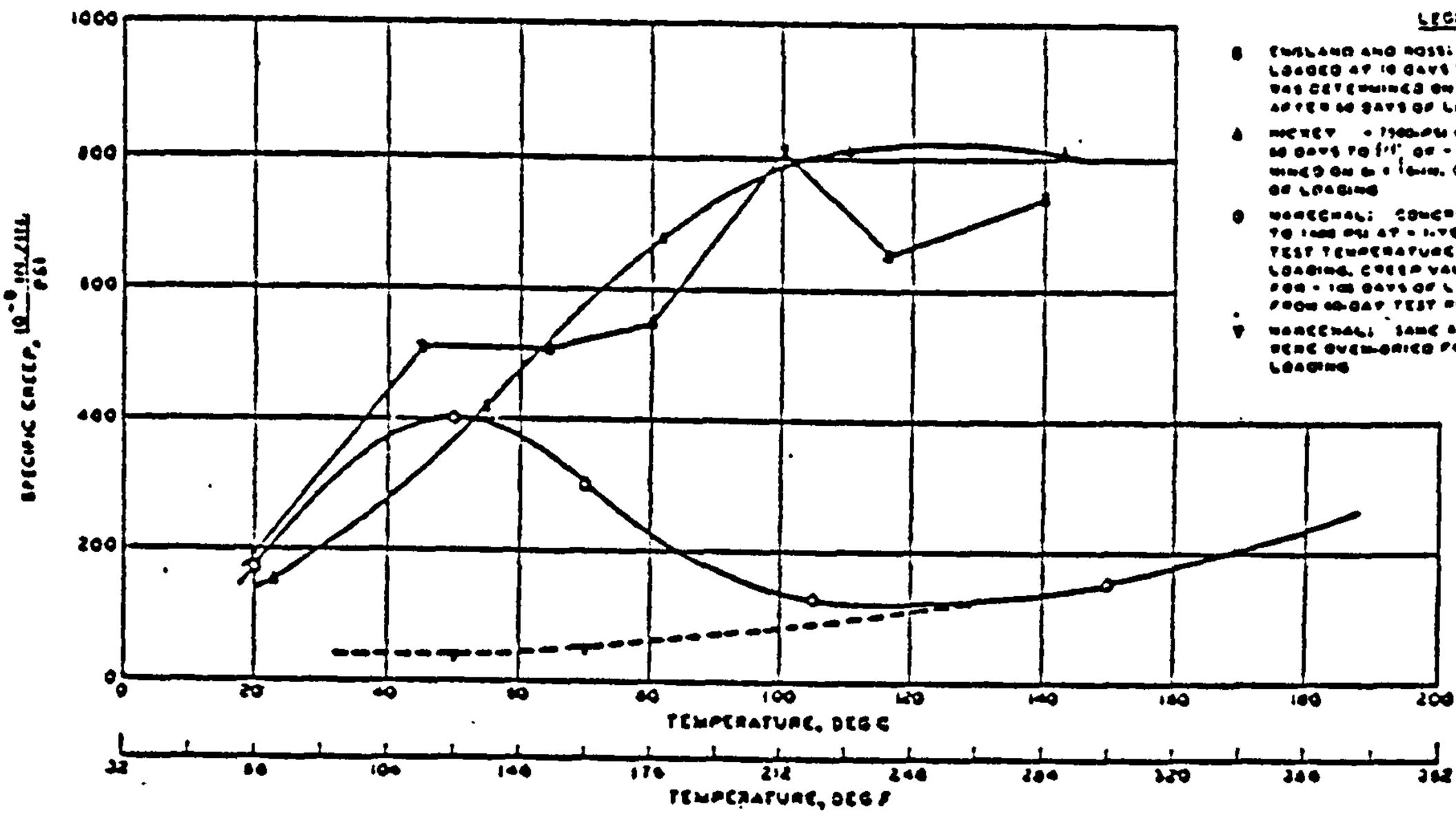

LEGEND

- ● England and Ross: Limestone concrete loaded at 10 days to f/f'_c of 0.25; creep was determined on 4 x 8 in. cylinders after 90 days of loading
- ▲ Hansen: Limestone concrete loaded at 90 days to f/f'_c of 0.10. Creep was determined on 6 x 12 in. cylinders after 107 days of loading
- ■ Hansen: Concrete of limestone loaded to 1000 psi at 1-year age; subjected to test temperature for 10 days prior to loading. Creep values plotted are those for 100 days of loading extrapolated from 90-day test results
- ▼ Hansen: Same as above, but specimens were oven-dried for 1 month before loading

INFLUENCE OF TEMPERATURE ON CREEP

UNSEALED SPECIMENS AFTER 60, 100, OR 107 DAYS OF LOADING

Fig 3-4 ref.(84)

Perusing further into the more recent literature revealed confirmatory and additional information on creep behaviour of concrete under sustained and cyclic temperature regimes.

Nishizawa and Okamura (44) loaded sealed concrete prisms to 26% of their cold strengths at the age of 28 days, and these were heated after 7 days from loading to 70°C or 90°C. During the first week of heating, a rapid increase in creep strains was observed followed by a steady increase which is shown to be linear with the logarithmic time scale. The creep strains recorded in the first day of heating amounted to about 150% of the initial elastic strain on loading at 20°C. Results obtained under cyclic temperature conditions between 20°C and 70°C showed a very rapid increase in creep strain in the first temperature cycle, but no further change was observed in the subsequent cycles; except that when a new higher level of temperature was applied, a further rapid increase in the creep strain occurred.

Fahmi, Polivka and Bresler (88) presented results of a creep study conducted on hollow cylindrical micro-concrete specimens in compression and torsion at 50 and 100% relative humidity. Most of these specimens were subjected to a sustained load for 37 days at 23°C and then heated to 60°C or exposed to thermal cycles between 23 and 60°C. An increase in creep strain and rate of creep was observed when the concrete was first heated and sustained at 60°C. After heating, the creep strain continued increasing with time for the 100% R.H. specimens, whereas for the 50% R.H. specimens the creep strain stabilized in about 2 to 3 weeks. The first thermal cycle caused the largest increase in creep strain. Although each subsequent thermal cycle caused a further increase in creep for the 100% R.H. specimens, no appreciable increase in creep was observed on the 50% R.H. specimens. They also concluded that the specific creep in torsion was higher than that in compression

at sustained normal, elevated or cyclic temperatures, and that most of the creep strain at elevated or cyclic temperatures was irrecoverable.

Results obtained by Hornby and Grainger* from tests on concrete cylinders confirmed the trend of increase in the creep with temperature, when a specimen was first heated to 75°C after being under sustained load for 893 days at 27°C. It was found that a year after the change in temperature, the creep rate approximately equalled the creep rate of another specimen which had been under load for the same time, but maintained throughout at the higher temperature.

Browne and Bamforth (56) showed results of creep tests on sealed limestone concrete cylinders, loaded at the age of 12½ years and stored under water at temperatures of 20°C and 95°C. It was observed that the 95°C specimens exhibited far greater rate of creep than those maintained under load at 20°C. After 102 days from loading, the higher temperature specimens indicated a specific creep strain value of 78×10^{-5} per N/mm^2 compared with 11×10^{-6} per N/mm^2 for the lower temperature specimens.

Browne and Blundell (68) published results (Fig. 3.5) of tests in which the temperature was increased and decreased on concrete samples which had been kept under sustained load at temperatures of 20, 65 and 95°C. It was observed that increase in temperature rejuvenated the creep rate, while a decrease in the temperature initially reduced the creep rate but after a period of time there was a substantial recovery to similar rate which would have occurred if the original higher temperature had been maintained.

Illston and Sanders (79) investigated the creep behaviour of saturated mortar tube specimens subjected to sustained torsional loading

---

*Reported in reference 89

and various temperature histories within the range 20 to 94°C. Their results (Fig. 3.6) showed that when the temperature was raised for the first time, the creep rate increased greatly in comparison with that of a similar specimen heated before loading. No such change of rate was observed when the temperature was lowered or when it was raised to a level previously attained. They concluded from this study the existence of a third component of creep strain designated 'transitional thermal creep' in addition to the commonly known components, flow and delayed elastic strains. This component is said to develop only when the temperature is raised to a new higher level, and it is of an irreversible nature. In a follow up study (10) they showed that the component has a limiting specific value which they expressed solely as a function of temperature.

3.2.3 High temperature creep

There have been several attempts to investigate the creep behaviour of concrete at high temperatures, and to answer the argument as to whether or not there is a further increase in creep with increasing temperatures.

Sullivan and Poucher (48) tested mortar and plain concrete beams which were subjected to mechanical load cycles in bending, and various thermal cycles in the range 20 to 400°C. They found that at 300°C the creep of mortar was twice that at 125°C, whereas the creep of concrete at 300°C was nearly three times that at 125°C, probably due to the development of micro-cracks between aggregate and mortar.

Wang (91) shows results of tests on concrete cylinders loaded to 40 and 60% of their strengths and heated at temperatures between 93.3 and 426.8°C for 326 days. At all temperatures and stress/strength

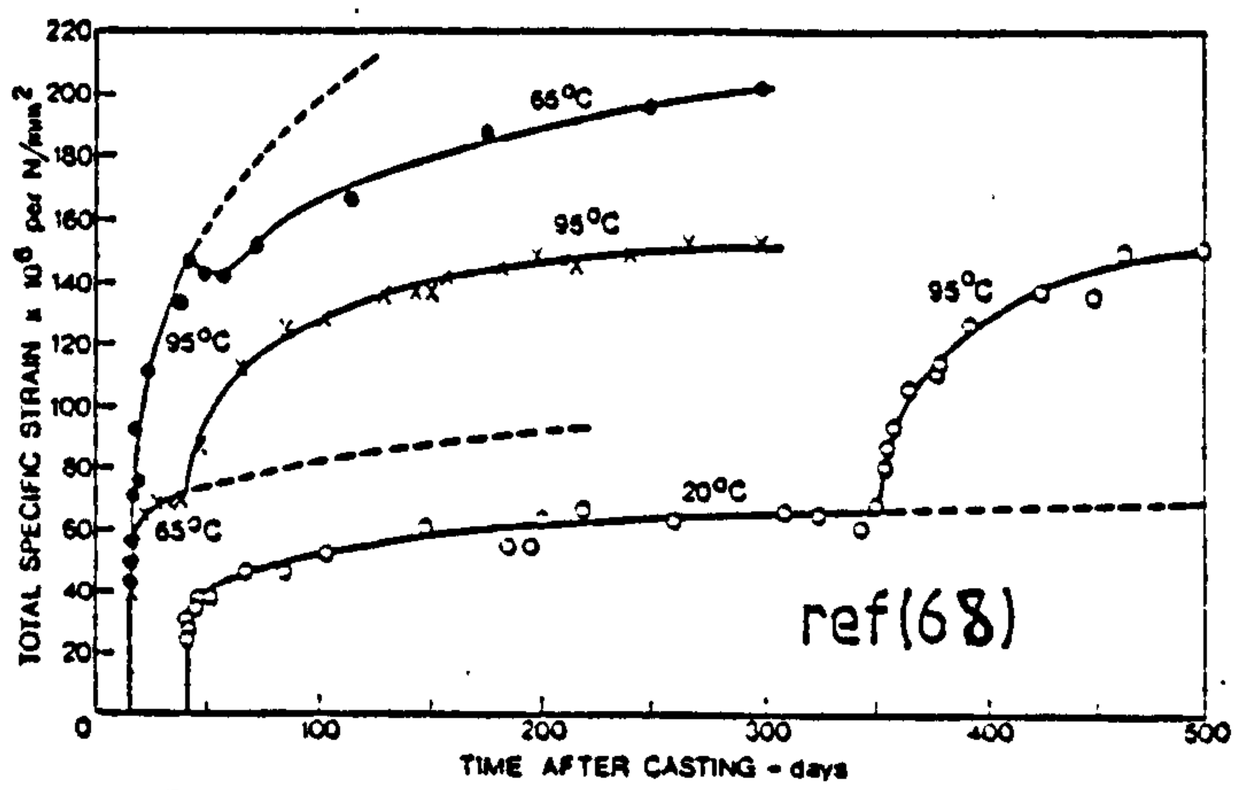

Fig.3.5 The effect of temperature variation upon creep of concrete

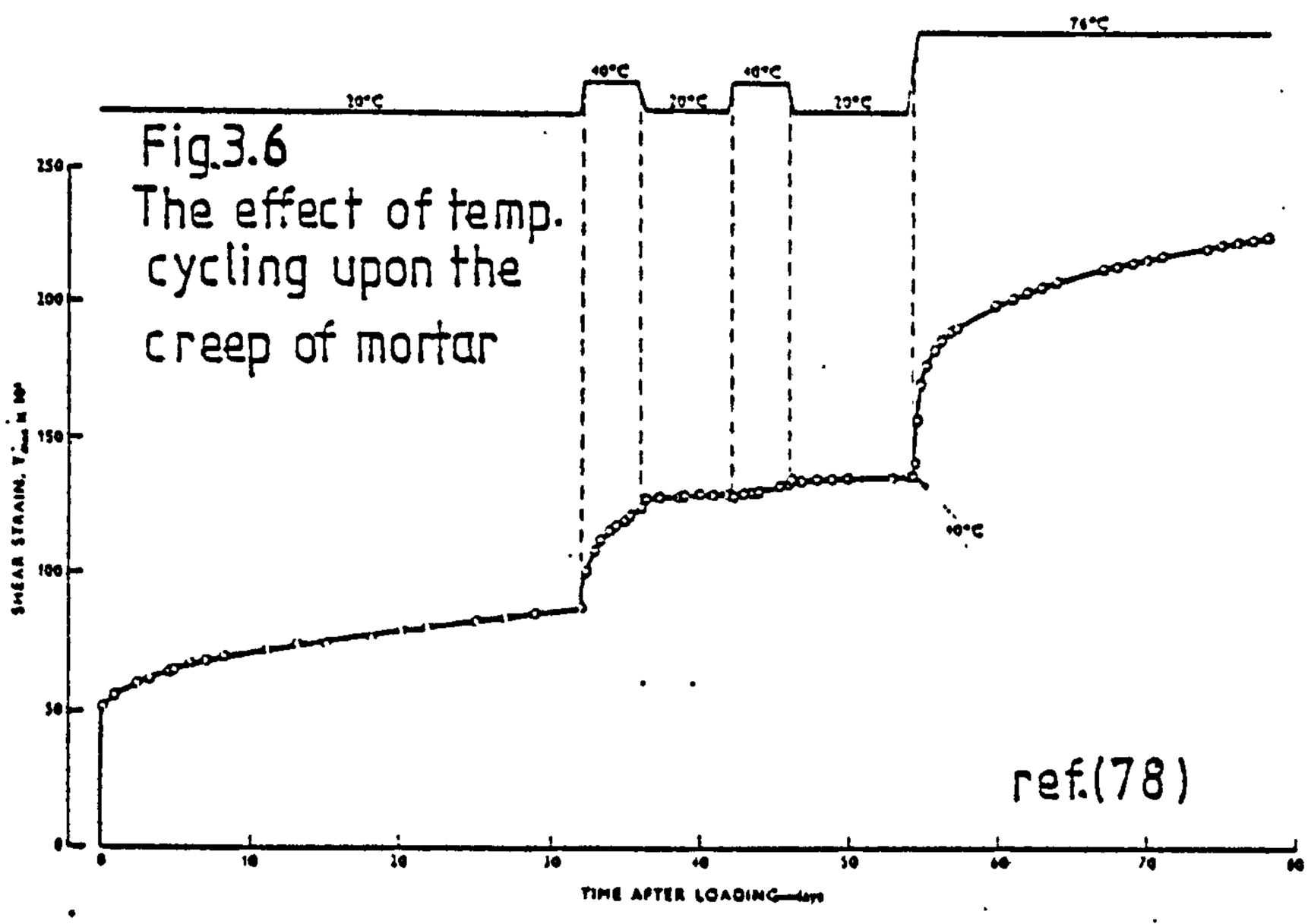

Fig.3.6
The effect of temp. cycling upon the creep of mortar

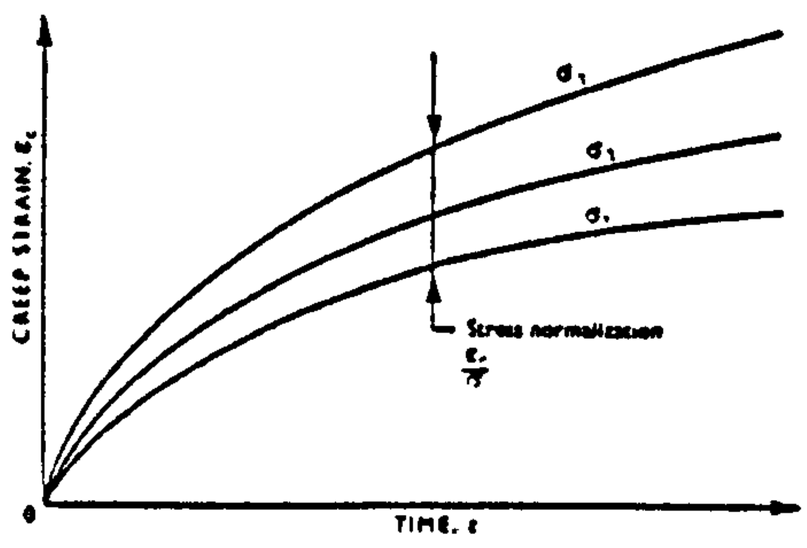

(a) Normalization of creep curves plotted for various stresses produces a single curve for each temperature

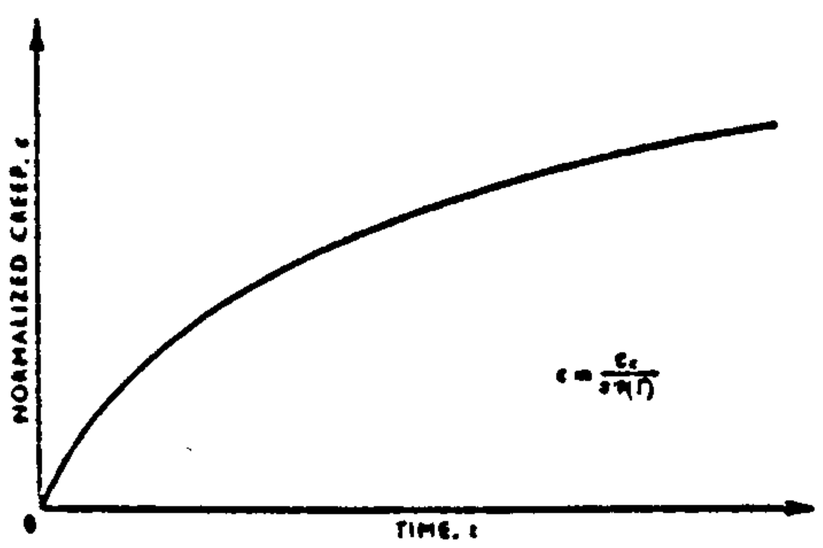

(c) Normalized creep or pseudo-time, ε

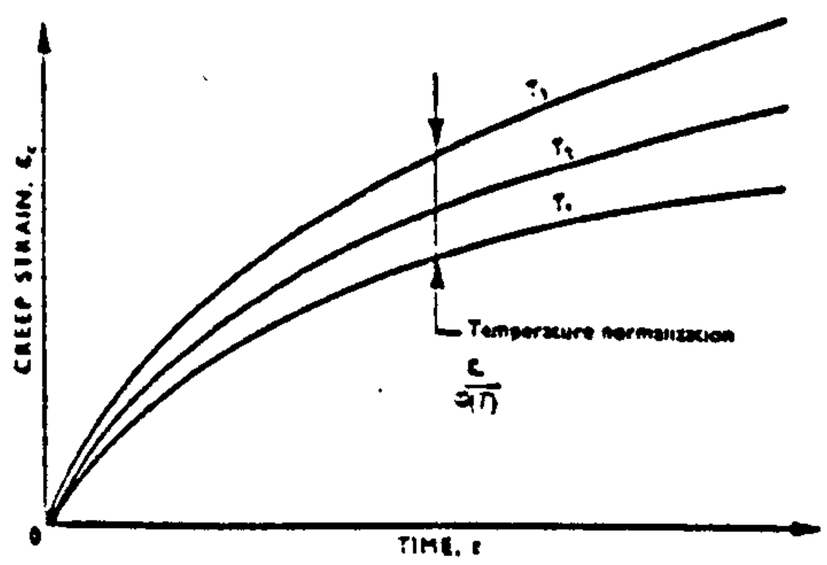

(b) Further normalization with respect to temperature produces the single curve shown in (c)

Fig 3·7 diagrammatic representation of the normalization of creep w.r.t. stress and temperature

ratios the creep generally increased with temperatures; the relationship between creep and stress/strength ratios was, however, found to be non-linear at all temperature levels investigated.

Gross (92) has conducted creep tests on unsealed concrete cylinders which were preheated to the desired temperature, then loaded for 7 days. He concluded that for conditions milder than stress/cold strength ratio equal to 0.66 and temperature 300°C, the total creep strains are linear in the stress variable within these limits, also he reduced the non-linear thermal creep phenomenon into a linear thermoviscoelasticity problem.

3.2.4 Influence of moisture content on creep

Creep occurring in the absence of moisture exchanges is commonly termed 'basic creep', while the additional creep induced by moisture movement to the surrounding atmosphere is termed 'drying creep'. Reutz (93) among others has shown that the influence of simultaneous drying is to cause a large increase in creep at first, but this is gradually decreased as the rate of drying diminishes. Re-wetting also increases creep, as according to one theory (94) the basic creep potential increases due to increase in the moisture content; this potential is reduced on drying, but drying creep takes place, so that each part of the cycle contributes to increased creep. Illston (95) postulated a creep to moisture content to be identical to shrinkage-moisture content relation when plotted non-dimensionally. Recently, Gamble and Parrott (96) published experimental results on creep during drying-and-wetting. It was observed that the development rate of drying creep was linearly related to that of concurrent shrinkage. Specimens re-wetted under load exhibited wetting creep, which was linearly related to concurrent swelling.

Hannant (83) found that preheated concrete samples, to a weight loss of 80% of the mixing water, which were subsequently sealed and loaded, virtually reached their creep limit after 20 days. Zielinski and Sadowski (97) observed inappreciable creep in fully dried specimens tested at 20 or 60°C. However, similar tests carried out on specimens with various moisture contents showed almost linear relationship between creep and moisture content.

3.2.5 Shape and size effects on creep

It is to be expected from the argument of Section 3.2.4 that the size of a concrete member affects drying creep, as it governs the amount of moisture lost to the surrounding environments. The concept of surface/volume ratio as a good indicator for the shape and size effect is assumed by Ross (69) to apply for creep as well as shrinkage. Hansen and Mattock (70) arrived at similar conclusions to that for shrinkage regarding the use of the S/V ratio, as being a suitable parameter for use in structural design. They also concluded that the size and shape of member only affected the rate of creep during about the first three months, and that both the rate and final value of creep decreased with increase in the member size.

3.2.6 Normalization of creep data

It is generally accepted that at normal temperatures and working stress levels (below 50% of ultimate strength) concrete possesses a linear stress/strain relationship in both elastic and creep regimes. This has provided a convenient basis for normalizing creep data with respect to stress into a single time variable commonly termed 'specific creep' strain, i.e. creep strain per unit stress. For moisture stable

concrete samples, the linearity of creep strain with stress has also been confirmed at temperatures below 100°C by the majority of investigators. It should therefore be possible to find a suitable expression to describe the creep-temperature-time relationship for use in time-dependent behavioural analyses of structures.

Browne (8) derived from his experimental data the expression:

$$\varepsilon = f(kT) + f'(kT).\ \log_{10}(1 + t)$$

where ε = specific strain, i.e. the sum of elastic and creep strains per unit stress, k = the age at temperature and load application in days, t = time in days, T = the temperature of concrete under load, and f(kT), f'(kT) = experimentally determined factors which depend on k and T.

Ross, England and Suan (16) have taken advantage of the stress-creep strain linearity at temperatures below 100°C and proposed the term 'specific thermal creep' which they defined as:

$$c = \frac{\varepsilon_c}{\sigma.\phi(T)}$$

where c = specific thermal creep strain, i.e. creep strain per unit stress per unit temperature, ε_c = creep strain, σ = applied stress, $\phi(T)$ = temperature-creep normalization function, which enable a family of creep curves determined under various constant temperatures to be reduced to a single data curve. In most instances, $\phi(T)$ is a simple polynomial in temperature T. The normalization procedure is shown diagrammatically in Fig. 3.7. The resulting single specific thermal creep curve can be used to replace time in the time-dependent constitutive laws, thereby simplifying the analysis of creep behaviour in structures subjected to temperature gradients, and allowing the analysis of mass

concrete structures by the methods of finite elements and continuum mechanics.

Fahmi, Bresler and Polivka (98) have developed a mathematical model for predicting creep of concrete at constant and variable temperatures, based on time-shift principle, for the so-called thermo-rheologically simple material. Such an approach requires that creep curves at different temperatures when plotted against the logarithm of the time are of the same shape. Some literature data on the creep of sealed concrete have been shown to conform to this principle within a temperature range of 20 to 80°C. Determination of the temperature function $\phi(T)$ (unlike that defined above) have been made numerically, and in one instance a third order polynomial in T was given.

At higher temperatures, Marechal (99) has shown that the Arrhenius activation energy principle applies to creep strain dependence on temperature and that linear stress/creep strain and semi-log creep strain-time relationships exist up to 400°C.

CHAPTER IV

THERMAL CREEP AND SHRINKAGE ANALYSES OF CONCRETE STRUCTURES

Chapter 4 - Synopsis

Methods of calculating the time-dependent stresses in materials subjected to non-homogeneous creep are discussed with particular reference to three methods; the iterative 'rate of creep'; the 'steady state'; and the 'variational power theory'. All the three methods have been developed for the analysis of a 3-span continuous prestressed concrete beam under the sustained influence of transverse loading and temperature cross fall. A numerical example is given, and close agreement of predictions for transient creep effects is shown between the iterative rate of creep solution and the direct solution of the variational power theory.

4.1 Introduction

For the time-dependent analysis of homogeneous concrete structures at working stress levels (below 50% of ult. strength), various constitutive relations exist, which enable a fairly accurate estimate of the service stresses to be made (creep and shrinkage effects) in structures under time-varying stress regimes. The simplest direct approach is that of the 'effective modulus' method, which accounts for the apparent decrease in concrete stiffness with time. Others include the methods of superposition, rate of creep and rate of flow. The principles and relative merits of these methods have been described and discussed by a number of investigators (100-102) to whom reference is made.

In the broader context of structural analysis, constitutive creep laws for concrete have been based on the concept of linear visco-elasticity. Mechanical analogues (Rheological models) of either Maxwell or Kelvin type, or combinations of the two simulating the deformational behaviour of concrete have been proposed to formulate stress-strain laws for the material. In general, such constitutive laws express either the total concrete strain in the form of an integral type equation involving an hereditary integral, or the time rate of change of the total strain in the form of a differential type equation. The integral type creep law is usually solved using superposition principle or convolution integral method, whereas the differential type creep law is solved using a rate of creep method. The solution scheme of either type is essentially an iterative one in which discretization in the time span is made. On the grounds of computational cost, particularly for large structural systems, differential type creep laws seem to have an advantage over the integral form creep laws since they only require the storage of the current values of stress and strain in contrast to the latter type.

In the circumstances where concrete properties are non-homogeneous, examples of which are structures subjected to spatial temperature variations, a particular form of stress history occurs. The analysis of time-dependent effects in these structures therefore requires more general forms of constitutive laws. These must account for the environmental effects on the various strain components, moisture movements and ageing properties of the material.

In recent years several attempts have been made to extend some of the existing creep theories to deal with thermal creep and other aspects, such as non-linear behaviour of concrete. While it is not intended herein to produce an exhaustive survey of such developments, the reader is referred to the reviews given by Neville (102) and Irving (54), or to the references (103-117) for direct access to some of the proposed methods.

Nevertheless, in spite of all the attempts, no realistic constitutive relation for the thermal creep analysis of concrete structures has yet emerged. It is, however, possible that good engineering solutions for a wide range of problems can still be obtained using some forms of creep laws developed on the basis of the specific thermal creep concept. One of these is the rate of creep method (110) which is adapted here for the step-by-step computer analysis of the experimental and other beam examples reported in this work. Two other direct methods, the variational power (114) and steady state (16,18,112) are also used to predict the steady state and transient stresses for the problems. Description of the principles and solution procedure of the rate of creep method is given in some detail in Section 4.2. Those of the 'steady state' and the 'variational power' theories are given in Sections 4.3 and 4.4 respectively.

4.2 The rate of creep method

The method is applied here to the problem of a symmetrical 3-span continuous prestressed concrete beam. The analysis is applied to one half of the structure as shown in Fig. 4.2.

4.2.1 Principles

The method uses a single specific creep curve for all ages of loading, hence the age-dependence problem of the creep is considerably simplified.

The time rate of change of total strain $\frac{d\varepsilon}{dt}$ is given by the relationship

$$\frac{d\varepsilon}{dt} = \frac{1}{E} \cdot \frac{d\sigma}{dt} + \sigma \cdot \frac{dC}{dt} \qquad (4.1)$$

where $\frac{dC}{dt}$ is the time rate of change of specific creep strain.

On the basis of specific thermal creep concept, the law expressed in real time by Eq. 4.1 is represented by the Maxwell law in pseudo time 'c' as,

$$\dot{\varepsilon} = \frac{\dot{\sigma}}{E} \cdot + \sigma . \phi(T) \qquad (4.2)$$

in which the dot notation refers to differentiation with respect to 'c', and $\phi(T)$ = creep-temperature normalization function, Fig. 3.7. This is often assumed as a linear or polynomial function of T in degree Celsius.

General Comment

A recognised deficiency of this law is that it neglects the recovery (delayed elastic) strains when stresses decline, which makes it rather inaccurate for the analysis of creep at normal temperatures. However, for thermal creep analysis, the importance of delayed elastic strains diminishes considerably. This is mainly because while the flow component of creep is greatly enhanced by temperature rise, its delayed elastic component remains sensibly unaffected (81,82,101). On the other hand, where it is necessary to include the recovery strains in the constitutive relationship, more complicated models, such as the four element Burger's representation (116) must be used.

4.2.2 General procedure

For the numerical step-by-step analysis of non-homogeneous concrete structures (i.e. having different creep properties across each section) discretization in time, as well as space, needs to be made. The time (real or fictitious) is divided into discrete intervals and the continuum of the structure into a number of finite elements. With regard to beam and plane frame structures, the elements are further divided across their sections into a number of sub-elements. The number of these divisions is usually dictated by the geometry of the structure and the boundary loading. The lengths of the time intervals, however, should be chosen so that only small amounts of creep develop during these intervals in order to justify the basic assumption of the approach; that the stresses remain constant during each interval while strains are allowed to develop.

The general routine of the procedure as applied to a typical structure can be summarized as follows:-

1. At the start of the first time interval the stress and displacements in every domain of the structure are those due to applied boundary loading including temperature (thermo-elastic).
2. The stresses determined at the start are sustained through the interval while each sub-element is allowed to deform freely (thermo-inelastic deformation).
3. At the end of the interval, the strain compatibility and force equilibrium are examined for each section. Where these are violated, they should be restored by elastic adjustments to the forces in the section.
4. The integrated effects of these adjustments on the boundary forces and displacements of the structure are determined, then superimposed to those prevailing at the start of the interval.

The procedure is then taken through steps 2 to 4 for each successive time interval using the stresses determined at the end of the preceding interval, until the material is considered to have undergone sufficient creep.

In what follows, the behaviour of an un-reinforced concrete member element subjected to the combined actions of temperature cross-fall, load moment and axial prestress is investigated, over a typical time step during which small amounts of creep occurred. Basic expressions for calculating stresses and deformations in both analytic and numerical forms are derived. Some considerations for the changing concrete modulus of elasticity with temperatures over the depth of the section are given. Subsequently, the overall behaviour of a structure typical of the experimental beam is examined.

4.2.3 Basic expressions

Assumptions

1. Plane sections are to remain plane, so that the axial strain ε_a, and the curvature θ of the section can be related to the axial force N and bending moment M.

2. The instantaneous and creep strains are linear in the stress variable, so that the superposition principle is applicable to stresses and strains.

3. The tensile stresses are not to exceed the ultimate tensile strength of the concrete in order to avoid the development of cracking.

Consider a typical time step during which the section is allowed to deform freely, under a sustained stress system determined at the end of the preceding interval, to produce a free strain profile as shown in Fig. 4.1. These strains do not conform with the axiom of plane sections. To restore the compatibility of strains, therefore, a straight line B B' should be introduced, such that the strain associated with stress at fibre $x, \varepsilon_{s,x}$, can be related to the free strain, $\varepsilon_{f,x}$, curvature θ, and axial strain ε_a by the expression thus,

$$\varepsilon_{s,x} = \{(\varepsilon_a + \theta.x) - \varepsilon_{f,x}\} \qquad (4.3)$$

These strains must satisfy the equilibrium of forces on the section such that,

$$N = \int_{-D/2}^{D/2} b \,.\, E \,.\, \varepsilon_{s,x}.dx \qquad (4.4)$$

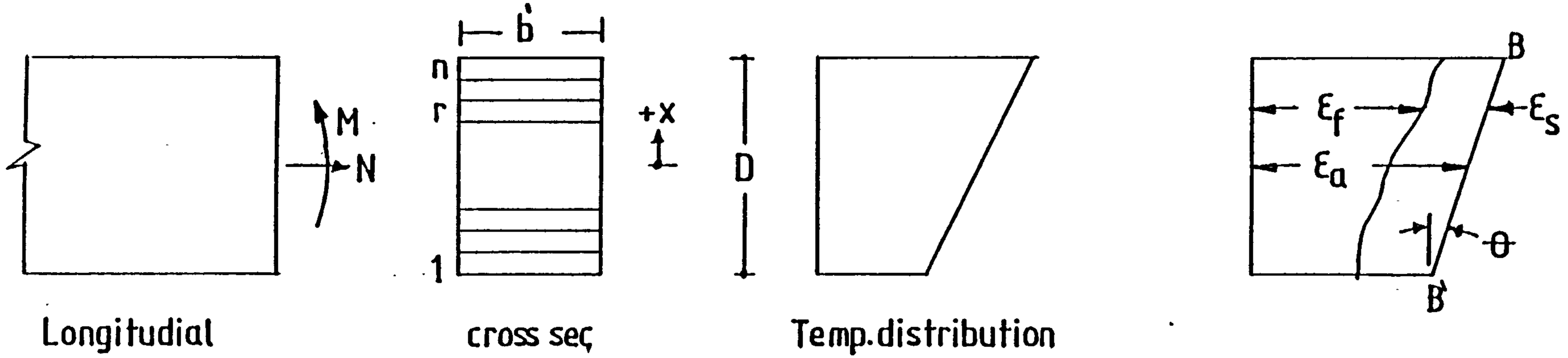

Fig 4-1 Strains by rate of creep method

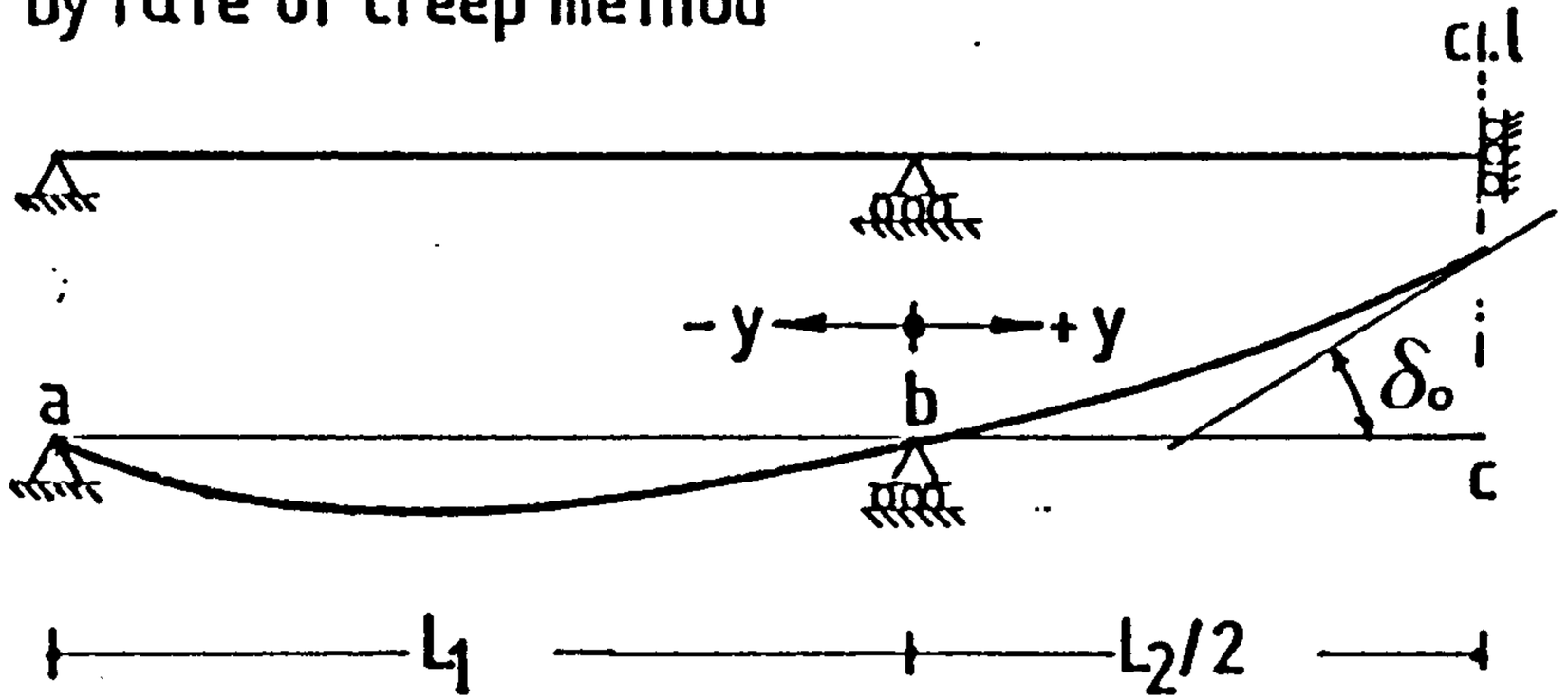

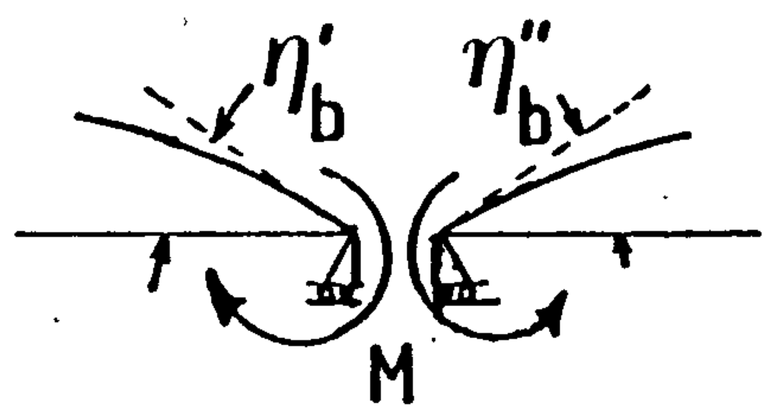

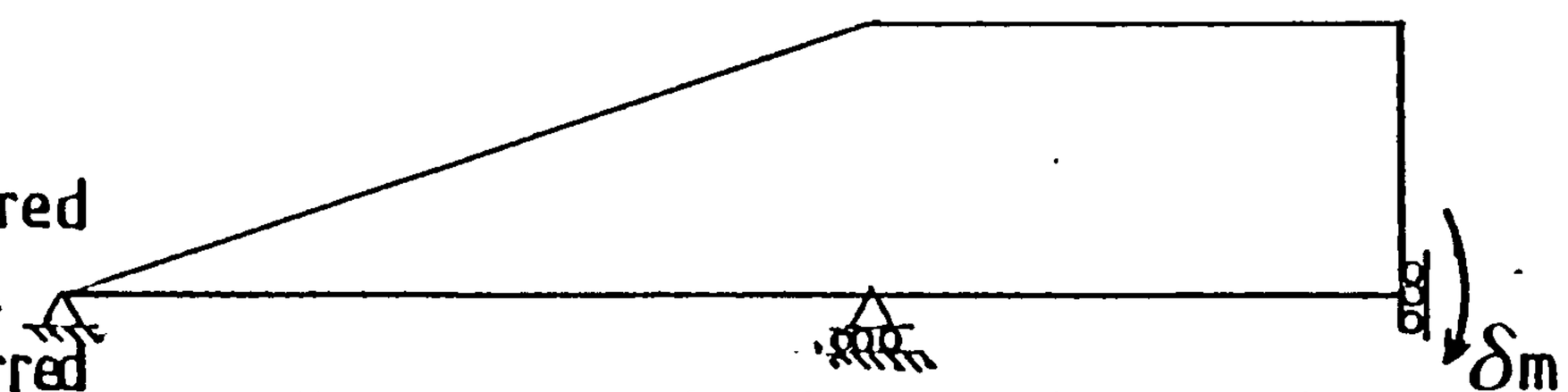

Fig.4-2 Analysis of creep effects on the external redundancy of the beam

and

$$M = \int_{-D/2}^{D/2} b \cdot E \cdot \varepsilon_{s,x} . x . dx \qquad (4.5)$$

Based on the data reviewed in Chapter 2, and on the reference (2,115) the concrete modulus of elasticity at a given temperature E_T may justifiably be assumed as a linear function of the modulus at 20°C, E. Such that, for a linear temperature crossfall, it can be expressed in terms of the space variable x thus,

$$E_T = E \cdot (p + q.x) \qquad (4.6)$$

where p and q are constants.

After substituting equations 4.3 and 4.6, the solution of the equilibrium equations 4.4 and 4.5 yields the following expressions for the axial strain and curvature of the section,

$$\varepsilon_a = \frac{12}{D(12p^2-q^2D^2)} \left[p \int_{-D/2}^{D/2} (p+qx).\varepsilon_{f,x}\, dx - q \int_{-D/2}^{D/2} (p+qx).x.\varepsilon_{f,x}\, dx + \frac{1}{E.b} \cdot (p.N - q.M) \right] \qquad (4.7a)$$

$$\theta = \frac{12.p}{(12p^2-q^2.D^2)} \cdot \left[\frac{12}{D^3} \cdot \int_{-D/2}^{D/2} (p+qx).x.\ \varepsilon_{f,x}\, dx - \frac{1}{D}.\frac{q}{p} \cdot \int_{-D/2}^{D/2} (p+qx).\varepsilon_{f,x}\, dx - \frac{q}{p} \cdot \frac{N}{E.b.D} + \frac{M}{E.I} \right] \qquad (4.8a)$$

If however the elastic modulus is to be assumed constant over the section, i.e. temperature-independent, then p = 1, and q = 0 and the above equations can be reduced to,

$$\varepsilon_a = \frac{1}{D} \cdot \int_{-D/2}^{D/2} \varepsilon_{f,x} \cdot dx + \frac{N}{E.b.D} \qquad (4.7b)$$

and

$$\theta = \frac{12}{D^3} \cdot \int_{-D/2}^{D/2} \varepsilon_{f,x} \cdot x \cdot dx + \frac{M}{E.I} \qquad (4.8b)$$

The integral terms in the above equations can be evaluated numerically by dividing the section of the member into 'n' number of elements as shown in Fig. 4.1. Accordingly,

$$dx = D/n$$

and

$$x = \frac{D}{2n} \cdot \{(2r-1) - n\}$$

Then, the axial strain and curvature expressions take the following forms,

$$\varepsilon_a = \frac{12}{D(12p^2-q^2D^2)} \left[p.\frac{D}{n}. \sum_{r=1}^{r=n} [p+q.\frac{D}{2n}.\{(2r-1)-n\}].\varepsilon_{f,r} - q.\frac{D^2}{2n^2} \cdot \sum_{r=1}^{r=n} [p+q.\frac{D}{2n}\{(2r-1) - n\}].[(2r-1)-n].\varepsilon_{f,r} + \frac{1}{E.b} \cdot (p.N - q.M) \right] \qquad (4.7c)$$

$$\theta = \frac{12.p}{(12p^2-q^2D^2)} \cdot \left[\frac{6}{D.n^2} \cdot \sum_{r=1}^{r=n} [p+q.\frac{D}{2.n}\{(2r-1)-n\}].\{(2r-1)-n\}.\varepsilon_{f,r} - \frac{q}{p} \cdot \frac{D}{n} \cdot \sum_{r=1}^{r=n} [p+q\{(2r-1)-n\} \cdot \frac{D}{2.n}] \cdot \varepsilon_{f,r} + \frac{M}{E.I} - \frac{q}{p}.\frac{N}{E.b.D} \right] \qquad (4.8c)$$

Alternatively, for a uniform modulus of elasticity

$$\varepsilon_a = \frac{1}{n} \sum_{r=1}^{r=n} \varepsilon_{f,r} + \frac{N}{E.b.D} \qquad (4.7d)$$

and

$$\theta = \frac{6}{D.n^2} . \left[\sum_{r=1}^{r=n} . \varepsilon_{f,r} . \{(2r-1)-n\} + \frac{M}{E.I} \right] \qquad (4.8d)$$

Hence, with the knowledge of the moment M, the axial prestress N, and the distribution of the free strains at the particular instant, the axial strain and curvature are evaluated from equations 4.7 and 4.8. These are then substituted into equation 4.3 and the stress distribution can be obtained, using the appropriate values for 'p' and 'q', from

$$\sigma_x = E.(p+q.x) . [(\varepsilon_a + \theta.x) - \varepsilon_{f,x}] \qquad (4.9)$$

Build-up of free strains

The free strains generally consist of temperature, creep and shrinkage strains, i.e.

$$\varepsilon_f = \varepsilon_t + \varepsilon_c + S \qquad (4.10)$$

At a particular level of a given section, the free strain at the end of the first interval,

$$\varepsilon_{f,1} = \varepsilon_t + \delta\varepsilon_{c,1} + \delta S_1$$

Then, if the temperature remained constant, the free strain at the end of the second interval,

$$\varepsilon_{f,2} = \varepsilon_{f,1} + \delta\varepsilon_{c,2} + \delta S_2$$

In general, the free strain at the end of interval j, for time invariant temperature is ·

$$\varepsilon_{f,j} = \varepsilon_{f,j-1} + \delta\varepsilon_{c,j} + \delta S_j \qquad (4.11)$$

where, $\varepsilon_{f,j-1}$ refers to the total free strain at the end of the preceding interval, and $\delta\varepsilon_{c,j}$, δS_j are the increments of creep and shrinkage strains developed during the interval.

If the Maxwell representation for the creep law is assumed to apply, then based on the specific thermal creep concept, the free strain at the end of interval j will be,

$$\varepsilon_{f,j} = \varepsilon_t + \sum_{i=1}^{i=j} \{\sigma_{i-1}.\phi(T).\delta c_i + \delta S_i\} \qquad (4.12)$$

where σ_{i-1} refer to the stress determined at the end of the preceding interval, $\phi(T)$ = temperature-creep normalization function,

δc_i = specific thermal creep increment.

4.2.4 Changes in the redundant forces of the continuous beam over a typical time step

At the commencement of a particular time step, the symmetrical half of the beam, Fig. 4.2, is assumed to be in a static equilibrium with its boundary actions. The beam is then released (moment release) through the interval allowing it to deform freely without restraint. Consequently, a change in discontinuity (rotation) at the release occurs. By utilizing the v.w. principle the change in discontinuity at the end of the time interval can be determined, such that

$$\delta d_0 = \int_{-L_1}^{L_2/2} (\theta_{2,y} - \theta_{1.y}).M_1.dy \qquad (4.13)$$

in which $\theta_{2,y}$ and $\theta_{1,y}$ refers to the curvatures at the end and commencement of the time interval with the subscript 'y' refers to the section coordinate and M_1 refers to the unit action moment distribution.

In order to restore the structure compatibility, the change in discontinuity must be counteracted by a moment, which can be determined on an elastic basis such that,

$$\delta.m = -\delta\theta/d_{11} \tag{4.14}$$

where d_{11} is the rotation caused by a unit moment at the release.

The moment distribution prevailing at the start of the interval should therefore be adjusted by an amount

$$\delta.M = \delta m.M_1 \tag{4.15}$$

As a result of this change, the curvatures determined at the end of the interval should be corrected by an elastic amount,

$$\delta\theta = \delta M/EI \tag{4.16}$$

Compatibility of the slopes at the interior support

In Fig. 4.2a the slope of the end tangents at support b is indicated by η_b' for the end span and by η_b'' for the centre span. As a condition of slope continuity of the uncut elastic line over the support b

$$\eta_b' = -\eta_b'' \tag{4.17}$$

where

$$\eta_b' = -\frac{1}{L_1}\int_0^{-L_1} \theta_{2,y} \cdot (L_1-y).dy \qquad (4.18)$$

and

$$\eta_b'' = -\int_0^{L_2/2} \theta_{2,y}.dy \qquad (4.19)$$

If, $\eta_b' + \eta_b'' \neq 0$, say $= \delta\eta_b$ then the compatibility of the slopes can be restored by applying a couple given by,

$$\delta_m = -\delta\eta_b/d_{11} \qquad (4.20)$$

The moments and curvature adjustments are then made in the manner described above.

4.2.5 Stresses at the end of the time interval

With the curvatures computed and corrected at the end of the interval, the axial strains are calculated from eq. 4.7. In this equation the current value for the prestress force should be used, unless the prestress is considered to be of the follow-up type, or the estimated loss due to creep is insignificant. The stress distributions are then concluded from Eq. 4.9 substituting the same free strains used to calculate the curvatures.

4.2.6 Beam deflection

To determine the deflection profile of the beam at any time step, the simplified approach of the Virtual Work Principle may be employed. This involves the application of a unit force successively at a number of sections along the released structure at the end of the particular time step. Then, the vertical displacement of a point C anywhere along the beam may be calculated from,

$$\gamma_c = \int_{-L_1}^{L_{2/2}} \theta_{2,y} . M_{1c} \cdot dy \qquad (4.21)$$

in which $\theta_{2,y}$ is the distribution of curvature determined and corrected at the end of the time interval, and $M_{1,c}$ is the moment distribution produced by the unit action applied at point C.

4.3 Steady state theory predictions

It is commonly accepted that redistribution of stress generally occurs between any two zones of concrete maintained at different temperatures, and between concrete and steel when reinforcement is present. When loads and temperatures are sustained, the stresses approach a steady state (16), provided the creep capacity of concrete is sufficient to allow the process of redistribution to become complete.

England (112) proposed a method by which the steady state stresses can be evaluated using elastic analogy. It demands that the elastic modulus of concrete be replaced by the reciprocal of the creep-temperature normalization function $\phi(T)$. This means that the conventional elastic analysis may be used to determine the steady state stresses by the simple inclusion of a spatially varying elastic modulus,

such that, with reference to Fig. 4.1, the s.s. stress at fibre x may be calculated from

$$\sigma_x = \frac{A + Bx}{\phi(T)} \tag{4.22}$$

where A and B are the specific rates of change of axial strain and curvatures respectively. These are independent of time by hypothesis of the invariance with time of $\sigma.\phi(T)$, and are constants for a particular cross-section. The distribution given by eq. 4.22 must satisfy the equilibrium conditions of structural mechanics, such that

$$\int_{-D/2}^{D/2} b.\,\sigma_x.dx = N \tag{4.23}$$

and

$$\int_{-D/2}^{D/2} b.\,\sigma_x.x.dx = M \tag{4.24}$$

when N and M are the axial force and moment acting on the cross-section at the steady state. Then, after substituting for σ_x from eq. 4.22 into the equilibrium equations, a solution for A and B results, which take the form

$$A = a_1.M + b_1.N \tag{4.25}$$

$$B = a_2.M + b_2.N \tag{4.26}$$

Here the a and b parameters will depend upon data relating to the cross section and the temperature distribution. For a rectangular cross-section, and linear temperature distribution of the form $(\alpha + \beta.x)$ these are found to be:

$$a_1 = \frac{\beta}{b.D} \quad , \qquad b_1 = \frac{\alpha}{b.D}$$

$$a_2 = -\frac{\beta^2}{b.D} \cdot \frac{\log_e(T_1/T_2)}{[\beta.D-\alpha.\log_e(T_1/T_2)]} \quad , \qquad b_2 = \frac{\beta}{b.D}$$

Evaluation of the A and B parameters for the particular section rests on the knowledge of N and M values at the steady state. The total change in the prestress force N due to creep may be estimated by any other method, if it is not of the follow-up type; whereas determination of the steady state moments M require further formulation based on consideration of the boundary conditions on the structure. This is illustrated in the following section in relation to the continuous beam example.

4.3.1 Steady state moment distribution over the continuous beam

By invoking the moment area theorem, the difference in slopes between two points a and b can be obtained from the curvature distribution between these points. Then, with reference to Fig. 4.2

$$\eta_a - \eta_b = \int_b^a \theta . \, dy \qquad (4.27)$$

A similar statement can be made for the difference in the rates of change in slope with respect to pseudo-time,

i.e., $$\dot{\eta}_a - \dot{\eta}_b = \int_b^a \dot{\theta} \, .dy \qquad (4.28)$$

Similarly, the rate of change in the slope at a,

$$\dot{\eta}_a = \frac{1}{L_1} \cdot \int \dot{\theta} \, .y.dy \qquad (4.29)$$

also,

$$\dot{\eta}_c - \dot{\eta}_b = \int \dot{\theta} \, . \, dy \qquad (4.30)$$

But, from consideration of symmetry, the slope at point c = zero,

i.e., $\dot{\eta}_c = 0$.

Therefore, by combining eq. 4.29 with 4.30 and subtracting from eq. 4.28 the following equation results,

$$\int \dot{\theta} \, .dy - \frac{1}{L_1} \int \dot{\theta} \, . \, y.dy = 0 \qquad (4.31)$$

By definition, $\dot{\theta} = \frac{d\theta}{dc} = B$

hence, eq. 4.31 becomes $\int B \, dy - \frac{1}{L_1} \int B.y.dy = 0 \qquad (4.32)$

Then, if the s.s. moment distribution M is expressed in terms of the distributions of a point load moment* Mp and an unknown support moment M_s in equations (4.25 and 4.26, then the integration of eq. 4.32 yields the following solution for the redundant support moment at the steady state,

$$M_s = \frac{9}{8} \, . \, M_p + \frac{7}{6} \, . \, \frac{b_2}{a_2} \, . \, N \qquad (4.33)$$

This leads to the determination of the steady state moment, and hence the distributions of A and B along the beam.

* See fig. 4.3

4.4 The variational power method

Although historical methods of analysis can be made to generate almost exact solutions to many creep problems, their running cost can be prohibitively high for the analysis of large and complicated structural systems. Other methods which can yield acceptable solutions directly without having to rely on their intermediate phases are therefore always desirable. One of such methods, the 'Variational Power' has been described by England (114). The logical principle of his theory is based on the assumption that an energy change rate with respect to variations of the stresses from the true state is a minimum. His interpretation for the theory in relation to a body resting on rigid supports can be briefly summarized as follows.

A body or structure, which is said to be in a transient stage of creep deformation is at any instant in equilibrium with its boundary actions, and the strain and displacement rates are compatible. By invoking the principle of virtual work at any time, t, it is possible to state that the products of the actual internal strains, $\varepsilon(t)$, with a set of equilibrium stresses $\delta\sigma_i$, will be zero when integrated over the entire volume of the continuum

$$\text{i.e.} \qquad \int \varepsilon(t).\delta\sigma.dv = 0 \qquad (4.34)$$

Since this statement is true for all t, it is possible to make the additional statement,

$$\int \dot{\varepsilon}(t).\delta\sigma.dv = 0 \qquad (4.35)$$

in which $\dot{\varepsilon}(t)$ represents the internal strain rates.

Equation 4.35 requires that the constitutive stress/strain relationship of concrete is specified in such a manner that the strain rate is a function of the stresses and the time derivatives of the stresses only.

The detailed formulation of the problem to be solved by this theory, however, depends upon a stress representation of the following form being adopted,

$$\sigma = \sigma_o + \sum_{i=1}^{i=n} a_i \sigma_i \qquad (4.36)$$

in which σ_o is any distribution which satisfies the statistical boundary loading on the structure, and the distribution $\delta\sigma_i$, i = 1 to n, represents self equilibrating sets of stress components. The a_i terms are weighting parameters, which are functions of time and become the unknowns in the creep problem.

In the following section, the theory is applied to the same continuous beam example used previously, to illustrate the solution procedure and to compare the predictions with those given by the iterative rate of creep method.

4.4.1 Transient creep solution of the continuous beam

The state of stress at any section along the beam is clearly dependent upon the applied mechanical loading and the redundant support reaction, which here varies in the transient period. The redistribution of stress over any particular section, therefore, is due partly to the differential creep behaviour of the section, and partly to the time-varying external redundancy.

Because stresses vary in both the x and y directions in this example, the transient stress distributions are represented by more than one function. After suitable scaling in the x and y directions, and writing $X = x/d$, $Y = L_1$ and with reference to Fig. 4.3, these are

$$\sigma = f+2.\psi(P-R_1).Y.X + \{R_2(X^2-\tfrac{1}{3}) + R_3.X^3\}.Y \quad \ldots\ Y = 0 - \tfrac{1}{2}$$

$$\sigma = f+\psi(P-2R_1.Y).X + \{R_2(X^2-\tfrac{1}{3}) + R_3.X^3\}.Y \quad \ldots\ Y = \tfrac{1}{2}-1 \qquad (4.37)$$

$$\sigma = f+\psi(P-2R_1).X \quad + \{R_2(x^2-\tfrac{1}{3}) + R_3X^3\} \quad \ldots\ Y = 1\ \tfrac{5}{3}$$

Where $\psi = \frac{3}{4} \cdot \frac{L_1}{bd^2}$, f = mean prestress, P = applied point load, and R_1, R_2 and R_3 represent the redundancies in the problem, such that at time zero, R_1 = thermo-elastic support reaction,

$$R_2 = R_3 = 0$$

The variational principle of equation 4.35 takes here the form,

$$\int_{-1}^{+1} \int_{0}^{5/3} \dot{\varepsilon} \frac{\partial \sigma}{\partial R_i} \cdot dY.dX = 0 \qquad (4.38)$$

Introducing the stresses from equations 4.37 into equation 4.2 yields expressions for the total strain rates along the beam. Considerable simplification results from the assumptions that the concrete modulus of elasticity is uniform over the beam section, and that $\phi(T) = T = (\alpha + \beta X)$. Then after substituting for $\frac{\partial \sigma}{\partial R_i}$ from equations 4.37 and the spatial integrations are carried out separately for each value of i where i = 1 to 3, three differential equations result, which are written in matrix form, viz.

Fig.4-3 Variational power method analysis of the beam

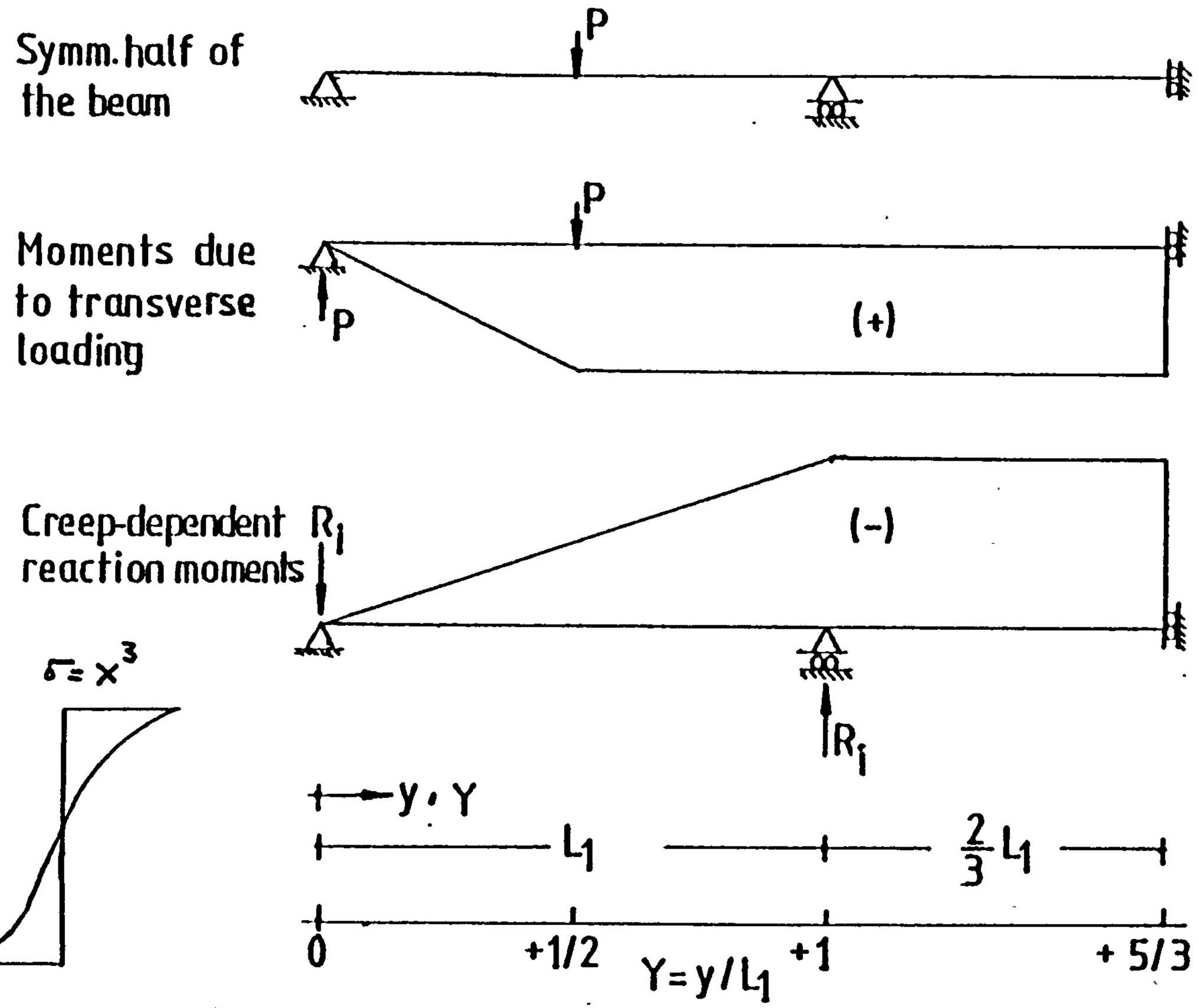

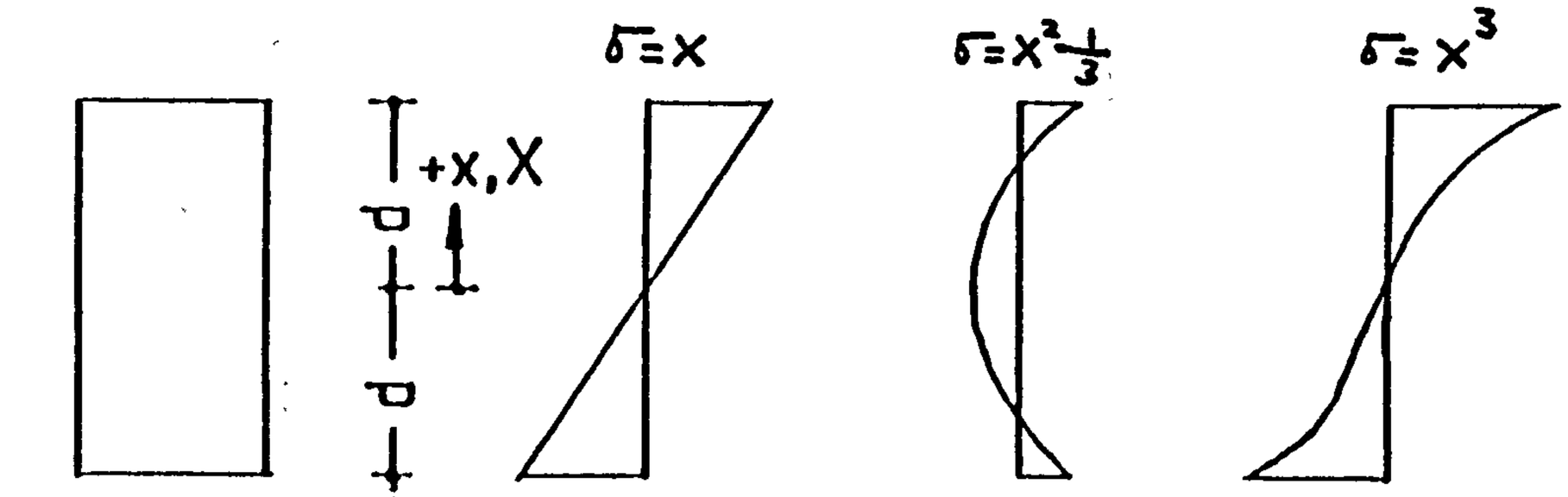

$$\begin{bmatrix} 1 & 0 & -\frac{3}{10} \\ 0 & 1 & 0 \\ -\frac{14}{5} & 0 & 1 \end{bmatrix} \cdot \begin{bmatrix} \dot{R}_1 \\ \dot{R}_2 \\ \dot{R}_3 \end{bmatrix} + E \cdot \begin{bmatrix} \alpha & \frac{4}{15}\frac{\beta}{\psi} & -\frac{3}{10}\cdot\frac{\alpha}{\psi} \\ -2\psi\beta & \alpha & \frac{6}{7}\ \beta \\ -\frac{14}{5}\alpha\psi & \frac{8}{15}\beta & \alpha \end{bmatrix} \cdot \begin{bmatrix} R_1 \\ R_2 \\ R_3 \end{bmatrix}$$

$$+ E \cdot \begin{bmatrix} -\frac{9}{16}P & -\frac{7}{12}\frac{f\beta}{\psi} \\ \frac{9}{8}P\psi\beta & \\ \frac{7}{10}\left(\frac{7}{3}f\beta + \frac{9}{4}\psi P\alpha\right) & \end{bmatrix} = 0$$

In general form, these can be written as

$$A \cdot \dot{R} + B \cdot R + C = 0 \qquad (4.39)$$

The solution of equation 4.39 has the form,

$$R = e^{-[A].[B].c} \cdot K - [B]^{-1} \cdot [C] \qquad (4.40)$$

where K is a vector dependent upon the initial conditions at time zero, here we have

$$R_1(0) = \frac{9}{16} \cdot P - \frac{7}{9} E\, \bar{\alpha}_c \cdot \beta,$$

$$R_2(0) = R_3(0) = 0$$

Therefore,

$$K = [R(0)] + [B]^{-1} \cdot [C] \qquad (4.41)$$

Equation 4.40 may be solved, using a general numerical procedure (117), described in the Appendices. It consists of expanding in series form the exponential matrix for a small value of the exponent $[A]^{-1}.[B].c$

by suitably selecting a value of c, and then summing the series in truncated form to a predetermined degree of convergence. Solutions for other values of c are readily obtained for all such values as 2^n. c by simply squaring and re-squaring the sum of the truncated series.

Stresses calculated for the point load section of the beam at some significant values of pseudo-time c are listed in Table 4.1, Col. 'V.P.'. These are compared to exact solution from a step-by-step computer analysis, Col. 'EX'.

Numerical data

The following numerical data have been used in the analysis procedures:

beam cross-section:	b.D = 101.6 × 152.4 mm
end span:	L_1 = 914.4 mm
centre span:	L_2 = 1219.2 mm
mid-end span point load:	P = 8.0 KN
applied uniform prestress:	f = 6.2 N/mm^2
modulus of elasticity of the concrete:	E = 34.5 GN/M^2
coefficient of thermal expansion of the concrete,	$\bar{\alpha}_c = 12.5 \times 10^{-6}/^oC$
the uniform temperature over the beam section:	$\alpha = 68\ ^oC$
the applied temperature gradient over the section:	$\beta = 0.236\ ^oC/mm$
the Sp^{th} creep value used in the V.P. analysis,	$c = 1.45 \times 10^{-6}$ per N/mm^2 per ^oC
the number of pseudo-time steps used in the r.o.c. analysis:	$= 400 \times 1.45 \times 10^{-8}$ per N/mm^2 per ^oC

Table 4.1

c =	0	0.145		0.290		0.580		1.160		Steady State	
$\frac{8.x}{d}$	Th.el.	EX.	V.P.	EX.	V.P.	EX.	V.P.	EX.	V.P.	EX.	V.P.
7	13.72	12.12	12.20	11.00	11.37	9.73	10.45	8.87	9.74	8.63	9.48
5	11.58	10.57	10.62	9.84	9.97	8.97	9.19	8.32	8.60	8.11	8.39
3	9.43	8.96	8.99	8.59	8.57	8.10	8.02	7.68	7.59	7.52	7.44
1	7.28	7.28	7.31	7.23	7.15	7.12	6.88	6.96	6.65	6.85	6.57
-1	5.13	5.51	5.55	5.76	5.66	6.00	5.72	6.11	5.75	6.09	5.75
-3	2.98	3.68	3.69	4.17	4.08	4.74	4.51	5.13	4.82	5.22	4.92
-5	0.84	1.76	1.71	2.45	2.37	3.30	3.19	3.97	3.81	4.21	4.03
-7	-1.31	-0.24	-0.4	0.60	0.49	1.68	1.70	2.61	2.68	3.02	3.04

Stresses over the point load section of the beam calculated from two separate analyses:

i. Exact solution from a step-by-step computer procedure, Col. 'EX'.

ii. Approximate solution from the variational principle method, Col. 'V.P.'.

Notes:

Units of stress are in N/mm^2

pseudo-time 'c' units are $\times 10^{-6}$ per MN/M^2 per ^oC

tensile stress = (negative)

The method reveals satisfactorily the stress-redistribution features associated with non-homogeneous creep. The errors shown are, however, acceptably small for creep calculations and have thus illustrated the ability of this method to provide economical creep solutions.

By including the creep recovery explicitly in the analysis and adopting the four element Burger's representation (117) for example, an improvement in the accuracy can be obtained if required. However, this has to be judged carefully against the additional effort required for carrying out the integration of eq. 4.35 and subsequently the solution of the resulting exponential matrix equation.

CHAPTER V

Experimental Work - Part 1

Design, construction and testing procedure of a post-tensioned concrete beam with an elastic inclusion

Chapter 5 - Synopsis

This Chapter describes the design and testing of a 3.2 m prestressed concrete beam. It was tested over three spans as a continuous member symmetrically loaded in the end spans only and subjected to sustained transverse temperature crossfall everywhere. The aim was to monitor the stress variation with time within the central span directly using an elastic inclusion technique. In addition, the internal support reactions were recorded and the experimental data were used to assess the usefulness of the steady state and the rate of creep theories. The test results and conclusions are given in Chapter 6.

5.1 Objective

Under the combined-actions of sustained loading and temperature crossfall, the external boundary forces in some concrete structures may undergo substantial changes with time, as a result of differential thermal creep behaviour of the material. This has been verified in some experiments cited in Chapter 1. However, because the external actions constitute an integral response of the internal stresses over the entire volume of the structure, changes of the kind have been coupled to a process of stress redistribution. Since it has not been possible to determine explicitly the stresses in the experimental structures, they have been inferred from support forces measurements and from the use of constitutive relationship relating stress to creep strain.

An attempt has been made here to explore the possibilities of finding a suitable technique to achieve the objective of directly monitoring the development of stresses in a non-isothermally heated and loaded statically indeterminate beam structure. Unfortunately, no direct stress measuring device of certain reliability, applicable under such test conditions, has apparently been developed yet. The only available alternative was the 'elastic inclusion' technique, by which stresses can be correlated to the strains observed in a homogeneously elastic body incorporated into the structure. Its use in concrete research has so far been limited to short-term non-heated experiments, as has been successfully demonstrated by Stanculescu (40) on plain concrete beams tested close to and up to ultimate load.

An assembly of elastic elements has been designed to fit in between two identical concrete prisms, such that when they are axially stressed they form a rigid beam structure. This was subsequently

tested as a three span continuous beam with the elastic inclusion situated at a constant moment zone. A detailed description is given in Section 5.4.

5.2 General considerations

In developing the design of the elastic inclusion, the following considerations were given:-

1. The material should have completely elastic and time-invariant homogeneous properties, and under the operating temperature and stress conditions exhibit no significant time-dependent strains;

2. The material stress response should be such as to justify the use of a mechanical strain gauge device;

3. The geometry of the inclusion system should be such as to allow free passage for a set of prestressing wires required for the post-tensioning operation;

4. The number of independent elastic elements across the beam section should be sufficient to identify clearly the field stress profile.

5.3 Choice of the inclusion material

Aluminium was chosen as the inclusion material, primarily for the convenience of strain measurements with mechanical rather than electrical strain gauges, due to the latter's uncertain reliability. A secondary factor which influenced the choice was based on previous findings (40) which concluded in favour of the aluminium when comparing it to other materials in respect to stress measurements.

5.4 General description of the composite beam design

After considering the various aspects of the problem a comparatively simple design for the elastic inclusion and hence the composite beam was developed. A number of identical aluminium I-section elements was chosen and arranged into a stack forming a laminated rectangular block of cellular cross section, as shown in Fig. 5.1a. With specially made mild steel bearing plates attached to the ends of each individual element, the block was then interposed longitudinally between the ends of two identical concrete prisms, having uniform cross-sections concordant with the end planes of the block. The assembly was subsequently stressed axially by a set of prestressing wires, thus forming a monolithic composite beam structure, Fig. 5.1b.

5.5 Section and size of the beam

Proportioning of the beam cross-section was dictated by two factors, (1) the size of the aluminium elements available and (2) the maximum fibre stress allowed.

The nearest practical size available for the I-section elements had 38 mm (1½in) wide flange and a depth of 101.6 mm (4.0 in). Hence, by adopting this size, the width of the beam section was fixed, i.e. by the depth of the I-section.

In order to maintain the operating stresses within the working stress range (below 50% of ultimate strength) within which creep strains are generally believed to be linear in the stress variable, the maximum fibre stress at any section was limited to about 14 MN/M^2. About half this amount was assigned to the prestress on the beam, and in order to ensure the uniformity of prestress over the beam section it was decided that it was desirable to use an evenly distributed

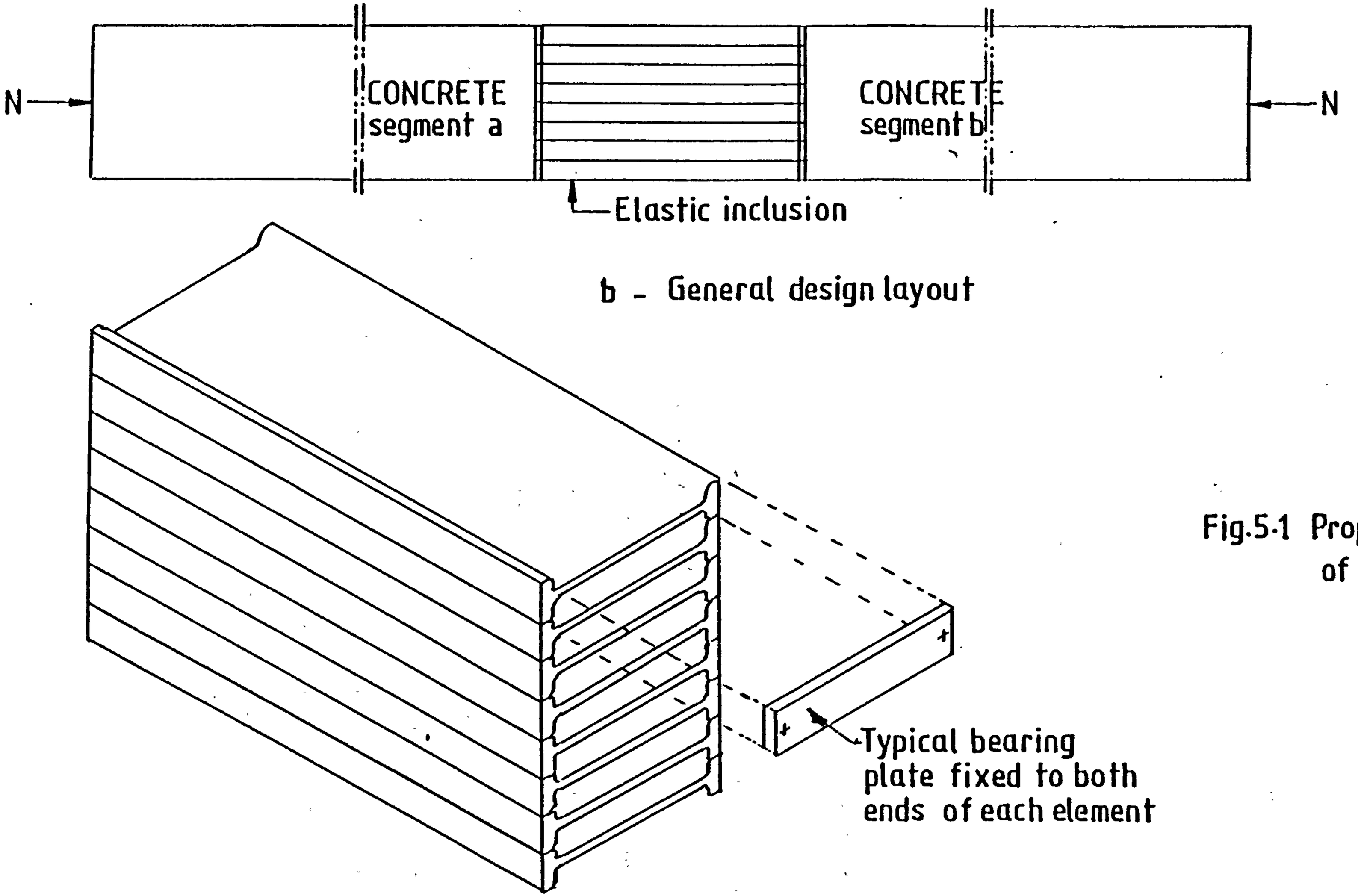

b - General design layout

a - Elements assembly

Fig.5.1 Proposed design layout of the beam experiment

number of prestressing wires for such purpose. Also, by using small sized wires it would offset the need for larger cavities within the inclusion block, and hence would enable the use of a larger number of elements within a given depth.

A rectangular arrangement of six 5 mm ϕ cold drawn steel wires having ultimate tensile strength of about 34 KN was chosen. By symmetrically reducing the flanges of the aluminium I sections to half their original widths, i.e. to 19 mm, a clearance gap of about 14 mm deep sufficient to accommodate 10 mm plastic duct tubing was obtained; and by utilizing only about 45% of ultimate strengths of the wires (in order to minimize losses of prestress due to relaxation of steel) a conveniently worked out cross-section of 101.6 × 152 mm (4.0" × 6.0") resulted. This permitted the use of eight I-section elements across the depth of the beam at 19 mm c/c.

With respect to the size of the beam, an overall length of 3.2 m was deemed adequate for the test, thus making it possible to utilize one of the standard formworks of the laboratory; and since the beam was to be symmetrically supported over three spans, adequate proportioning of the centre and end spans was necessary. After preliminary calculations were performed a centre/end span ratio of 1.33 resulted. This was translated into 1.22 m (48") for the centre and 0.91 mm (36") for each of the end spans, after allowing 76.0 mm (3.0") from either end of the beam to the nearest support. The section and size proportioning of the beam are detailed in Fig. 5.2.

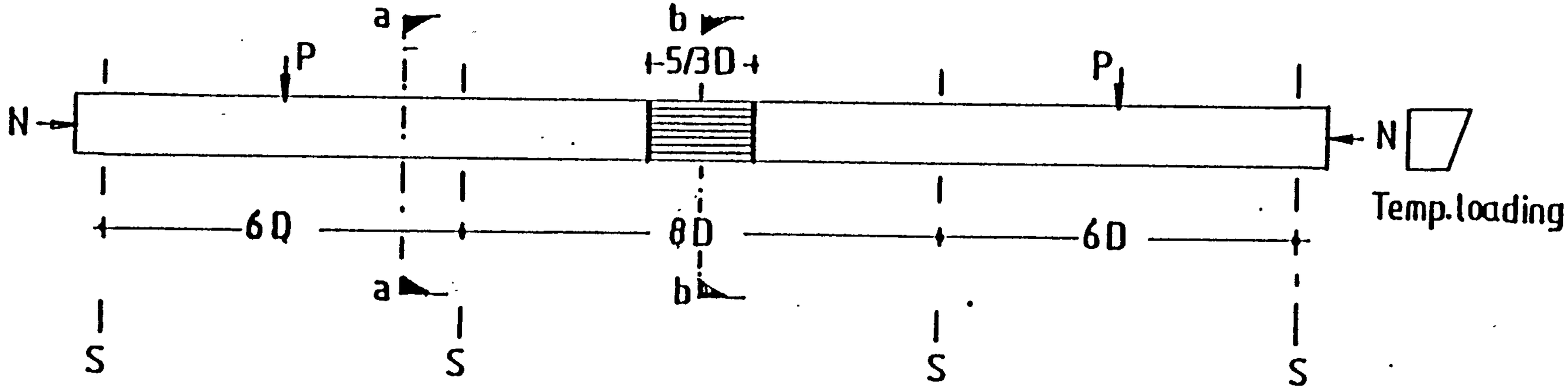

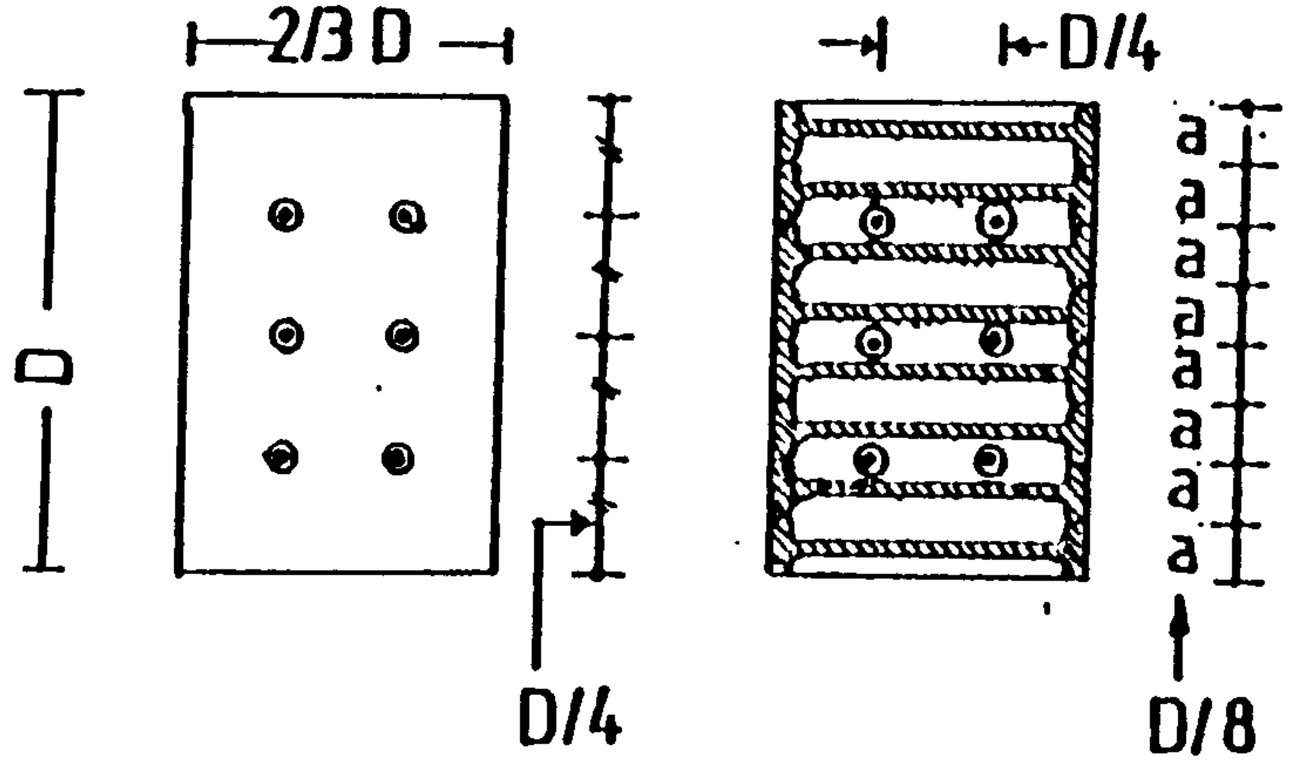

Sec.a-a Sec.b-b

Fig.5.2 Section and size details of the test beam

Note

D=152.4 mm

Cross-section area of the inclusion = 8×687.2 sq.mm

5.6 Technical requirements

The main technical requirements called for by the present investigation included:-

1. Supporting apparatus,
2. a system by which to ascertain at all times, and subsequently maintain a constant prestress force,
3. mechanical transverse loading system,
4. temperature loading and measuring facilities, and
5. strain and deflection instrumentation.

5.6.1 Supporting apparatus

The beam was mounted on four supports provided into a purpose-built rigid frame made of standard steel channels. Details of its construction as well as the supports are depicted in Fig. 5.3. The end supports were moment-free and one of them provided longitudinal translatory freedom, as well as the two interior proving ring supports. The manner in which the proving rings were mounted onto the main girder of the frame (see Plate 5.1) provided the additional freedom of varying the levels of the supports. This may either be required to maintain the supports in a co-linear position, or to impose a prescribed amount of displacement on either or both of the supports. The relative movements of the supports were monitored via a set of four dial gauges; the two external support gauges were clamped to the uprights of the frame, and the other two inner support gauges were clamped to the bending free top member of the frame.

Provisions were made in the apparatus for measuring the beam deflection. These consisted of a series of three 25 mm square section

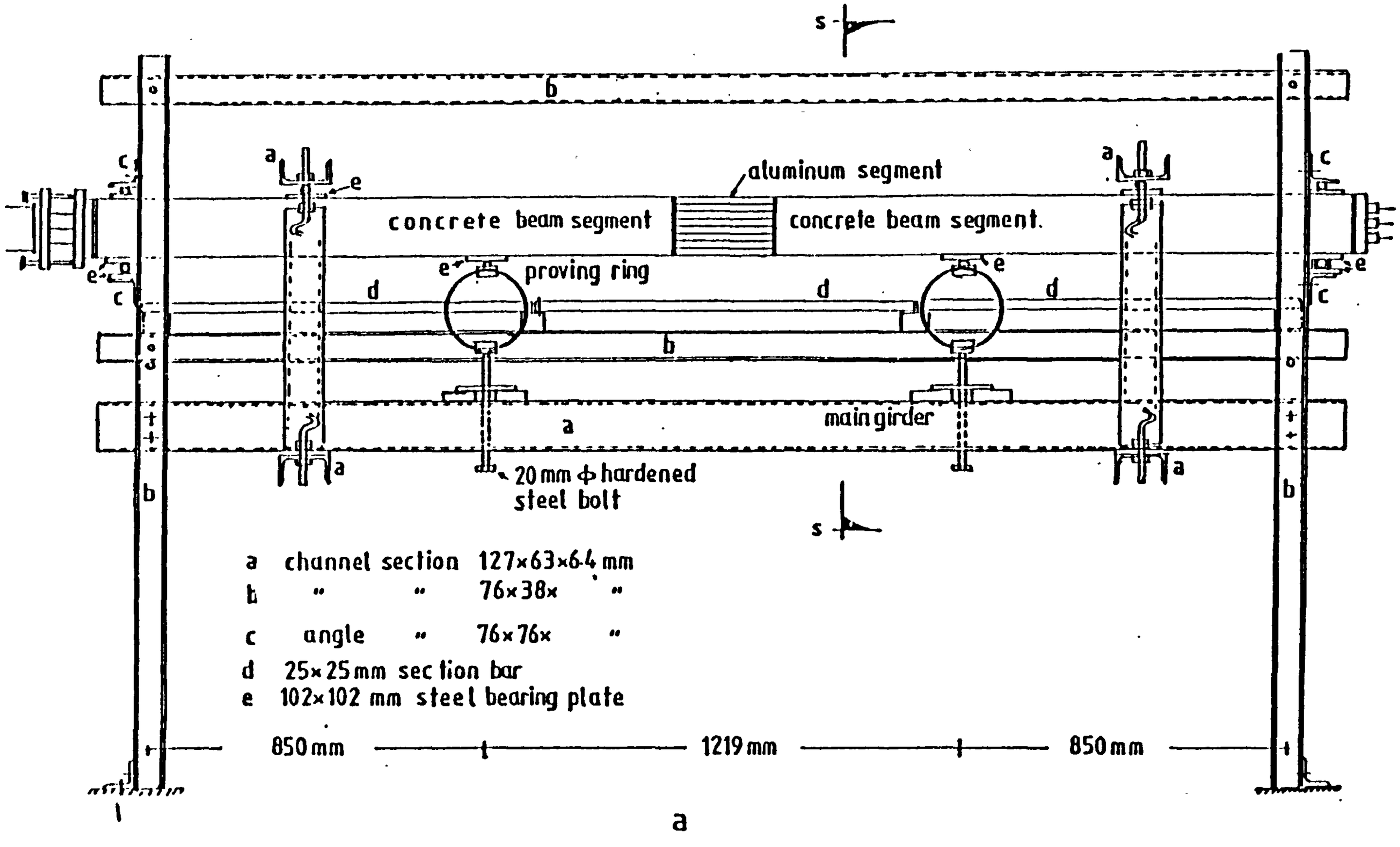

a

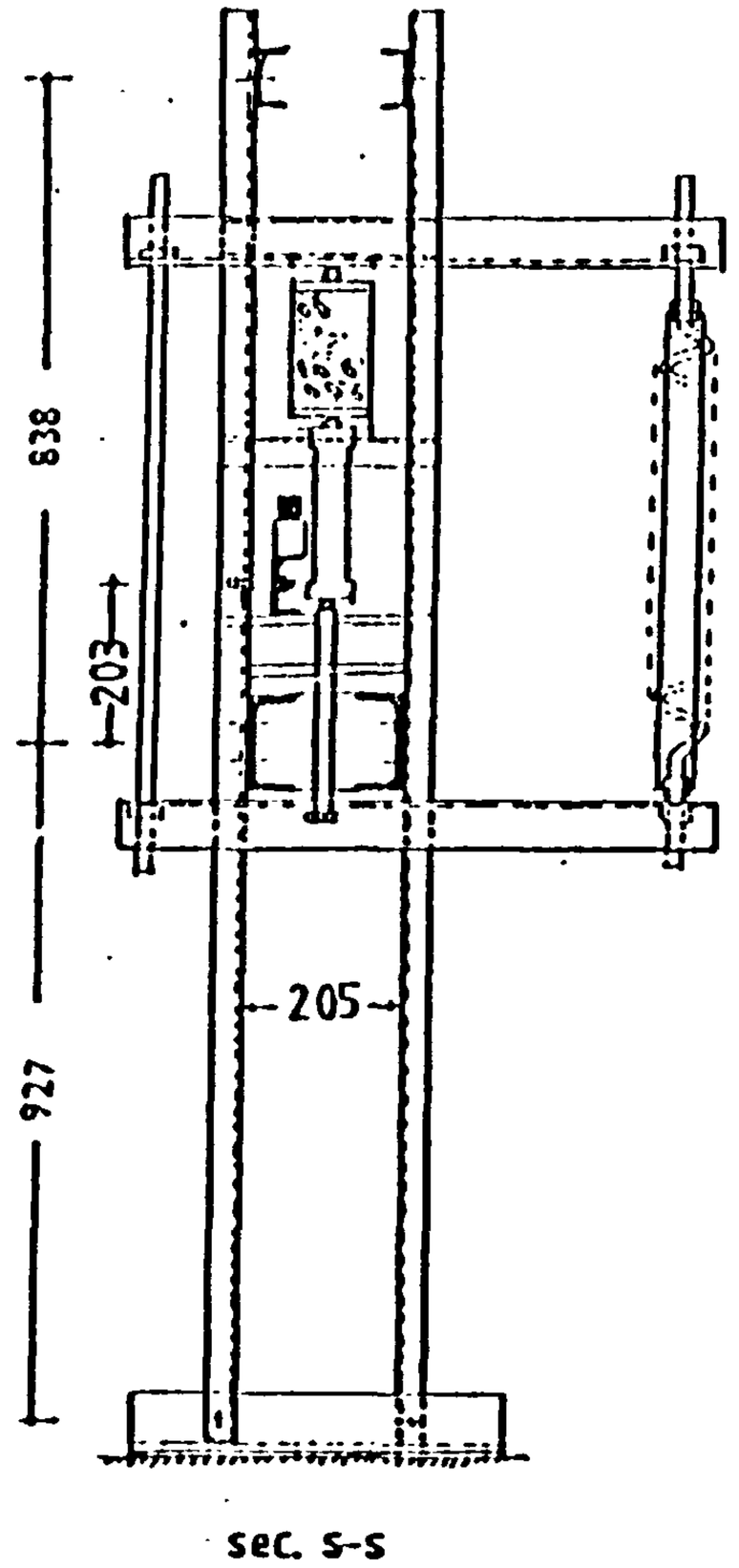

sec. s-s

b

Fig 5.3 General design of the mounting frame

bright mild steel bars simply supported, to eliminate bending effects due to ambient temperature fluctuations, over one channel section. This channel was also simply supported between the frame posts, to eliminate in-plane bending of the main frame. The deflection gauge and technique used in conjunction with this system are described under Section 5.6.5.

5.6.2 Prestressing system

In order to ascertain the total prestress force over the beam section and to restore future losses in prestress due to creep, a dynamometer steel tube assembly was mounted in series with the beam. A brief description of this assembly is given here, in the meantime reference should be made to Fig. 5.4 and Plate 5.2 for a more detailed description.

The ends of a 114 mm ϕ and 305 mm long steel tube were located between two 12 mm thick mild steel recessed circular flanges, one of which was attached to a 19 mm thick hardened steel triangular plate. Screwed through the corners of this plate were three 19 mm ϕ finely threaded hardened steel bolts. These were supported on steel balls seated in spherical grooves provided in a similar plate, directly bearing on the end plate of the beam. Minimum clearance holes were carefully drilled in all these plates to enable the prestressing wires to be passed through the assembly.

The system operates in such a way that after stressing the wires, the total force is transmitted by the anchorages, through the dynamometer tube and three steel bolts to the beam end plate. The total prestress force can then be ascertained from the tube deformations measured over three meridians at 120° by a demountable strain gauge. This system

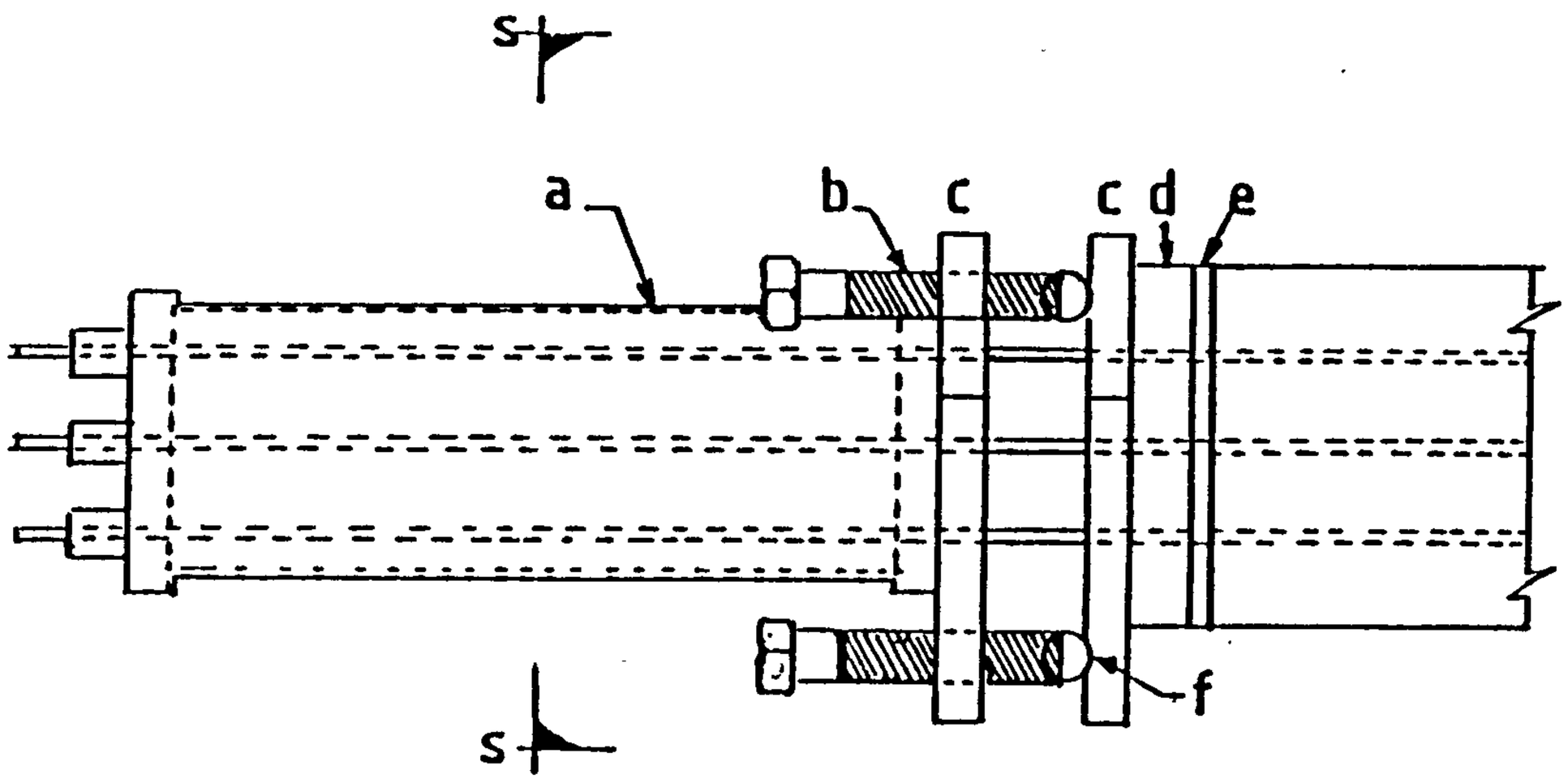

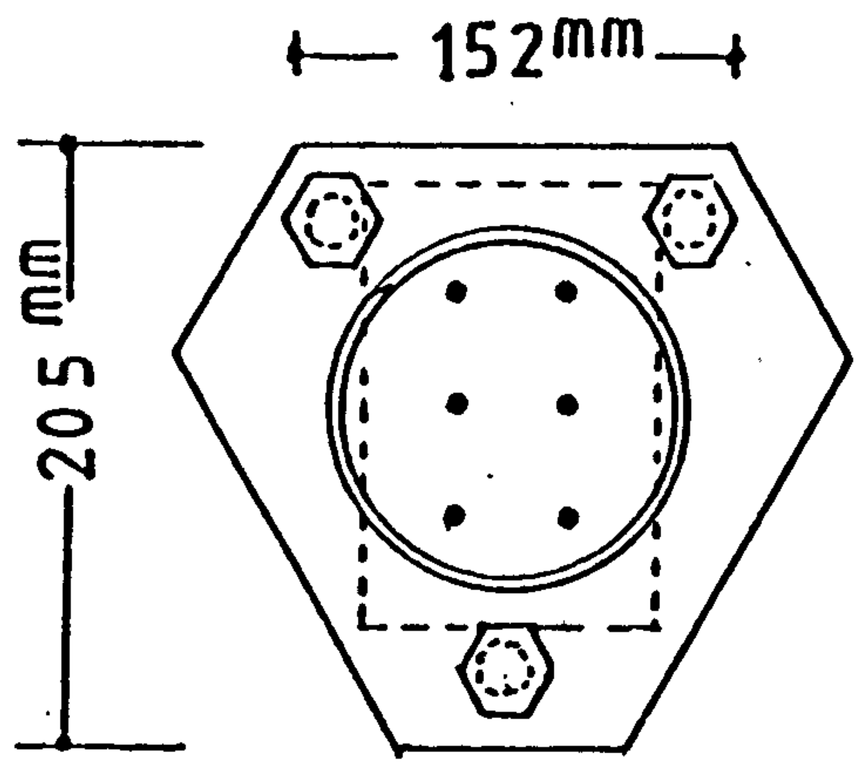

Key:

a–110mmϕ x 300mm M/S tube

b–19 mmϕ hardened steel bolt

c–25 mm thick st plate

d–32 mm thick steel end-plate

e–13 mm thick asbestos plate

f–20 mmϕ ball bearing

Fig 5.4 Prestressing system assembly

offered the advantage of easily restoring prestress losses by tightening the bolts. Also, through these bolts it would be possible to compensate for any irregularities in the uniformity of the initial prestress which might be caused as a result of the end planes of the beam not being parallel, in addition to the ease with which the wires could be destressed at the end of the test.

5.6.3 Transverse loading

Since it was decided to create a uniform moment zone over the elastic inclusion section of the beam, loading was restricted to the end spans only. Provisions for the application of a point load over each of the spans were made. These were in the form of reaction frames made of precalibrated stiff springs, tension rods and channel sections mounted in the manner shown in Fig. 5.3b. The system works in such a way that the tension applied to the springs is transferred by levering action onto the beam through ball bearing provided over the loading points. The amount of extension induced in each spring is determined by an extensometer attached to it, and from the load-extension graph predetermined for each spring and the lever arm-ratio the force is determined.

5.6.4 Temperature loading and measuring facilities

The maximum hot concrete fibre temperature aimed at for the test was in the region of 90°C. This was expected to drop to about 50°C at the lower face of the beam. Direct heating of the aluminium block was, however, to be avoided in order not to introduce additional temperature stresses into the problem. Careful considerations were consequently given to ensure symmetrical thermal loading over the concrete segments.

The power requirements to achieve the specified temperature crossfall was approximately estimated to be about 50 watts per linear meter of the beam. A single 12 m long minerally insulated and stainless steel sheathed element made by Pyrotenax Ltd. was provided for the purpose. The element was bent three times over each segment as shown in Fig. 5.5, in order to ensure uniform heating over the width of the beam. The cable was fed through a variable transformer provided to step down the mains voltage, and was connected in series with a Bercostat to provide independent power adjustment which might be necessitated by variations in the heat flow properties of concrete.

Temperature measurements in the concrete segments

Transverse temperature distributions were established over four different sections along each concrete segment, from six equally spaced fixed stations across the depth of the beam, as illustrated in Fig. 5.6. The measuring technique employed a set of detachable copper constantan thermocouples inserted at will, into 3 mm O/D, 80 mm long copper tubules each with a sealed end cast into concrete at each station as shown in Fig. 5.6b. The thermocouples were connected to an electronic thermometer, made by Comark Electronics Ltd. The instrument, illustrated in Plate 7.2, has an automatic cold junction and is fitted with an external reference facility enabling an improved accuracy related to cold junction stability to be achieved. It is claimed to have an accuracy of $\pm 0.5^{o}C$ over a range of $400^{o}C$ and gives direct readings in ^{o}C with a resolution of $0.1^{o}C$ per division. The instrument used was a battery operated type, fitted with a 10 input selector switch and was calibrated by the manufacturer to BS 1828. Frequent checks were being made, while in use, against two fixed temperatures, the boiling point of water and the melting point of ice.

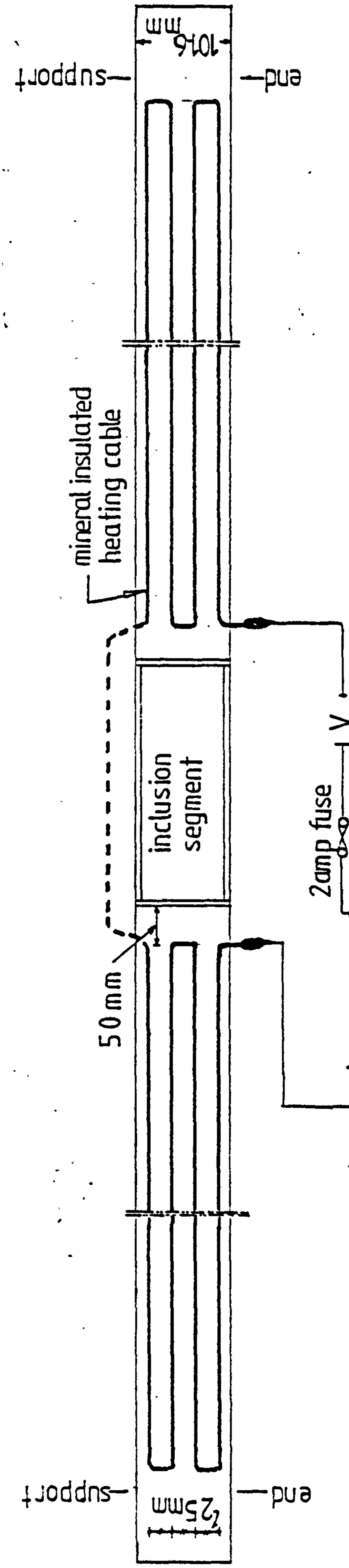

Fig.5.5 Heating circuit diagram

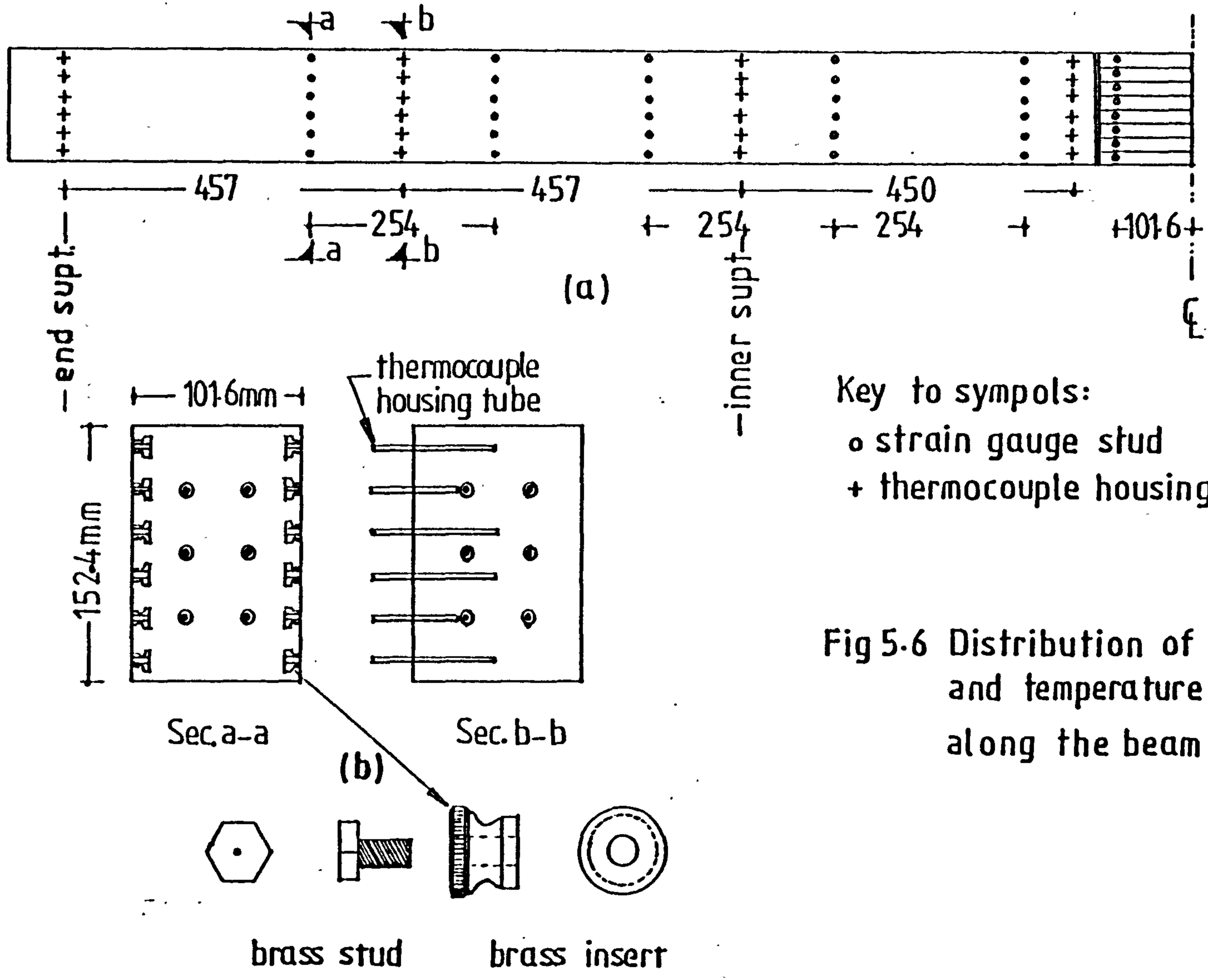

Fig 5.6 Distribution of strain gauge and temperature measuring points along the beam

Temperature measurements over the aluminium block

In view of the higher sensitivity of aluminium to temperature changes, it was decided that it was desirable to ascertain the temperature distribution across the block by two methods. In the first attempt, the surface temperature of each individual element was measured at three locations, two near the ends and one at the centre, by temporarily attaching, with a strong adhesive tape, three from the same set of thermocouples. The temperatures were subsequently checked, using a spring loaded surface probe compatible with the measuring instrument. In the majority of cases, however, both methods were found to give almost the same results. On few occasions where discrepancies of $0.5^{o}C$ or more arose between the two measurements, the procedures were repeated.

5.6.5 Strain and deflection instrumentation

Strain measurements

Decision was taken, at the early stages of planning for the experiment, not to use surface electrical strain gauges for measurements of strain over the elastic inclusion block, because of their doubtful performance under the present test conditions. The demountable type mechanical strain gauge appeared to be a convenient alternative. Hence, a 200 mm Demec gauge (Plate 5.3) was chosen for the purpose. Pairs of strain gauge points were precisely drilled symmetrically on both flanges of each element. It was found possible to reproduce strains with this gauge to about 4.8×10^{-6}. On converting this to stress at the corresponding concrete fibre yields, about 0.05 N/mm^2. Such a degree of accuracy was considered quite adequate.

With respect to concrete strain measurements, three sections were selected for each segment; under the point load, over the interior support and at the centre span, as shown in Fig. 5.6a. Here, in view of the limited depth of the beam, it was not possible to use embedment type strain gauges in a sufficient number to adequately define the strain profile across the depth of the beam. Therefore attention was again focussed on mechanical type strain gauges, which resulted in the choice of a 254 mm Whittimore gauge (Plate 7.2). The strain gauge points were provided in hexagonal brass studs screwed into brass inserts (county caps), (Fig. 5.6b), fixed in position during casting of the concrete. Only six of these points, 25 mm apart, were provided on opposite sides across the depth of each section, so as to permit free flow of concrete around the inserts.

Deflection measurements

Changes in the deflection profile of the beam were established by measuring the vertical movements of 21 equally spaced points relative to the reference bar system which was mounted parallel to the underside of the beam. A single demountable dial gauge attached to a special jig, (Plate 5.3), was used for all except the support points. The gauge was used in such a way that the plunger of the dial gauge was sunk in and the jig was clamped to the bar by a thumb screw; the plunger was then carefully released until it touched a thin glass disc, previously stuck to the underside of the beam at the given point, and the reading of the dial gauge was subsequently recorded.

5.7 Concrete mix design

The aim was to provide a concrete mix of adequate quality, both in terms of strength and workability. A reasonably workable concrete was considered important in order to ensure the flow of wet concrete around the wire ducts and all other embedded accessories. From a number of trials, a mix in the proportions of 1 : 1.88 : 2.82, and W/C ratio of 0.45 was finally adopted. This mix gave a cold 28-days strength of about 45 N/mm^2. More details on the mix and the elastic properties of hardened concrete are given in the Appendices.

5.8 Manufacture of the test beam

In order to preserve the symmetry of material behaviour on both sides of the inclusion, it was considered necessary that the specimens should have consistent geometrical and material properties. Close matching of these properties was thought possible to attain, through formwork design, and by ensuring the specimens the same batch of concrete, casting procedure, and storing environments.

Also, in order that the elastic inclusion should fulfil its intended function, it was considered essential that lack of fit between the various elements and the adjacent concrete fibres should not arise to such a degree as to significantly affect the state of applied stress. The risk of encountering such a problem in the present set-up appeared to be high, which required exceptional attention. As a result, it was considered worthwhile to construct a pilot beam to observe the behaviour of the inclusion under stress and to ascertain the workability of the technique employed.

In the event, a pilot beam was constructed in such a way that both ends of the aluminium elements were anchored to the adjacent

prisms during casting. The outcome of the pilot test indicated the need for certain changes in the integration process of the inclusion with the concrete segments. After a careful study, it was considered feasible to anchor only one end of the element into the concrete, leaving the other end free so that corrective measures, for lack of fit for example, might be effected should such a problem arise. This technique, which finally proved successful, is now described in some detail in the following sub-sections.

5.8.1 Formwork design

The mould provided was made of two duralumin channel section beams fixed on to a plane steel bed, and joined at the ends with 25 mm thick mild steel end plates (see Plate 5.4). The backs of the channels were lined with metal-faced ply. Before these were fixed to the channels, the county caps were attached with counter-sunk screws at the exact positions allocated to the strain gauge points. Thermocouple positions were carefully marked on one of the lined channels through which close fit holes were drilled to enable the insertion of the copper tubes during the casting operation.

The mould was then divided into two independent compartments by a plane mild steel plate fixed vertically across the mould normal to the axis of the beam. The plate was located in such a way as to coincide with the free end plane of the aluminium block. The bearing plates of this end of the block were carefully assembled and fixed onto the other side of the intersection plate, in order to be anchored to the end of the adjacent concrete prism, as illustrated in Plate 5.4.

5.8.2 Casting preparations

With all parting surfaces lubricated, the formwork components were loosely assembled onto the steel bed. The aluminium elements were then inserted into the mould and aligned with the plane of the intersection plate. After tightening all bolted connections of the mould, the inclusion assembly was locked in position.

At this stage, the plastic tubing ducts were introduced into the compartments and were tightly held to the end plates. The prestressing wires were subsequently inserted, passing through close fit and wide apertures provided in the end and intermediate plates respectively. Using a 'single wire system' prestressing jack, the wires were stressed, after installing the dynamometer assembly, to about 7 kN each. This operation was intended to maintain a straight profile for the ducts during casting and until setting of the concrete.

Finally, the thermocouple housing copper tubes were fitted into positions through the respective sides of the mould.

5.8.3 Casting procedure

The concrete mix was carefully proportioned, mixed under carefully controlled conditions (blending of dry ingredients, addition of water, duration of mixing, etc.) and then placed simultaneously into the compartments by two operators. An electric hammer was moved along the base of the mould by a third operator, while casting was in progress. When concreting reached the top, an immersion vibrator was used to ascertain full compaction of the concrete. An additional layer of about 20 mm thick of concrete was added on top with the help of long wooden strips clamped along the edges of the mould. This was subsequently chopped off with a trowel after a short vibration. The object was to

obtain a homogeneous distribution of material across the beam depth.

After levelling the surfaces of the specimens, a layout for the heating cable was carefully marked and embossed on both surfaces, using specially formed lubricated steel wires. The specimens were subsequently covered with thick polythene sheets and left to cure in the mould for two days. Then the wires were de-stressed by loosening the bolts of the dynamometer assembly, cut and removed. Following that, the main channels of the mould were carefully removed, leaving the metal faced ply in contact with the concrete surfaces. Each segment was then wrapped in polythene sheeting and transferred to the curing room where they were left to cure in such conditions until the age of 21 days, when they were transferred to the testing laboratory and prepared for sealing.

5.8.4 Sealing and curing

Preliminary tests were carried out on some cube specimens coated with different layers and types of resins, and heated in an oven at temperature of about 100°C for a period of six weeks, during which frequent weight changes were observed. Based on the results of these tests, a Bakelite resin compound, with a base, grade R18774/1 and a hardener, grade Q19159, was selected.

In establishing the sealing procedure for the specimens, it was decided that the surface under consideration should not be exposed to the atmosphere longer than the time necessary to complete the operation. In general, the side to be coated was set facing upwards and the area was cleaned with a wire brush, and the sharp corners were filed with a carborundum stone. Greased wooden strips were clamped around the area to enable 'ponding' of the resin around the edges.

After mixing a sufficient quantity of the base and hardener, the resin was applied to the surface with a paint brush. Air bubbles formed on the surface in time were pricked and those found later were scraped and filled with the resin. Two coats were applied to each surface in such a way that one coat was given in the morning and the second coat in the afternoon.

Sealing progressed from the upper to the lower surfaces, through the sides and finally the far ends of the prisms. While coating the top surfaces of the specimens the heating cables were fixed into the grooves and painted over with the resin. The load bearing plates, if any, were firmly fixed into their exact locations before the resin became tack-free.

Prior to application of the resin to the sides of the specimens, the ply boards were released and the strain gauge studs were screwed into the county caps. Care was taken to ensure that sufficient resin was ponded around the strain gauge studs and the thermocouple housing tubes. The far ends of the prisms were thinly coated and subsequently attached to their Sindanyo asbestos boards, cut to size and had holes drilled in them to suit the positions of the prestressing wires. These were intended to provide some heat insulation to the prestressing system.

5.9 Control tests

A set of six 100 mm cube and six 108 mm ϕ cylinder specimens from the same batch of concrete as the beam, in addition to a similar set from a different batch, were cast to determine the elastic material properties, namely compressive and tensile strength, as well as the concrete modulus of elasticity. These were tested at room temperature at the ages of 28 and 56 days to coincide with the loading and heating ages of the beam. These are detailed in the Appendices.

As regards uniaxial creep and shrinkage control tests, these were incorporated into Part 2 of the experimental program expounded in Chapter 7.

5.10 Pre-stressing set-up and procedure

At the age of 28 days from casting, preparations were made to integrate, by axial stressing, the two beam segments on the test apparatus. Two portable jacking devices were mounted across the main girder of the frame, temporarily replacing the proving ring supports during the prestressing operation. Each segment was in turn carefully handled and mounted between the relevant end and intermediate supports. One of them was supported on two rollers, so that it could be easily manœuvred relative to the other, during setting for the prestress. The prestressing wires were guided through the whole system including the dynamometer at one end, and were then anchored to the steel end plate at the other end. At this stage, datum temperature and strain gauge measurements were established on both sides of concrete, and the aluminium block.

The two segments were brought into close contact with their longitudinal axes set approximately in the same vertical plane. With the help of the supporting jacks and the reference bar and deflection gauge system, the segment's interface was accurately set into a vertical plane. Before proceeding with the stressing process, initial deflection gauge readings were recorded, so that after completion of the process, the existence or otherwise of eccentricity could be determined.

Using a hollow ram jack, and starting with the middle two through wires at the opposite corners, each wire was tensioned in steps of 2 to 3 kN up to a maximum of 16 kN. The force in each wire was read from the

previously calibrated gauge of the prestressing and was ascertained by measuring the wire extension. The total force and force distribution across the beam was ascertained from the strain profile of the aluminium block. The results obtained from the first attempt were, however, not satisfactory, and a second attempt had to be made, which involved repetition of the whole process.

After successfully achieving the desired stress pattern (see Chapter 6) the provisional supports were replaced by the proving rings, and the beam was prepared for the application of transverse loading.

5.11 Load and temperature applications

After assembling the reaction frame components around the centre point of the end spans, a set of temperature, strain and displacement gauge readings was recorded. The loading springs were subsequently tensioned simultaneously by two operators until the pre-determined extensions were achieved. The relative support movements indicated by the support gauges were eliminated by adjusting the levels of the internal supports. The immediate elastic response of the beam, including support reactions, strains and deflections were recorded. Similar observations were frequently made during the next 33 days when the beam was exposed to non-uniform heating.

In preparation for heating, the beam was wrapped (except the underside) with a 25 mm thick glass wool insulation (see Plate 5.5). Then, after making the necessary connections to the heating circuit, and establishing the initial strain, temperature and displacement readings, the power was switched on to the circuit. Because strain and deflection measurements had to be done manually, it was possible to record these parameters during the early hours of heating, except the support movements and reactions. The first complete set of observations

was however recorded after about 48 hours when the temperatures reached their maximum stable values.

5.12 Cycle and frequency of observations

The cycle of observations generally consisted of measurements of the following parameters:-

1. Support displacements and reactions
2. beam deflections
3. overall temperature distributions
4. concrete and aluminium strains
5. total prestress force

Except during the first two weeks of heating, the reactions, strains and beam deflections were usually recorded after alignment of the support levels. The above observations were recorded at 2, 5, 7, 10, 14, 16, 21 and 28 days from heating, subsequently at about 2 to 3 weekly intervals.

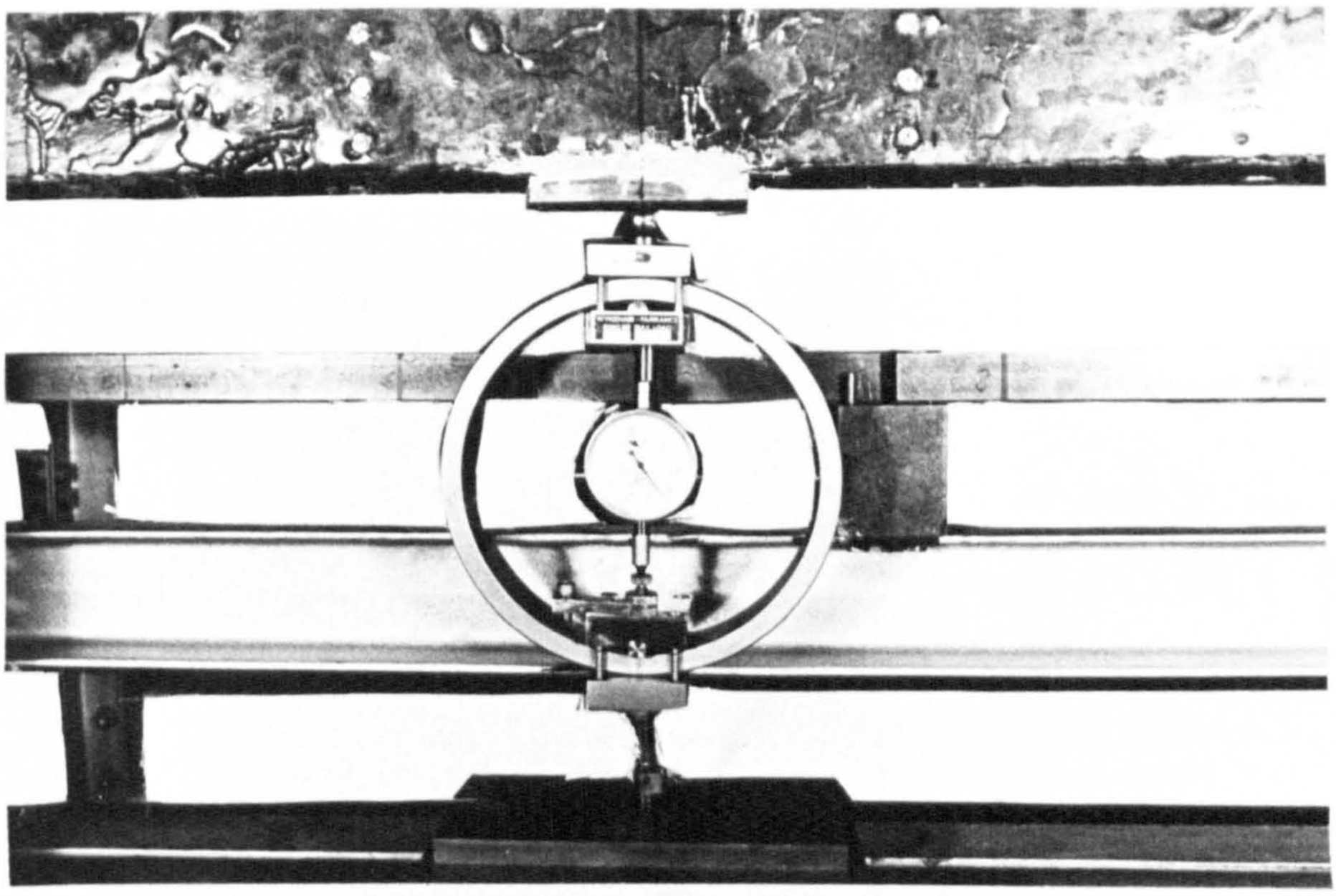

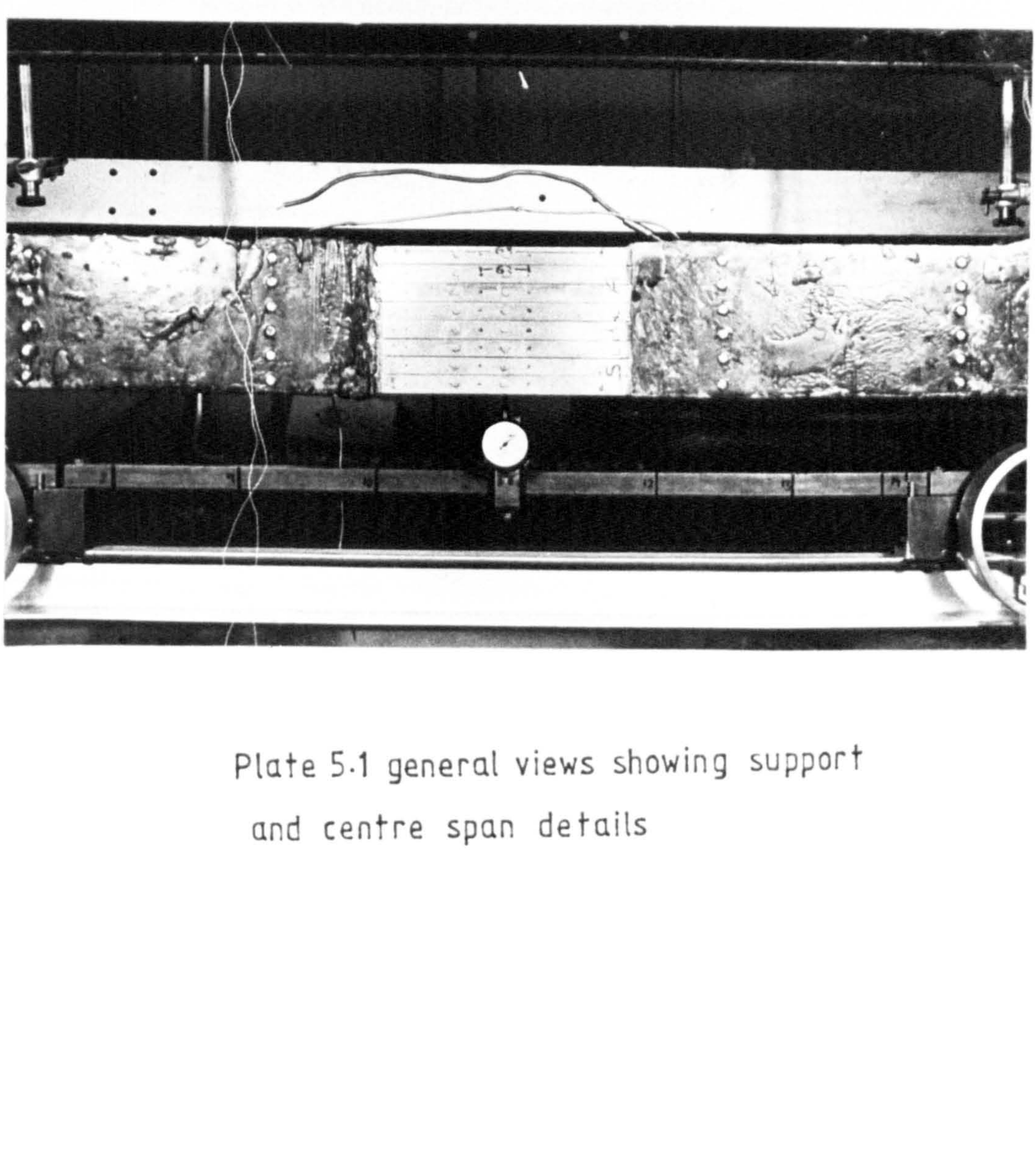

Plate 5.1 general views showing support and centre span details

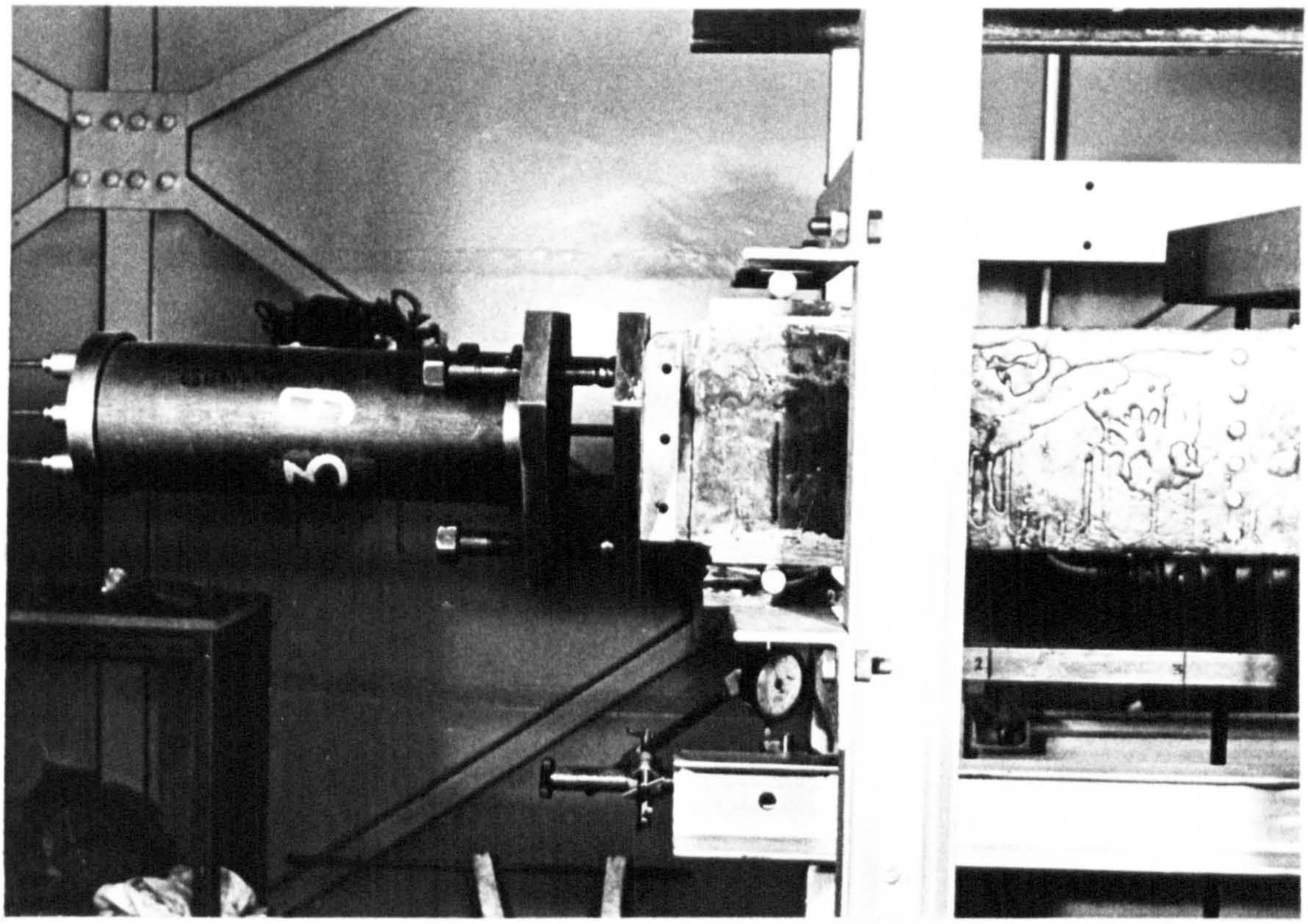

Plate5·2 dynamometer assemply

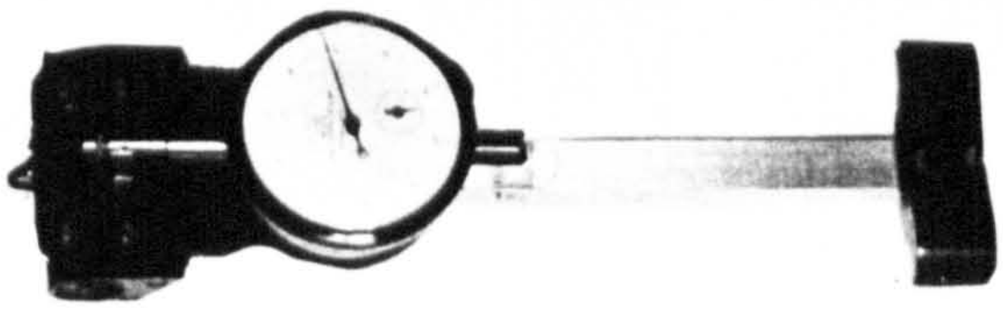

Demec Gauge

Deflection Gauge

Plate 5·3 Mechanical Instrumentation

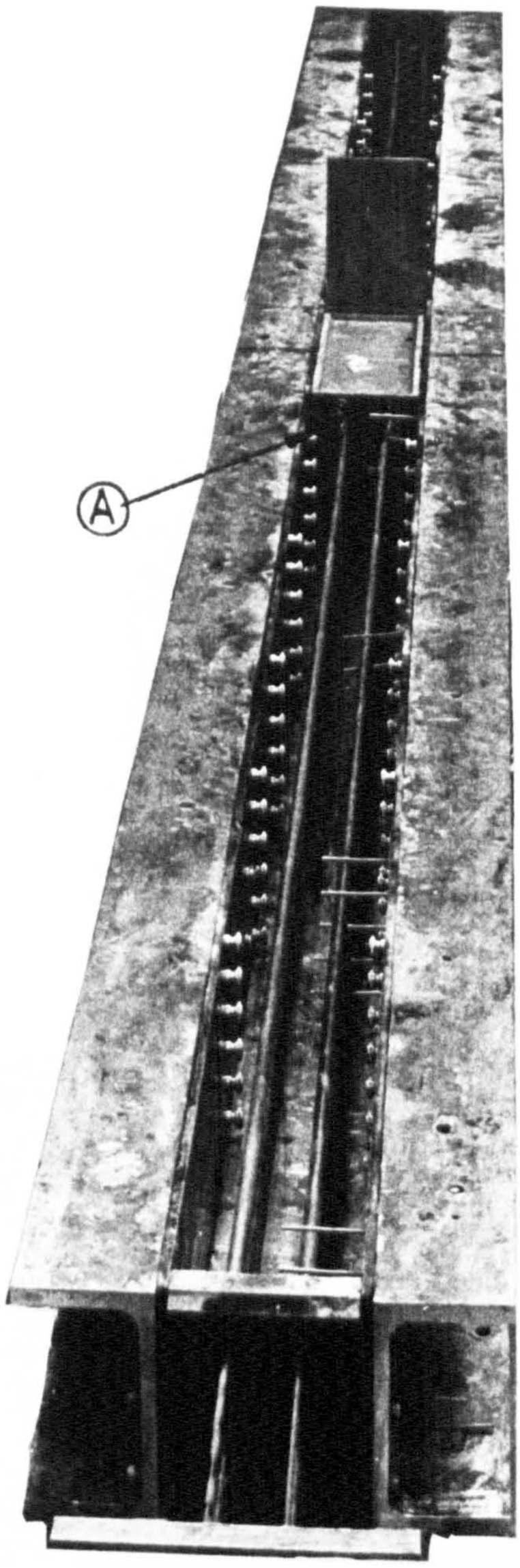

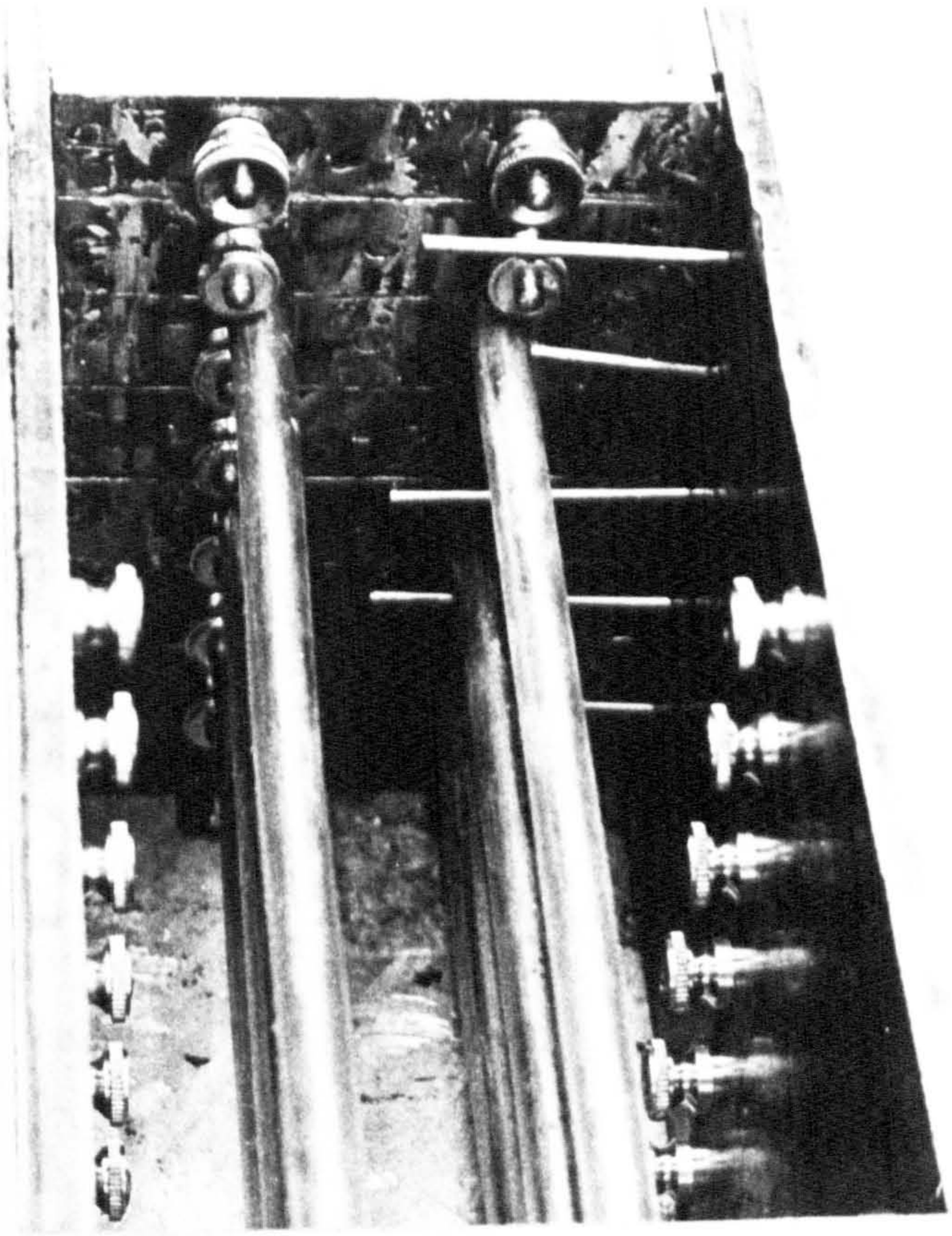

detail A

Plate 5.4 Formwork construction details

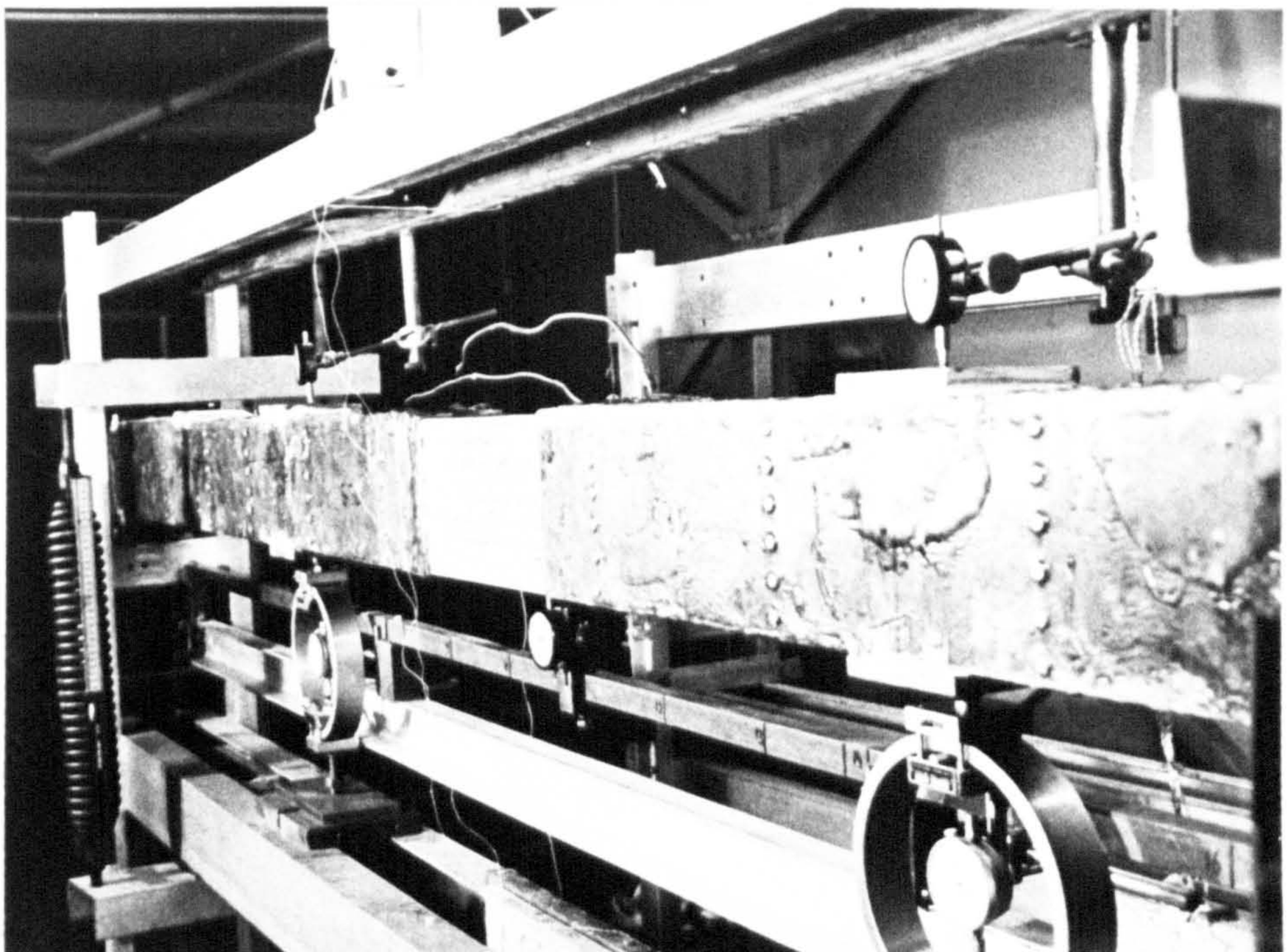

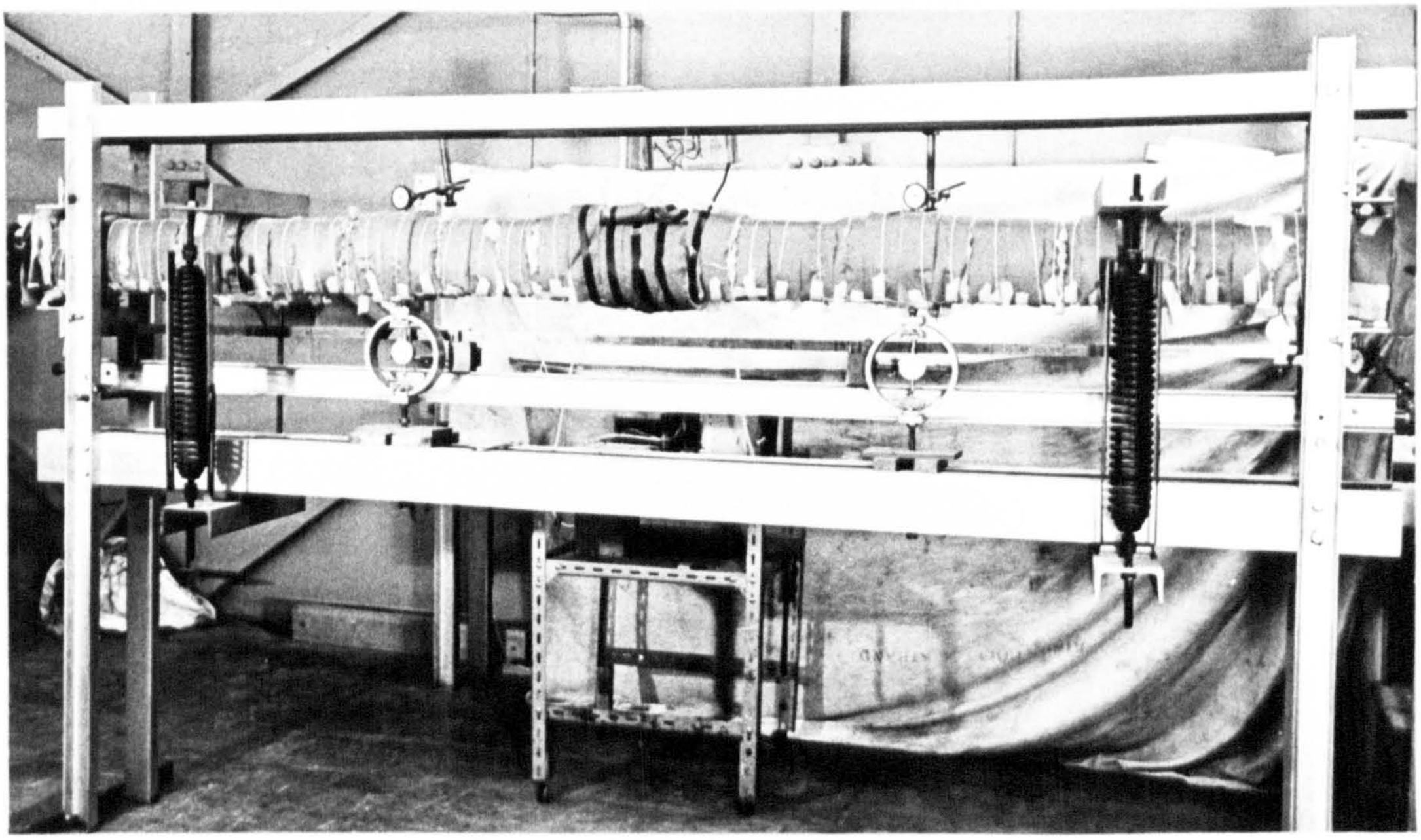

Plate 5.5 geneneral view of the testing rig showing the beam before and after heating

CHAPTER VI

TEST RESULTS AND THEORETICAL PREDICTIONS OF THE CONTINUOUS BEAM BEHAVIOUR

Chapter 6 - Synopsis

This chapter presents the test results of the continuous beam experiment described in the preceding chapter alongside the theoretical predictions of the steady state theory and the rate of creep method. The results reveal that significant redistribution of stresses and moments did occur due to the differential thermal creep behaviour of the material. The redistribution process occurs fairly rapidly but slows down with time, indicating the tendency of stresses towards a limiting long-term state.

It is concluded that the rate of creep method is able to predict satisfactorily the stress and moment redistribution phenomena due to non-homogeneous creep of the material. At large values of the specific thermal creep the method predicts closely the long-term state of stress consistent with the predictions of the quasi-elastic steady state theory.

The data obtained from the composite concrete/aluminium beam experiment described in Chapter 5 are presented and compared to theoretically predicted values. Analyses of both the short and long-term stresses have been carried out using the simple elastic theory of bending and the quasi-elastic approach of the steady state theory respectively, whereas historical analyses of the stresses and displacements have been performed using the iterative rate of creep method.

In presenting the results, use has been made of the close similarity in the behaviour of the beam about its vertical line of symmetry. The observations recorded on both sides of the centre line have therefore been averaged and introduced as representative of the behaviour of the symmetrical half of the beam.

6.1 Temperature state

6.1.1 Temperature gradients and mid-depth temperatures

The distributions of temperatures over the beam reached stable values after approximately two days from the start of heating. At all times of measurements, and at almost every section of the concrete segments, the distributions were found to be very nearly linear. Typical distributions of temperatures across four of the concrete sections, as well as over the aluminium block recorded at different ages are shown in Fig. 6.1.

For the purpose of analysis, the least square method has been utilised to obtain the best straight line fit for the temperature data and therefore to evaluate both the temperature gradients and mid-depth temperatures.

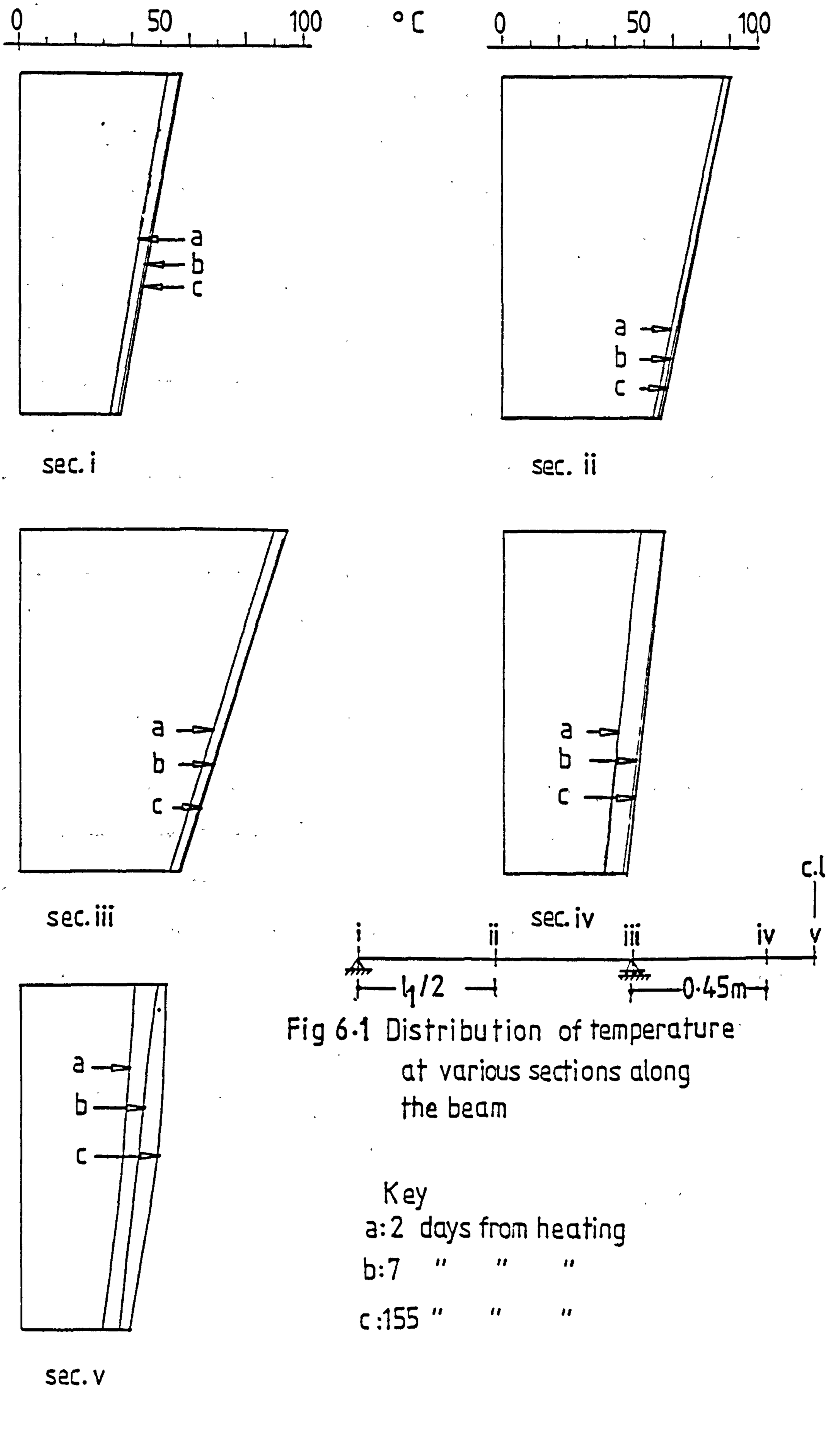

Fig 6·1 Distribution of temperature at various sections along the beam

Key

a: 2 days from heating

b: 7 " " "

c: 155 " " "

6.1.2 Distribution of temperatures along the length of the beam

The loops of the heating cable were stopped approximately 50 mm short of the end support line and the aluminium block in an attempt to avoid excessive heating over these regions. As a result of this, and because of poor insulation, both the temperature gradients and mid-depth temperatures dropped considerably. Over the point load sections, similar but less severe drops occurred in these quantities due to heat losses through the loading platens.

In Fig. 6.2 are shown the mean distributions of the surface temperatures and the calculated temperature gradients along the beam. The points shown in these graphs include those obtained from surface temperature measurements, in addition to others calculated from the internal temperature distributions.

6.1.3 Time variation of temperature

The time-variations of both the temperature gradients and mid-depth temperatures over the various sections of the beam are represented in Fig. 6.3. The plots show that over the long range these temperature parameters remained in general reasonably constant, apart from small fluctuations from the initially stabilized values, which are believed to have occurred as a result of one or more of the following factors.

1. Fluctuations in the mains supply voltage and therefore the wattage output of the heating cable.
2. Changes in the heat flow properties of the concrete.
3. Fluctuations in the laboratory temperatures.

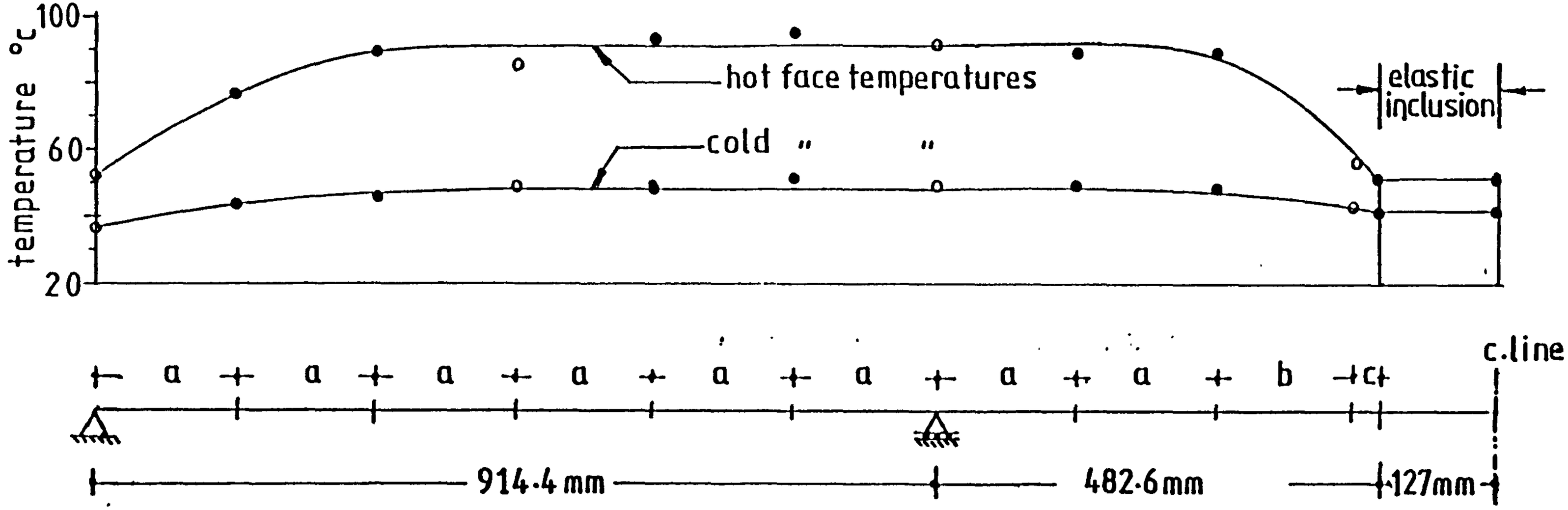

Fig 6·2 Distributions of surface temperatures and temp. gradients along the beam

Notes: spacing a=152·4 mm
b=146·0 "
c=32·0 "

[•] values from surface temp. measurements
[o] " " internal " "

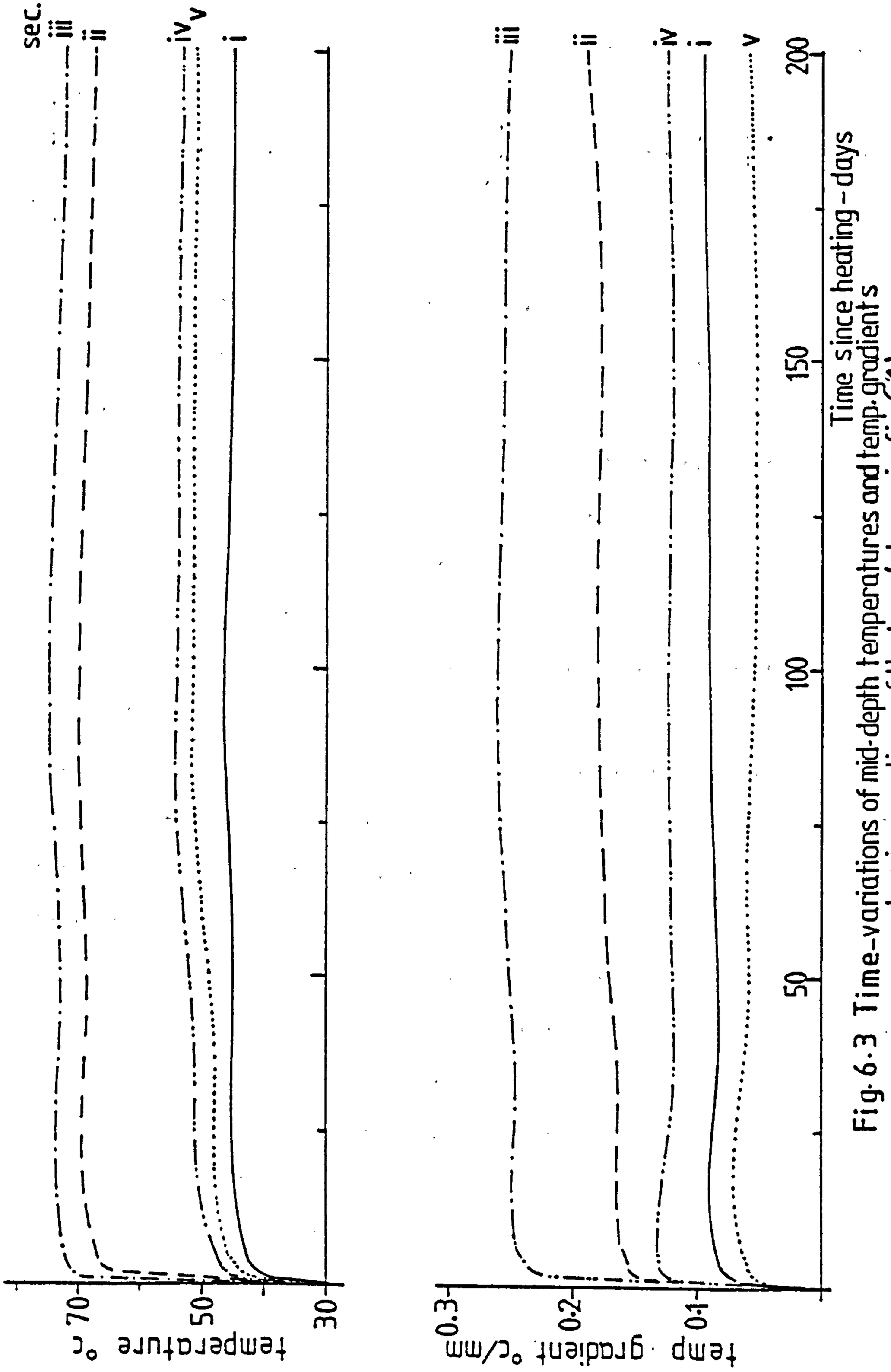

Fig·6·3 Time-variations of mid-depth temperatures and temp. gradients at various sections of the beam (shown in fig 6·1)

6.2 Variation of the support reaction with time

The interior support force recorded immediately after the application of transverse loading amounted to 4.425 KN. In comparison, the elastic theory predicted a value of 4.469 KN, i.e. an overestimate of less than 1%. It is of interest to note, however, that for a monolithic concrete beam structure the elastic calculations yield a value for the support force of 4.50 KN. Thus, the presence of the elastic inclusion within the beam structure reduced the theoretical support reaction only by about 1.67%.

Over the cold test period, the reactions increased only slightly, such that at the loading age of 33 days, i.e. just before heating commenced, the mean force reached a value of 4.475 KN.

On first heating, the reactions decreased rapidly although the total short-term effect of the temperature was not permitted to develop as the interior supports were allowed to move freely as the beam curved upward (Fig. 6.4). This was intended to reduce the thermo-elastic bending moment and therefore to eliminate the development of cracking. After about the first few hours of heating the reactions started to increase despite the fact that the temperature was still rising. The increase in the reactions continued with time accompanied by gradual diminution of the differential settlement of the supports caused during first heating, Fig. 6.5. However, the remainder of the differential settlement was finally eliminated by elastic adjustment after about two weeks from the start of heating. The reactions continued to increase thereafter under co-linear support conditions, and at the heating age of about 19 days the initial effect of heating was completely nullified. The rate of increase appeared to diminish with time and after about three months of sustained heating the reactions seemed to stabilize,

Notes

a immediate change due to upward movt. of 0·235mm

b " " " " downward " " 0·505 "

c & d " " " " removal of these displacements

age of concrete at loading = 28-days

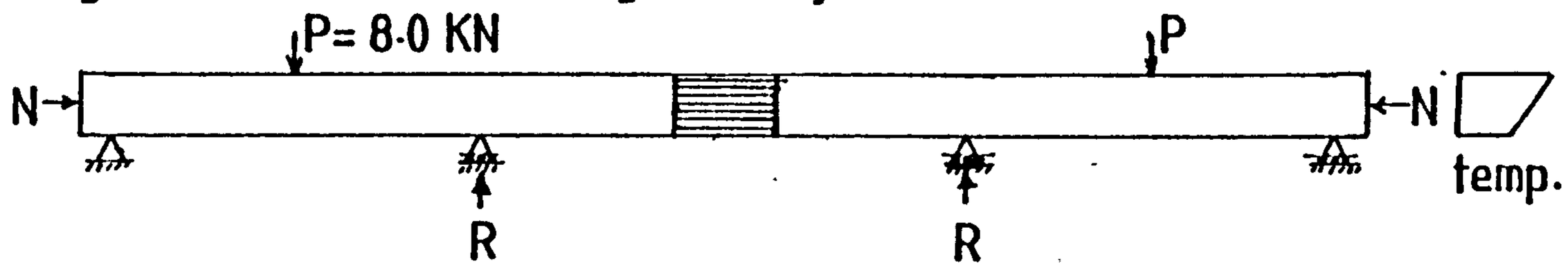

Variation of support reaction with time

Fig 6.4

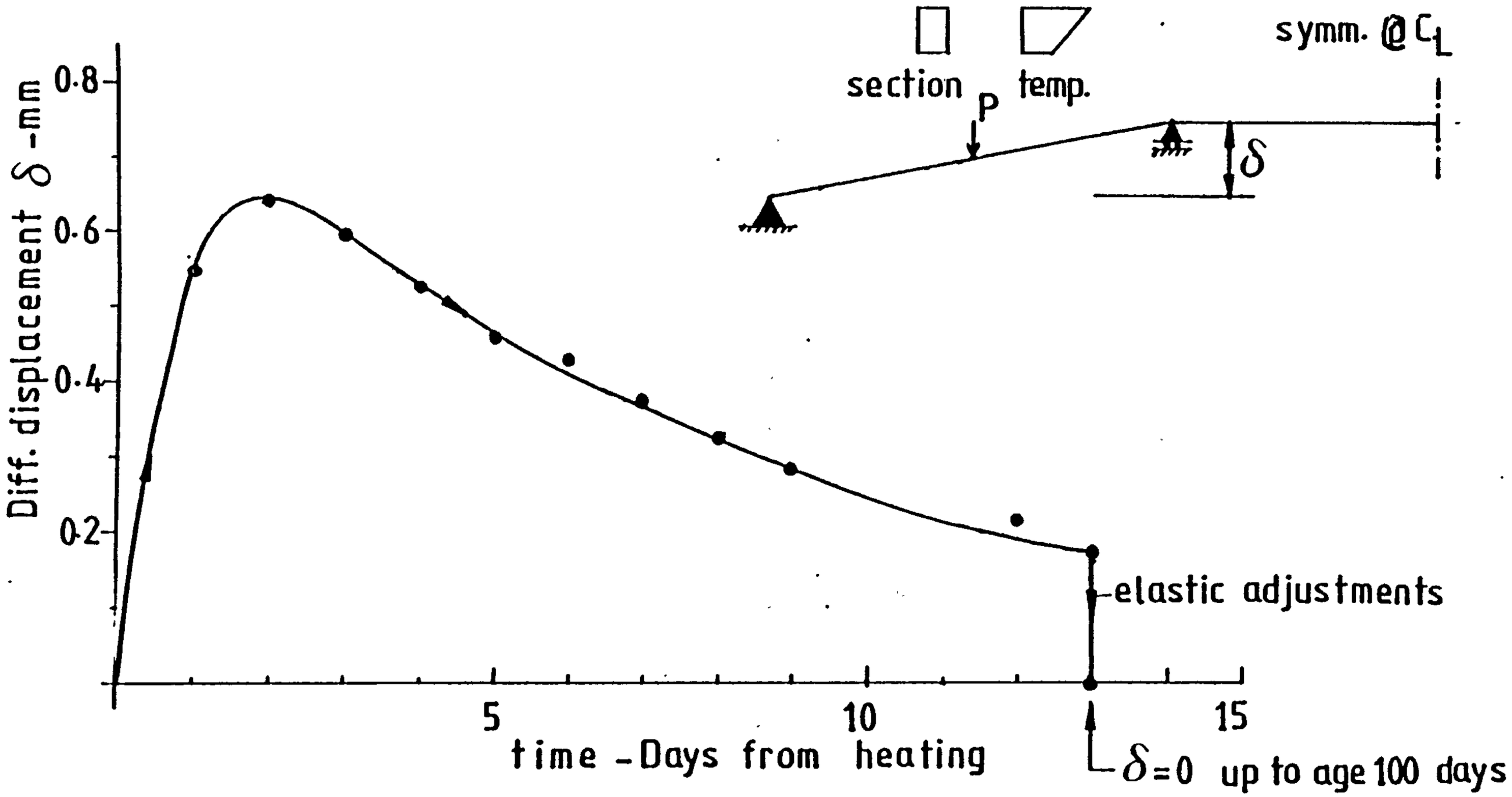

Fig. 6·5 Variation of differential displacement δ with time after heating

indicating that they were approaching an upper limit, which is better known as the steady state value. However, to ascertain the existence of such a state, the beam was further tested with its supports subjected to and maintained under differential displacements, as illustrated in the following sub-section.

6.2.2 Reactions' behaviour under sustained displacements of the supports

At the heating age of 100 days, the interior supports were displaced vertically about 0.235 mm above the level of the end supports. This resulted in immediate increases in the reactions, which amounted to an average of 0.436 KN. However, with the sustainment of the differential displacement, the reactions exhibited a general decline over the subsequent test period, which lasted for 56 days. In Fig. 6.4, it can be seen that the plot of the test data over this particular period appear as part of a relaxation curve. Nevertheless, after the restoration of the beam supports to the co-linear state, the reactions behaviour appeared to continue in the same general pattern observed before the imposition of the displacement.

It is clearly apparent from the above account that under both test conditions, the reactions tended towards a common long-term value. Such a behaviour was in general agreement with the steady state theory concept, which implies that when loads, temperatures and/or displacements are sustained, there is always a preferred long-term state to which the stresses, and hence their integrated boundary response, will tend to, provided that there is sufficient creep capacity in the material to allow this process to become complete.

A further attempt was made to observe the reactions' behaviour under sustained differential settlements of the interior supports. On

the 187th day of heating, the interior supports were displaced about 0.505 mm downward below the level of the exterior supports. Immediately, the reactions decreased by an average of about 0.888 KN, and on maintaining the imposed displacement, they exhibited gradual increases over the subsequent two weeks' period. However, some irregularities in behaviour did occur later, as a result of small variations in the applied temperature gradient caused during the attempts made to regulate the supply voltage to the heating circuit.

6.2.3 Effects of a temperature cycle on the reactions

After a period of 250 days of sustained heating the beam was finally subjected to a temperature cycle prior to the termination of the test. However, before the temperature gradient was first reduced, the interior supports of the beam were restored to the co-linear level with the outer supports. This brought the values of the support faces to an average of 5.645 KN, which was slightly below the value reached before the displacement was imposed.

On the first attempt, cooling was performed on two stages over a period of two days. With the reduction of the applied temperature gradient, the reactions increased sharply, such that on complete cooling, the average force reached a value of about 8.673 KN, that is to say, nearly twice the initial value observed on loading. Nevertheless, a general decline was observed during the following 22 days' cold period of the cycle. Nearly the same short-term effect and the general pattern of behaviour were also observed when and after the beam was finally cooled.

On re-heating, however, the reactions dropped sharply, and over the hot part of the cycle they exhibited an increasing pattern, very

similar to that observed on first heating. In Fig. 6.4, evidence is shown that the short-term response of the support forces was to some extent greater on heating than on cooling. The mean force of the two supports increased on both cooling occasions, for example, by an average of 3.0 KN, while the reduction due to heating amounted to about 3.225 KN. The reason for such discrepancy, however, is thought to be related to some of the loss incurred by heating on the modulus of elasticity of concrete being recovered on cooling.

In the same plot of the results, it is shown that over the hot part of the cycle, the time rate of increase in the mean force was greater than the time rate of decrease over the cold part. This was understandably consistent with the general opinion that the creep rate of the material is greater at elevated temperatures.

6.2.4 Predicted limiting steady state reactions

The steady state theory predicted a value of about 5.55 KN (see the Appendices) as the upper bound value for the redundant support force likely to be reached under the sustained loading and temperature conditions. This value almost coincided with the experimental value recorded at the heating age of 100 days, when the rate of increase in the reactions was very slow indeed. The range of the long-term value, however, was subsequently identified from the observations made following the application and removal of the upward displacement to the interior supports, which was found to be between 5.915 and 5.666 KN. The theory predictions therefore underestimated the redundancy by between 2.0 and 6.2%, which in view of the approximations involved in the calculations, appeared to be very reasonable.

6.3 Time variation of moments along the beam

The time variation in the bending moment distributions over the beam, as inferred from the recorded values of the support reactions, are depicted in Fig. 6.6. The theoretical distributions of moments, on the other hand, are depicted in Fig. 6.6a. The diagram reveals some features of the redistribution of moments due to the differential thermal creep behaviour of the material. It shows that, as time progressed, creep caused the initial thermo-elastic moments to change sense and substantially in magnitude. This was accompanied by a time-dependent shift in the points of zero moments towards the centres of the end spans. Evidence that greater redistribution of stresses occurred over the intermediate span than elsewhere in the beam was given by the fact that this span experienced greater and more rapid changes in bending moments.

6.4 Removal of the vertical loads

On removal of the vertical loads, after being sustained for 408 days, the reactions immediately decreased by an average of 4.454 KN. This value differed from that observed on first application of the loads by a very small amount. Such result implies that the beam retained its elastic response throughout the test period. However, the fact that the loads were removed 78 days after cooling, renders it more likely that some of the loss in the elastic modulus of the concrete which could have been caused by heating, was recovered during the subsequent cold period.

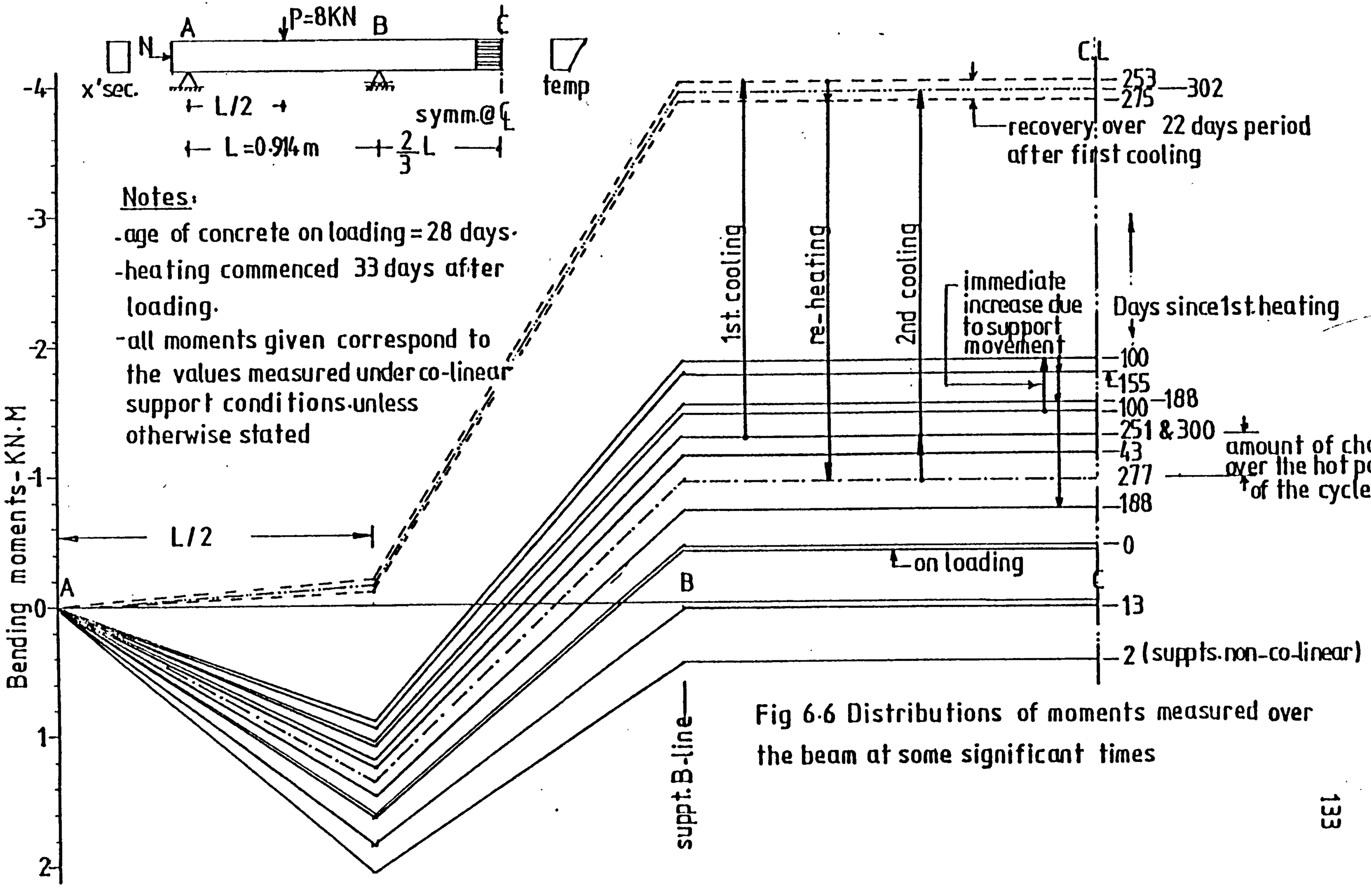

Fig 6.6 Distributions of moments measured over the beam at some significant times

Theoretical distributions of moments along the beam at some significant times after heating- elastic and step-by-step solutions.

Note :
all moments given correspond to co-linear support conditions unless otherwise stated

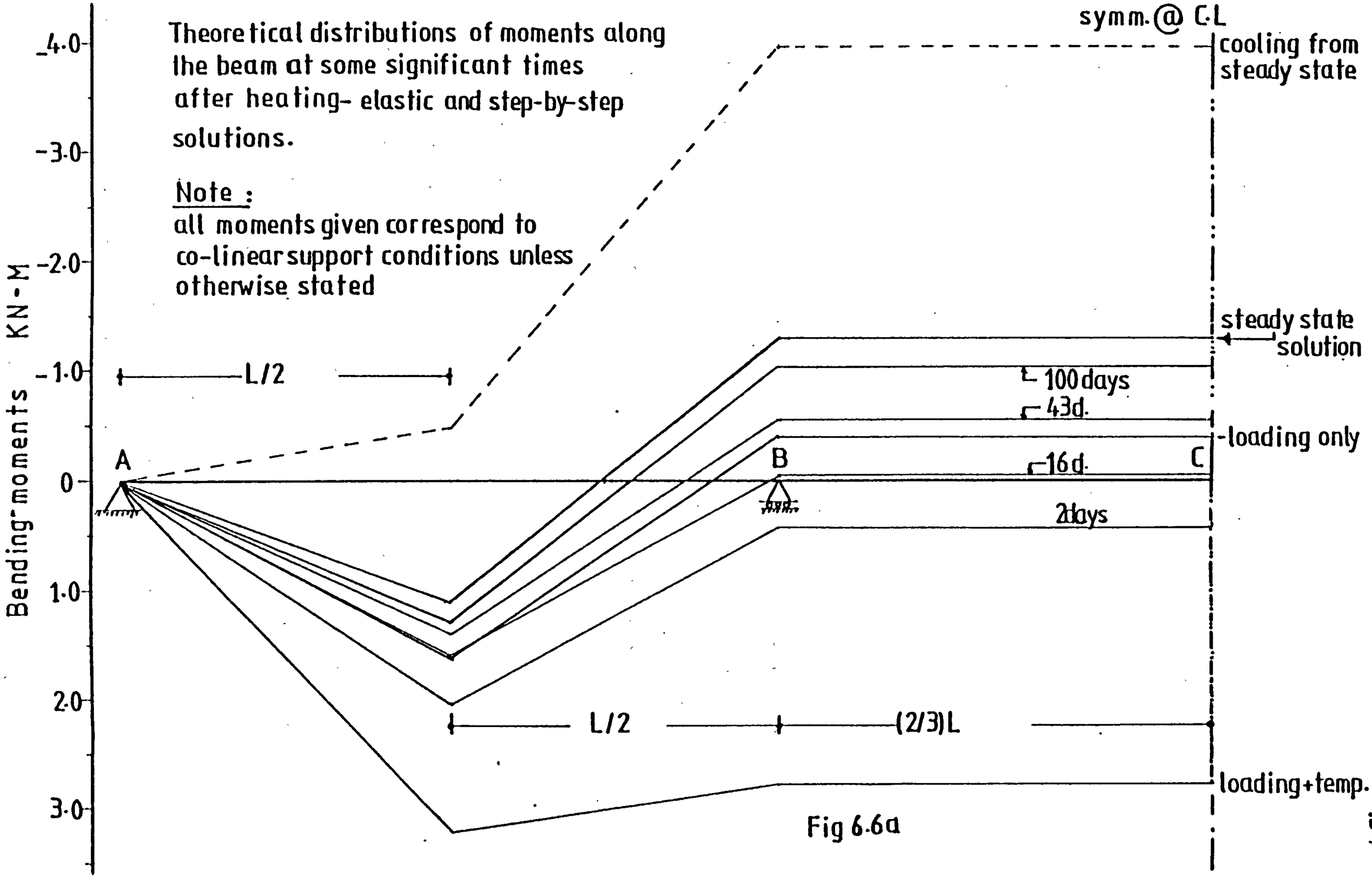

Fig 6.6a

6.5 Beam deflections

Changes in the deflection profile of the beam are displayed in Fig. 6.7. The data points in this figure represent the vertical displacements of a number of equally spaced points along the beam measured with respect to their positions prior to application of the transverse loading. The values given correspond to the conditions for which the supports were co-linear. The theoretical deflections are on the other hand depicted in Fig. 6.7a.

From an examination of both measured and predicted deflections indications are that the applied temperature gradient caused initially hogging and sagging deflections of the end and central span respectively. Subsequently, creep reversed the trend and caused it to increase with time at diminishing rates. The continuing deflection changes with time were indications of the effects of creep on the beam curvatures.

6.6 Curvature changes

Fig. 6.8 shows the time-dependent changes in the curvatures of three given sections along the beam measured over the first 100 days of heating. Evidence is shown that the curvatures of the three sections were reduced considerably on first heating. These reductions were however greater for the support and central span sections than that recorded over the end span section. This can be related to the comparatively greater changes in the bending moments of the former two sections caused by heating, as previously shown in Fig. 6.6.

As heating was sustained, the curvatures of all the three sections concerned showed increasing trends with time in conformance with those of the many other test parameters being

Key to the defln. profiles

- • on loading (age = 28 days)
- ° before heating (age = 61d.)
- ⋇ 15 days after heating.
- ✱ 29 " " "
- □ 56 " " "
- ♦ 155 " " "
- × 250 " " "

Notes

- the datum for all measurements is the beam axis prior to loading.
- spacing s = 152.4 mm

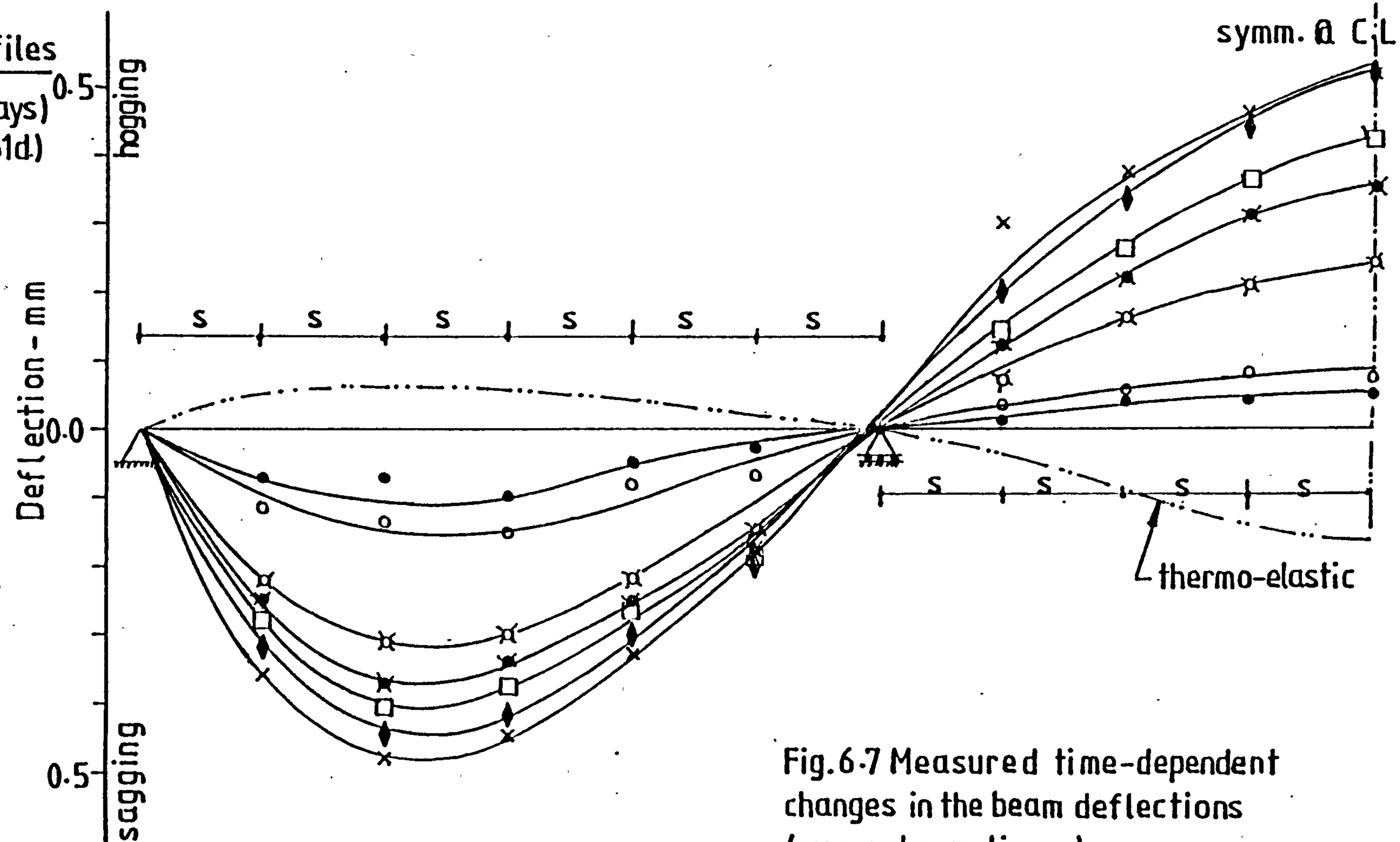

Fig. 6·7 Measured time-dependent changes in the beam deflections (supports co-linear)

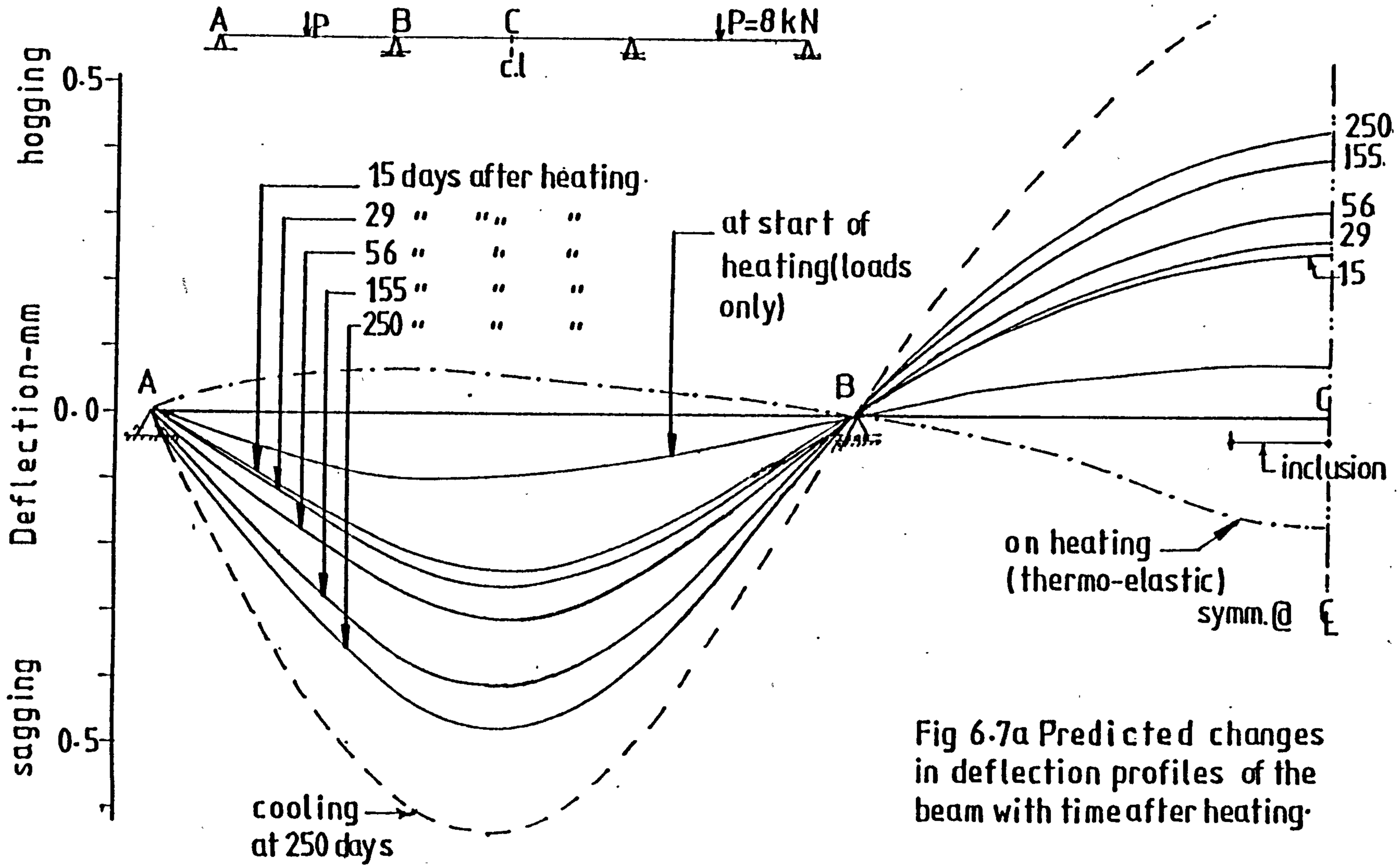

Fig 6.7a Predicted changes in deflection profiles of the beam with time after heating.

Note:
the temp.state used in the analysis is given in fig. A-1 of the Appendices

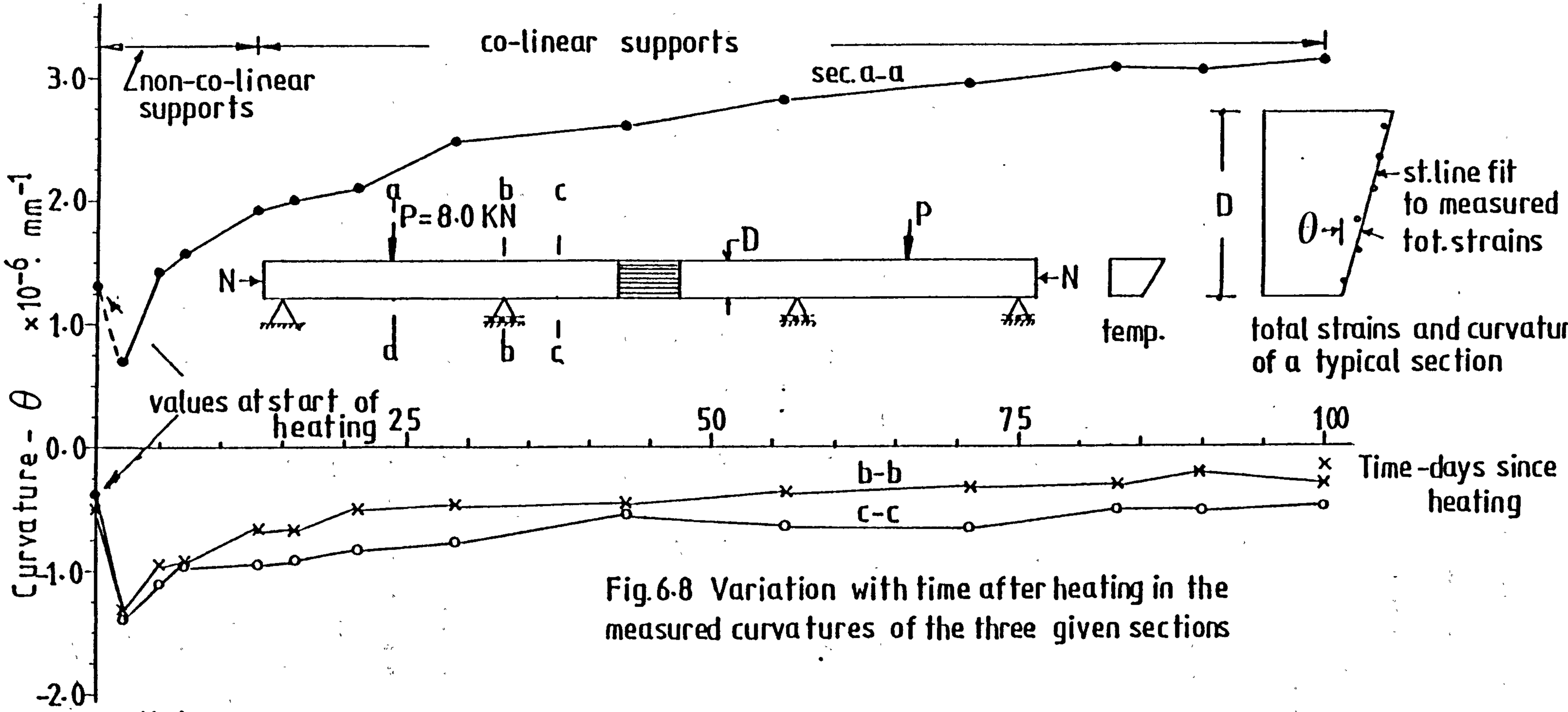

Fig. 6·8 Variation with time after heating in the measured curvatures of the three given sections

Notes:

- age of concrete on loading = 28 days
- " " " " heating = 61 "
- the temperature state is shown in fig 6·2

observed. That is to say, they increased at continually decreasing rates. In general, the rate of increase in curvature of the end-span sections was considerably higher than those of the other two sections. The following explanation for such behaviour is offered:

The imposition of the temperature gradient on the beam created the most severe stressing condition over the point load sections, with their extreme upper fibres being exposed to the maximum compressive stresses. The combined effects of higher stresses and temperatures, therefore, resulted in the development of higher creep rates and consequently more rapid curvature changes over these sections than elsewhere along the beam.

The results of Fig. 6.8 give indications that after about the first two months of heating the curvature changes over the support and middle span sections became more or less stable. However, the observations of moment and deflection changes over these sections indicated otherwise. The fact that the curvature values plotted have been deduced from the slopes of the straight line fit of the total strain distributions which is an approximate procedure may account for this inconsistency.

6.7 Direct measurements results of stresses within the central span

The strain data recorded from the elastic inclusion incorporated into the beam structure have been processed to indicate the force patterns created across the assembly due to axial prestress and transverse load applications. And then, to indicate separately the magnitudes of temperature and creep effects in form of incremental force changes occurred across the elements after application of the temperature gradient on the beam. The corresponding total state of stress in the concrete and its variations with time are presented and compared to

theoretical predictions in a subsequent section.

Generally, the stress in the concrete at the level of a particular element ($\sigma_{c,r}$), which is assumed uniform over the concrete bearing area of the element ($A_{c,r}$) is calculated from:

$$\sigma_{c,r} = \frac{f_r}{A_{c,r}}$$

where f_r is the axial force in that element and which is calculated from

$$f_r = \left(\frac{n_d}{K} - \bar{\alpha}_r.\Delta T_r\right) \cdot E_r \cdot A_r$$

in which, n_d = total number of strain gauge divisions deviated from the reference state

K = gauge factor

ΔT_r = change in the element temperature from the reference state

$\bar{\alpha}_r$ and E_r = the coefficient of thermal expansion and Young's modulus of the elements' material respectively

A_r = cross-section area of the element.

The average numerical constants used in the above calculations are as follows:

$E_r = 66.6\ GN/M^2$, $\bar{\alpha}_r = 23.0 \times 10^{-6}/^oC$

$A_r = 687.2\ mm^2$, $A_{c,r} = 1935.48\ mm^2$

6.7.1 Initial response of the inclusion to prestress and load applications

Fig. 6.9 illustrates the observed responses of the inclusion elements to the applications of axial prestress and transverse loading on the beam. As can be seen in part 'a' of the figure, the distribution of prestress over the cross-section of the beam was very nearly uniform. Within the

accuracy of measurements, the mean prestress force recorded over the eight elements of the inclusion was about 11.75 KN giving a total force of about 94.0 KN. In comparison, the total force indicated by the dynamometer tube of the prestressing assembly was about 95.15 KN.

Part 'b' of Fig. 6.9 shows a very close agreement between the observed change in the force distribution over the beam section due to application of transverse loading and the change calculated by the elastic theory of bending for the composite beams. The total distribution of forces across the inclusion is depicted in diagram 'c', which is obtained by summing up diagram 'b' to 'a'.

6.7.2 Temperature and creep-dependent changes in the force distribution

Figures 6.10 and 6.11 illustrate the magnitudes of force changes observed across the inclusion at some selected times following the imposition of the temperature gradient. The reference state taken for these plots is that prevailing just before heating was due to begin. It then follows that the total force distribution across the inclusion, corresponding to a given age after heating can be obtained by superposing the relevant diagrams from these plots to diagram 'c' of Fig. 6.9. Attention is drawn here to the fact that for the reason stated previously, differential displacement between the interior and outer supports was permitted to develop freely during the first temperature rise. A large part of this was subsequently allowed to decay by creep until approximately the end of the second week of heating when the remainder was finally eliminated by elastic adjustments. Each of the first three diagrams in Fig. 6.10 therefore represents the distribution of forces developed under non co-linear support conditions.

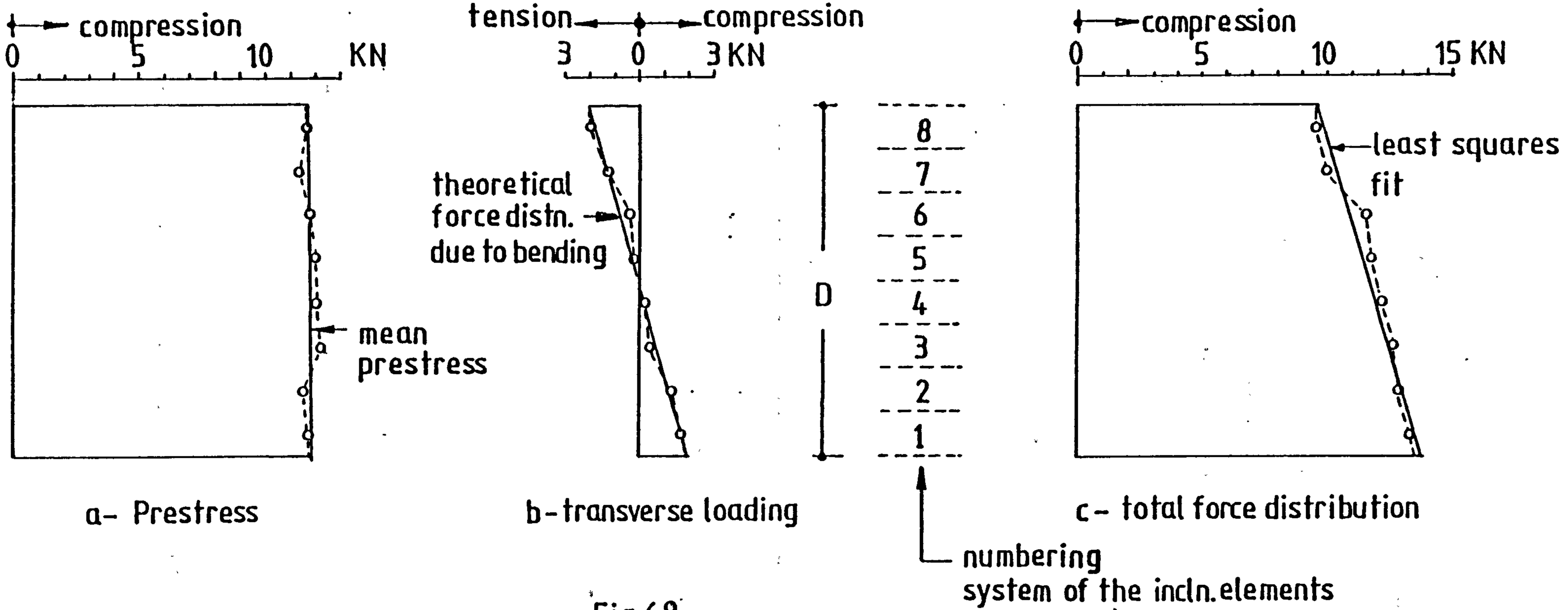

Fig. 6.9

Measured initial response of the inclusion elements to the applications of axial prestress and transverse loading

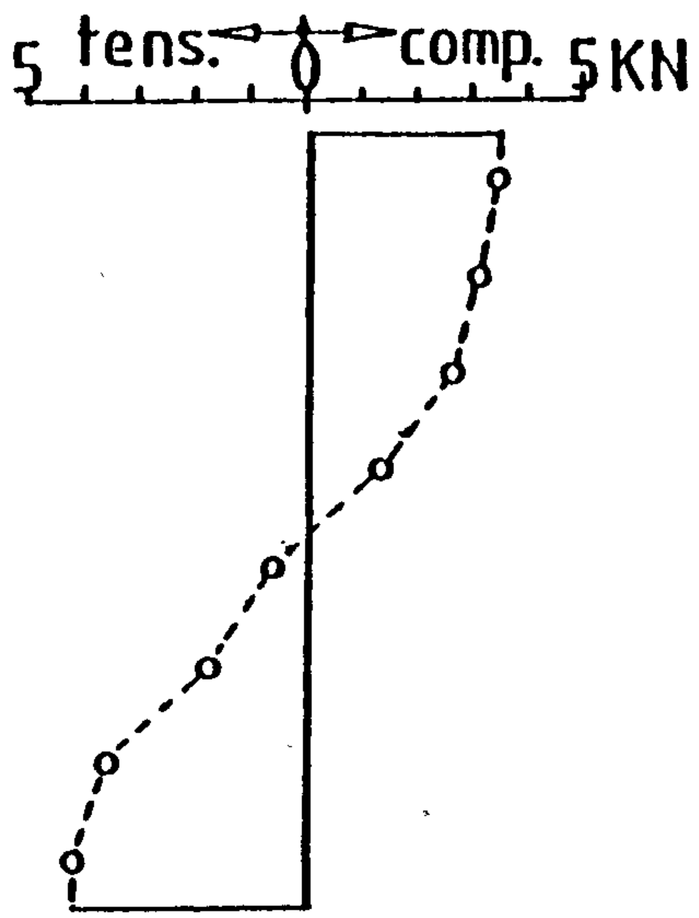

2-days

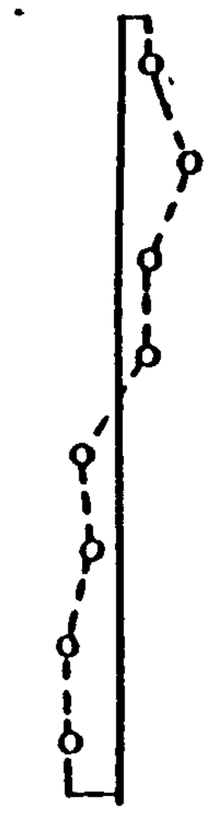

16-days

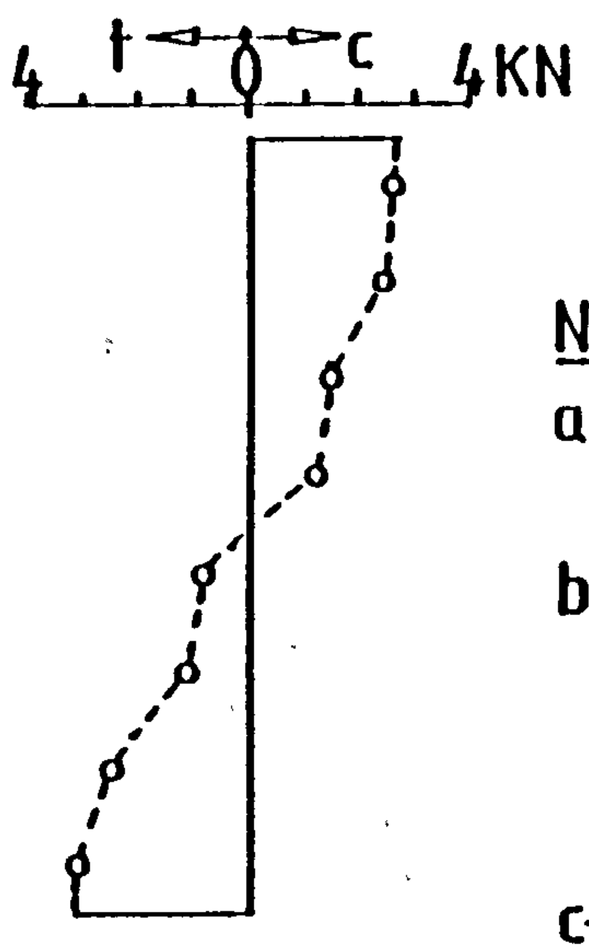

5-days

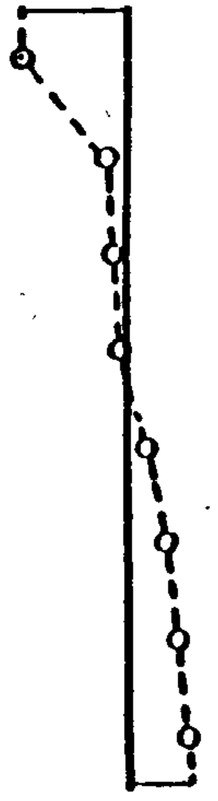

29-days

Notes:

a-all times given are from the start of heating.

b-the datum state for all measurements is that prevailing at the start of heating.

c-age of conc.on loading=28days

d- " " " " heating=61 "

e-supports non-co-linear for periods 0-13days thereafter co-linear.

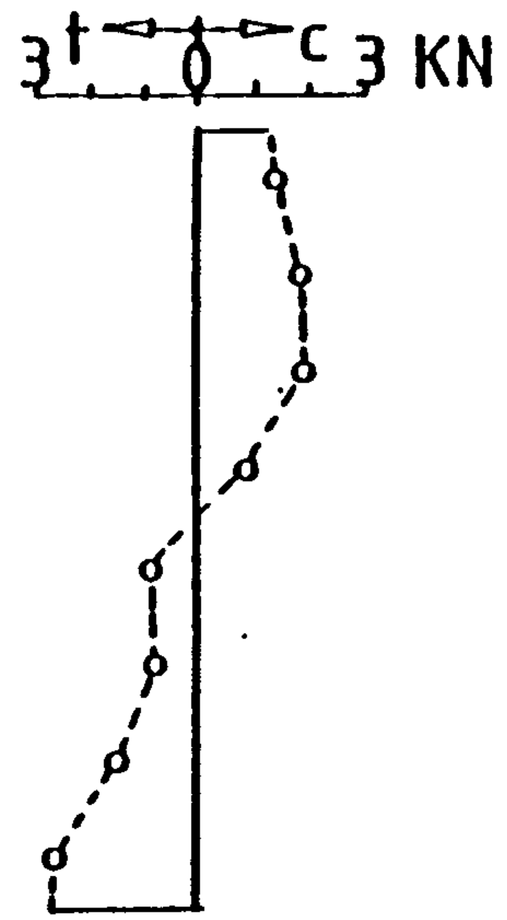

7-days

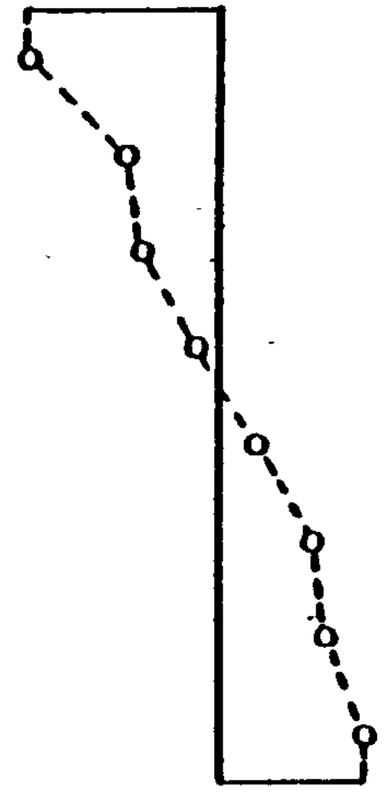

43-days

Fig.610 Changes in the force distns. measured over the inclusion section at the given ages of heating

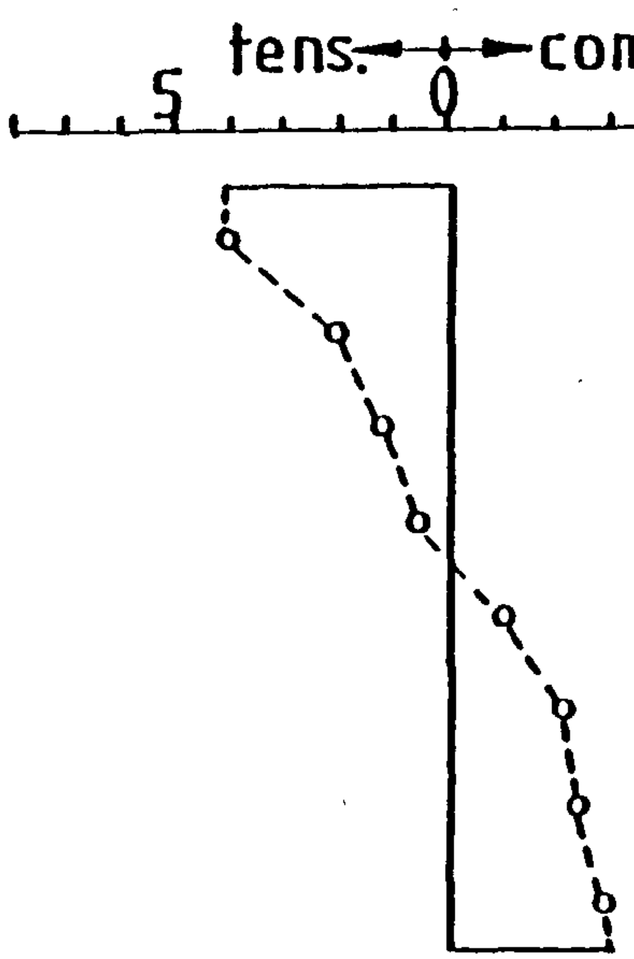

56-days since heating

Notes:

a-d notes given in fig.6·10 apply here.

e-supports co-linear unless otherwise stated.

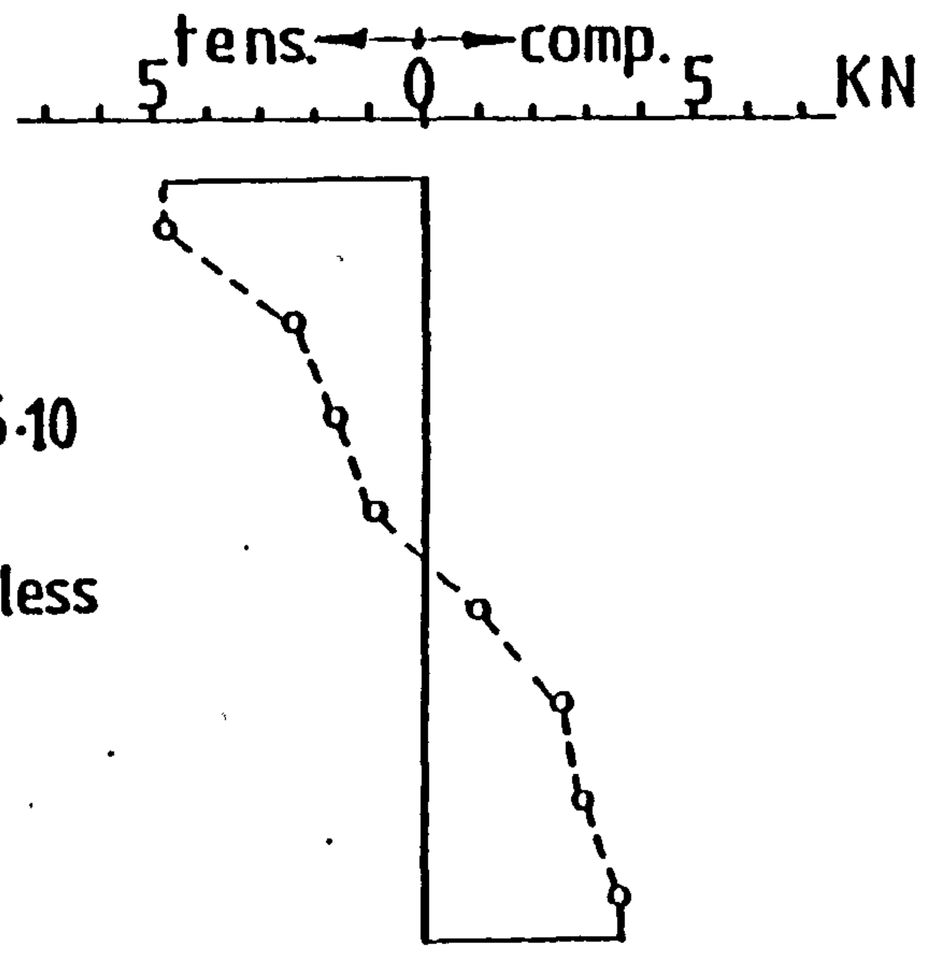

71-days

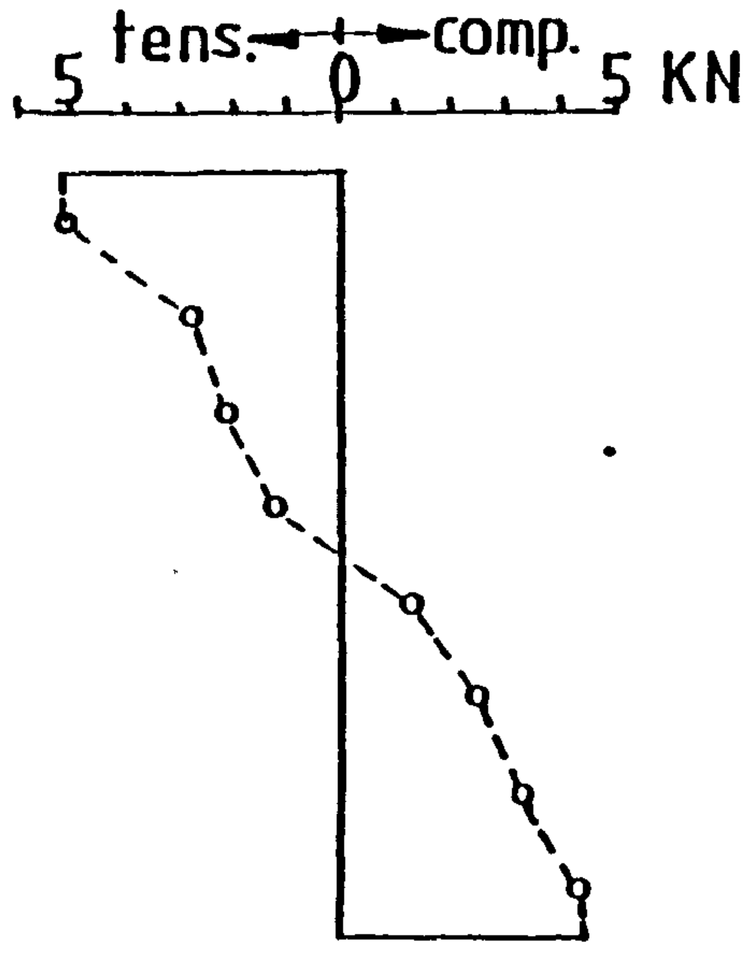

83-days

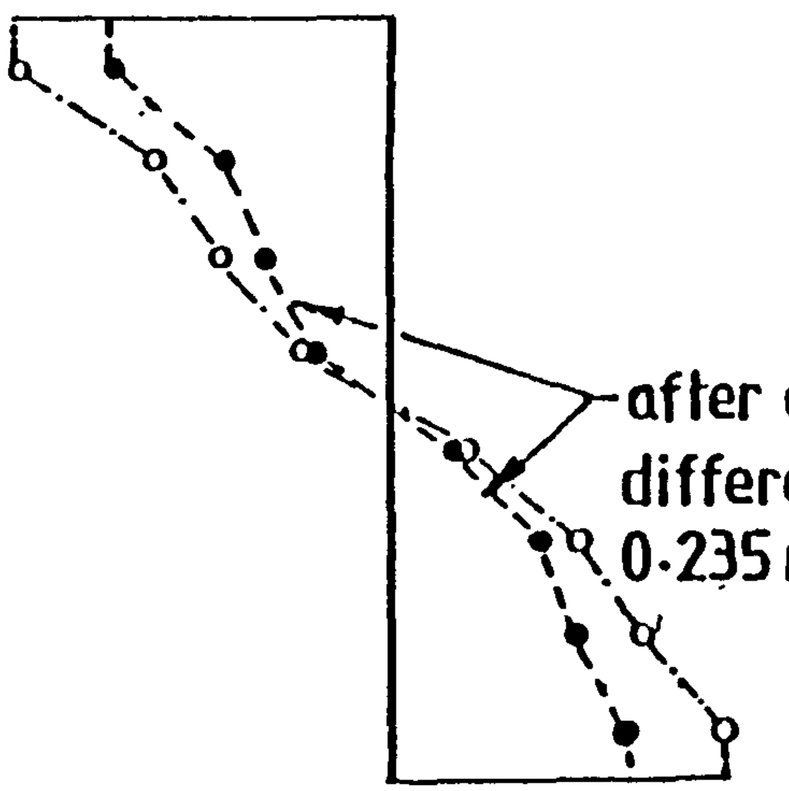

100-days

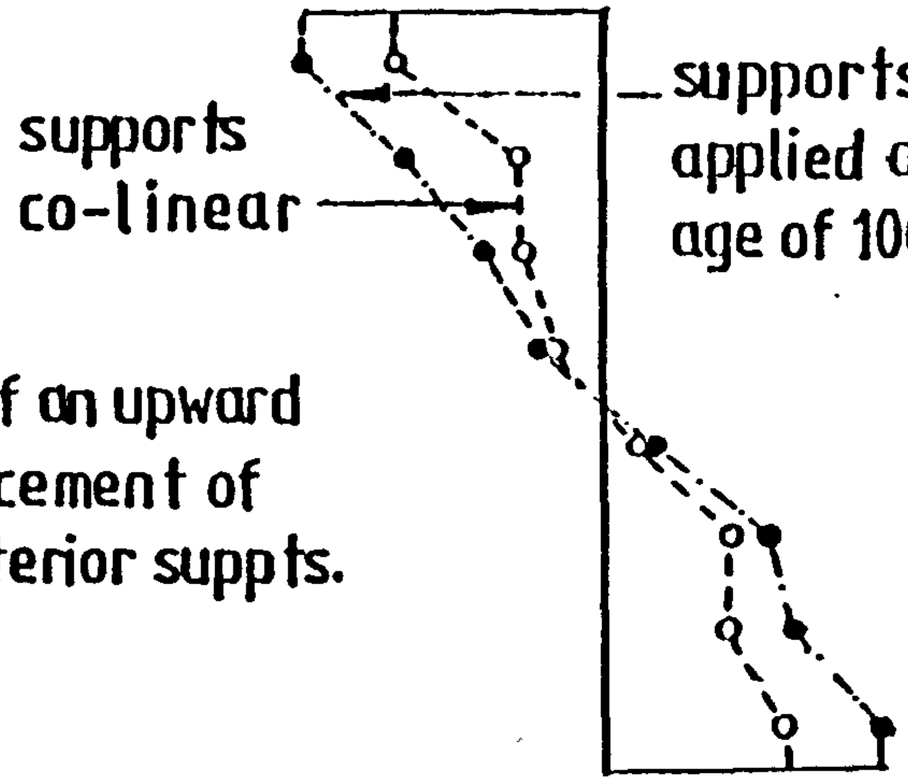

155-days

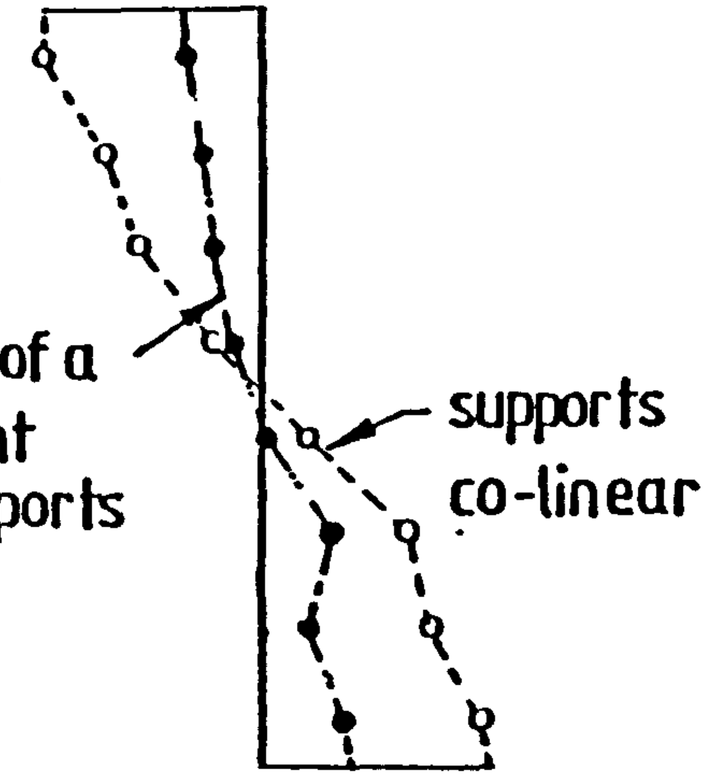

187-days

Fig.6·11 Changes in the force distns. measured over the inclusion section at the given ages of heating

Because of the rapid development of events in the test during the early hours of heating, it was not possible to record then the deformations of the inclusion elements, as this had to be carried out on both sides manually. The first set of results recorded, however, was when the temperatures reached their first stable state at the end of the second day of heating, at which time the interior supports were about 0.644 mm above the level of the end supports. Incidentally, this differential movement caused a maximum fibre stress variation of about 1.90 N/mm^2, or about 24% of the temperature stress, which could have had developed under a co-linear support situation.

From the data plot in Fig. 6.10, it is readily apparent that application of the temperature gradient gave rise to a sagging moment over the section, as confirmed by the observed reaction changes at the supports.

Examination of the data obtained at the successive ages of heating reveals that creep caused progressive decrease and the eventual removal of the initial temperature stresses created over the section. As time progressed, a force (or stress) system developed in the opposite sense, and continued to increase with time reflecting the observed increases in the hogging moment over the central span. Such increases in the section forces appeared to become progressively smaller with time, such that, at the third month of heating, the stress-inducing changes in the inclusion deformations could not be identified with certainty from the then measured total deformations. It was therefore reasonable to assume then that a steady state was being closely approached by the stresses at least over this section, and to carry out the sustained displacement tests referred to earlier, to ascertain the existence of such a state.

6.7.3 Behaviour under sustained displacements

The 100th day force diagram of Fig. 6.11 illustrates the immediate effects on the force distribution caused by the imposition of 0.235 mm upward displacements to the interior supports. As an illustration, the outermost elements of the inclusion block (i.e. No. 1 and 8) indicated an average force response of about 1.750 KN compared to a theoretical value of 1.731 KN calculated for a composite aluminium/ concrete beam.

While maintaining the differential displacements between the supports the elastic change in the force distribution showed a gradual diminution with time over the subsequent 55-days period of observation. It can be seen that the 155 day force profile, corresponding to the non co-linear support condition, approximates closely to that of the 100 day profile for which the supports were co-linear. This shows that creep almost completely nullified the effects of the differential displacements imposed on the supports. In consequence, the act of restoring the supports to the co-linear level, after the 55 days period, appeared to have the effects of newly applied downward displacements from a co-linear support situation. However, subsequent observations over the following 32-days period indicated an almost complete disappearance of these additional effects caused by the removal of the differential displacements. This can clearly be seen when comparing the 187th to the 155th days profiles corresponding to the co-linear support conditions.

On the same 187th day diagram of Fig. 6.11 are shown the immediate response of the inclusion elements to the imposition of a 0.505 mm differential downwards displacement applied between the inner and end supports of the beam. Once again the force response of the elements

compare favourably with the theoretical predictions. Nevertheless, unlike the previous displacement test, the forces measured at some later ages (see Fig. 6.12) indicated a rather unsettled pattern of behaviour after showing an initial tendency to recover. It is understandable, however, that in this case the situation was different in that both the amounts of displacements and the instantaneous effects on the force distribution were substantially greater. Furthermore, the test came at a later stage in time, when apparently the creep potential of the material was diminishing.

After being sustained for a period of 64 days, the differential settlements of the supports were finally eliminated in preparation for cooling.

6.7.4 Effects of a temperature cycle

Changes in the force distribution over the temperature cycle applied towards the end of the test are depicted in Fig. 6.12. It is evidently clear that cooling, as well as re-heating, with the supports co-linear caused the most severe stressing conditions over the section. The non-linear shape of the upper part of the stress diagram is an indication that cracking developed due to the sudden removal of the temperature gradient. The stress condition was, however, mitigated slightly over the subsequent cold part of the cycle, consistent with the observed recoveries in the supports' reactions over the same period of time.

The re-introduction of the temperature gradient on the beam significantly modified the total change in the force distribution previously reached under the sustained temperature regime. By superposing to the total force distribution in Fig. 6.9 it can be established that, after reheating, the state of stress was less severe than that

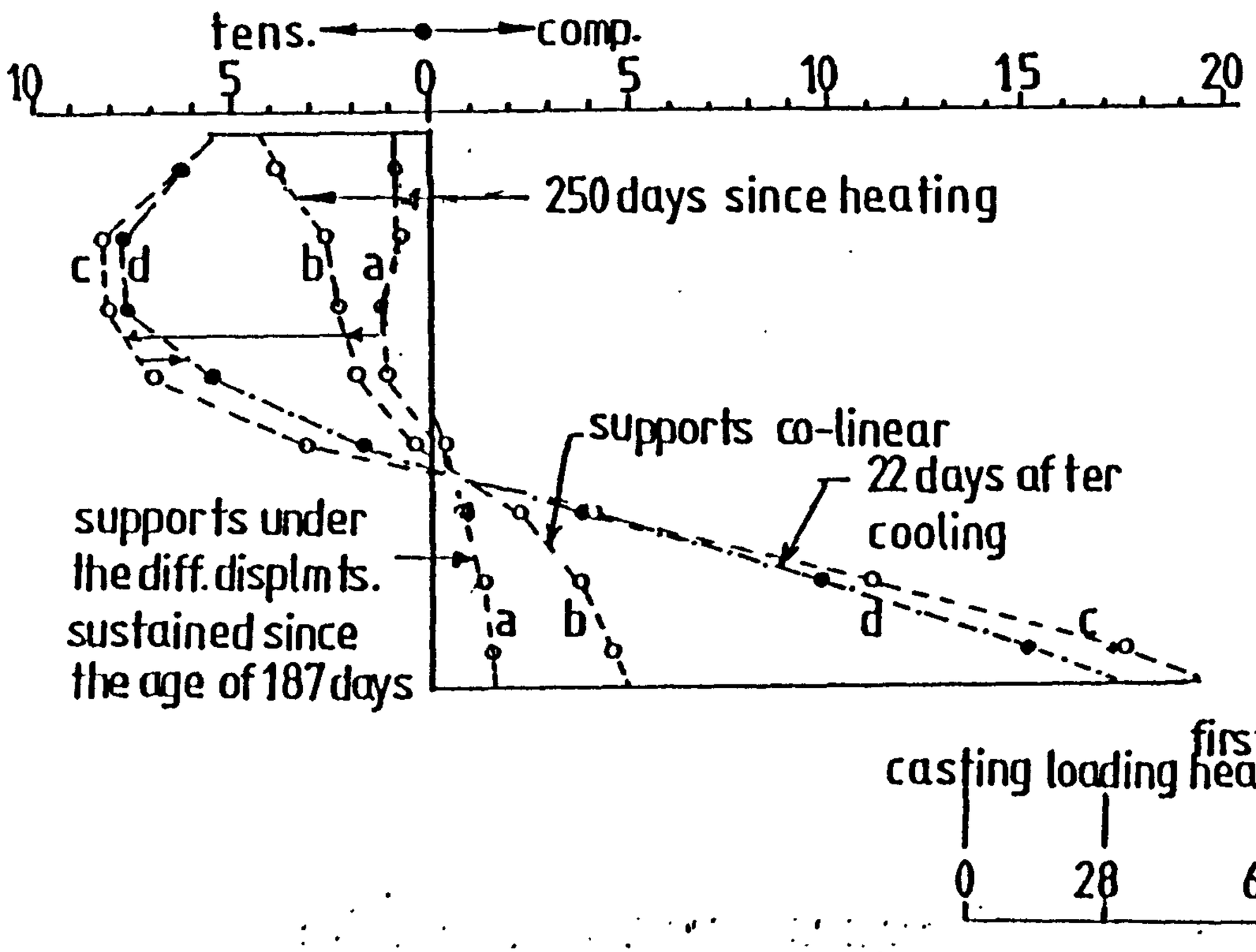

Notes on the illust. shifts of the force profiles:

a—►b immediate change due to removal of the differential support settlements

b—►c change on first cooling

c—►d recovery over the following cold period

d—►e change after first re-heating

e—►f change 23 days after re-heating

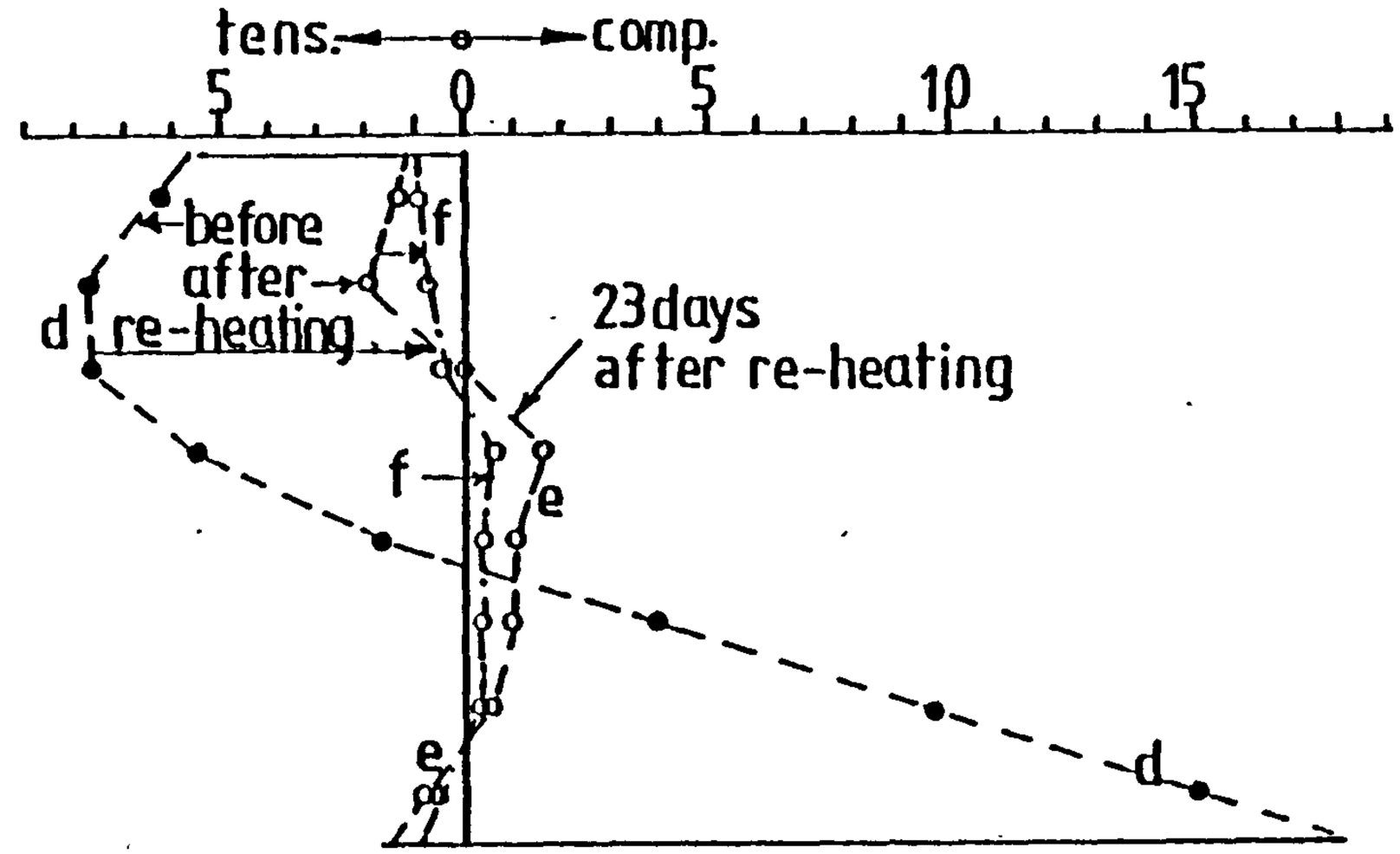

Fig. 6-12 Changes in the force distributions recorded before removal and after re-application of the temperature gradient. (the datum for all measurements is the state prevailing at start of heating)

existing before cooling was first applied. Although limited in scale, the results seemed to support the view that temperature cycling usually produces less severe stressing conditions than the sustained temperature regime.

6.7.5 Concrete stress redistribution over the intermediate span section - measured values vs. theoretical predictions

The time-dependent changes in the inclusion forces, observed under co-linear support conditions, which are described in Figs. 6.10 and 6.11, are superimposed to distribution, c, of Fig. 6.9; converted to concrete stresses, and plotted for some selected times in Figs. 6.13 and 6.14 against the step-by-step computer solutions. Specific thermal creep data used in the analysis have been evaluated from one set of the results expounded in Chapter 8. These were obtained from uniaxial creep experiments on laminated concrete specimens of the same material composition as the beam. The relationship between the specific thermal creep (pseudo-time) and real time in days since heating is displayed in Fig. A.3 of the Appendices. Numerical data and other relevant details of the analysis procedure are given in Table 6.1 .

Within the accuracy limits of the experiment, the comparison shows a good measure of agreement between theory and observations, in spite of the simplifications introduced in the analysis formulations. These concern the adoption of the specific thermal creep concept, the disregard of the delayed elastic strains, and the use of a constant uniform modulus of elasticity for the concrete, etc. The ability of this simplified approach to describe satisfactorily the process of stress redistribution over a non-uniformly heated member section is thus clearly demonstrated.

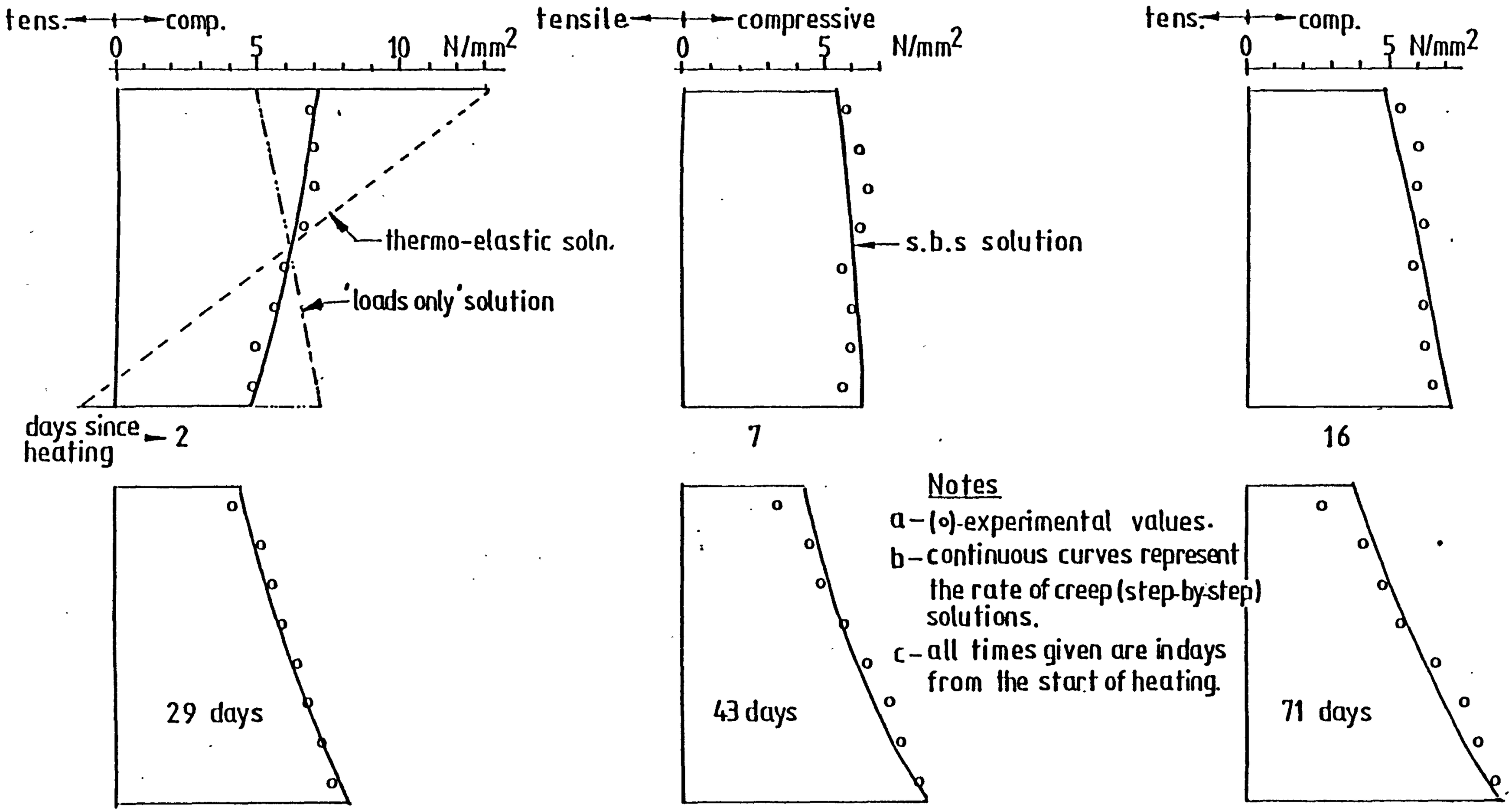

Notes

a – (o)-experimental values.

b – continuous curves represent the rate of creep (step-by-step) solutions.

c – all times given are in days from the start of heating.

Fig.6.13 Comparison between theoretical predictions and measured values of stresses at the given times

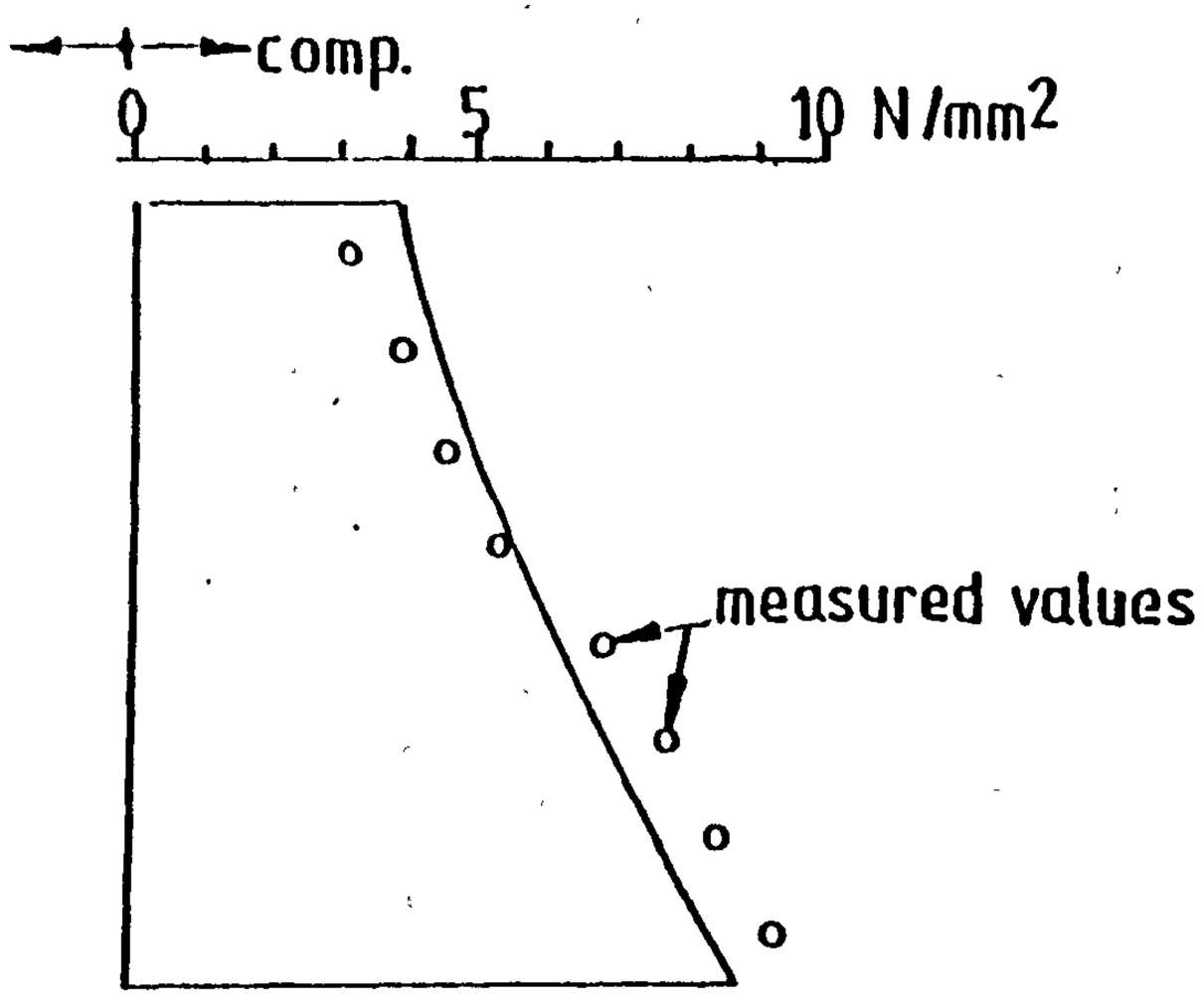

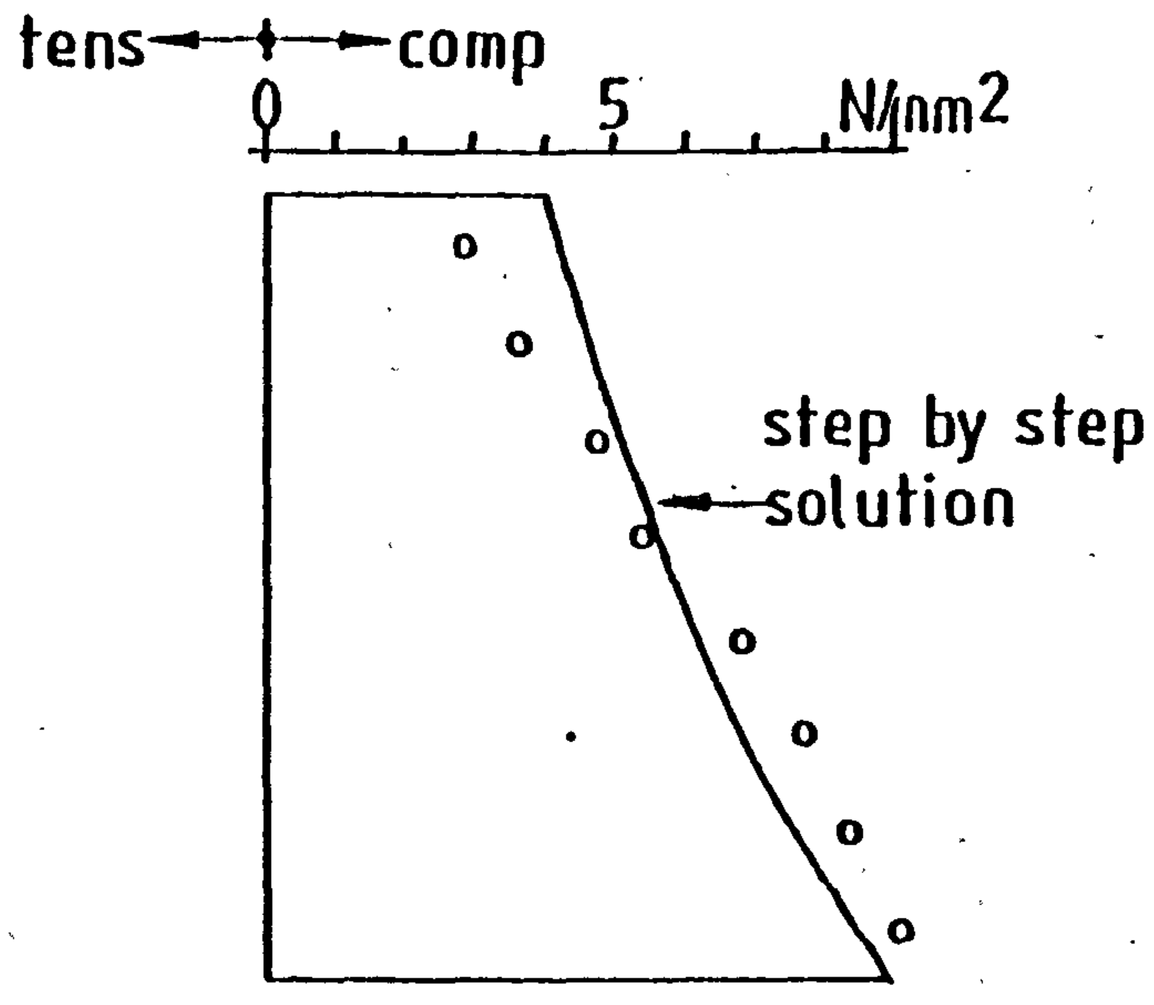

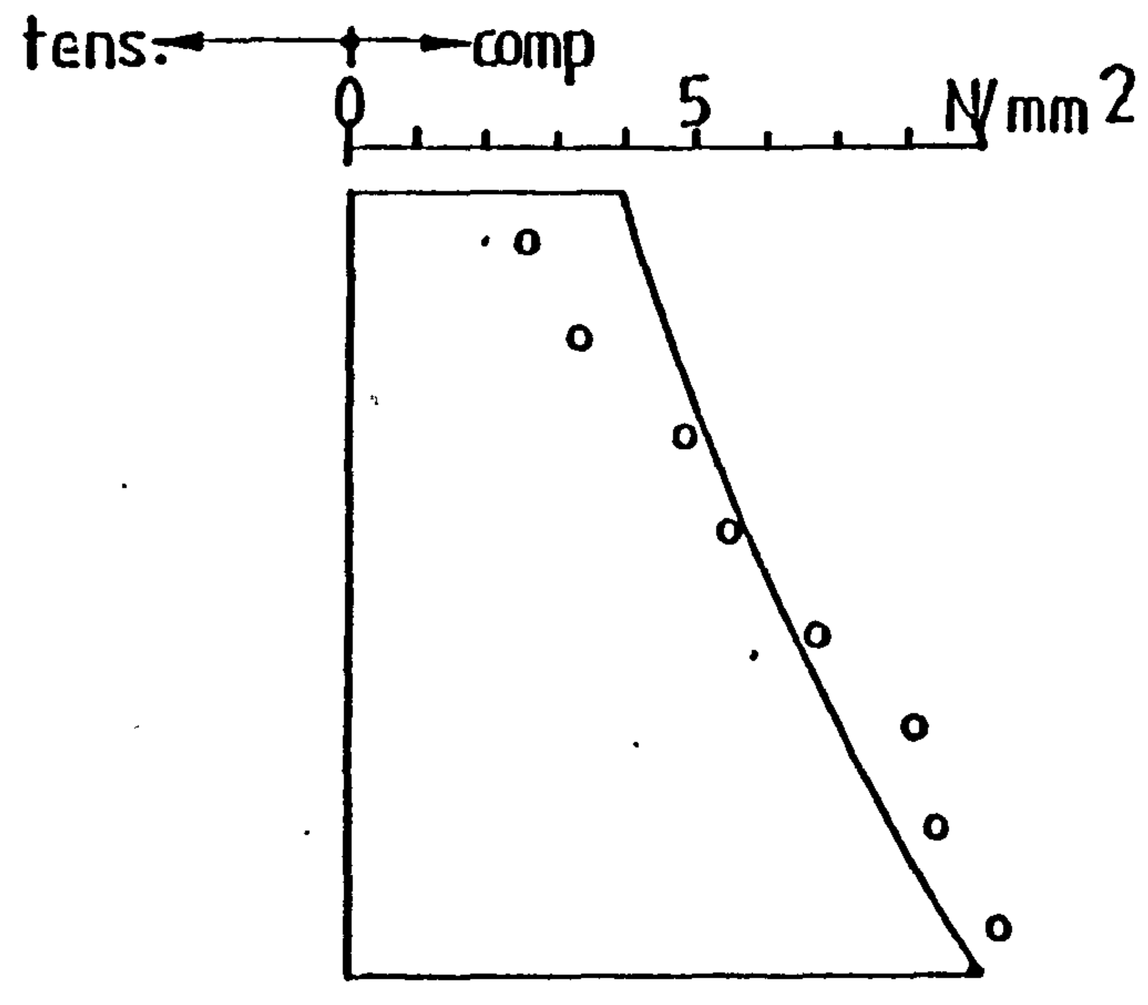

days since heating → 83 100 155

Fig 6.14 Comparison between theoretical predictions and measured values of stresses at the given times after heating. (see notes a, b & c in fig 6.13)

6.7.6 Stress redistribution over the mid sections of the end spans - theoretical solution

The states of stress over the point load sections of the end spans at some selected ages, as revealed by the analysis, are depicted in Fig. 6.15. The results indicate that both the rate and magnitude of stress changes due to creep were significantly smaller over these sections than those over the intermediate span. This was consistent with the observed changes in the span moments referred to earlier in Section 6.3. The results reveal also the diminishing trend of change in stresses with increase in the specific thermal creep value, in common with the behaviour of several other parameters observed.

When comparing these with the results of the other sections, it can be seen that the critical stress situation corresponding to time zero (an elastic theory prediction) was being shifted, at large times, from the section under the point load to that of the interior span. This indicates that the elastic theory cannot be relied on in predicting the stresses under such conditions.

6.8 Steady state stresses - Observations vs. predictions

The direct measurement results presented hereinbefore evidenced a progressive decrease with time in the rate of stress redistribution over the elastic inclusion section of the beam. This was such, that after about three months of sustained heating further stress changes were becoming insignificantly small and often uncertain, which signified that the stresses were approaching a limiting state. The 100th day distribution is regarded here as a close enough representation of such a state, and used as a basis for comparison with theoretical solutions.

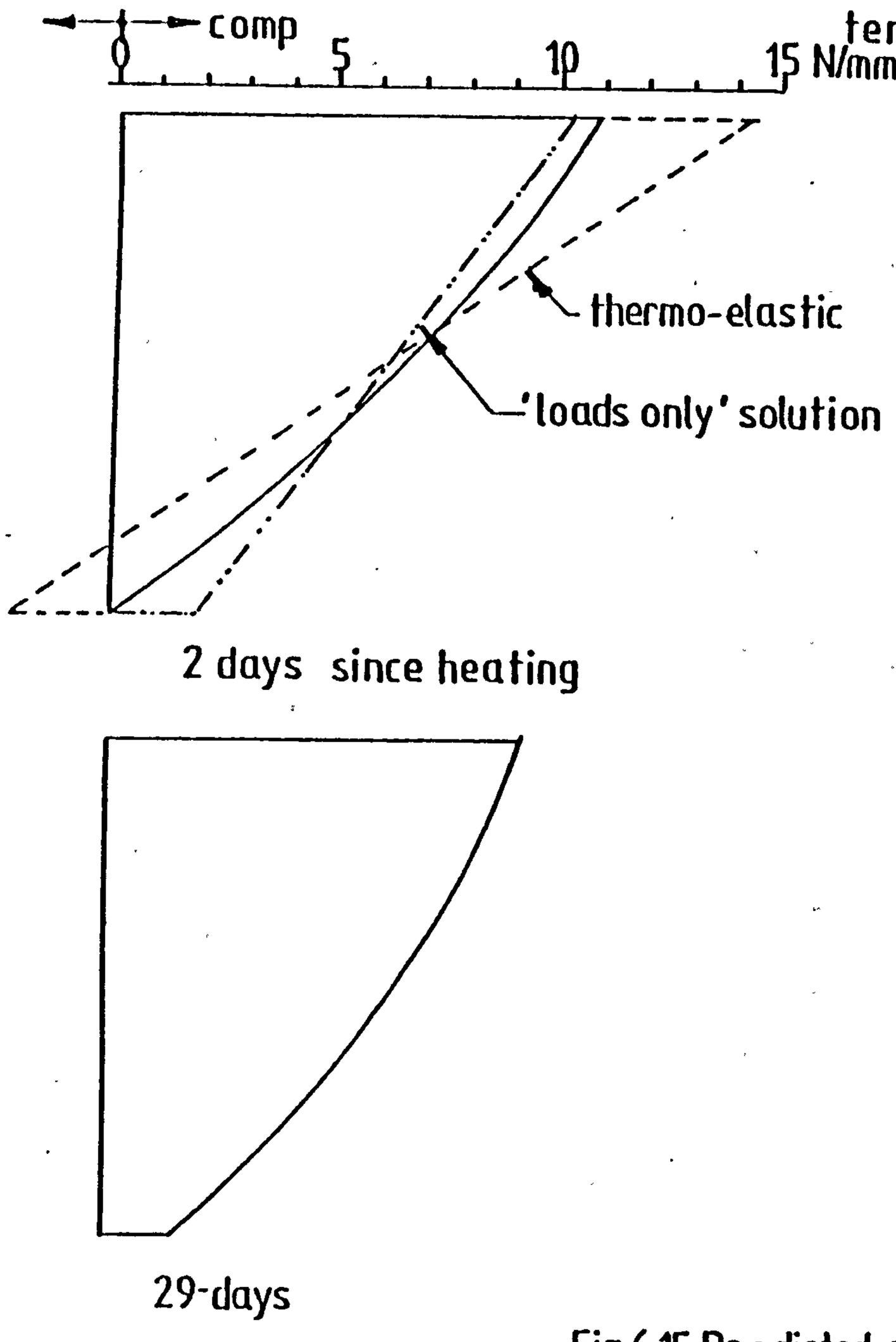

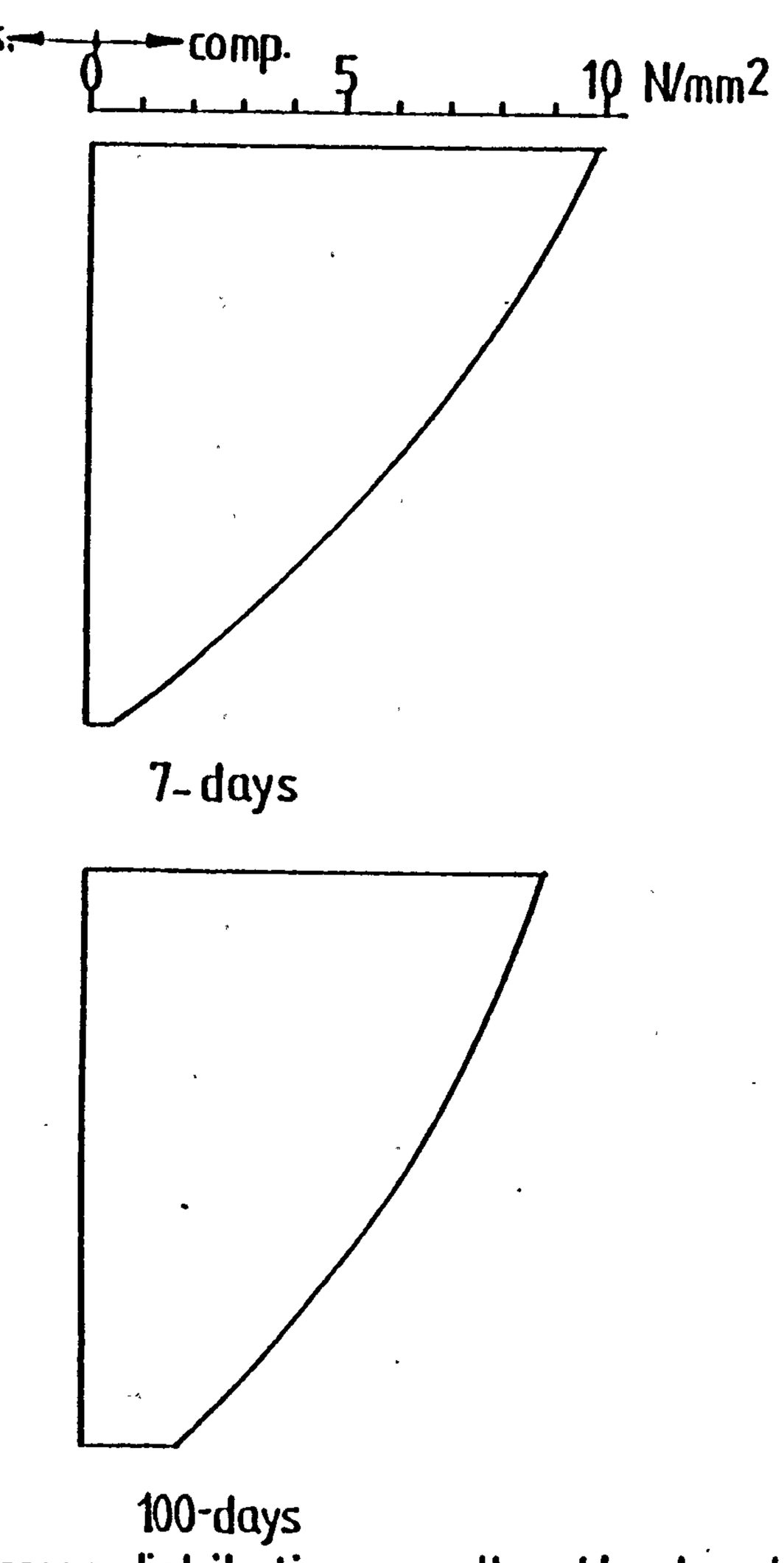

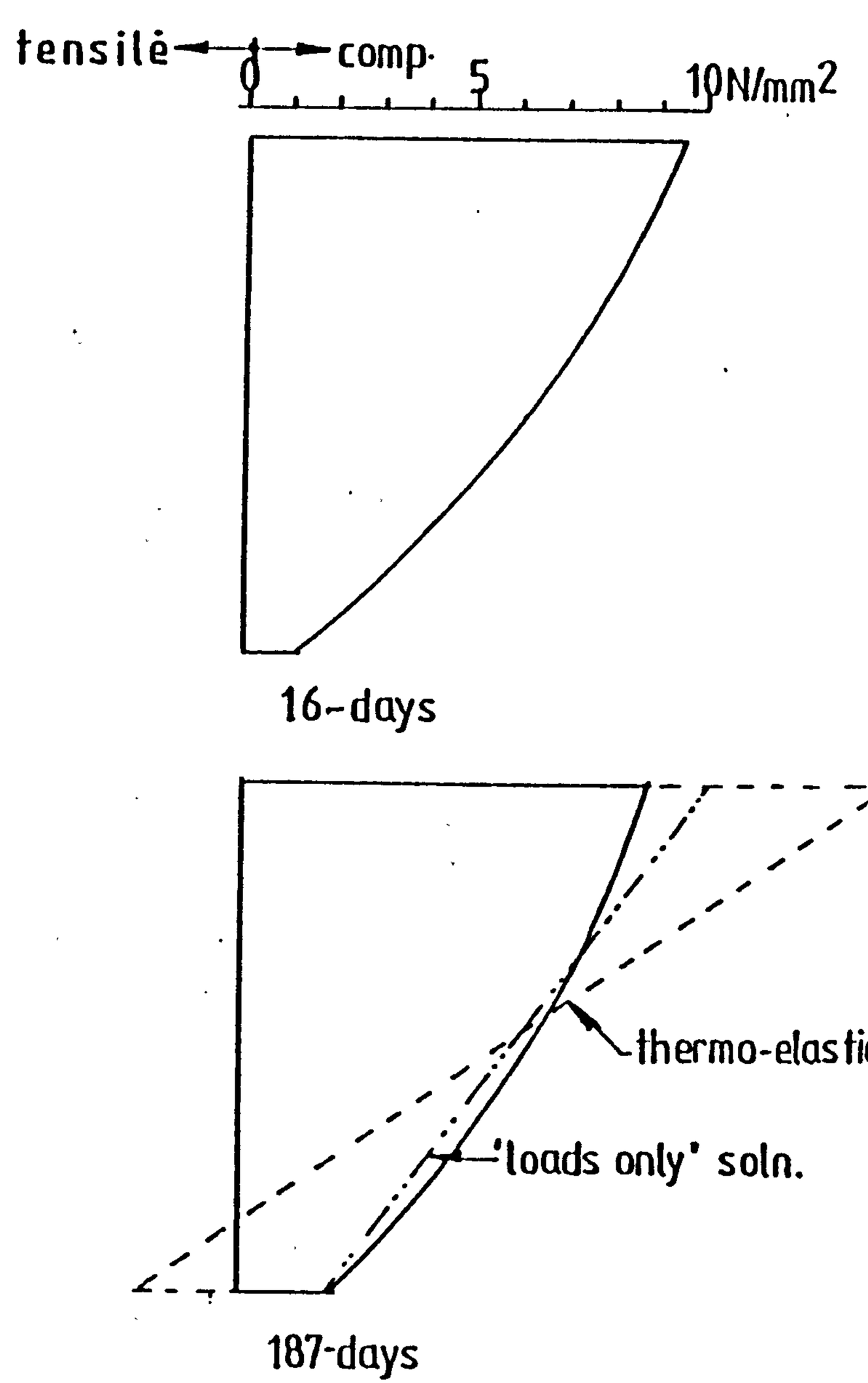

Fig.6-15 Predicted stress redistribution over the pt.load section

The 'steady state' theory approach, as described in Chapter 4, has been used to calculate the limiting long-term state of stress across the intermediate span section of the beam. Numerical data and calculation details are given in Appendix III. Almost identical results have been obtained from the iterative step-by-step analysis procedure at large values of the specific thermal creep. These are plotted against the 100th day stress profile in Fig. 6.16. The near correspondence of the predicted with the measured stress values can be seen at all but a few of the element levels over the section. The measure of disagreement at these levels, however, is shown to fall within a 0.50 N/mm^2 stress margin, which under the circumstances is considered to be acceptably small.

6.9 Influence of the elastic inclusion on the short- and long-term behaviour of the beam

The presence of the elastic inclusion within the structure of the concrete beam tested can be expected to cause bending stress concentration at the discontinuity sections, and would probably influence its behaviour. Thermo-elastic and creep-dependent stress analyses have consequently been carried out in order to assess the severity of the concentration and the extent of its influence on the beam behaviour.

In Table 6.1, the stresses calculated for the sections of contact and those under the point loads are listed and compared to a similar set of results obtained for a homogeneous concrete beam, i.e. having no elastic inclusion.

Examination of the results reveals a maximum disturbance in the thermo-elastic stresses of only ± 0.20 N/mm^2 to exist at the outermost fibres of the discontinuity sections. In practice such value should not have developed since the full temperature loading was not applied instantly

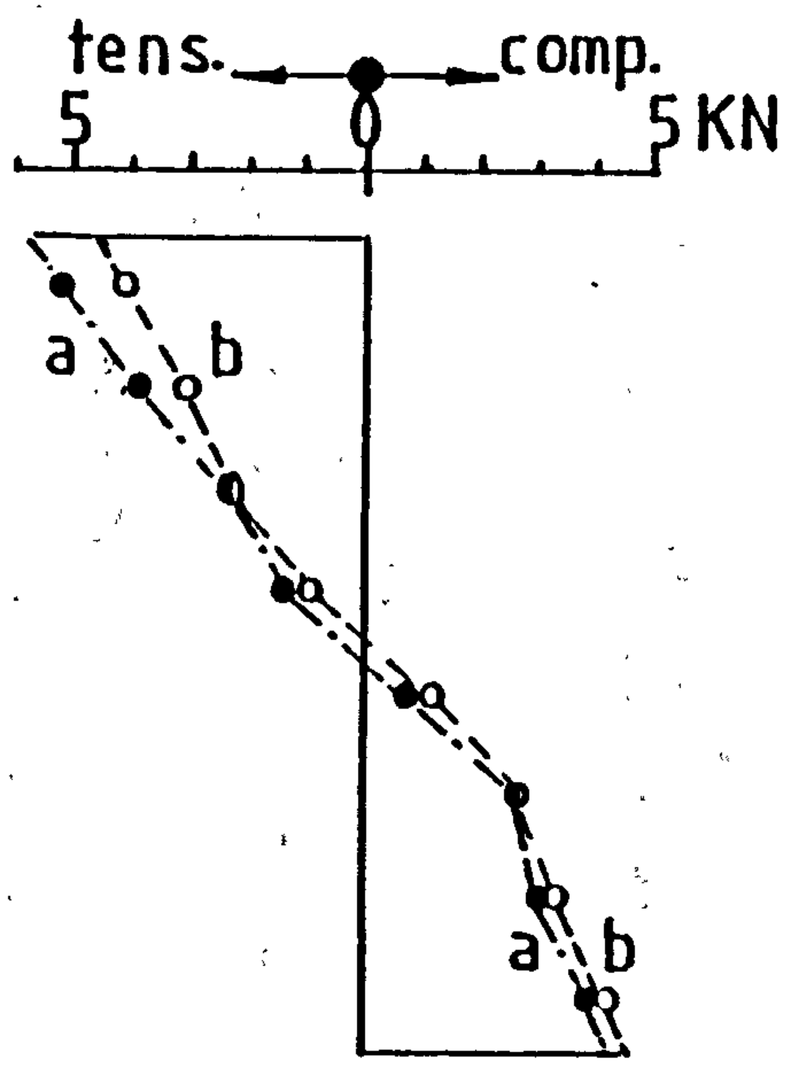

Combined plot of the net changes in the force distributions observed at two ages :
a - 100 days after heating
b - 187 " " "
] co-linear supports

Ref. State : Fig 6.9c

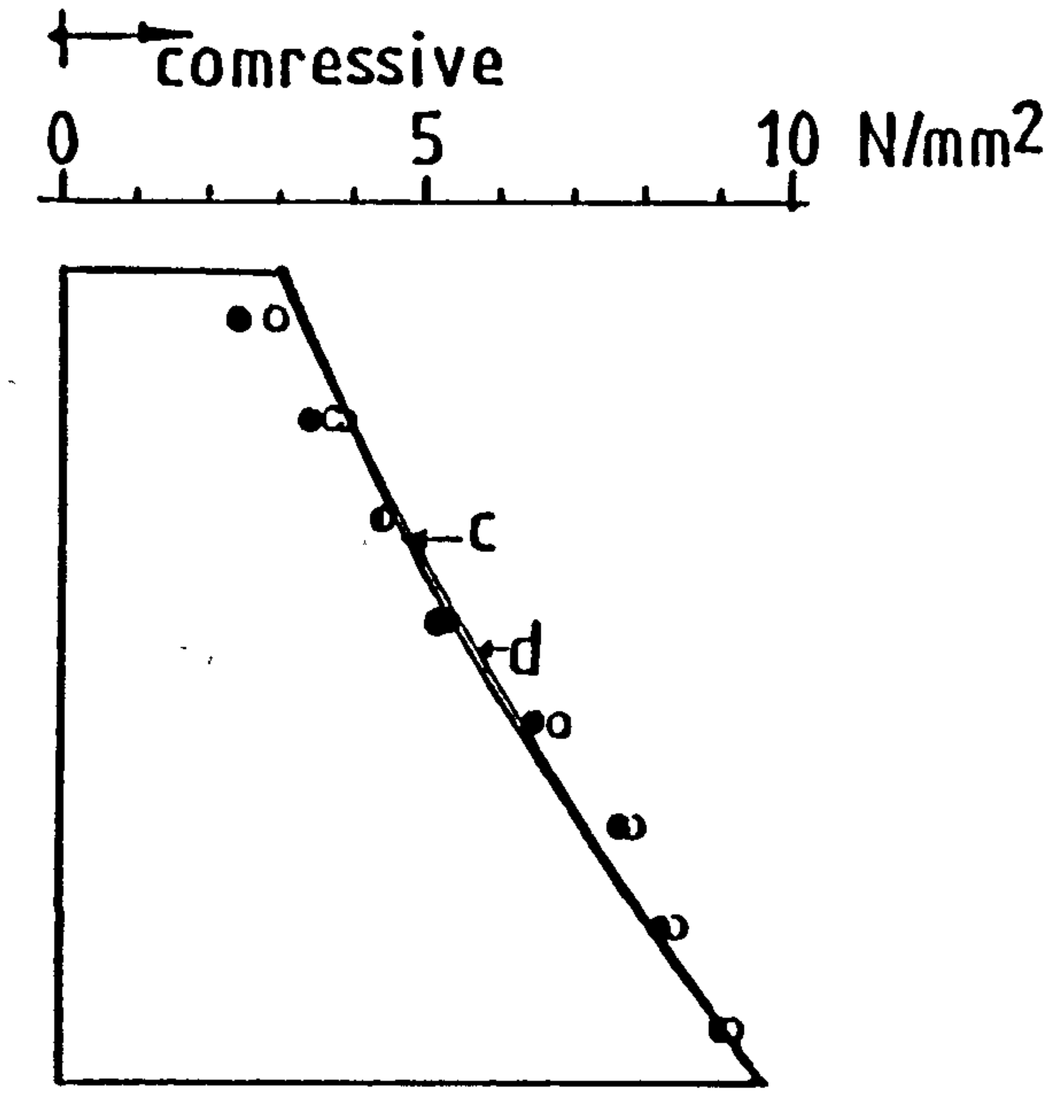

Stresses

Predicted solutions
c - steady state theory
d - rate of creep solution at 'c' = 2.4×10^{-6} per N/mm^2 per °C

Fig 6.16 Measured vs. predicted limiting long-term stresses within the central span.

Table 6.1

$c \times 10^{-6}$		0		0.40		0.60		1.20		2.40	
Section	Element No.	c	h	c	h	c	h	c	h	c	h
a-a	1	-1.23	-1.33	.78	.84	1.41	1.49	2.45	2.51	2.98	2.99
	2	.86	.79	2.60	2.64	3.09	3.15	3.83	3.87	4.14	4.15
	3	2.94	2.90	4.25	4.27	4.57	4.60	4.99	5.01	5.12	5.13
	4	5.03	5.01	5.74	5.75	5.87	5.88	5.98	5.98	5.87	5.97
	5	7.11	7.13	7.09	7.08	7.01	7.00	6.83	6.81	6.70	6.69
	6	9.20	9.24	8.31	8.28	8.02	7.99	7.56	7.53	7.34	7.33
	7	11.29	11.35	9.41	9.36	8.91	8.85	8.19	8.15	7.91	7.90
	8	13.37	13.47	10.40	10.34	9.68	9.61	8.75	8.70	8.41	8.40
b-b	1	- .27	- .46	4.65	4.77	6.04	6.20	8.17	8.29	9.14	9.17
	2	1.54	1.41	5.12	5.21	6.10	6.21	7.55	7.63	8.17	8.18
	3	3.36	3.27	5.56	5.61	6.13	6.20	6.94	6.98	7.25	7.26
	4	5.17	5.14	5.96	5.98	6.14	6.16	6.34	6.35	6.37	6.38
	5	6.98	7.00	6.33	6.32	6.12	6.10	5.75	5.73	5.55	5.54
	6	8.79	8.87	6.68	6.62	6.08	6.01	5.17	5.12	4.76	4.75
	7	10.60	10.73	6.99	6.90	6.02	5.91	4.60	4.52	4.02	4.00
	8	12.41	12.60	7.28	7.16	5.94	5.97	4.05	3.94	3.31	3.29

Effects of the elastic inclusion on the short- and long-term stresses over the two sections shown below

Notes: Col. (c) stresses calculated for the composite beam
Col. (h) stresses calculated for the homogeneous beam
Stresses in N/mm^2
Pseudo-time $c \times 10^{-6}$ per N/mm^2 per ^oC
Sign convention: compressive stress (+ve)

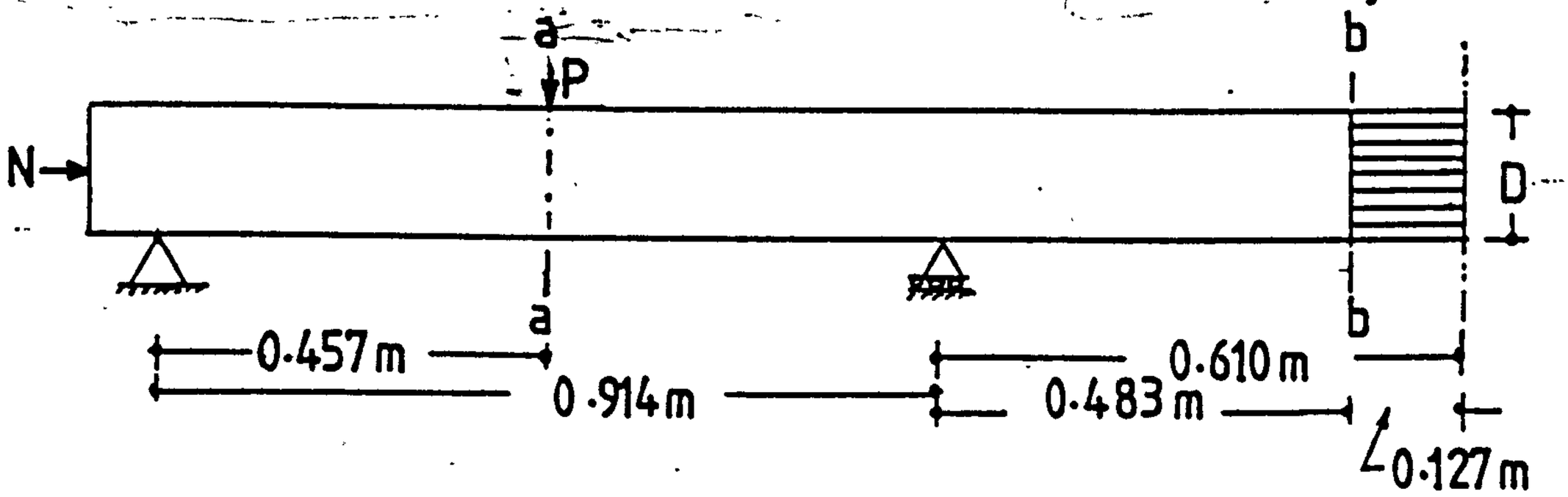

Numerical data

conc.sec. b×D = 101.6×152.4 mm
prestress N = 94.0 KN
transv.load P = 8.0 KN
the temp loading is that shown in fig 6.2
specific th. creep capacity of the concrete = 2.4×10^{-6} per N/mm^2 per ^oC
$E_c = 34.5\ GN/M^2$, $\alpha_c = 12.5\times10^{-6}/^oC$
mean cross section area of a typical inclusion element = 687.2 sq. mm
$E_a = 66.6\ GN/M^2$, $\alpha_a = 23.0\times10^{-6}/^oC$

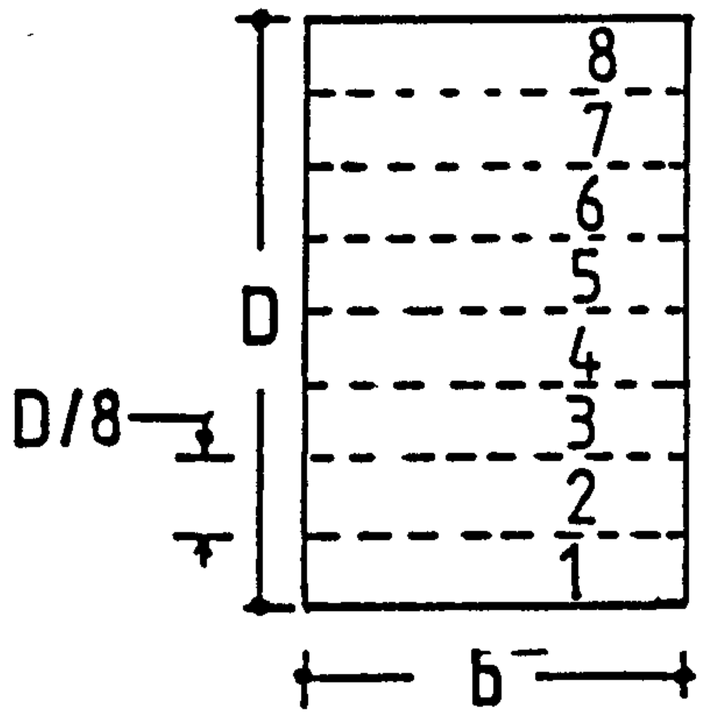

typical concrete sec. of the beam subdivided into eight equal elements

as assumed in the analyses. Nevertheless, this effect is shown to disappear with time and the corresponding stresses of the two solutions tend towards the same long-term values.

Further examination of the results reveals rather insignificant influence, and that concerns the stress redistribution rates with time. In the homogeneous beam these are slightly higher compared to the composite beam, because part of the latter was replaced by a non-creeping material.

6.10 Concluding remarks

The direct stress measuring technique employed in this investigation had successfully served its intended purposes with the minimum of interference in the results. In all stages of measurements, there had been a near total agreement between the moments indicated by the elemental forces of the inclusion and those indicated by the external boundary actions observed at the supports. The information gained from this experiment, within its limits, warrants the following conclusion being made.

1. Under the sustained influence of external loading and temperature crossfall, stresses and supports reactions undergo a process of redistribution with time.

2. The redistributions occur fairly rapidly but slow down with time, and tend to become stationary after a sufficiently long period.

3. The extent of redistribution is such that the initial thermo-elastic stresses disappear completely in a fairly short period of time, and with the sustainment of heating the moments at some sections change in both sense and magnitudes.

4. There always seems to be a preferred long-term state to which the stresses tend, although displacements may continue to develop with time.

5. Cooling, from the steady state or after a long period of sustained heating, usually brings about the most severe stressing over sections previously having experienced the largest stress changes due to creep.

6. Based on the specific thermal creep concept, the rate of creep method of analysis is able to predict closely the time-dependent stress changes, even when no consideration is given to the recovery strains.

7. Both the rate of creep method at large values of the specific thermal creep, and the steady state theory, are adequately capable of predicting the limiting long-term state of stresses.

CHAPTER VII

EXPERIMENTAL WORK - PART 2

DESIGN, CONSTRUCTION AND TESTING PROCEDURE OF A LAMINATED CREEP RIG

Chapter 7 - Synopsis

This chapter describes the construction and testing technique of a novel creep rig designed with the objective of investigating the influence on creep of the moisture flow caused by non-uniform heating. The especially designed rig permitted temperature gradients to be applied across laminated concrete blocks formed from a series of closely held rectangular columns (44.5 × 102 × 305 mm), while being loaded in compression independently, and free from interface stresses. 'No-load' comparison specimens were tested concurrently to provide shrinkage data for the creep tests. The test results are detailed in Chapter 8.

7.1 Objective

The thermal creep of concrete has broadly been studied on either moisture stable or drying samples with little or no attention to the effect of moisture movement caused by temperature gradients. In general, the material behaviour is sensitive to changes in its hygral state; and because the moisture movement may induce additional strains which could have some, as yet, unknown effect on the creep deformation, further investigations into this aspect of material behaviour are needed.

The experimental work described in the following sections was designed with the main objective of developing a better understanding of the creep behaviour of concrete within the sphere of influence of moisture movement. A secondary purpose was to investigate the temperature change effect upon the creep, after a long period of sustained heating at constant temperature.

To perform uniaxial creep experiments in attendance of temperature gradients a specially designed apparatus was developed. It enabled a set of rectangular section columns to be loaded independently, while being held in close proximity to each other forming a laminated block free from interface stresses.

Heating facilities were provided to create the desired temperature crossfalls and therefore to activate the moisture movements through the laminations of the test blocks. The same heating environments were provided across identical unloaded companion specimens, which were cast and tested concurrently with the loaded sets, in order to provide the necessary shrinkage data for the creep experiments.

A number of tests with different moisture flow and temperature conditions was carried out. The details of these and other tests carried out to investigate the influence of moisture flow on the coefficient of thermal expansion of concrete are given with the results

in Chapter 8. In the following sections, details are given of design of the experiments, the instrumentation and testing techniques employed.

7.2 Criteria of the specimen geometry

In uniaxial creep experiments, it is important that the initially applied uniform state of stress is maintained during the period of investigation. When a temperature gradient is imposed across the loaded section of the specimen the uniformity of stress is likely to be perturbed and flexural deformations may be introduced into the problem. It was considered possible, however, that such effects could be eliminated by opting for a laminated specimen instead of a solid one. In this case the temperature distribution is expected to be fairly uniform within the thickness of each lamina. Fig. 7.1 shows a schematic layout of the creep and its shrinkage control block proposed for the experiments. The arrangement appeared to be convenient for the application of temperature gradient symmetrically on both blocks, by introducing a single heat source in between.

7.3 Loading system

Although loading and strain measuring techniques may differ, the principles of determining the uniaxial creep characteristic of a given concrete are basically the same. The loading device, for instance, is required to produce a uniform state of stress on the specimen with reasonable speed and to be able to maintain such condition for the duration of the test with minimum attention.

Hydraulic pressure loading, though being increasingly used in the field of creep research, was excluded from these experiments in the early stages of planning for two reasons:-

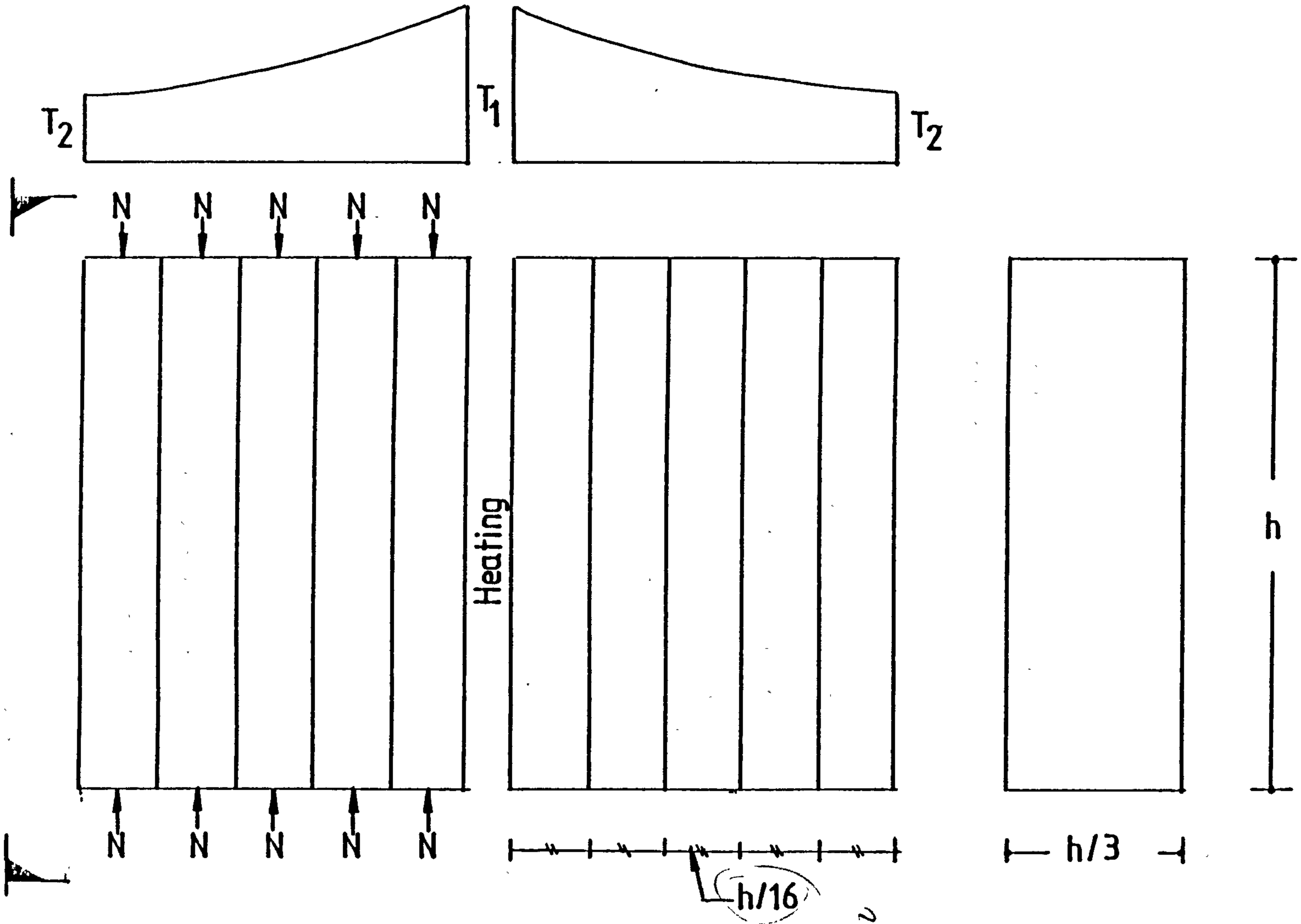

Fig.7.1 Schematic design layout of the laminated creep and shrinkage experiments

h=304.8mm (12.0 in)

1. the close proximity of the loading stations, as it was intended to load each lamina of the test block independently
2. the multiplicity of the pressure outlets required to load all the specimens incorporated in the experimental program.

In searching for an alternative method of loading, the system which utilises the energy stored in the highly strained members of a low stiffness frame appeared to be a convenient choice for these experiments. Although the task of loading using this method is somewhat tedious, the risk of load reduction compared with pressure loading is minimum.

Having adopted a mechanical system of loading, it was realised that the compression frame design should satisfy two main requirements:-

1. To carry the maximum load prescribed for the tests and to accomplish the above stated conditions of stress.
2. Its lateral dimensions should not exceed the thickness of the test piece so as not to inhibit positive contact of the concrete laminations incorporated in any one block.

As a result, a comparatively simple design of the compression frame was developed, a description of which is given in the following section.

7.4 Design layout of a typical creep rig unit

For the descriptions to follow, references are made to Fig. 7.2 and Plate 7.1.

Basically, each concrete test piece is mounted vertically in series with a thin walled dynamometrical tube (having the same outside dimensions) with a mild steel bearing plate at the joint interface. A system of mild steel rollers and bearing plates at the far ends of the column transmits the force applied by a bright mild steel compression

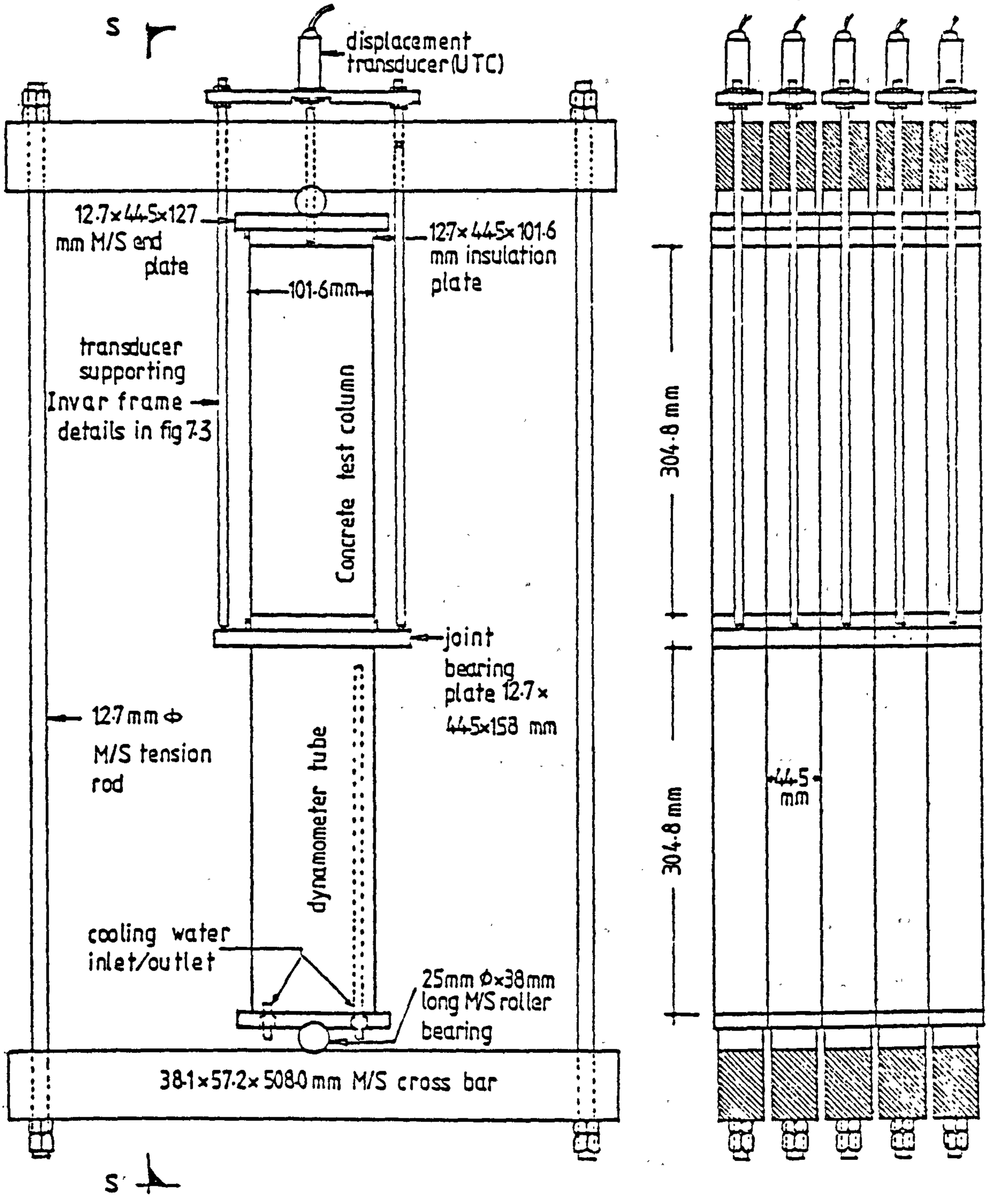

Fig 7·2 General design layout of the proposed creep rig

frame formed around and in the largest plane of symmetry of the central column by two rectangular section cross bars held by two tension rods. The force induced in the column is ascertained from the deformation of the pre-calibrated dynamometrical tube.

A displacement transducer mounted in an Invar frame through the overhead cross bars measures the time-dependent movement of the concrete test piece. A more detailed description of this system is given in Section 7.5.

7.4.1 Conceptual details and other considerations

In designing the compression frame, it was necessary that the tension rods were located at least 18.0" (457 mm) apart so as to allow sufficient access for measuring the tube deformations with mechanical strain gauge. A section of 1.5" × 2.25" (38.10 × 57.2 mm) and an overall length of 20" (508 mm) were arrived at. This gives a maximum load capacity of about 40 KN when the maximum stress/yield strength ratio of steel is about 54%. The tension rods used were 0.5" (12.7 mm) of the same steel quality as the cross bars.

All bearing plates used were 0.5" (12.7 mm) thick and having the same width as that of the concrete specimen, i.e. 1.75" (44.5 mm). The end plates were 5" (127 mm) long while the intermediate common bearing plate was made 1.25" (32 mm) longer for the purpose of displacement measurements described in Section 7.5. Four locating pins were fixed in each plate for the alignment of the tube and specimen axes with the point of loading. Provision for water circulation was made at the bottom plate in order to cool down the dynamometrical tubes if found necessary.

With the exception of specimens tested at room temperature, two Sindanyo asbestos plates 0.5" (12.7 mm) thick were precisely cut to the

size of the concrete section and bonded to the ends of the specimen, serving as heat insulation.

With regard to the dynamometrical tube, it was decided to go for aluminium rather than steel for two main reasons:-

1. the deformability of an aluminium tube is about three times that of a comparable size steel for a given load, thus allowing more accurate load measurements
2. as a need for water circulation into the dynamometer tube during the heating program was anticipated (although this was later found unnecessary) steel would rust
3. aluminium has a weight advantage over steel and this would help in the handling of the components and mobility of the rigs.

7.5 Strain instrumentation

The purpose of instrumenting the specimens was to obtain a record of strain history during loading under variable thermal conditions.

In deciding upon the appropriate instrumentation the use of internal strain gauges was eliminated at an early stage in this study, for a number of reasons:-

1. Since most commercially produced strain gauges are temperature sensitive and moisture dependent, an elaborate calibration and protection technique would be necessary in order to obtain meaningful data from the measurements
2. the presence of internal strain gauges within the relatively small thicknesses of the laminations might disturb the strain field and/or the transfer of moisture

3. in the likely event of gauge failure in any one or more of the test pieces, the risk of perturbing the results would be very high.

These have influenced the alternative choice of monitoring the movements by external sensors.

Universal Transducing Cells (UTC) made by Statham of the United States were selected for this purpose. These highly sensitive small displacement transducers are basically unbonded strain gauges having a nominal bridge resistance of 350 Ohm. A typical cell is shown in Plate 7.2. They have been used successfully in long-term experiments (60) in which they proved to have a remarkable degree of stability over a long period of time.

7.5.1 Transducer frame

The Statham transducers were mounted on specially designed Invar frames, with their probes pointing down the vertical axes of the concrete specimens in the manner shown in Fig. 7.3. Central Invar rods, precisely following the axial movements of the concrete specimens, were used to transmit these movements, by direct contact, to the transducer probes.

Each frame was made of 178 × 25 × 9 mm Invar plate and two 8.0 mm ϕ Invar rods. The plate was fastened to the threaded ends of the rods with steel nuts; this was preferred to permanent fixation, so as to allow the freedom of adjusting its level to suit the height of the central rod. In addition it would enable the starting of a new datum of measurements whenever the displacement range of the cell has approached its limit.

A 32 mm wide recess was made in the middle of the plate reducing the plate thickness to 4 mm and a 16 mm hole was drilled at the centre, in order to fasten the cell in the required position. Lateral stability

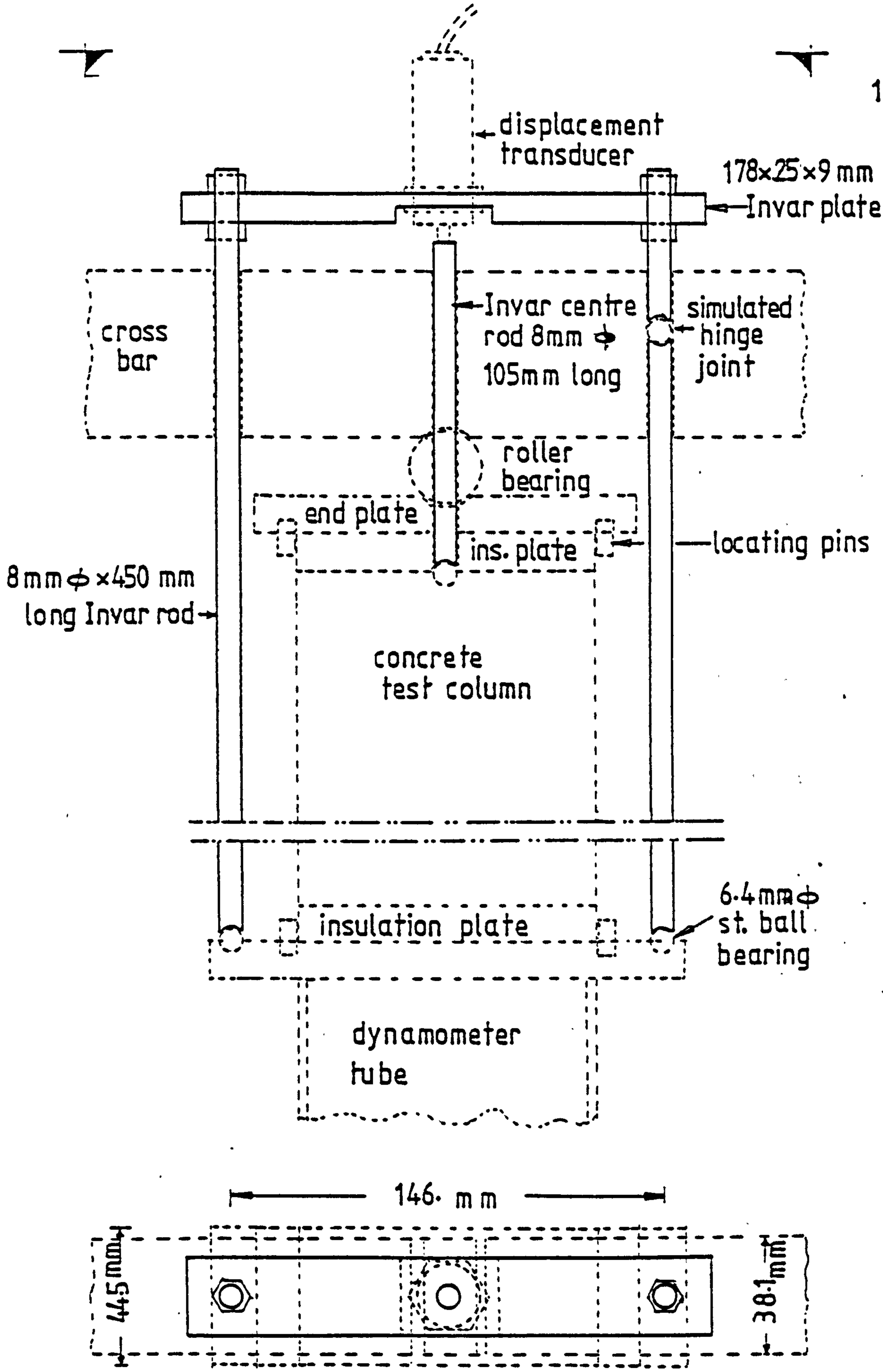

Fig. 7·3 Transducer mounting Invar frame

to the transducer frame and the central rod was provided by the top steel cross-bar of the loading frame. Free fit tapered apertures, having top and bottom diameters of 8 and 9 mm respectively, were drilled at the centre and at 146 mm apart symmetrically from the centre of the cross bar. The legs of the frame were inserted through the apertures and supported on 6.4 mm steel balls fixed in a ball seating provided on the lower steel end plate of the test piece. The frame supports were therefore acting as hinged supports where only rotations are allowed.

In order to eliminate the effect of thermal deformation, the frame was further simplified by introducing another hinge-like joint in one of its upright members. This was achieved by seating a 6.4 mm steel ball within a cut section just below the threaded portion of the rod.

The central Invar rod was made 150 mm long of the same diameter as the frame rods. It was provided with ball seating at one end precision flat finish at the other. The rod was provided with free access directly to the top of the concrete specimen, where it was seated on a 6.4 mm steel ball which was partly cast at the centre of the concrete section.

7.5.2 Strain indicator

In the early periods following load and temperature applications, during which the creep rates were highest, it was important that successive readings of signals from all the transducers in each set were to be made fairly rapidly. For this purpose, it was necessary that all the cells were to be maintained continuously energised over such periods, or preferably throughout the test period. A multi-channel conditioning unit was consequently developed, such that only the return could be switched through to a transducer digital indicator.

The conditioning unit, which can cater for up to 25 cells, was designed and manufactured specifically for these tests by 'Shape Instruments Ltd.'. A brief description of this unit, as part of the strain measuring system used, is given as follows:

The system consisted of two separate units (see Plate 7.2)

a) The Conditioning Unit

b) Digital display unit

The conditioning unit comprises a mains-driven M series power supply which is connected permanently to the 25 channels. Each channel has a 5 pin D.I.N. socket and mating plug supplied, into which the 25 channels of instrumentation is connected. The bridges are supplied with 5 V D.C. and produce a full-scale output of 16 mV/V nominal.

Zero and span adjustment controls for each channel are fitted to provide at least ± 10% adjustment, as well as a 25 way stud switch to select the required bridge.

The display unit comprises a mains-driven digital indicator and push button calibration switch. When pushed, this shunts a precision resistor across one arm of the selected bridge.

7.5.3 Calibration of the transducer

The Universal Transducing Cell model UC3 has a displacement range of 0.005 in (0.127 mm) which corresponds to a full scale output of 80 mV. The signal read out system was designed so that the full scale output can be divided into 500 units of 0.16 mV; hence the aim was to calibrate the transducer so that a displacement of 10×10^{-6} in (254×10^{-6} mm) corresponds to one unit of the digital voltmeter reading.

The transducer was mounted horizontally on a jig with its probe set against the moving armature of a precision micrometer (see Plate 7.2)

and connected to the relevant channel in the signal conditioning unit.

Starting from electrical zero, the armature of the micrometer was moved forward until a positive contact with the cell probe was made, as indicated by a deviation of 5 or 6 units. After restoring the zero reading by the channel zero control the armature was moved forward to 80% of the interval and the span control was turned until a reading of 400 was attained. Starting again from zero, intermediate readings corresponding to known increments of displacements between nought and the full interval were taken to establish the linearity of the cell. Once this was ascertained, the calibration button was pushed to shunt a precision resistor across one arm of the relevant bridge.

To ascertain that the zero and span adjustments thus being made remain so throughout the test period, a subsidiary cell allocated to a particular channel was used as a reference to all others in the following manner:

The reference cell was connected to its channel and mounted with its probe in a vertical position on to a bracket attached to a vertical post. Calibration of the reference cell was first established by recording the signal produced by the 50 gm calibration weight when seated on the probe, in addition to the signal corresponding to zero load. The same procedure and observations were made when the reference cell was connected to the channels of the test cells in turn. Therefore, any further changes in the zero or span controls could be restored with the help of the reference cell.

7.5.4 Mechanical strain measurements

The need for a subsidiary strain measuring system arose for the following reasons:-

1. To measure the elastic strain component immediately after the imposition or removal of the load, which it was not possible to achieve with the Statham transducers
2. To ascertain the amount of deformation occurring during the short interval when the transducers are withdrawn from service for calibration checks. However, from first experience this was found unnecessary because the cells were first checked after one month of operation, when the rate of deformation was expected to be low.
3. As a contingency measure against cell or power failure. The latter has however occurred on three occasions outside the control of the operator.

The Whittimore 254 demountable strain gauge was chosen for the purpose. Brass studs screwed into county caps which were cast into both sides of the laminations as used in the beam test served as gauge points, Fig. 7.4. With this system, the measurements were found to be reproducible to approximately 5 microstrains.

7.6 Concrete Mix

In order to utilize some of the creep data produced in the experiments in the analysis of the beam test results, it was decided to use the same mix proportions throughout the tests. Details of the concrete mix are given in the appendices.

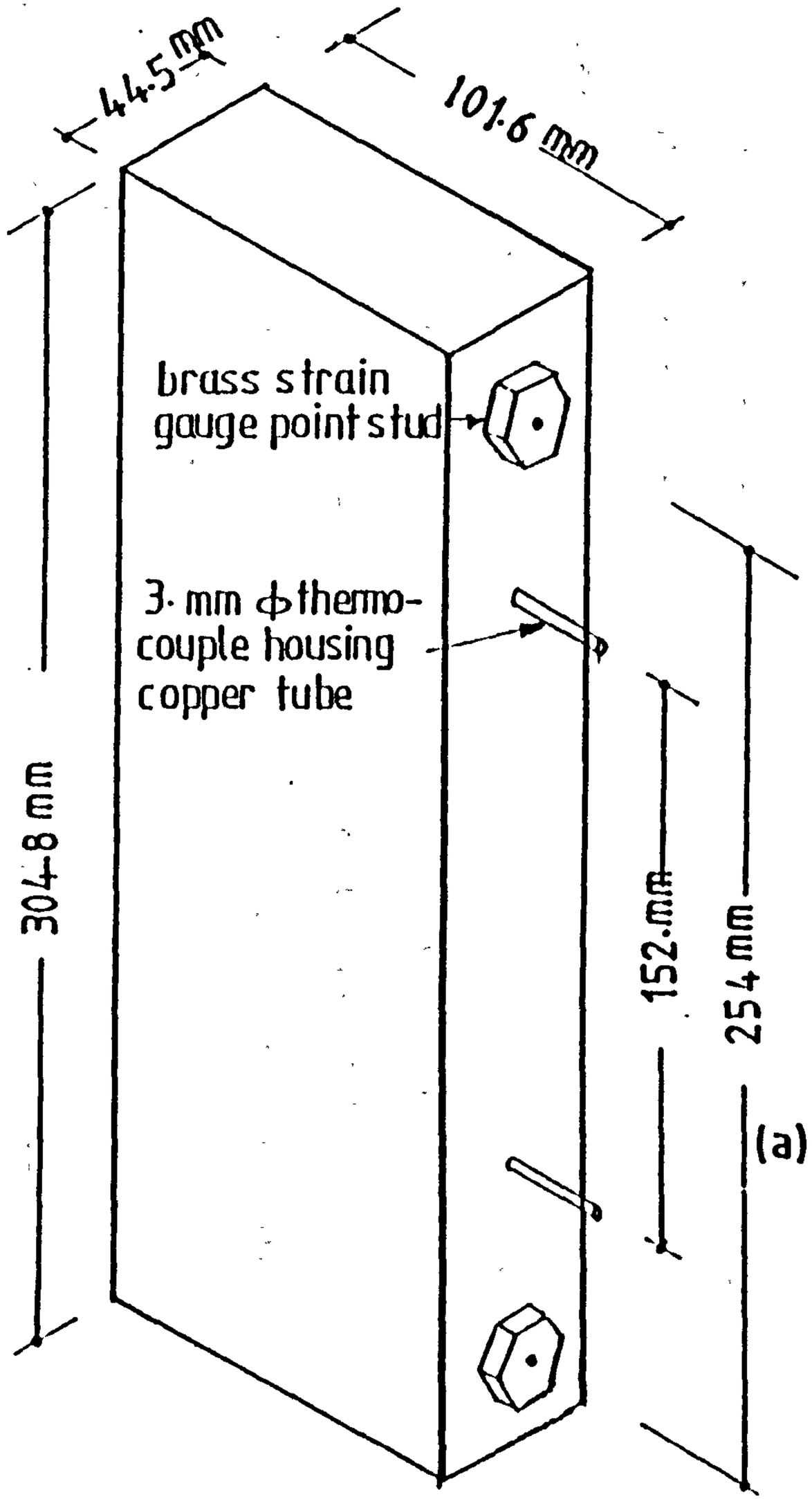

(a) mechanical strain, and temperature measuring attatchments

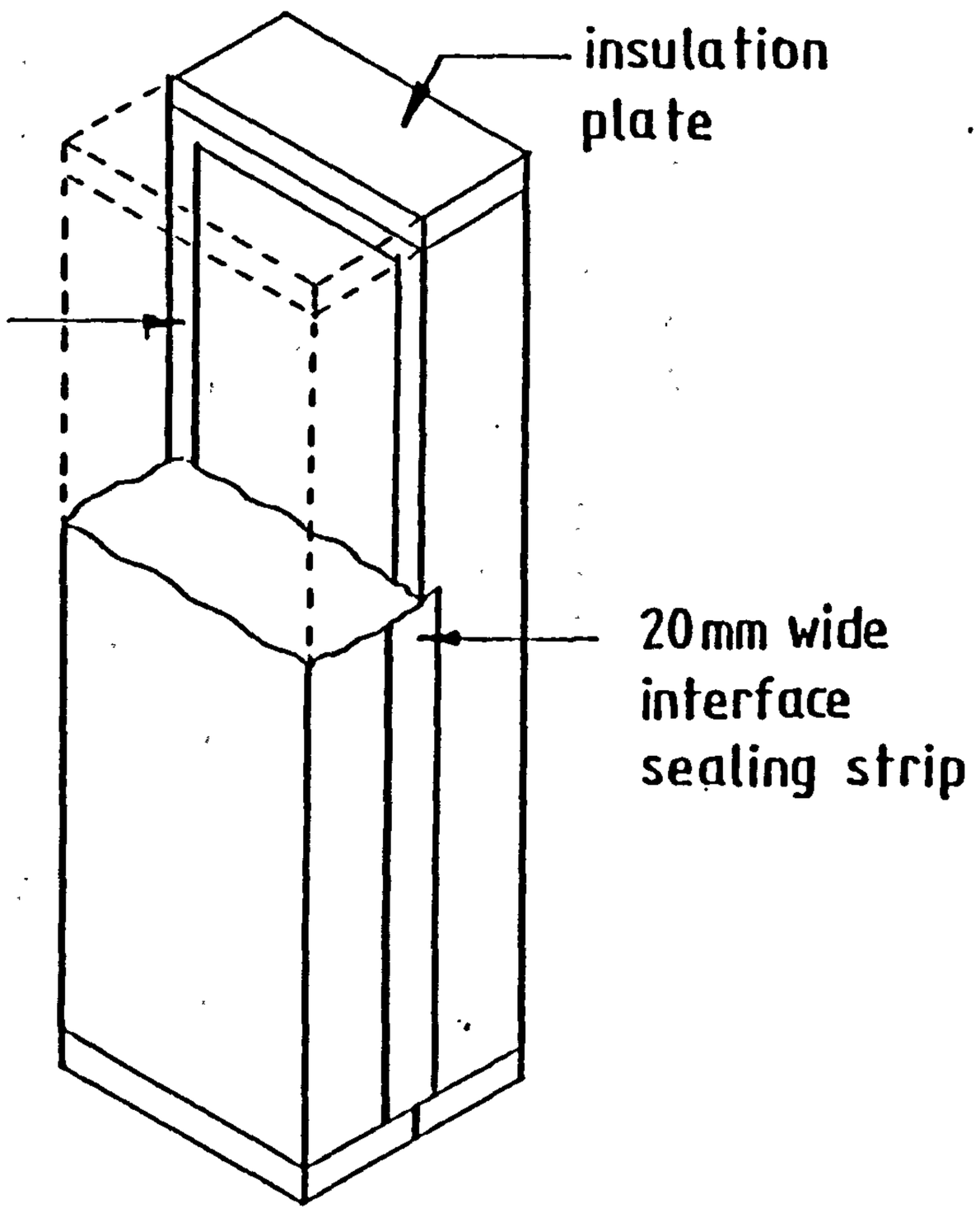

(b) method of edge and interface sealing of two typical adjacent laminations

Fig 7.4

7.7 Manufacture of the concrete laminae

The aim was to establish a manufacturing procedure for the test specimens, such that their characteristics would not significantly influence the results of the experiments. Conditions of homogeneity, shape and planeness of the specimens' ends were the major influencing factors which were given careful consideration.

In order to normalize the behaviour of the specimens around their axes, the axial symmetry ought to be preserved. The decision was therefore taken to cast the specimens in a vertical position, thus alleviating conditions of non-homogeneity which might otherwise be significant.

The uniformity of the cross section and planeness of the specimens' ends are particularly important parameters in establishing the specified state of stress during loading. Mild steel moulds of cellular construction were therefore designed and precisely fabricated, which enabled sets of five laminations to be produced in close conformance to the shape of an ideal rectangular section prism.

Reference is made to Plate 7.3 for the following description of a typical mould used in this study.

Unequal pairs of 12.7 mm thick mild steel plates were joined vertically to form a hollow rectangular box section. This section was then divided into five separate compartments by means of a set of four 6.4 mm thick mild steel plates. The dividing plates were held in vertical positions parallel to each other in between grooves accurately machined on the inner surfaces of the longer side plates.

The dimensions and spacing of the mould's components were so proportioned that the formed compartments coincided with the specified size of the test laminations.

Two sets of holes were provided in each mould to enable the embedment of the brass inserts and the insertion of the thermocouple housing tubes during casting of the concrete.

The methods adopted for the manufacture of any two sets of laminations can be described as follows:

With all the parting surfaces of the moulds lubricated and the brass inserts screwed in position, the main plates were loosely joined and mounted on plane steel plates provided with four locating pins. Subsequently, the dividing plates were thrust in between the slots and the whole assembly was fastened and firmly clamped to a vibrating table along with moulds of the property control specimens.

At this stage, the concrete mix was carefully proportioned, mixed and placed in the various compartments in sequence of about 12 to 15 casts. Just before casting reached the level of either thermocouple, lubricated dummy steel rods were inserted through the apertures provided in one side plate of each mould. These rods were made such that they could only travel up to the vertical axis of each compartment.

As casting approached the top of each compartment, strips of wood were placed around the perimeter so as to enable an additional layer of about 20 mm thick to be added on top of each mould. Thereafter the vibration was stopped and the excess concrete was chopped away with a spatula. About 2 mm of concrete was further abraded from the top of each compartment for the formation of the end caps.

The dummy rods were then withdrawn and replaced by the thermocouple housing tubes and the vibration was resumed for a further 10 to 15 seconds. The moulds were finally covered with polythene sheets to prevent evaporation of the moisture.

Typical cut sections through two sets of specimens cast at the same time are shown in Plate 7.4, and it can be seen that the concrete in both sets was quite homogeneous.

End Capping

The end capping operation was performed shortly after casting, when some initial set had occurred.

The various compartments were topped up with a neat cement paste. A straight edge was used to disperse the paste evenly and level it with the square machined edges of the plates. The surface was then worked on with a plane until a satisfactory smooth finish was obtained. The centre of each compartment was then carefully marked and steel balls were subsequently seated and sunk to about 4 mm below the surface. The tops of the moulds were then carefully covered with polythene sheets and left to cure in this condition until demoulding date.

7.8 Curing and sealing

Two days after casting, the specimens were demoulded, wire brushed and had their sharp corners filed with a Carborundum stone. They were then immediately weighed and the brass studs screwed to the inserts and the datum gauge readings were established. The specimens were left to cure in the room, having a mean temperature of about 18±2°C and relative humidity of about 85±10%. At the age of 28 days the weights and gauge readings were recorded, then each specimen was wrapped in a polythene sheet and transferred to the testing laboratory where the sealing operation was carried out.

Two types of sealing compounds were used; for pilot tests, which were carried out at room temperatures, the surfaces were painted with two coats of Araldite resin. For the main heating tests Bakelite resin was used instead.

In an attempt to obtain a satisfactory moisture seal at the interfaces of the adjacent laminations while retaining their freedom of movement, the following technique was adopted.

In the first stage, before the laminations were assembled on to the rig, strips of insertion rubber about 10 mm wide and 1.5 mm thick were stuck with the resin around the perimeter of each one of the two opposing surfaces as illustrated in Fig. 7.4. The gap thus created was to be filled with thin sheets of card, which permit the flow of moisture from one slice to the next. In the second stage, after the specimens were loaded and assembled next to each other and before heating was due to start, other strips of the same rubber about 20 mm wide were stuck along the near edges of the specimens, to prevent the escape of moisture from interfaces. This technique was however used with all but the specimens which had all round seal where no moisture transfer took place.

In general, the procedure for sealing the surfaces of the specimens was carried out as follows:

A sufficient quantity of the sealing compound was prepared by thoroughly mixing the base and hardener in the correct proportion. With the surfaces set facing upwards, greased thin wooden strips were clamped around the edges of the area. The sealing compound was then carefully applied with a paint brush to each surface in turn. Air bubbles formed on the surfaces were either pricked in time or scrapped later after hardening, when a second coat was applied before turning to the other sides. Because of the high viscosity of the resin, it was easily possible to pond it around the copper tubes and gauge studs, as well as the edges.

7.9 Heating facilities and instrumentation

It was intended to provide adequate heating facilities which would enable a state of non-uniform temperature to be imposed across the laminated creep and shrinkage blocks in both sustained and cyclic manners.

In deciding upon the appropriate system of heating for these experiments, it was considered important that the thermal environments which would be created in a creep test should be consistent with those prevailing in its shrinkage counterpart. It was thought possible to achieve such conditions by placing the shrinkage block in close proximity with the creep rig and interposing a single heat source in between the two exposed surfaces. The temperature crossfalls would thus develop symmetrically across the two sets of laminations, both in time and space.

A 25 mm thick concrete plate, cast around two silica glass tubes, was used to diffuse the heat produced by spring heating elements housed in the glass tube ducts. The surface area of the plate was made to coincide with that of the exposed surface of the block and the tubes were positioned 50 mm apart symmetrically in the cross section of the plate.

Preliminary estimates of the power requirements to produce temperature crossfalls around 40 and up to 80^{o}C was roughly found to be between 25 to 60 watts. However, a circuit delivering up to 100 W of power from a 100 V supply was designed utilizing the 1000 W commercially available spring heating elements. Two of these elements were connected in series with a 50 ohm Bercostat. A variable transformer was used to step down the mains voltage for five heating circuits. The heating circuit diagram for the five experiments is shown in Fig. 7.5. The function of the Bercostat in each circuit was to provide independent control of the

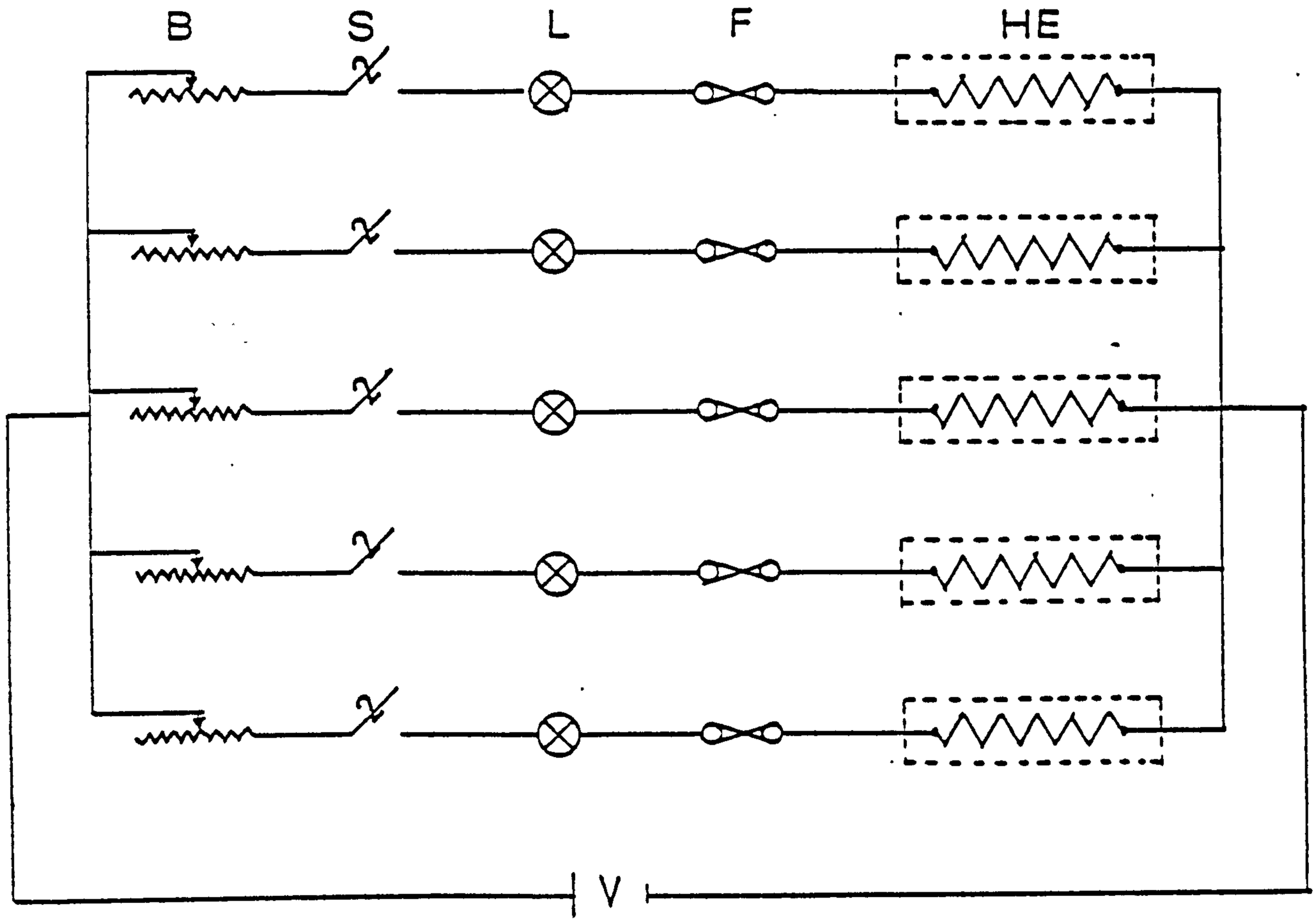

B=50 ohm Bercostat S=two way Switch L=Lamp

F=1.5 amp Fuse HE=Heater Elements V=Variac

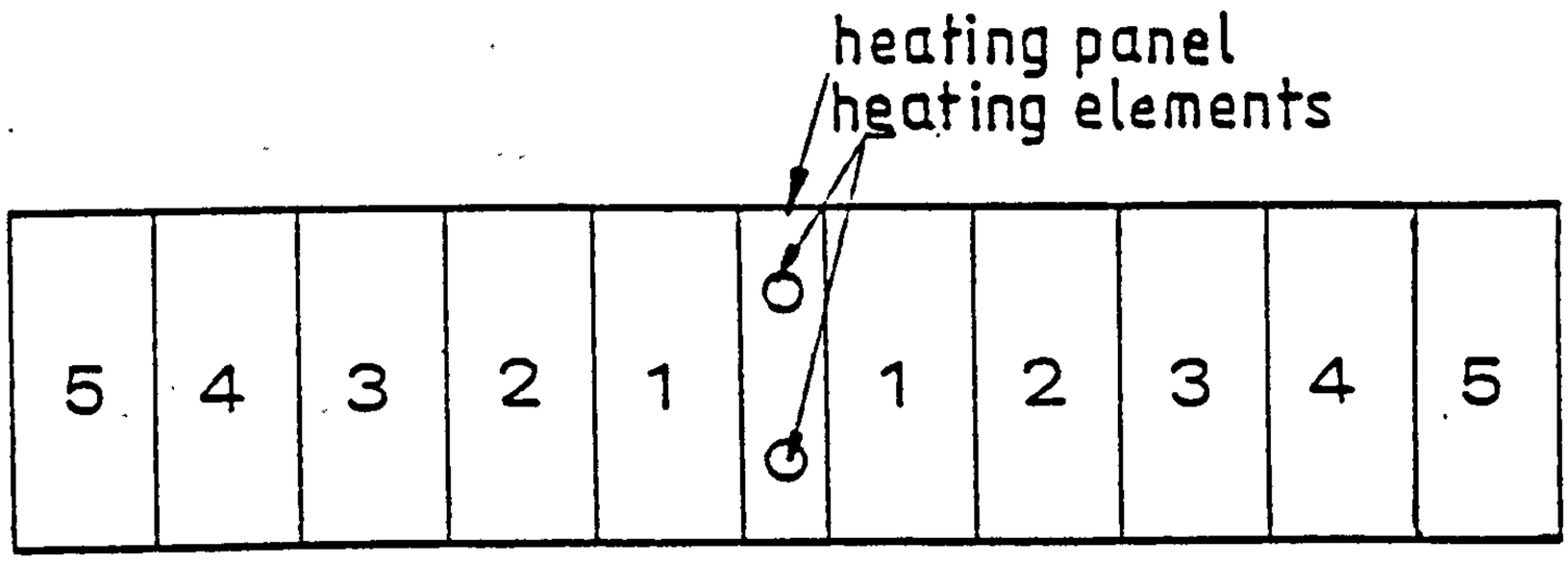

Typical test set

Fig 7.5 Heating circuits diagram for five test sets

thermal loading to each rig which might be necessary due to changes in the heat flow properties of concrete or during the thermal cycling program. Independent adjustments were also needed when not all of the heating elements were switched on at the same time.

7.9.1 Temperature measurements

In order to separate the observed total strain into thermal mechanical strain components, accurate knowledge of the temperature history in each lamina is necessary. The accuracy of the temperature measuring technique adopted in the beam test was however considered to be sufficiently high to warrant its use in these experiments.

Copper tubes 3 mm O/D and 64 mm long sealed at one end were cut 76 mm from both ends in the vertical plane of symmetry of each lamina. The closed ends of the tubes were aligned with the vertical axis of the specimen thus providing access for copper-constantan thermocouples to sense the temperature through to the centre. The internal concrete temperatures as well as the surface temperatures of the aluminium tubes were measured with the same equipment used in the beam experiments. Frequent checks were made to ascertain the accuracy of the system by measuring the temperatures of melting ice and boiling water.

7.10 Loading: set-up and procedure

At 50% of the yield strength of steel, the maximum load capacity of a creep rig unit is about 37.0 KN. It is however possible to double this value without overstressing the aluminium tube by reducing the lengths of the cross bars to half their existing lengths, provided an alternative technique for measuring the aluminium tube strains is substituted for the Whittimore gauge. It was decided nonetheless to

apply a uniaxial load of about 31.1 KN on all test laminations; this is equivalent to a uniform stress of about 6.9 MN/M^2.

The ages of the specimens at loading however varied from approximately 28 days for specimens tested at room temperature to about 32 days for those tested under heated environments, but only one test group of laminations forming a single block was actually loaded at any one date.

In the setting-up process of the individual creep rig units for loading, careful consideration was given to satisfy the following requirements:

a. that the various components of each unit should be assembled so as not to inhibit the full surface contact of the concrete laminations incorporated in any test block

b. that the loading planes should be aligned with the planes of the load bearing elements of the rigs so that the specified state of stress on all the specimens could be established as closely as possible.

In order to achieve the delicate alignment operation successfully, each unit was assembled on a horizontal plane provided with locating pins for the various components of the rig. Upon completion, the assembly was then locked in position by finger-tightening the nuts of the tension rods, carefully lifted and mounted on to a cantilever frame rigidly fixed to the wall. Every unit was prepared in the same way, and assembled closely together on the wall frame. A typical view of five assembled units can be seen in Plate 7.5.

Prior to load application, datum measurements of temperatures and gauge lengths on the aluminium tubes and concrete test pieces were established. Then the central Invar rods were inserted through the

relevant apertures, while the transducers were plugged into the respective channels and fitted to the Invar frames ready to be installed soon after loading.

Loading was first applied to the specimen closer to the wall by simultaneously tightening the nuts of the two tension rods with ratchet spanners, until the two gauge lengths of the dynamometer tube indicated approximately equal deformations of about 500 microstrains, which are equivalent to 50 gauge divisions. In some cases, however, a variation of about 2% from the mean value in either gauge length was tolerated.

Immediately after loading the specimen, measurements of the concrete strains were recorded, followed shortly by installing the transducer assembly and recording the initial voltmeter reading.

It should be remarked that the speed and efficiency with which the above process was implemented without significant loss of value, was greatly helped by the experience gained from a pilot test staged ahead of the main tests. Consequently, it was possible to impose the full loading within 3 minutes' duration and to measure the concrete strains and install the transducer within the next 2 minutes approximately. On a few occasions, when it took slightly longer to accomplish any one of the above steps, the specimen under consideration was de-stressed and re-loaded.

7.11 Heating: arrangements and application

The thermal gradients scheduled for application on these experiments were actually imposed after approximately 22 days from loading. The tasks of sealing the interfaces of adjacent laminations, in the manner described in Section 7.8, as well as the application of the insulation, were however accomplished the previous day. To carry out such operations,

it was necessary to dismantle temporarily the Invar frames carrying the transducers. Before this action was taken, the current temperatures and digital voltmeter readings were recorded. Further measurements were also made, using the Whittimore gauge, to assess the amount of deformation which occurred while the transducers were out of service.

With respect to the shrinkage control block, the procedure was to record the weights before and after sealing of the interfaces, wrap the insulation and record strains and temperature readings. The block was then mounted opposite the creep rig as shown in Plate 7.6, and the heating plate was interposed between the two blocks. The exposed sides of the heating plate were covered with glass wool insulation.

Just before switching the heat on, datum measurements of strains and temperatures were established on both experimental blocks in addition to the aluminium tubes. The datum readings of the digital voltmeter were however set up following the procedure described in Section 7.12.

7.12 Transducer datum set-up

The procedure adopted for establishing the datum of displacement measurements was such that, immediately after loading, the probe of the transducer was brought into contact with the central Invar rod until about 80 to 90% of its displacement range was initially exhausted. At the commencement of heating, however, the datum was set in the reverse order, i.e. by initially inducing a small amount of displacement (10 to 20%). The residual amount was taken by the thermal movement of the specimen, while its temperature was rising, until it reached a steady state, when the starting procedure was repeated.

It should, however, be noted that it was only necessary to set the datum once at the start of the tests and twice on the first day of heating

for the hottest specimen, and twice during the following period. In each case, it took only a few seconds to set the datum, which was easily accomplished by loosening and twisting one of the Invar rods of the frame.

7.13 Cycle and sequence of observations

The observation cycle generally consisted of recordings of temperatures, output signals from the transducers, and gauge readings of the shrinkage control specimens; in addition to temperatures and gauge readings on the dynamometrical tubes, although not as frequent.

During the test period preceding heating the above observations were usually taken at 1, 3, 5, 7, 10, 14 and 21 days from loading. Subsequent to heating the observations were taken at similar frequencies, followed by approximately 10 days' interval up to the first two months, extended from 2 to 3 weeks thereafter towards the end of the test at the sustained temperature regime. During the temperature cycling program, the observations were taken at close intervals depending on the length of the cycle period at the time.

Other observations were frequently made of the power supply and output of the heating circuit.

Finally, the results derived from these experiments are presented and discussed in the next chapter.

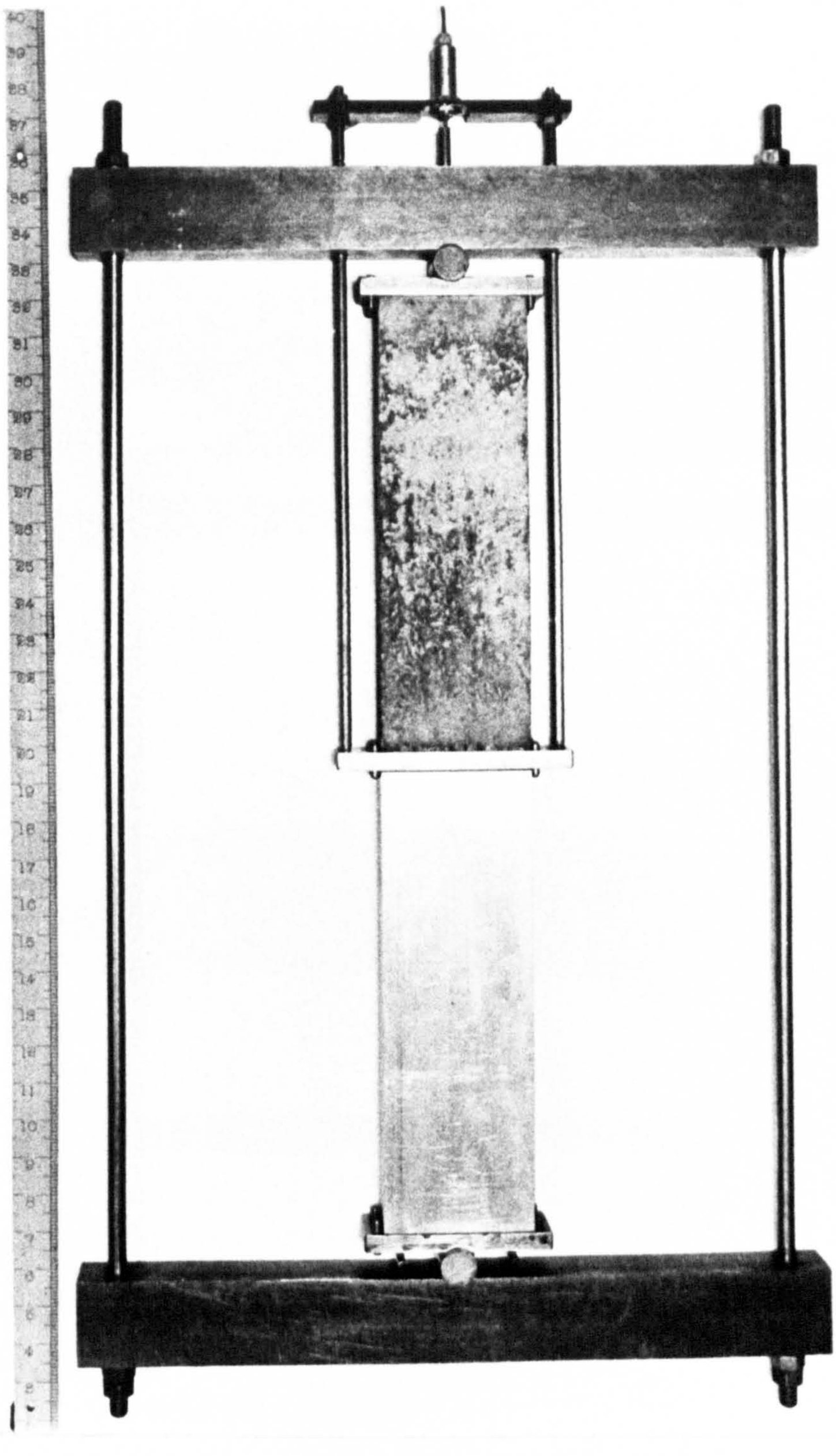

Plate 7.1 general view of a typical creep rig unit

note: insulation plates are not shown

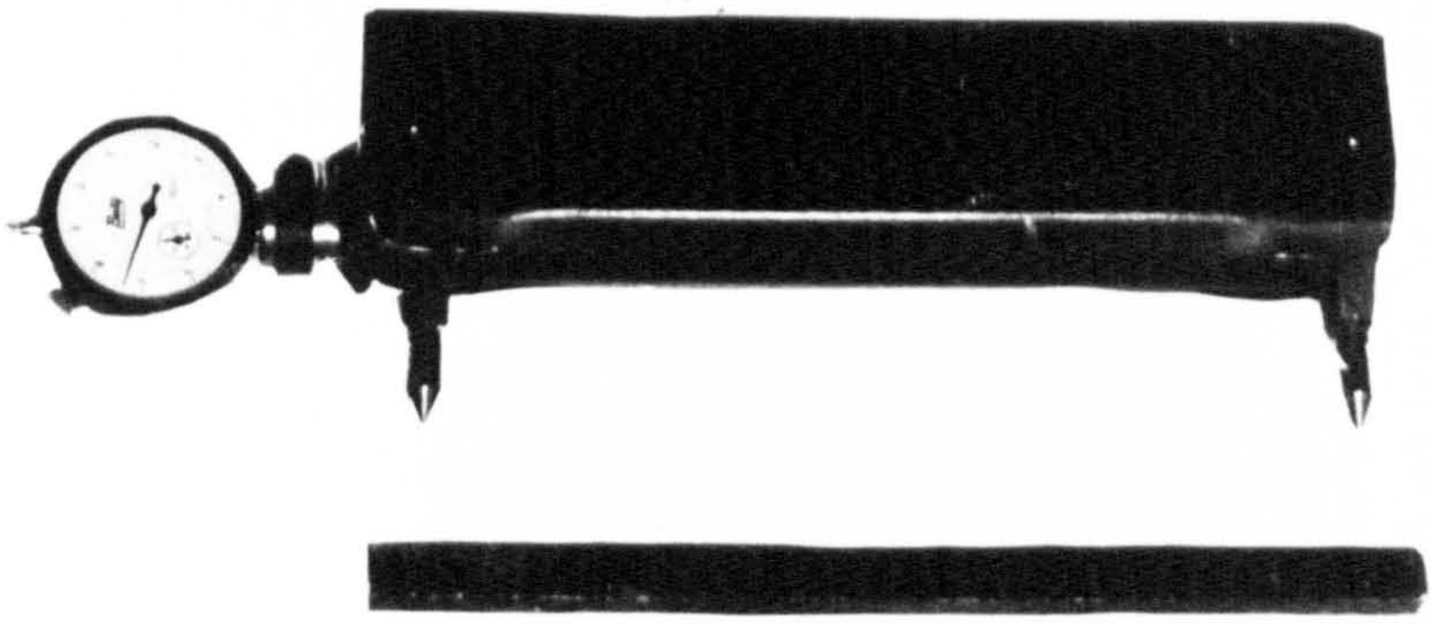

1) digital display unit
2) 25 channel conditioning unit
3) transducer's calibration micrometer
4) a typical transducing cell UC3
5) mechanical strain gauge (Whittimore)
6) Comark electronic thermometer

Plate 7.2 strain and temperature instrumentations

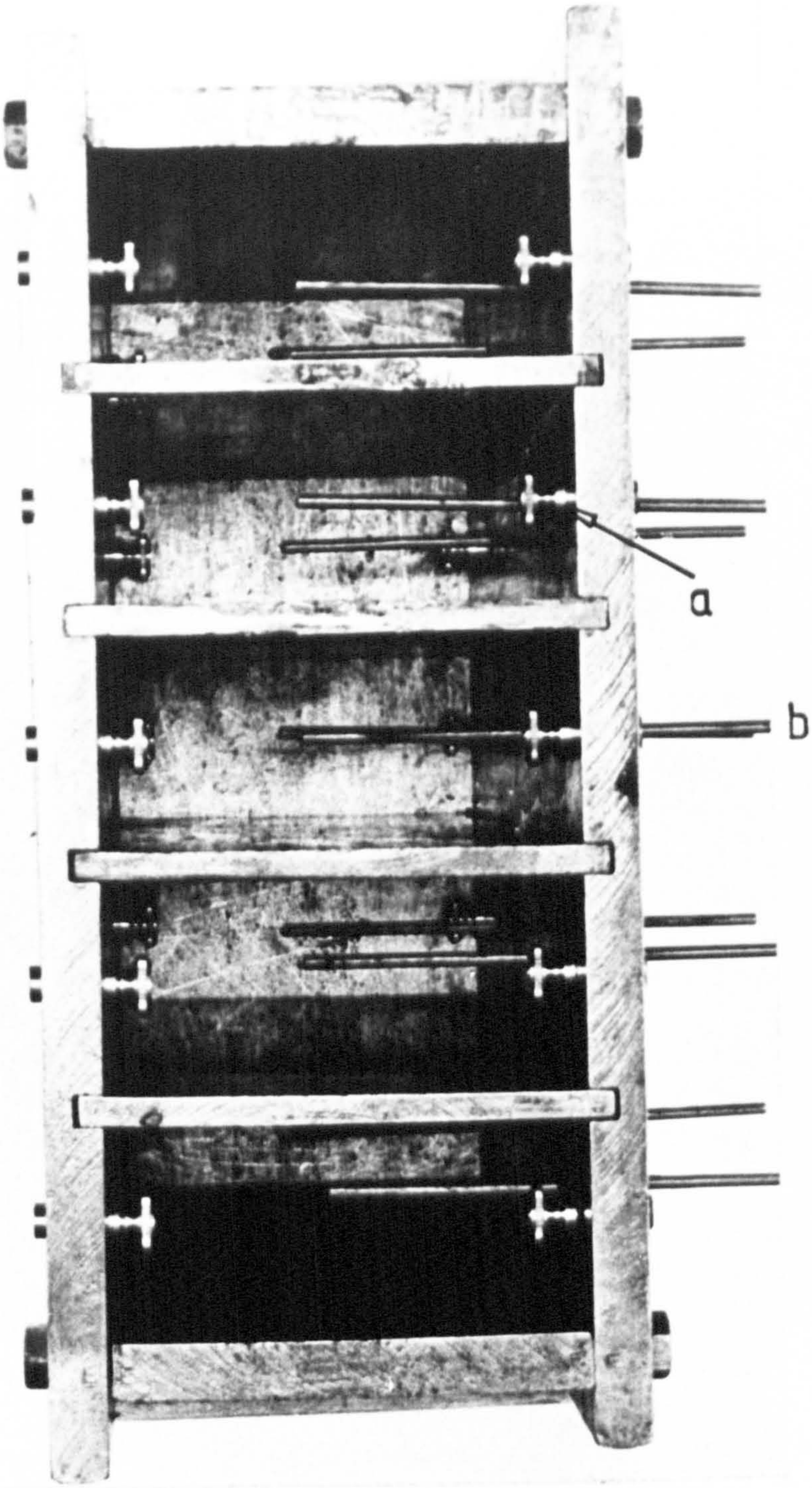

Plate 7.3 general view of the casting mould

a- strain gauge brass inserts

b- thermocouple housing tube

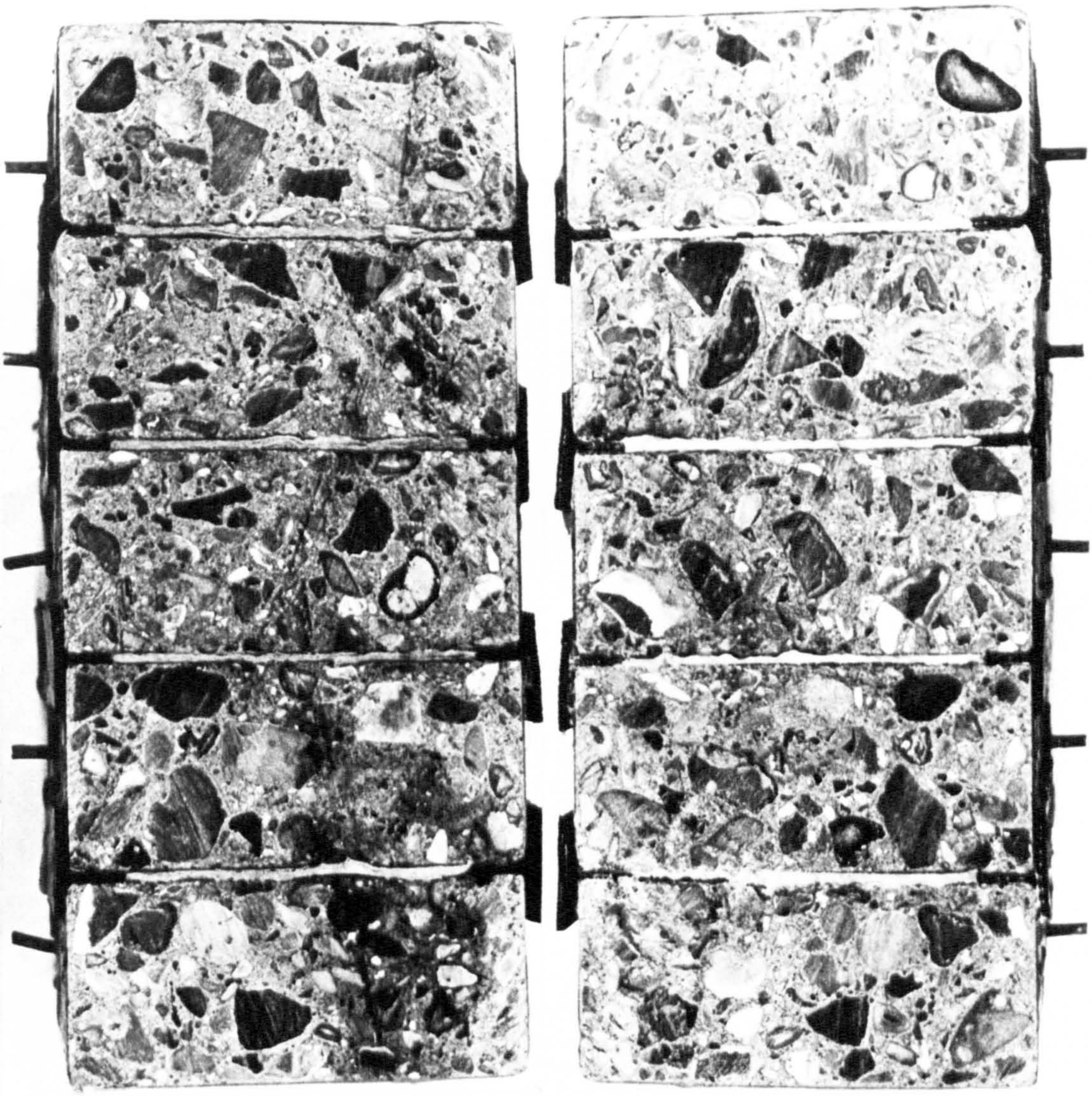

Plate7.4 view of typical sections accross
the creep and shrinkage blocks

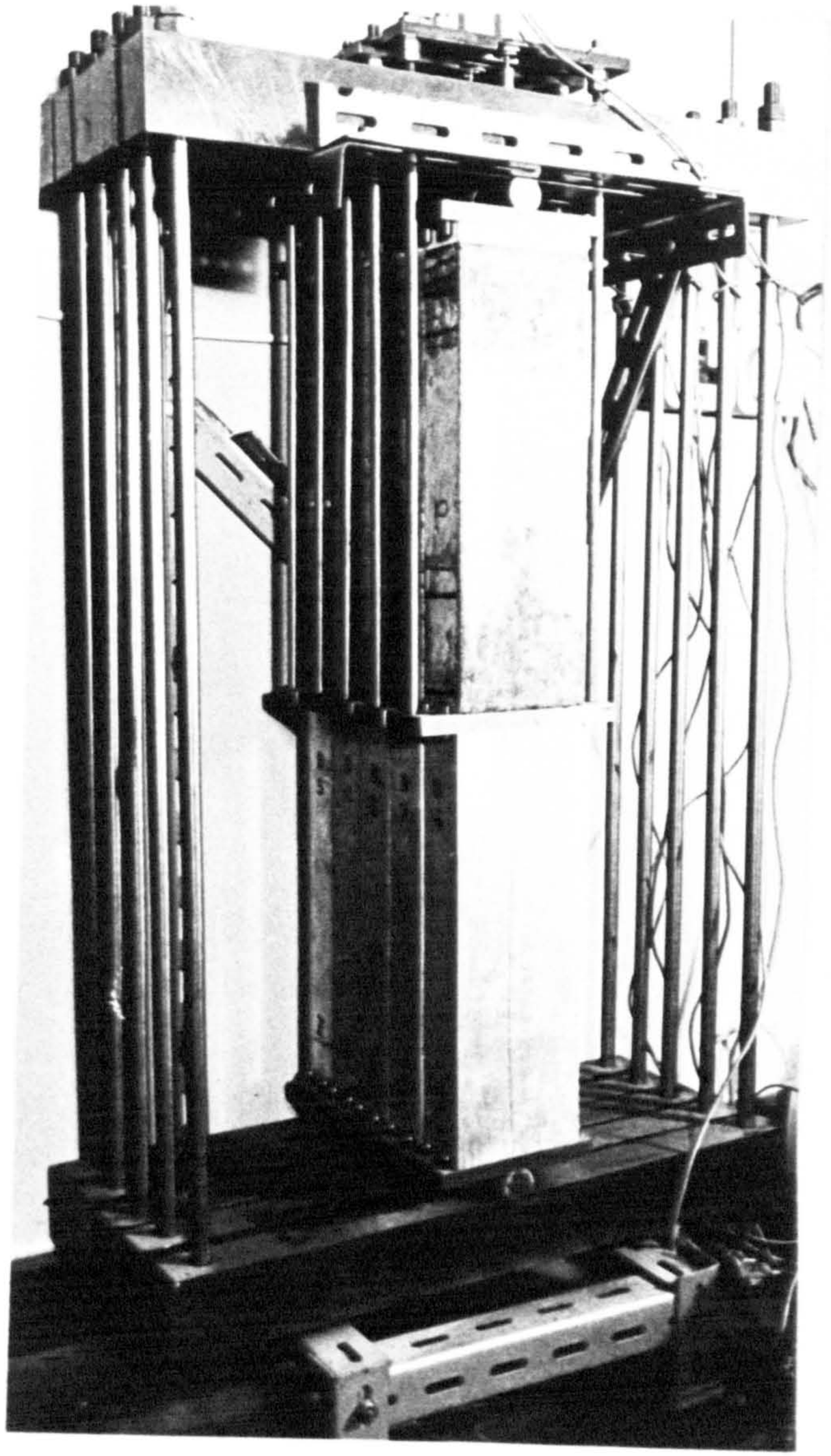

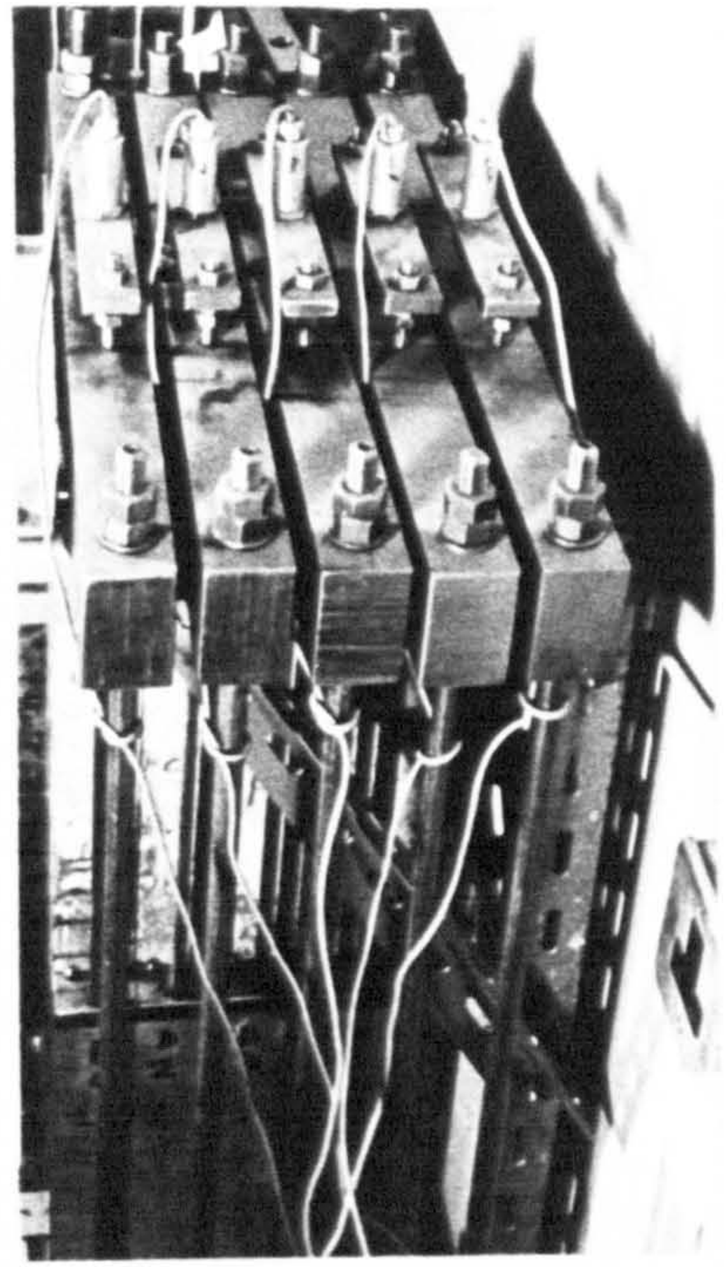

overhead view

Plate 7.5 general arrangements of the creep rig units

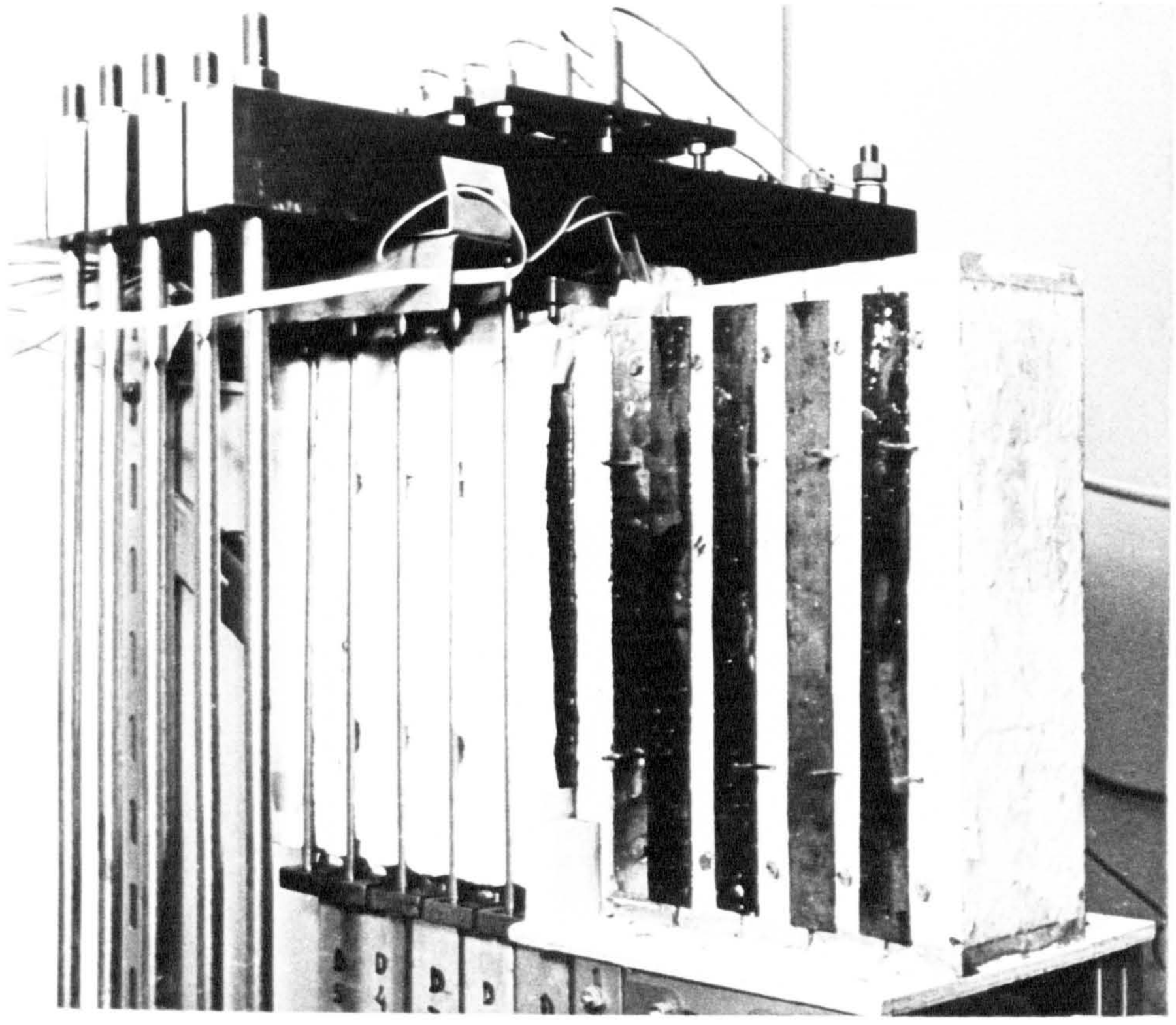

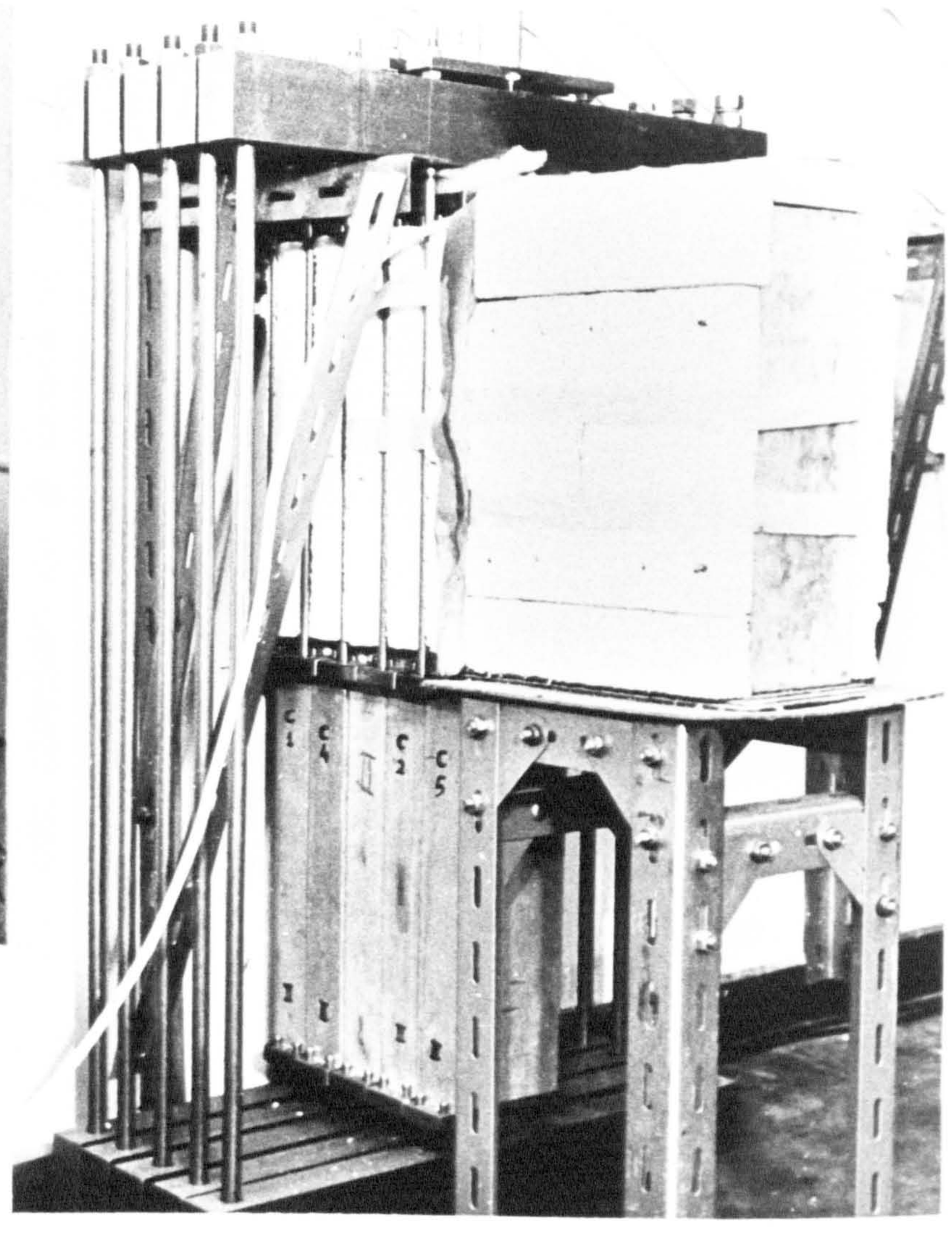

Plate 7.6 general layout of the tests

CHAPTER VIII

DISPLAY OF RESULTS OF THE LAMINATED CREEP RIG AND SHRINKAGE EXPERIMENTS

Chapter 8 - Synopsis

The results of the laminated creep and shrinkage experiments are presented. Four test series having different moisture flow conditions were heated under load in conjunction with identical 'no-load' comparison specimens. In addition, one set was tested for creep and shrinkage at room temperatures, and another set was heated without load, to investigate the time-variation of the coefficient of linear expansion of the concrete with moisture flow. Various temperature histories were investigated including temperature cycling after sustained heating periods of up to 200 days. The test temperatures covered a range of between 22^{o} and 114 ^{o}C. It is concluded that the creep rate increases with temperature and with an increase in the migration rate of the moisture. It can be expected to decrease whenever moisture concentration increases. Temperatures cycling between specified limits produce no sudden change in creep of the concrete maintained under either stable or variable moisture state, after the first temperature increase.

8.1 Introduction

This chapter collects the results of the author's experiments, which were designed primarily to investigate the long-term influence of moisture movement associated with temperature gradients on the in-elastic behaviour of the material. Results of heated moisture-stable, and non-heated drying experiments are also included, in addition to results of subsidiary tests carried out to determine the effects of the main test variables, i.e. temperature and moisture flow conditions, on the expansion behaviour of the material. A diagrammatic representation of the various test groups, and conditions of exposure are shown in Fig. 8.1. The type and number of tests carried out on each group are summarized in Table 8.1.

TABLE 8.1

Type and number of tests

Specimen group	Creep	Shrinkage	Coeff. of expansion	Remarks
A	1	1	-	Atmospheric drying (no heating)
B	1	1	1	Constant moisture content
C	1	2	1	Temperature gradient-activated moisture flow
D	1	1	-	
E	1	1	-	

Note: all creep specimens were loaded to about 6.9 N/mm^2, i.e. were loaded to a stress/28-day cold strength ratio of 0.15

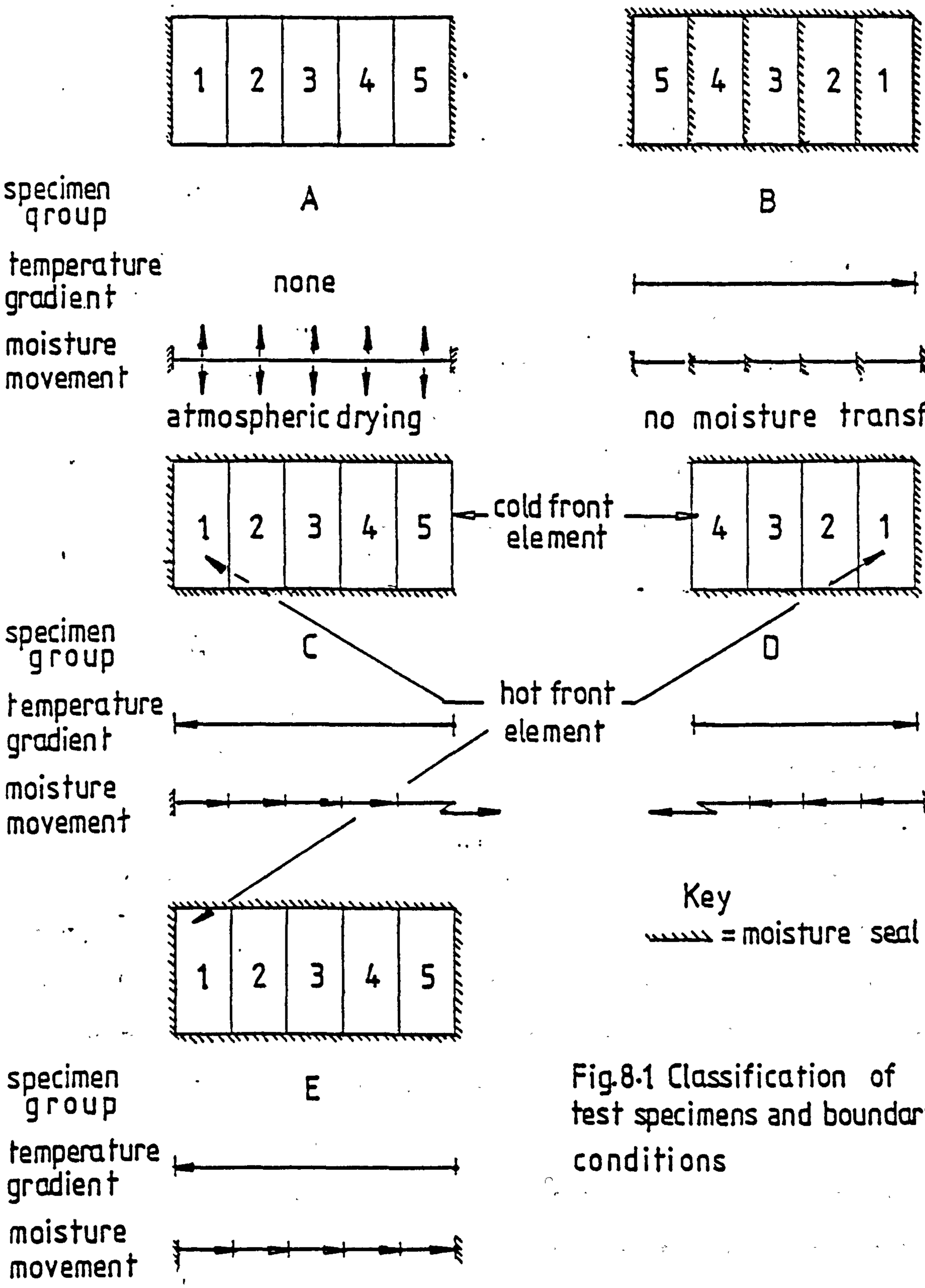

Fig.8.1 Classification of test specimens and boundary conditions

---

Description code for the test specimens

Specimes are referred to in the text by the group name A, B, C, D or E followed by number 1 or 2 to indicate the shrinkage or creep block. A particular element of a given test set may be described by a second number e.g.

E2-4 and C1-2

refer to the 4th element of the creep block from group E
and " " 2nd " " " " shrinkage " " " C respectively.

8.2 Strain behaviour of the test specimens at normal temperatures

8.2.1 Initial strains on loading

These are defined here as the total strain observed approximately 0.0014 days (2.0 min) after application of the stress. The mean instantaneous strain response of all the test group elements to stress of about 6.90 N/mm^2 applied at the age of 32 days was about 192×10^{-6}, with a standard deviation of about 10.6×10^{-6}. This gives a mean value for the elasticity modulus of the material of 36.0 GN/M^2.

8.2.2 Creep and shrinkage

For similar conditions of exposure, elements of the main test series B, C, D and E exhibited reasonably close deformations with time over the period preceding commencement of the heating programme. This concerns the two exposed front elements of series C and D block specimens, and the remaining 17 unexposed elements of the four test series under consideration. The comparative creep strain behaviour of the laminations tested under the two different conditions of exposure mentioned, is described in the combined plot of the results in Fig. 8.2. In arriving at the creep data displayed in this figure, account has been taken of shrinkage, as indicated by the non-loaded companion block specimens. Incidentally, shrinkage could only be detected at the two drying front elements, which at the end of the period exhibited approximately an average of 90 microstrain.

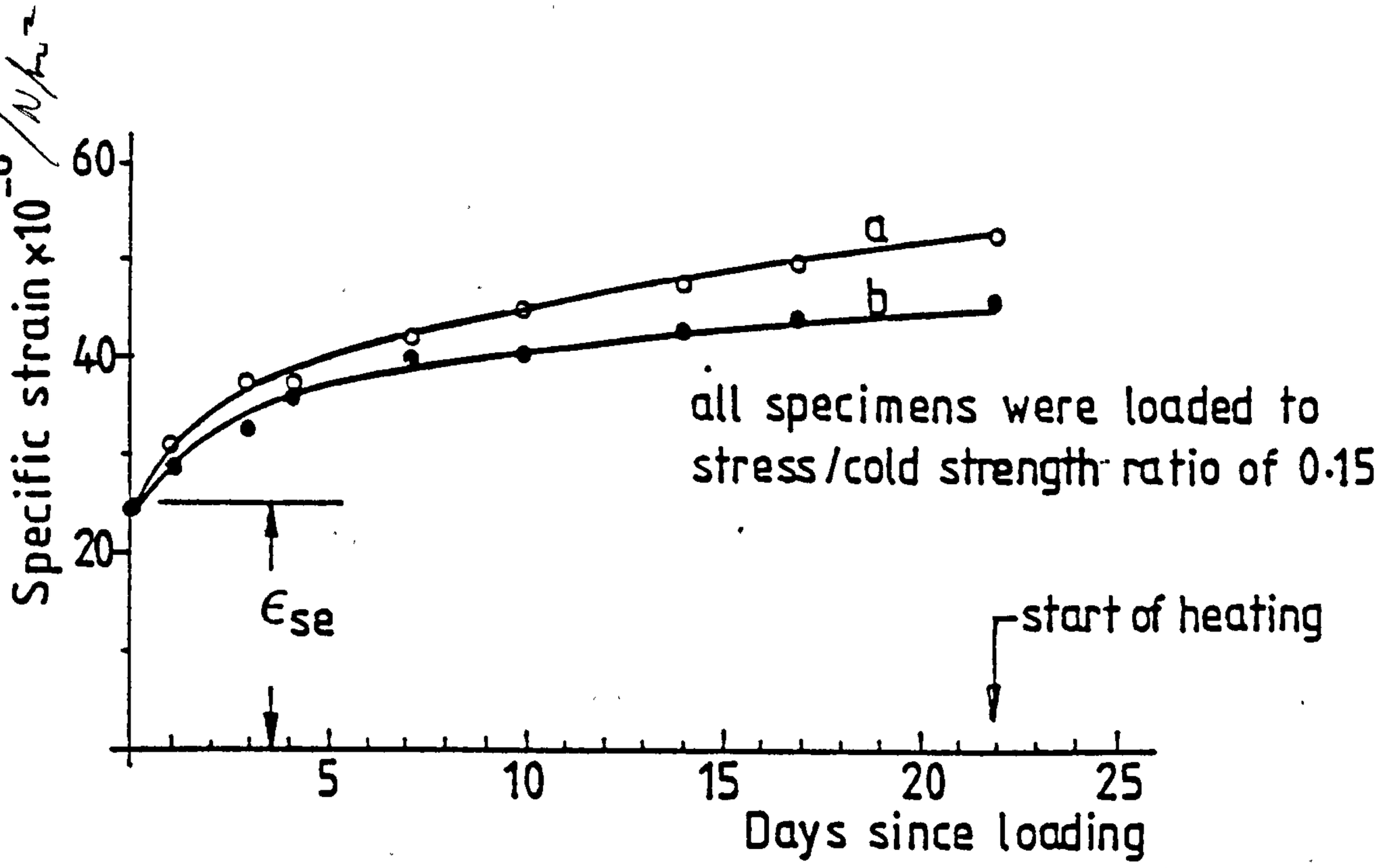

Fig 8.2 Plot of the mean specific strain vs. time prior to heating

curve(a) represents the mean behaviour of the two exposed elements C2-5 & D2-4

curve(b) represents the mean behaviour of the sealed or un-exposed elements of the laminated blocks B2, C2, D2 & E2 (a total of 17 elements)

Note:
the creep behaviour of these specimens under elevated temperatures is described in figs. 8.17 - 8.22

8.2.3 Creep of drying specimens

One experiment, which was originally intended as a pilot to the measuring equipment and testing procedure was conducted and extended for a period of over 14 months. The specimen block, test series A, had both its end faces sealed, thus allowing the laminations equal evaporation drying surface areas.

The total strain histories recorded for the laminations loaded to stress of 6.9 N/mm^2, and their non-loaded companion set are shown in Fig. 8.3. The observed difference in the total axial strain across the laminations of either set at any particular time was within a maximum of 40 microstrain. In view of the complex nature of drying and its subsequent effects on the material behaviour the extent of agreement between the results was considered reasonable. Hence, a single specific creep profile based on the averaged results of both sets representing the mean axial creep behaviour of the five elements is drawn in Fig. 8.4.

8.3 Strain behaviour of the test specimens under sustained elevated and cyclic temperature states

8.3.1 Coefficient of thermal expansion

Tests were carried out to determine the coefficient of linear expansion across the sections of the two laminated block samples B3 and C3 subjected to non-uniform heating. For the constant moisture content sample B3, the test carried out was of a short duration, whereas a long-term test was performed on the latter, to study the influence of the continuing moisture movement on this parameter.

Specimen B3 was exposed to various temperature crossfalls over a period of about 72 hours. Observations of temperature and length changes during heating and/or cooling provided the basic information

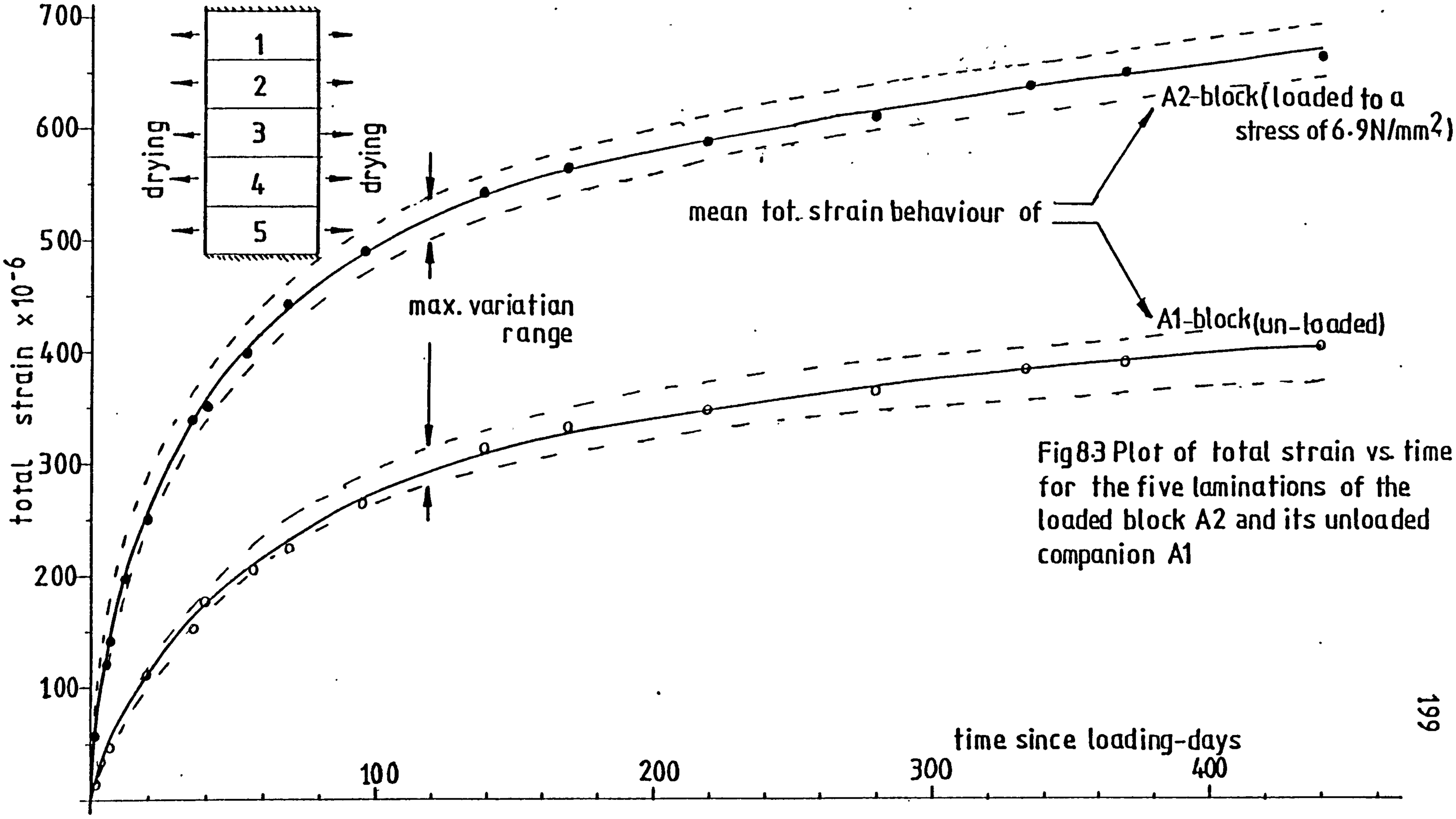

Fig 8.3 Plot of total strain vs. time for the five laminations of the loaded block A2 and its unloaded companion A1

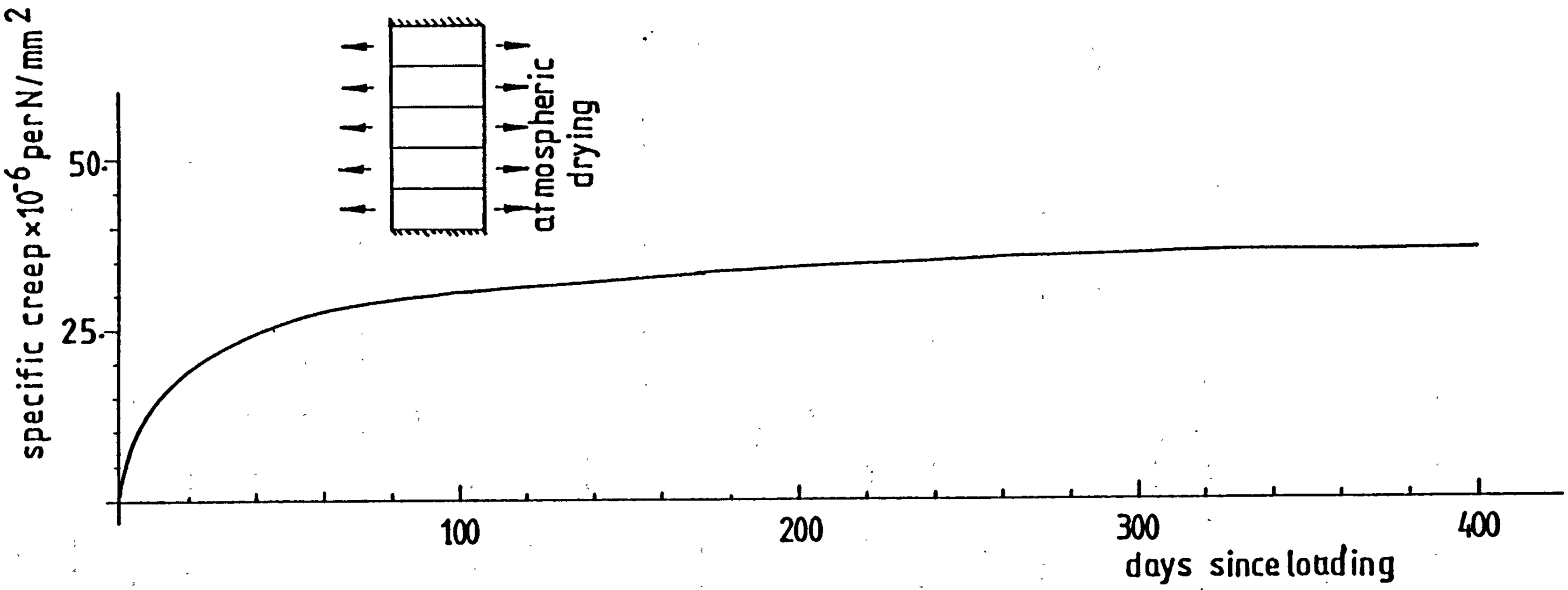

Fig.8.4 specific creep-time relationship
for A2 - block laminations drying at 19°c±2°c
and 60 ± 5% relative humidity
age at loading = 28 days
applied stress = 6.9 N/mm²

needed to determine the expansion coefficient for each element. However, because no clear trends were established between values determined during cooling and re-heating the results obtained for each temperature state were averaged, and are here presented in Fig. 8.5. The results showed relatively small variations in the expansion coefficient with temperature, over the temperature range of 25°C to about 100°C. It varied between a minimum value of about $12.2 \times 10^{-6}/°C$ to a maximum of approximately $13.0 \times 10^{-6}/°C$.

With regard to specimen C3, heating was applied simultaneously on a similar specimen C4, which served as a shrinkage control, and therefore as an indicator to the water phase in the specimen. This test was considered desirable since no other attempt was made to monitor the water distribution directly, although time-dependent changes in the total weights of the specimens were being regularly observed.

A temperature crossfall of about 36.5°C was symmetrically applied on both specimens, and sustained for a period of 200 days, interposed by short cooling intervals of 2 to 3 hours, for evaluating the coefficient of expansion across C3 block. Then, following a cooling period of about 12 days, both sets were subjected to a temperature cross-fall of about 72.0°C, with a maximum hot face temperature of about 110°C. These temperature states are depicted in Fig. 8.6.

Curves plotting the coefficient of thermal expansion against time for the five elements of C3 block are displayed in Fig. 8.7. The relevant data from this plot was utilised in deducing the shrinkage profiles of the companion set, which are displayed in Fig. 8.8. The shrinkage–moisture loss relation for the companion block C4 is on the other hand depicted in Fig. 8.9. Because it was only possible to record the total weight loss from the whole block, the shrinkage values plotted are evaluated by averaging the shrinkage strains of the five block laminations recorded at the same age.

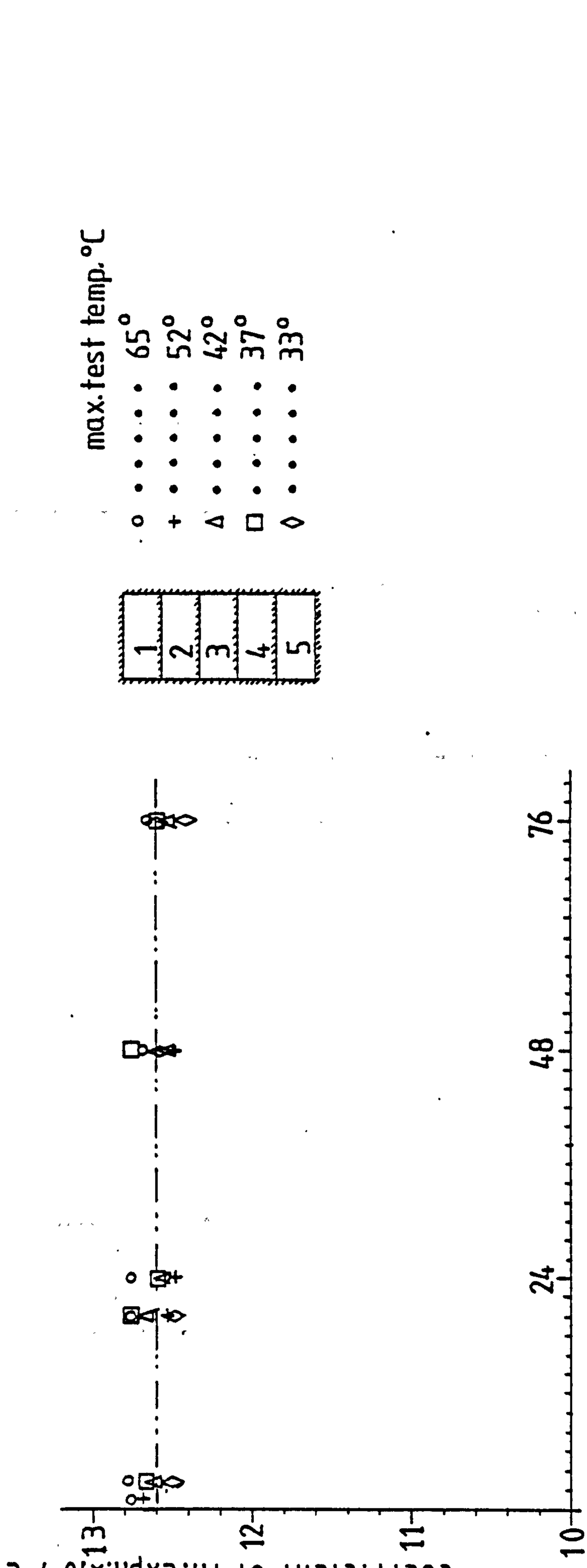

Fig.8.5 Variation of the coefficient of linear expansion with the moisture-stable block B3 across the moisture-stable block B3

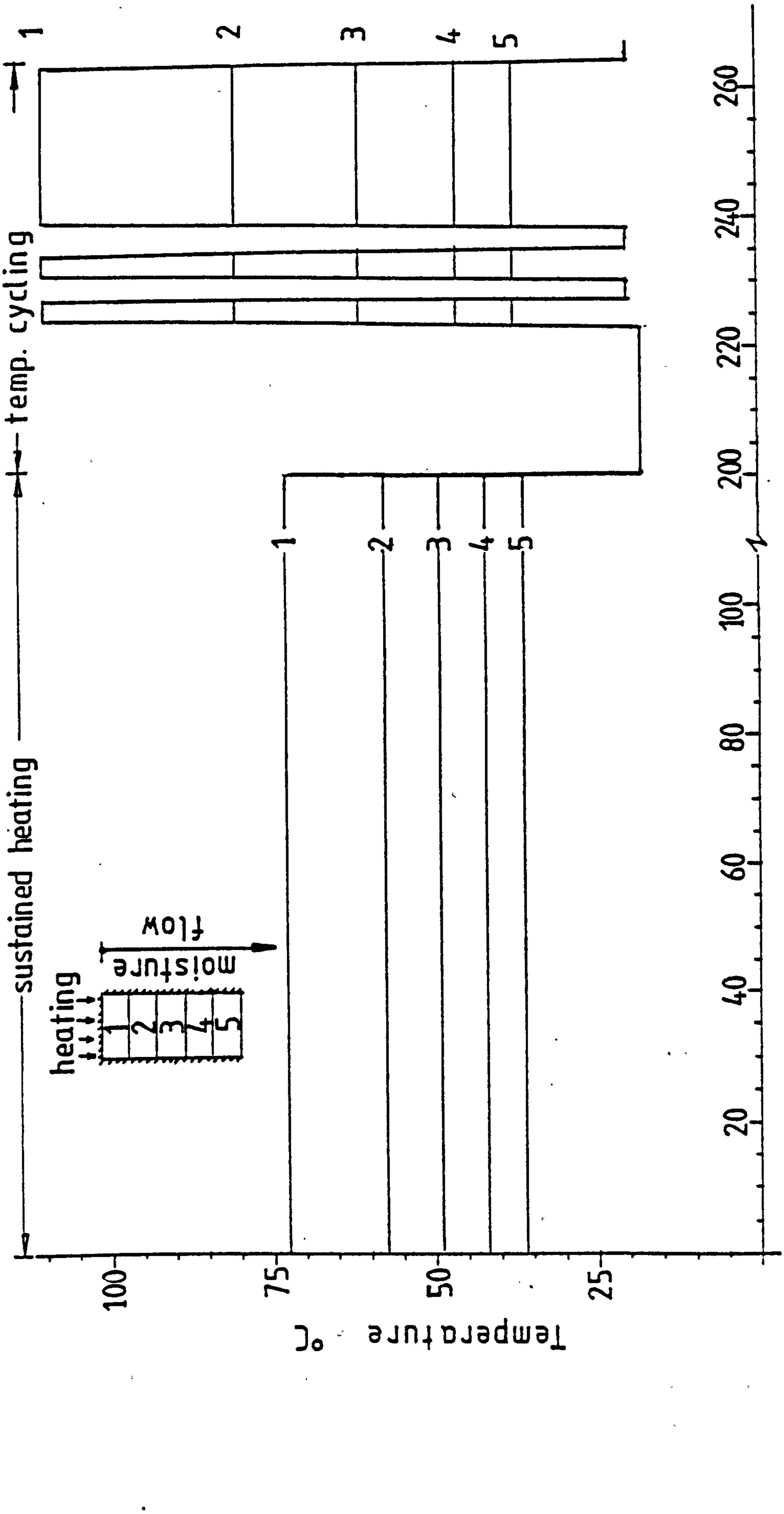

Fig.8.6 Temperature histogram of specimen C4 and the expansion specimen C3

Fig. 8·7 Variation of the coeff. of linear expansion with time in attendance of moisture flow accross the specimen (C3-block)

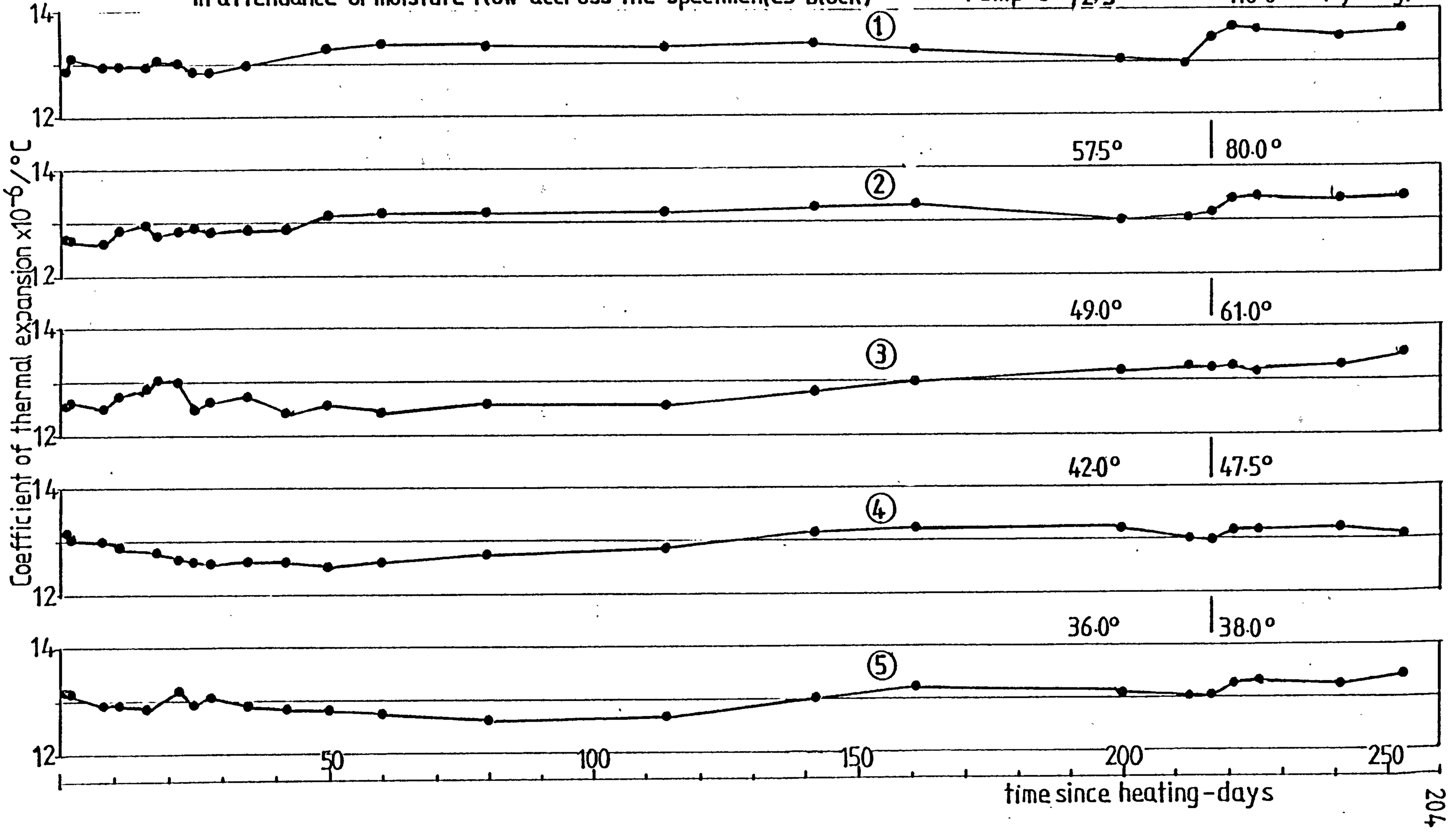

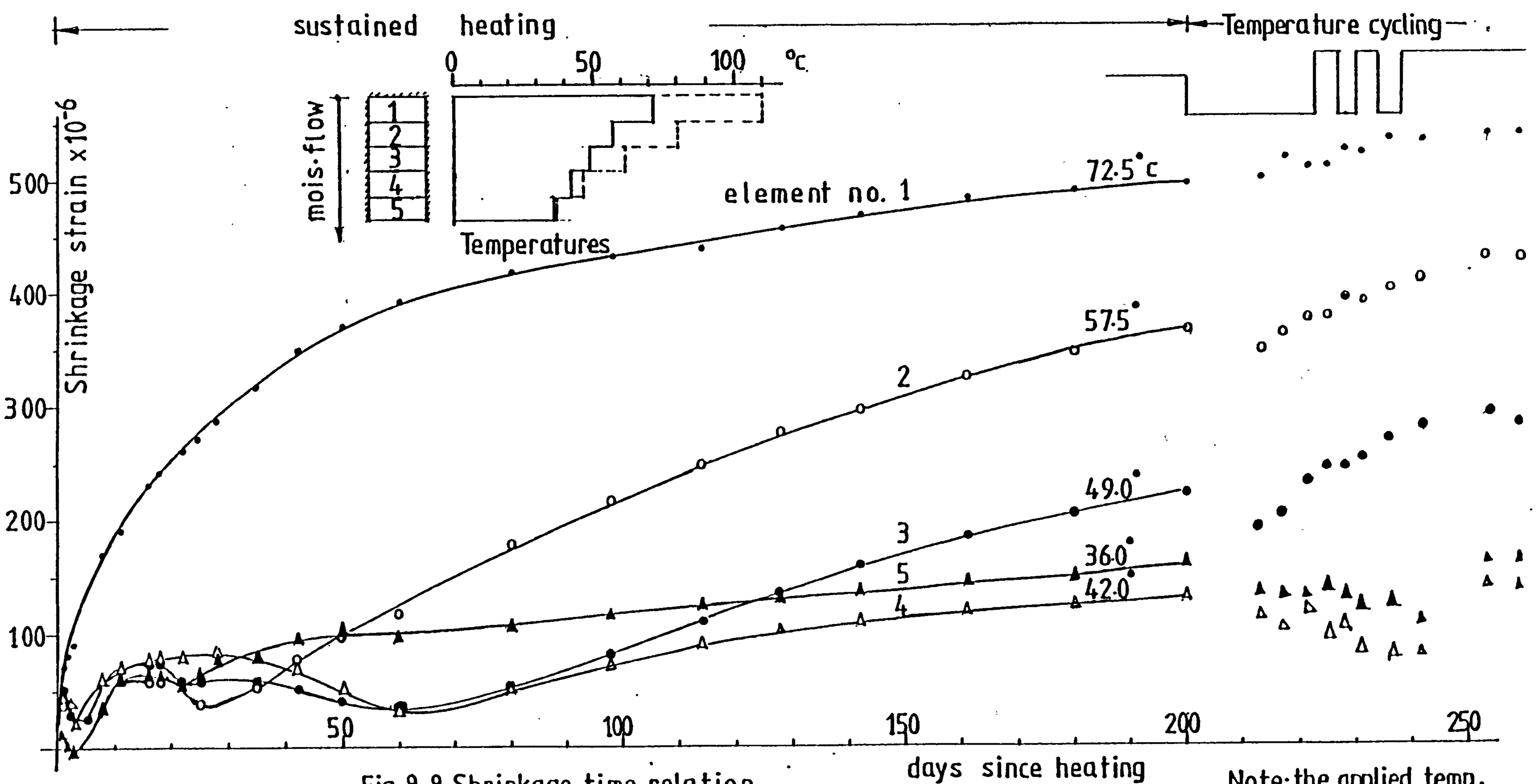

Fig. 8-8 Shrinkage-time relation specimen C4

Note: the applied temp. regime is given in Fig 8-6

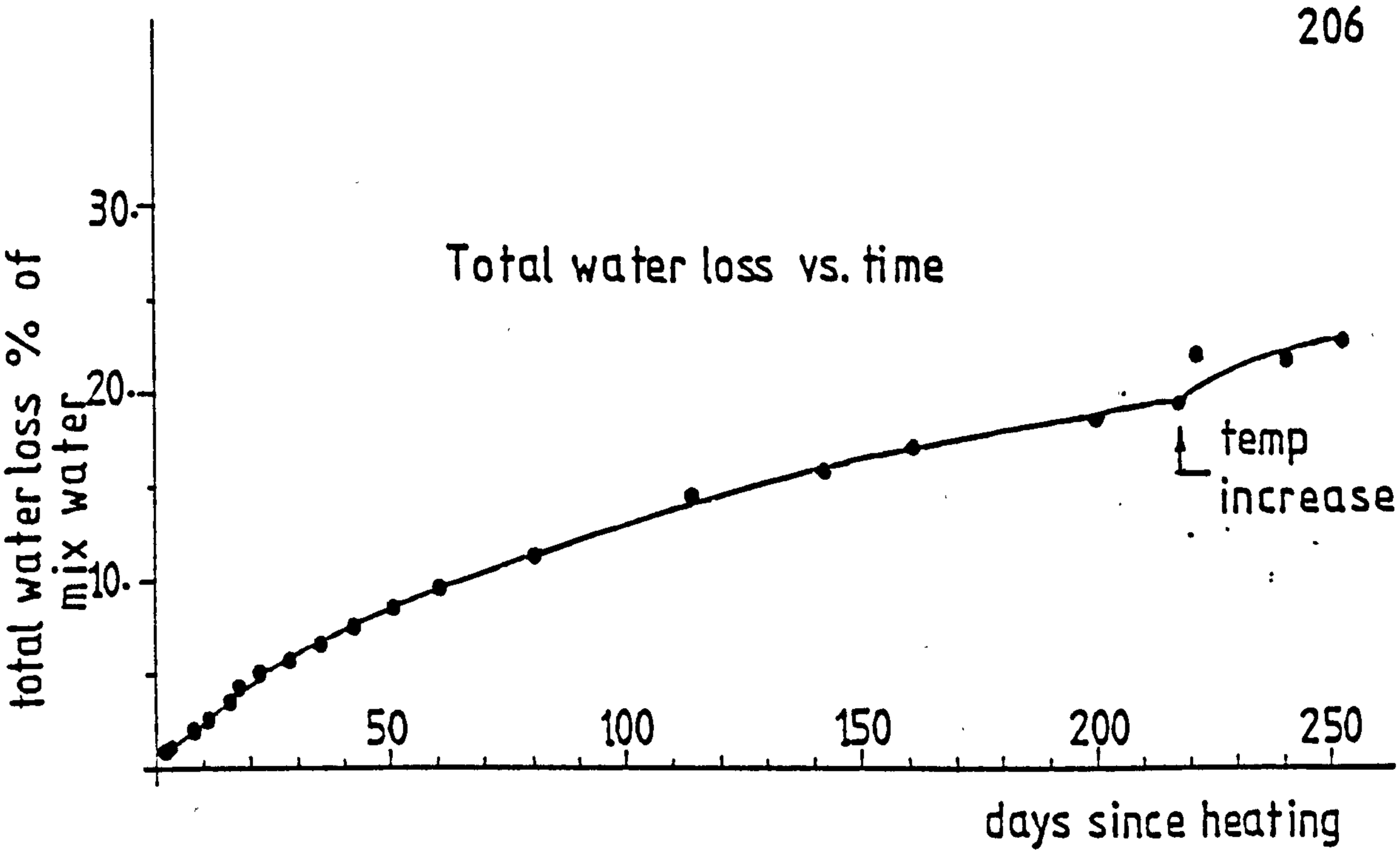

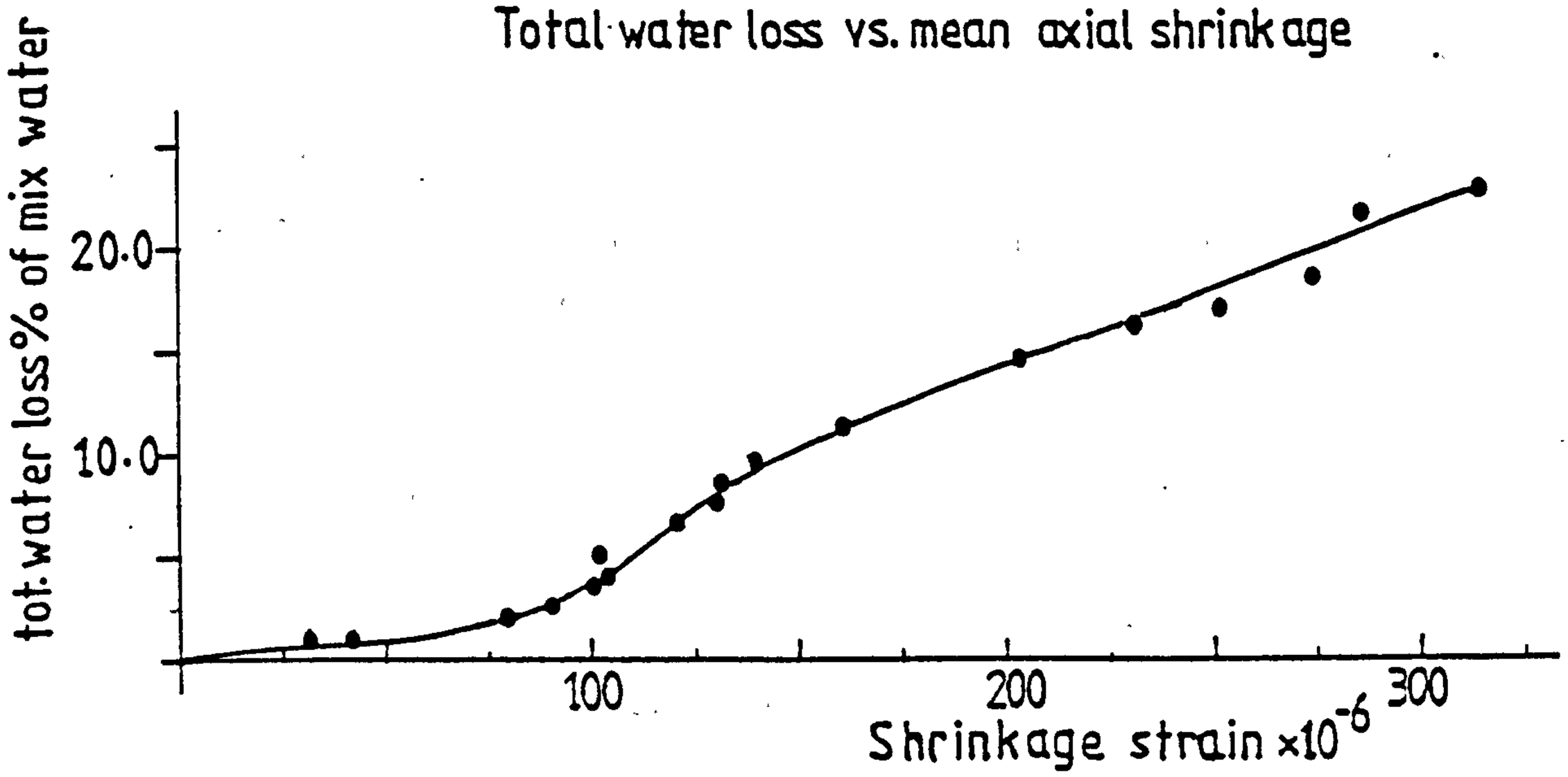

Fig.8.9 Variations of total moistur loss with time and the mean axial shrinkage of specimen block-C4 laminations

Although the observed variations in the coefficient of thermal expansion over the specimen's section were comparatively small, for the test conditions prevailed, the trends indicated by the results were clear. By inference from the shrinkage behaviour of the companion set (Fig. 8.8) the intermediate and cold front elements of C3 block (Nos. 2, 3, 4 & 5) experienced drying retardation during the first few weeks of heating. Over approximately the same period of time, their expansion coefficients were initially reduced slightly and/or remained fairly constant for a while.

In time, when drying became dominant, the expansion behaviour of elements Nos. 3, 4 and 5 exhibited rising trends with time, as indicated by the lower three curves of Fig. 8.7.

In general, the maximum observed difference in the expansion coefficient across the laminated specimen at any one time was about $1.0 \times 10^{-6}/^{o}C$. It varied between 12.4×10^{-6} and $13.45 \times 10^{-6}/^{o}C$ for the middle and hot front elements during the first heating phase. The variation during the second heating phase, however, ranged between a value of $13.0^{-6}/^{o}C$ for the fourth and fifth elements, and a maximum value of about $13.70 \times 10^{-6}/^{o}C$ for the hot front element, No. 1.

8.3.2 Temperature states in the main experiments

The first stage of heating was applied to the specimens approximately 22 days after loading, and sustained for up to 200 days. Thereafter all, except series D, specimens were exposed to various temperature cycling regimes spread over extended periods of up to 75 days. These temperature histories are described in Figures 8.10 to 8.13.

The temperature crossfalls were established over the specimens approximately 24 hours after the power was switched on to the heating

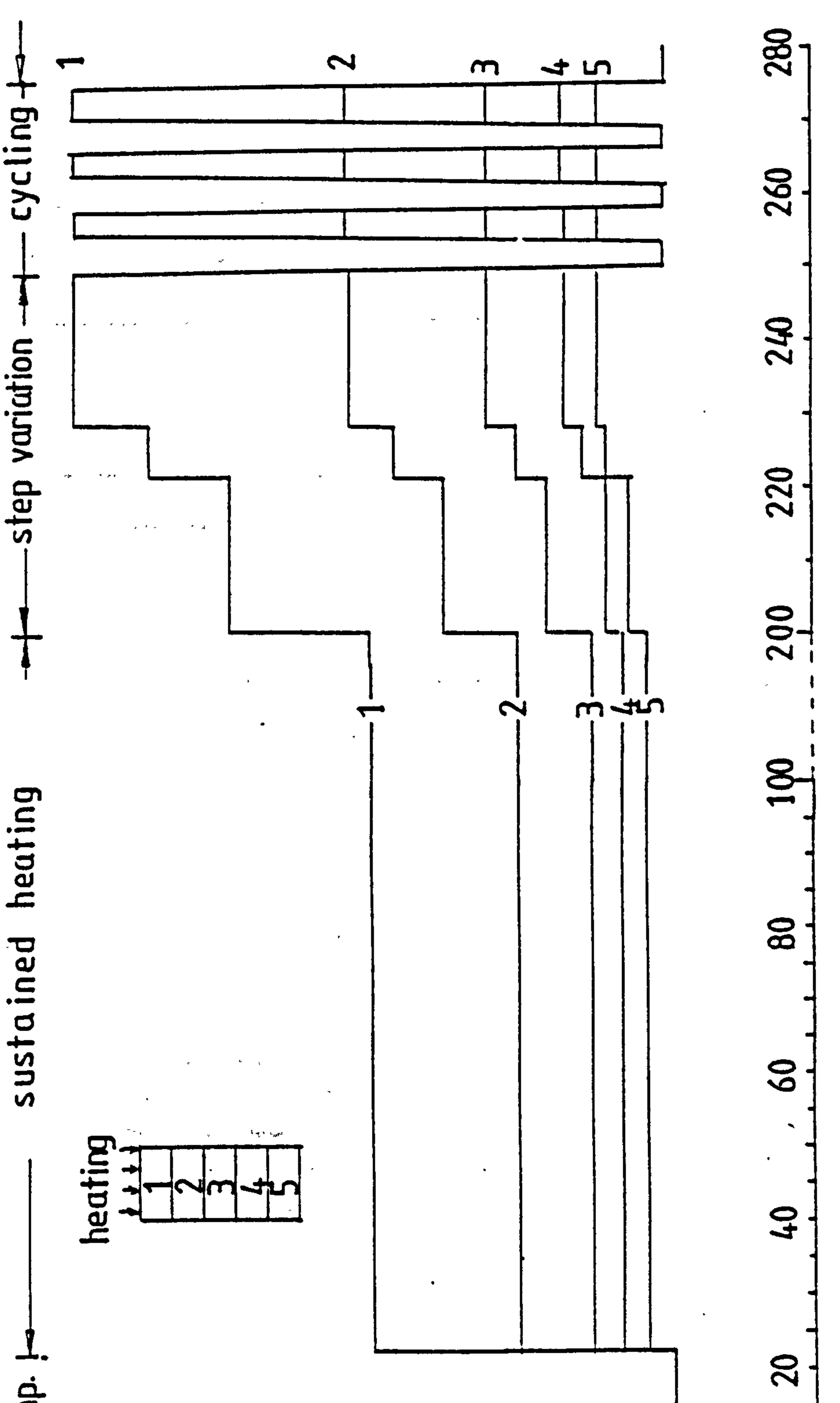

Fig.8.10 Temperature histogram of specimens B1 & B2

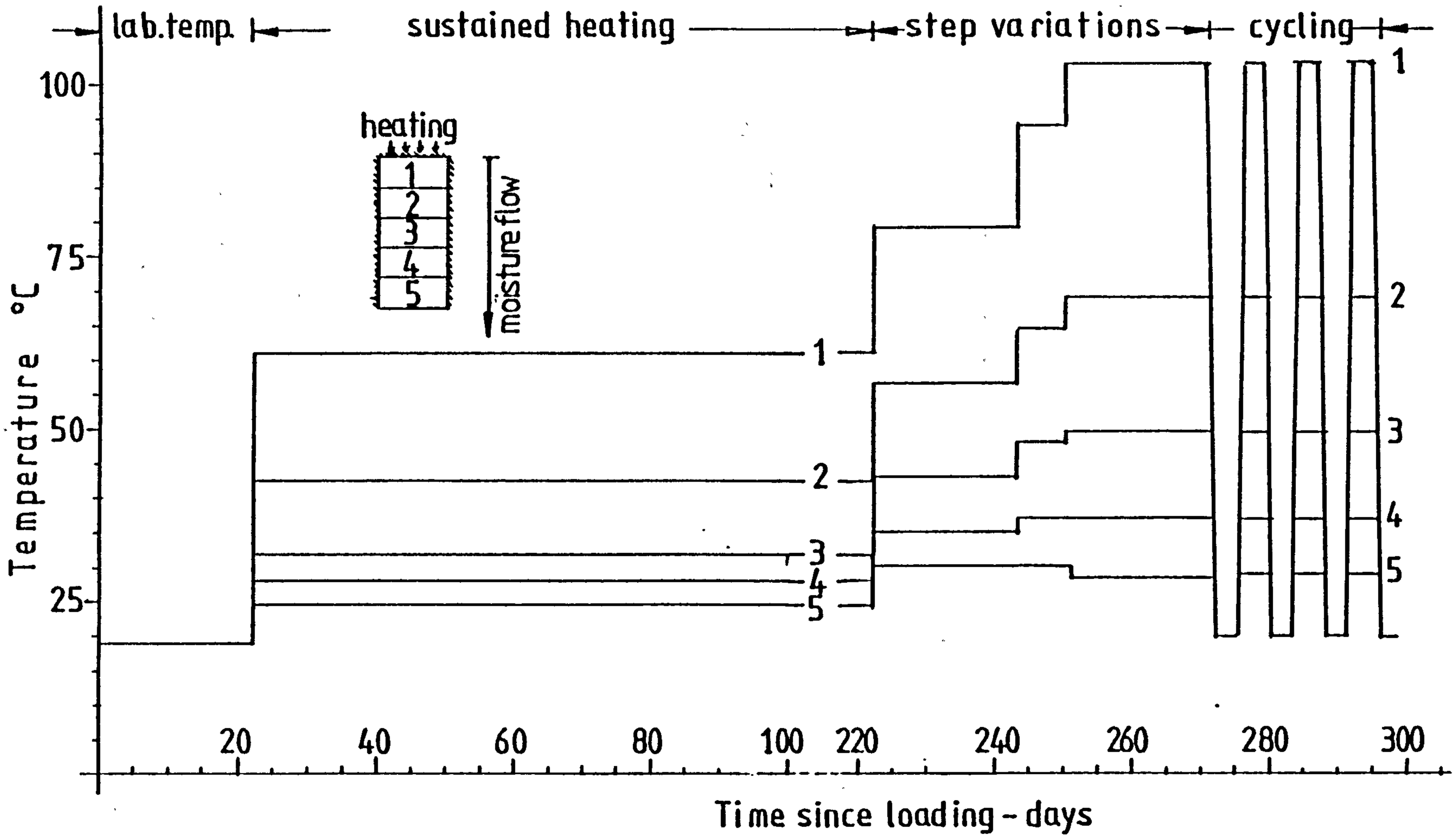

Fig.8·11 Temperature histogram of specimens C1 & C2

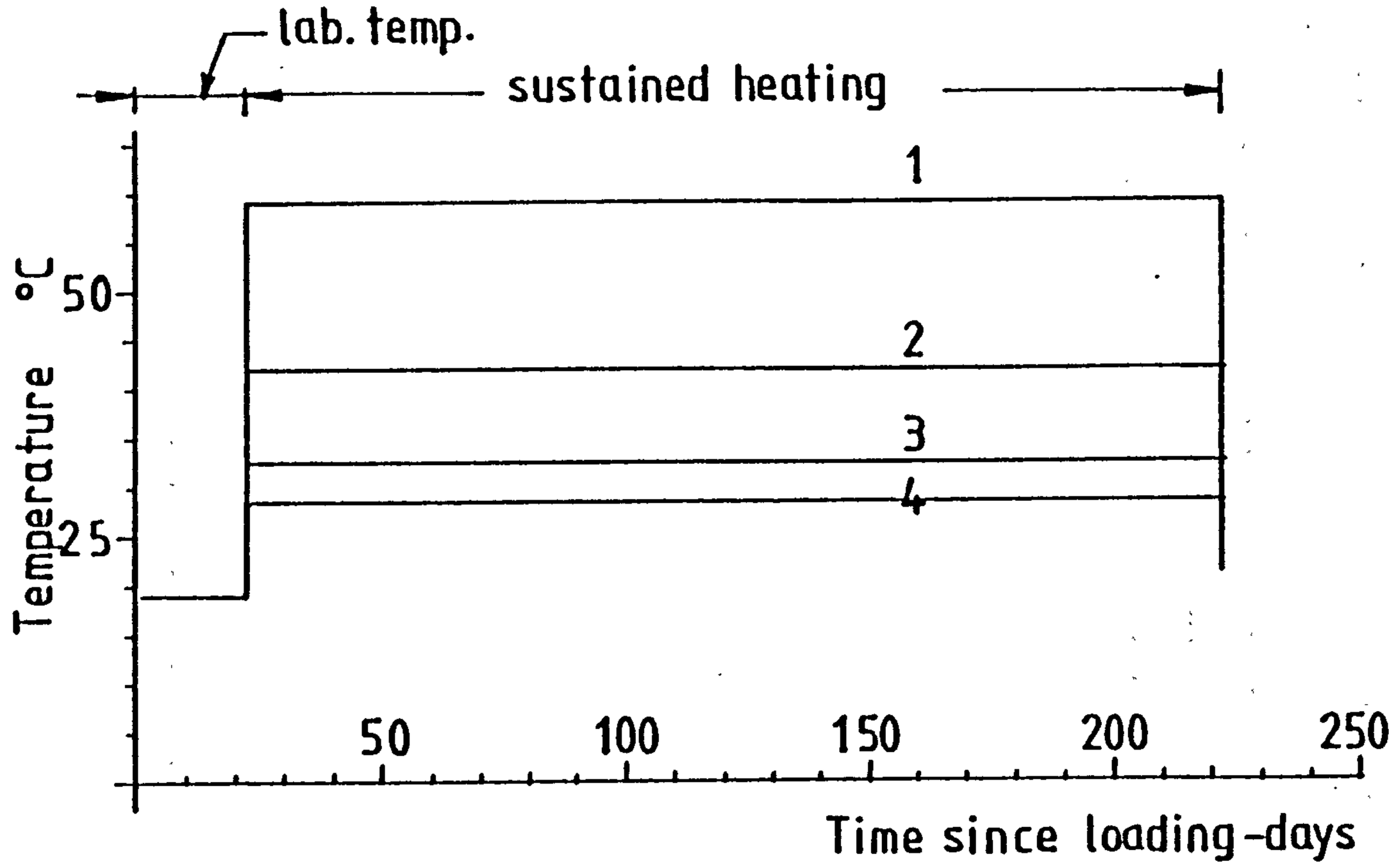

Fig.8-12 Temperature regime for specimens D1 & D2

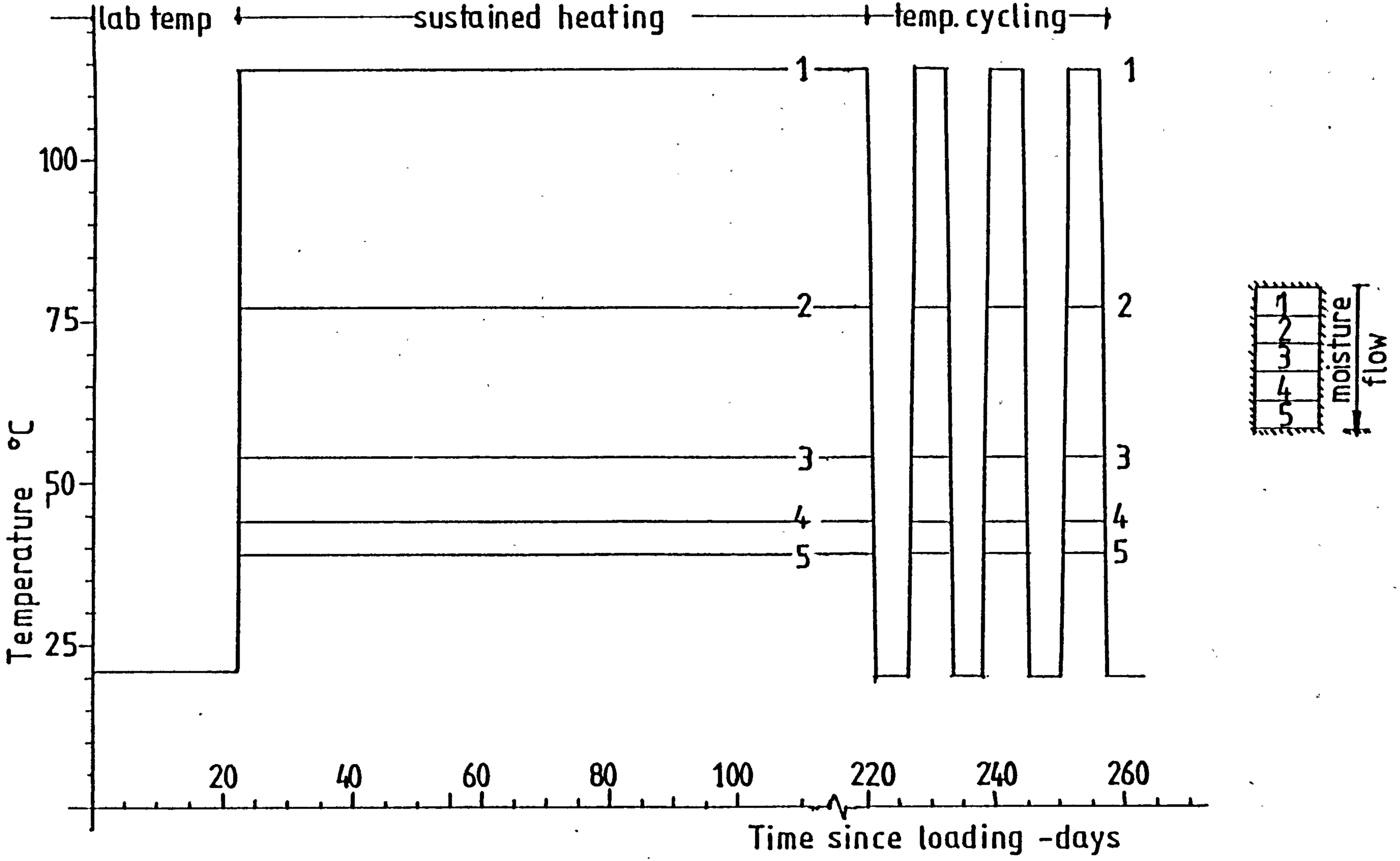

Fig. 8.13 Temperature histogram of specimens E1 & E2

circuits. The resulting distributions of temperature across each loaded set and its companion were generally the same. In one or two cases, however, variations of up to 2.0°C were observed between the temperatures of the intermediate elements of some experimental sets with the loaded ones being on the lower temperature side. This was largely due to heat losses from the ends of the loaded elements, for which it was not possible to ensure sufficient and equal insulation as for their opposite numbers in the shrinkage specimen.

With regard to specimens from the different test series, it was intended that series B, C and D were to have equal distributions of temperatures. Eventually, some success in this direction was achieved. All of these specimens were ascertained almost the same hot face temperature and the nominal temperature gradients, i.e. the temperature crossfall divided by the length of the specimen. Table 8.2 gives the mean temperatures and the resulting nominal temperature gradients sustained across the various sets, including the much higher values sustained on series E specimens.

Table 8.2

Test series	Mean temperature of the elements					Length of specimen mm	Nominal temp. gradient °C/mm
	1	2	3	4	5		
B	60.0	40.0	30.0	26.0	22.5	222	0.17
C	61.0	42.5	32.5	28.0	23.5	222	0.17
D	60.0	42.0	32.5	28.5	-	178	0.18
E	114	77	54	44	39	222	0.34

The differences shown between the temperatures of the intermediate elements of series B and both C anc D specimens are believed to be due to differences between the thermal conductivities of the interface materials, namely the Bakelite resin coating and the card sheeting. In the event, it was found practically impossible to generate equal temperatures for the said elements without having to adjust the spacings between those of the test series C and D.

Over the test periods small fluctuations in the temperatures arose largely as a result of similar variations in the laboratory temperature. More noticeable changes, however, were observed in the experiments involving moisture movements, where temperatures of the elements down the moisture gradients showed a tendency to decrease with time. These necessitated small changes to be made in the input power supply to the heating circuits.

8.3.3 Shrinkage

Curves describing the development of shrinkage strains with time for the laminations of C1 block specimens are displayed in Fig. 8.14. The data points shown on each curve were calculated by deducting from the observed total strain, the temperature strain components, using the appropriate value for the coefficient of expansion for the relevant element from Fig. 8.7.

The trends of behaviour indicated by the results of this test bear a close similarity to those indicated by the results of the previous experiment, shown in Fig. 8.8. Examination of both sets of results, however, reveals evidence of a number of well-known and other interesting features. For instance, both figures show clear evidence that the continuing migration of moisture from the hot front elements, i.e. No. 1,

Fig.814 shrinkage-time relation
specimen C1

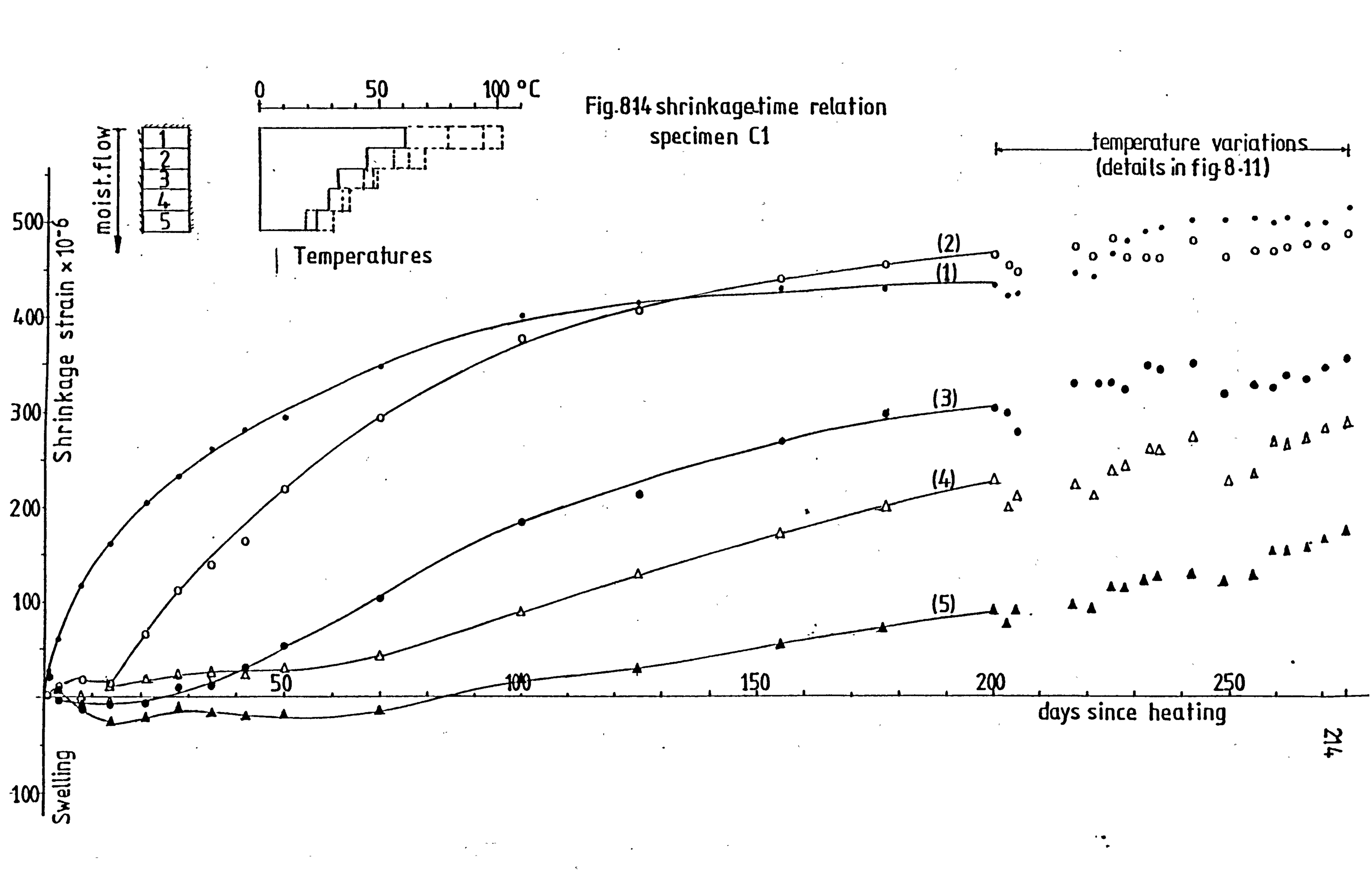

caused retardation of drying in the nearby cooler elements. Subsequently, the shrinkage rates in these parts of the sections were considerably reduced.

It is of interest to note that for the specimen having lower operating temperatures, the effects of the continuing water migration gave rise to swelling in the exposed cold front element, No. 5, which persisted for a period of over three months. In general, the effects on the intermediate parts of C1 block compared to those induced on the similar parts of block C4 were less severe. The reason may, however, be attributed to the fact that since the hot front temperature of the latter specimen was considerably higher than that of the former, the initial rate and amount of water migrating into the cooler parts of the specimen were obviously higher.

Close examination of Fig. 8.14 reveals that following the stepping up of the temperature gradient a general decline in the shrinkage of elements Nos. 2, 3, 4 and 5 occurred. This could be interpreted by the continuing migration of moisture from the higher to the lower temperature elements of the block. Apparently, due to the easing off of the moisture flow from the whole block, a rejuvenation of the shrinkage, or migration rate, occurred in all elements, after the first three weeks period. However, there were no indications of significant recovery or otherwise in shrinkage on cycling within the same temperature levels.

Fig. 8.15 illustrates the shrinkage behaviour of the four laminations of specimen D1, which was exposed to a sustained temperature crossfall of about 31.5^{o}C. This gives a nominal temperature gradient of about 0.18^{o}C/mm which is slightly greater than that of C1 and C4 blocks. It can be seen from this figure that shrinkage, or drying was developed at the colder end of the specimen with considerably less difficulty and delay. Such behaviour is a clear indication of the significant effects

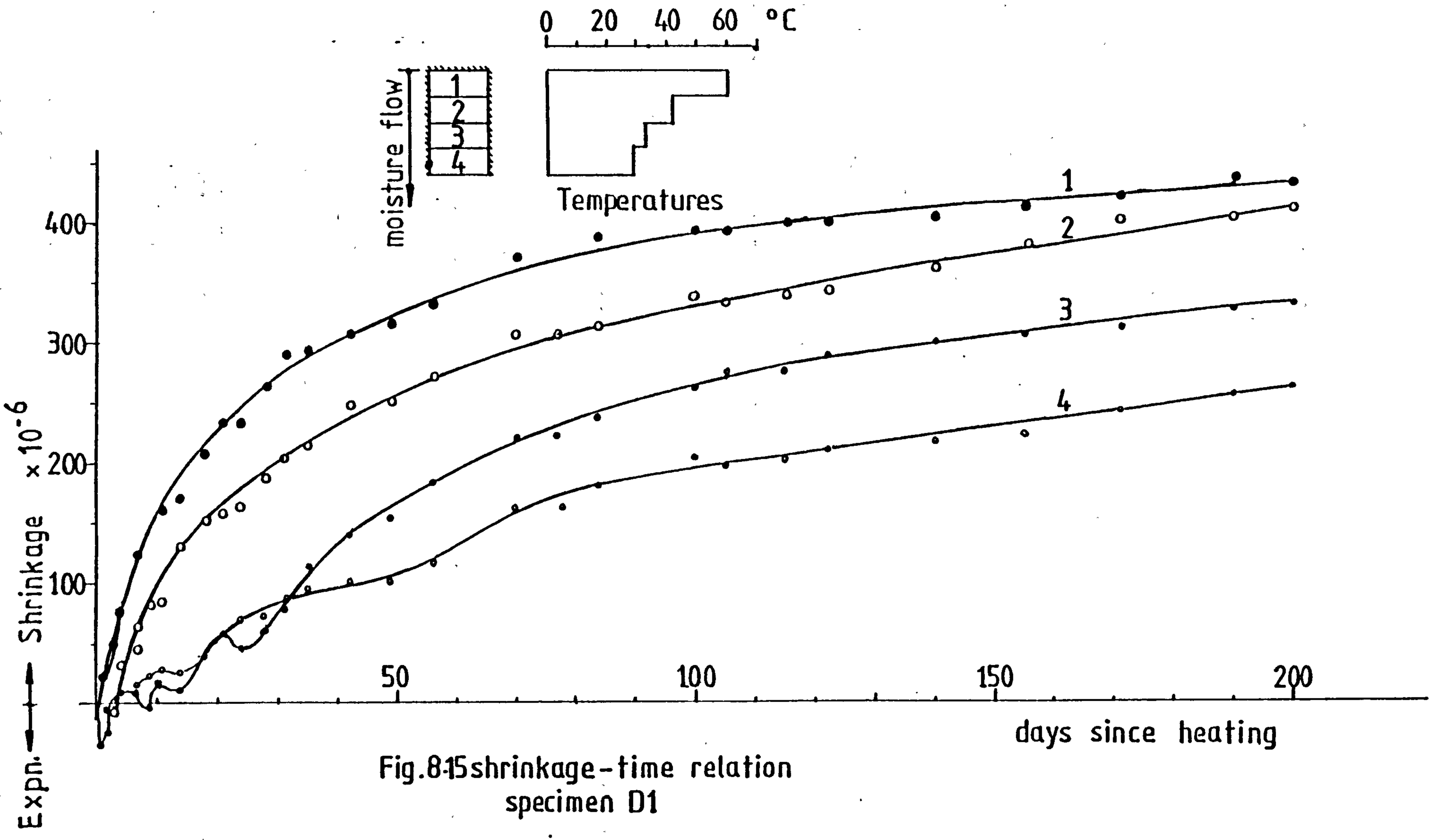

Fig.8.15 shrinkage-time relation
specimen D1

of both the moisture path length and the operating temperature gradient on the movement process of moisture. The rates of drying are greater the shorter the moisture path length and the higher the temperature gradient.

Fig. 8.16 plots the shrinkage data obtained from the experiment on specimen E1, which was subjected to a sustained temperature crossfall of about 75°C with a maximum hot face temperature of 114°C. Although the test was designed with the intention of containing the moisture movement within the specimen's boundaries, unfortunately moisture seal failure occurred apparently at the two fronts of the specimen. Close examination of the results indicates that, as a result of the high operating temperature, the seal at the hot front failed some time during the second day of heating, as suggested by the sudden increase in the shrinkage rate during this period. Whereas at the cold front the seal failure appears to have developed between the second and third week of heating, probably as a result of concentration of substantial amount of water.

The results show that due to the rapid release of free water from the hot front element, a major part of its 200 days' shrinkage has developed over a fairly short period of time. As an example, about 90% of this amount was reached at the heating age of 27 days. In respect of the second element of the group, however, the results showed that from the age of two days onwards, the moisture migrated from the element was obviously greater than the amount migrated into it from the hot front. On the other hand, the results show that swelling caused initially in the colder parts of the specimen eventually dissipated, apparently after the release of moisture from the cold end.

Examination of the results during the cycling temperature regime reveals no evidence of any significant changes in behaviour as a result of cooling or subsequent temperature cycles.

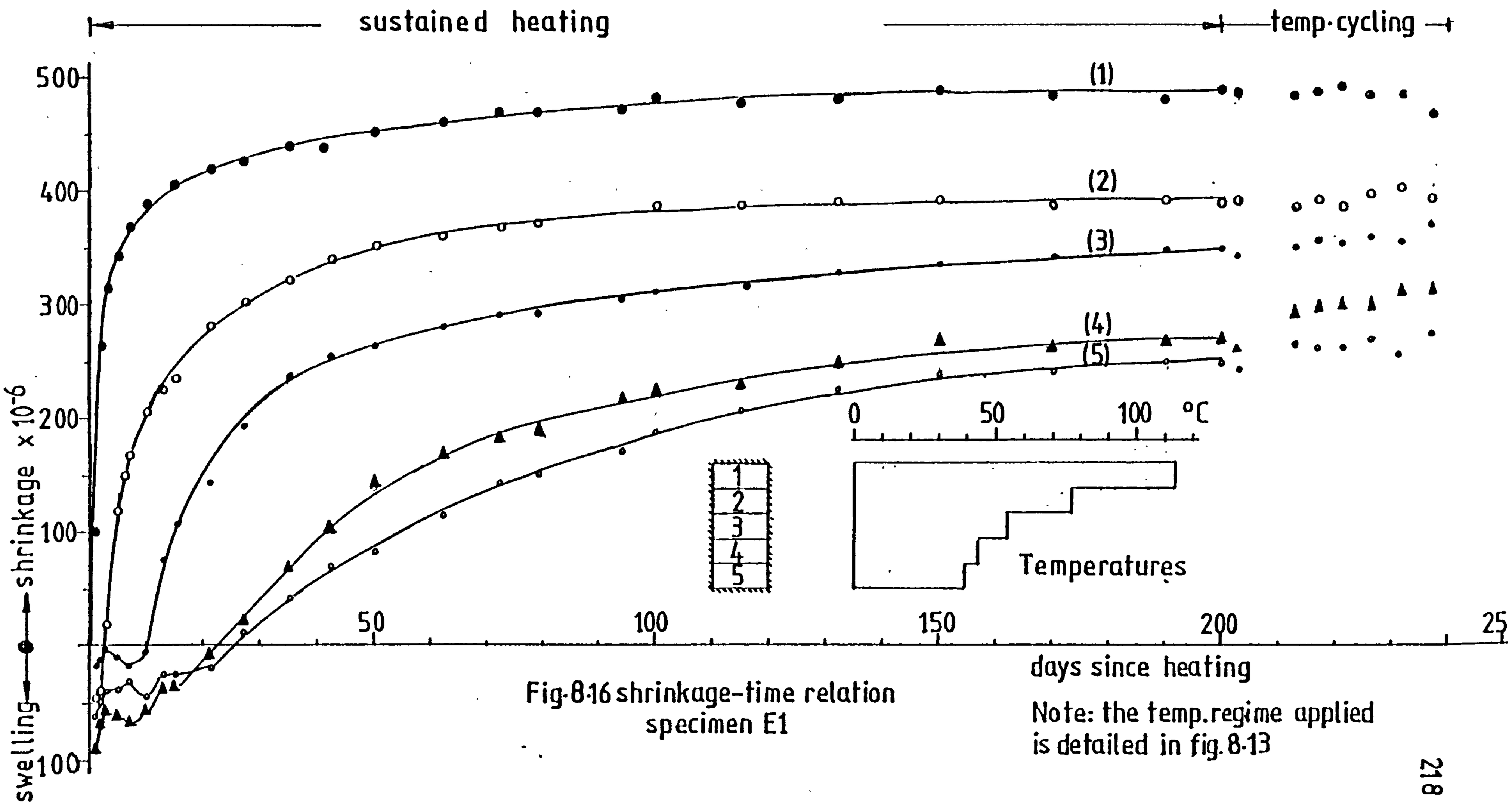

Fig·8·16 shrinkage–time relation specimen E1

Note: the temp.regime applied is detailed in fig.8·13

8.3.4 Creep under constant moisture content

Effect of sustained elevated temperature

The uniaxial creep behaviour of the moisture stable elements of B2 block under the various temperature states is described by the specific creep profiles drawn in Fig. 8.17. Over the sustained temperature regime, the results indicated trends which were, in many aspects, consistent with those of previous findings. For instance, the creep rates of the five elements were increased sharply during and shortly after heating, which was applied 22 days after loading. Also, there was a continuous increase of creep with time, which at the upper temperature levels appeared to follow the same general pattern of creep at the lowest temperature level.

Values of specific creep strains at significant times are re-plotted against temperatures in Fig. 8.18. The plot shows that between temperatures of 22.5°C and 60°C, the creep-temperature relationship over approximately the first month of heating was very nearly linear. At later ages, however, there was some deviation from this trend at 60°C, although the relationship remained linear between 22.5°C and 40°C throughout the period under consideration.

Effects of increase and cycles of temperature

The observations recorded during the subsequent phases of heating were also in broad agreement with those of earlier studies. For instance, there is evidence that the creep rates accelerated as the temperatures were stepped up for the first time. One interesting feature revealed by the results, however, was the apparent existence of a threshold temperature value above which the effect of a given temperature increment on the creep rate became more pronounced. On examination of

age of conc. at loading=32 days
" " on first heating=54 days
creep prior to htg. is shown in fig 8.2
applied stress=6.9 N/mm²

Fig 8.17 Specific creep-time relation for the sealed group B2

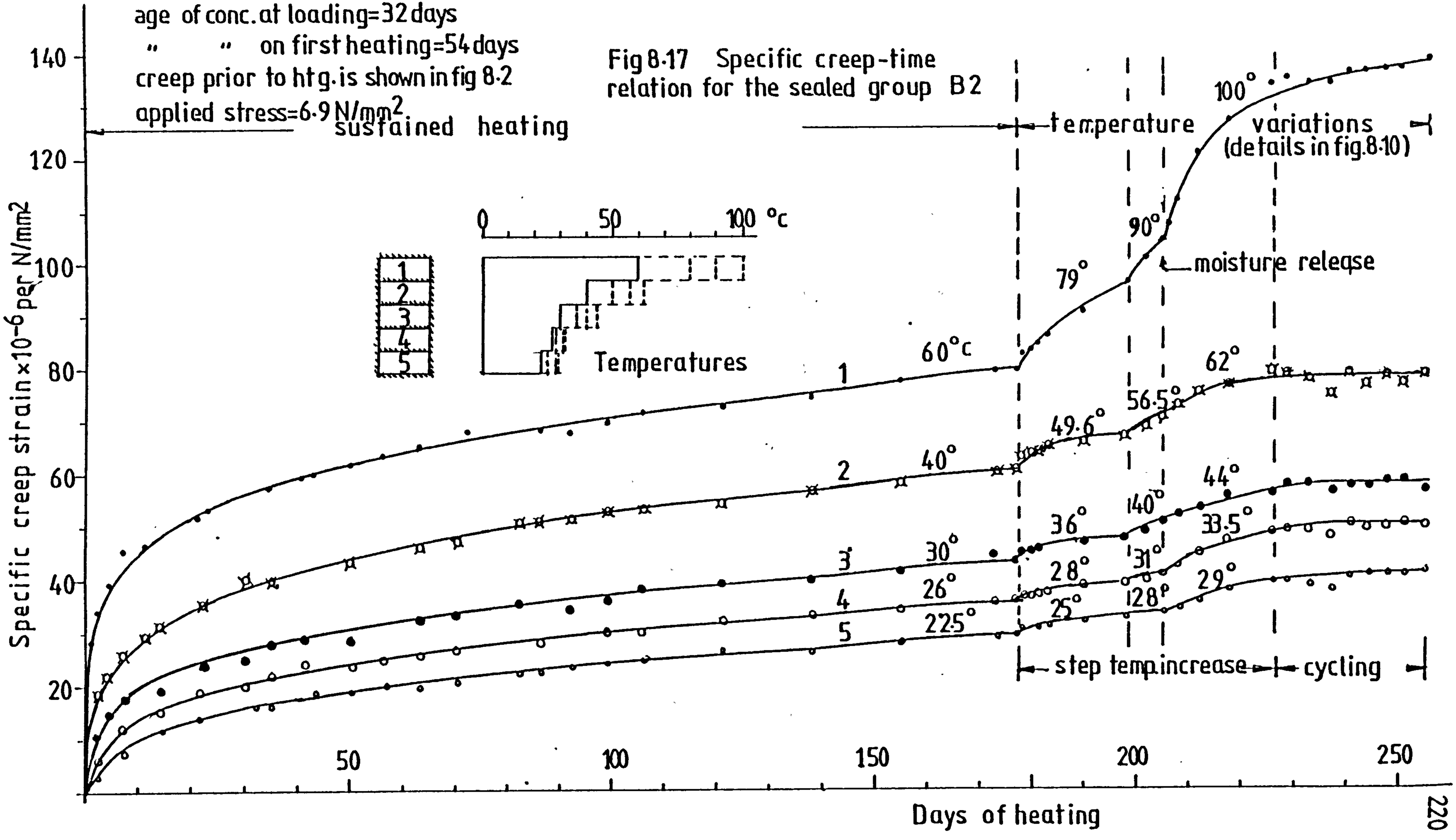

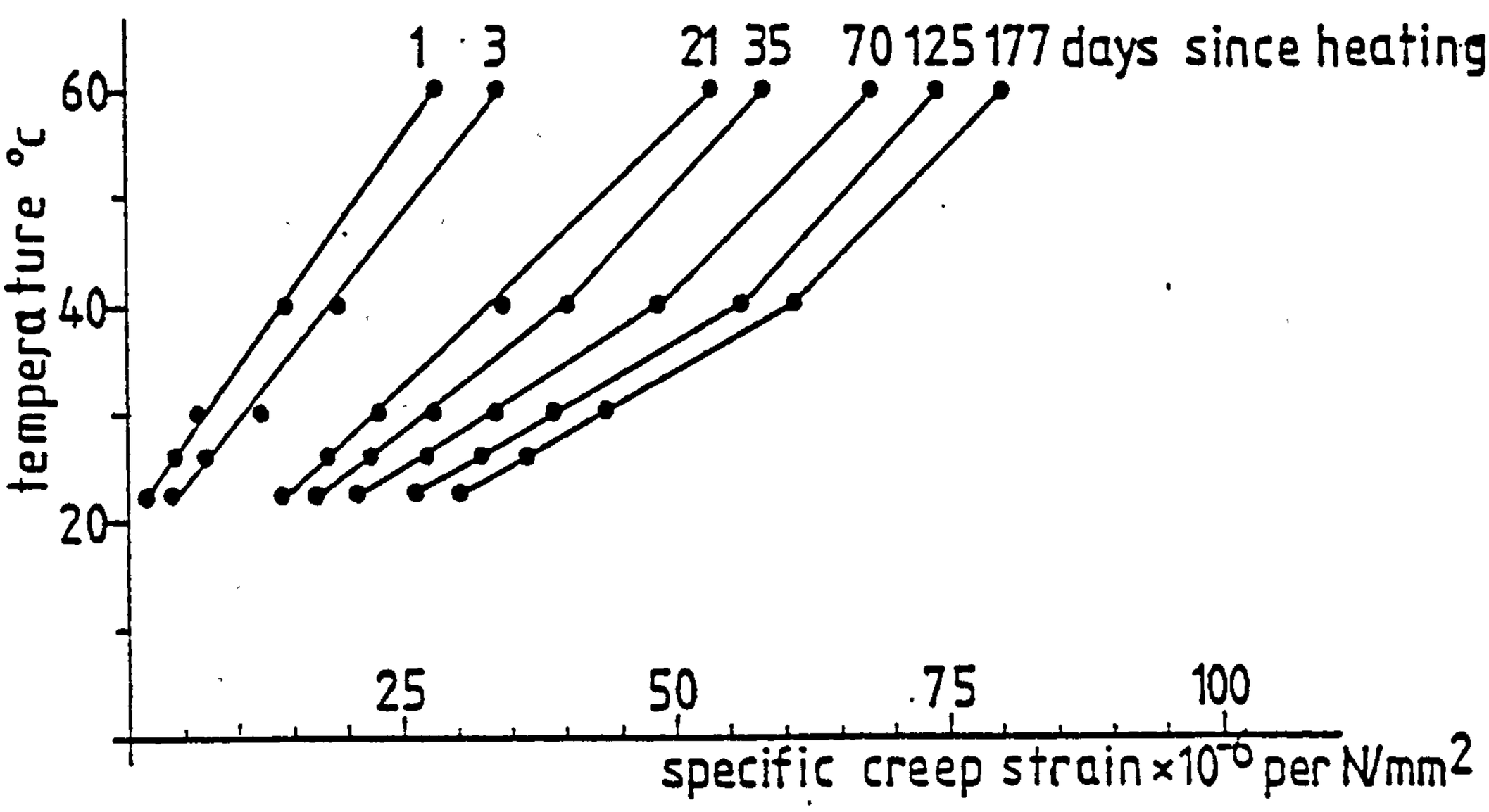

Fig.8.18 Specific creep-temperature relationship for specimen B2

the results described by the lower two curves of Fig. 8.17 this threshold value appears to be about 30°C. It is likely that the modulus of elasticity of the concrete started to decrease as its temperature was raised beyond this level.

Further increases in creep were observed during the second and third temperature step rises. The effect of the latter step on the creep of the hot front element was more pronounced as a result of the sudden failure of the moisture seal and the rapid release of free water from the element as its temperature was raised above 100°C.

The results show evidence that creep continued to increase with time during both temperature cycling and gradual cooling stages, with no signs of recovery.

8.3.5 Creep with simultaneous moisture flow through the specimen

Effects of constant temperature gradients

Curves plotting the variations of specific creep strain against time for the elements of C2 and D2 block specimens, which were tested in attendance of moisture flow, are displayed in Figures 8.19 and 8.20. The results show evidence indicating that both temperature and moisture movement played important roles in the development of creep strains in these specimens. The creep rates of all the elements concerned, for instance, accelerated greatly during and shortly after the temperature rises. In comparison to the behaviour of the sealed elements of B2 block, depicted in Fig. 8.17, the increases on first heating in the creep rates of the elements of these two blocks were, for similar temperature conditions, significantly greater. Such a behaviour illustrates the tendency of creep to increase more for a given temperature rise, when there is a migration of moisture from the continuum than when migration is prevented.

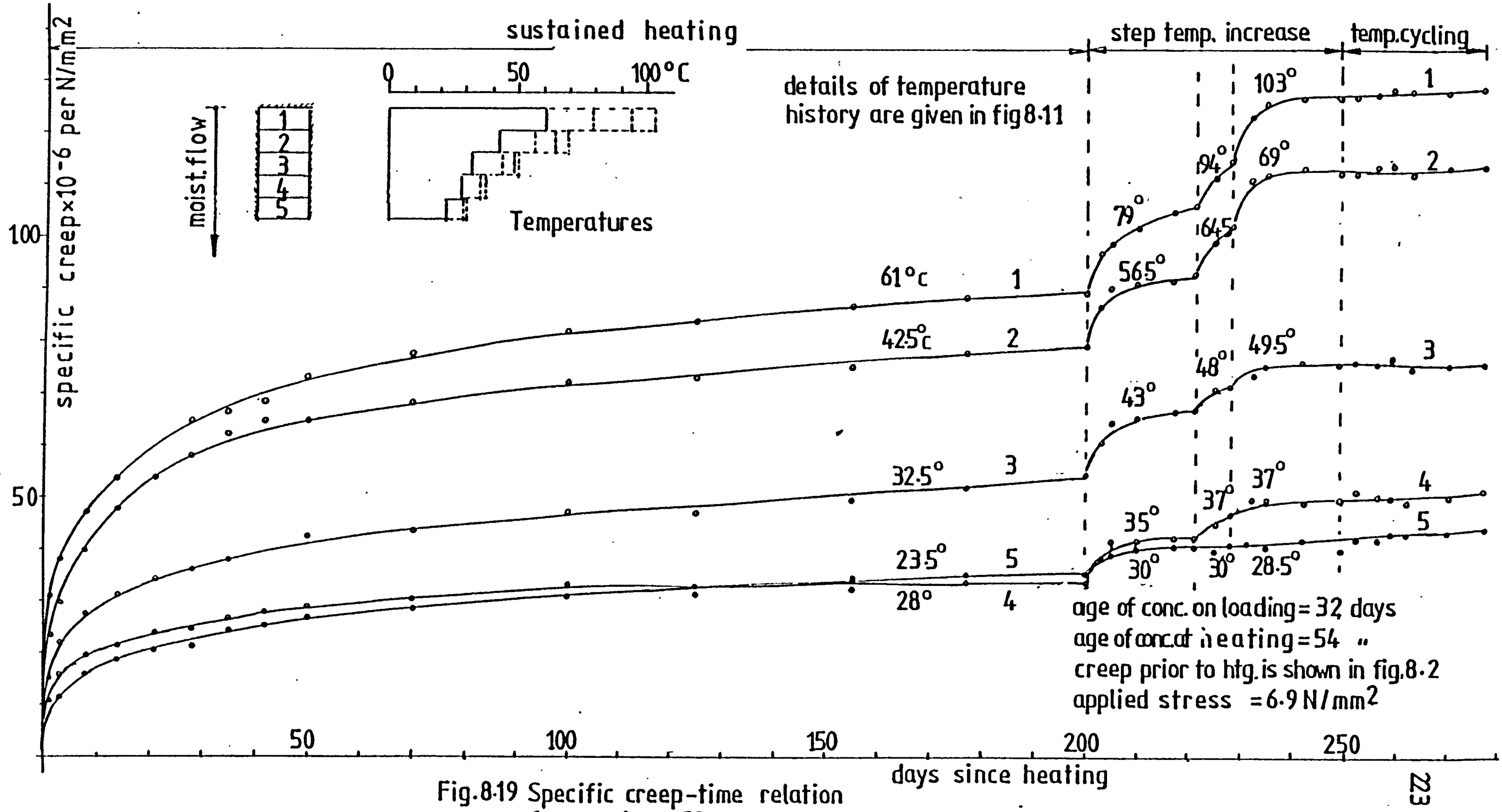

Fig. 8·19 Specific creep-time relation for specimen C2

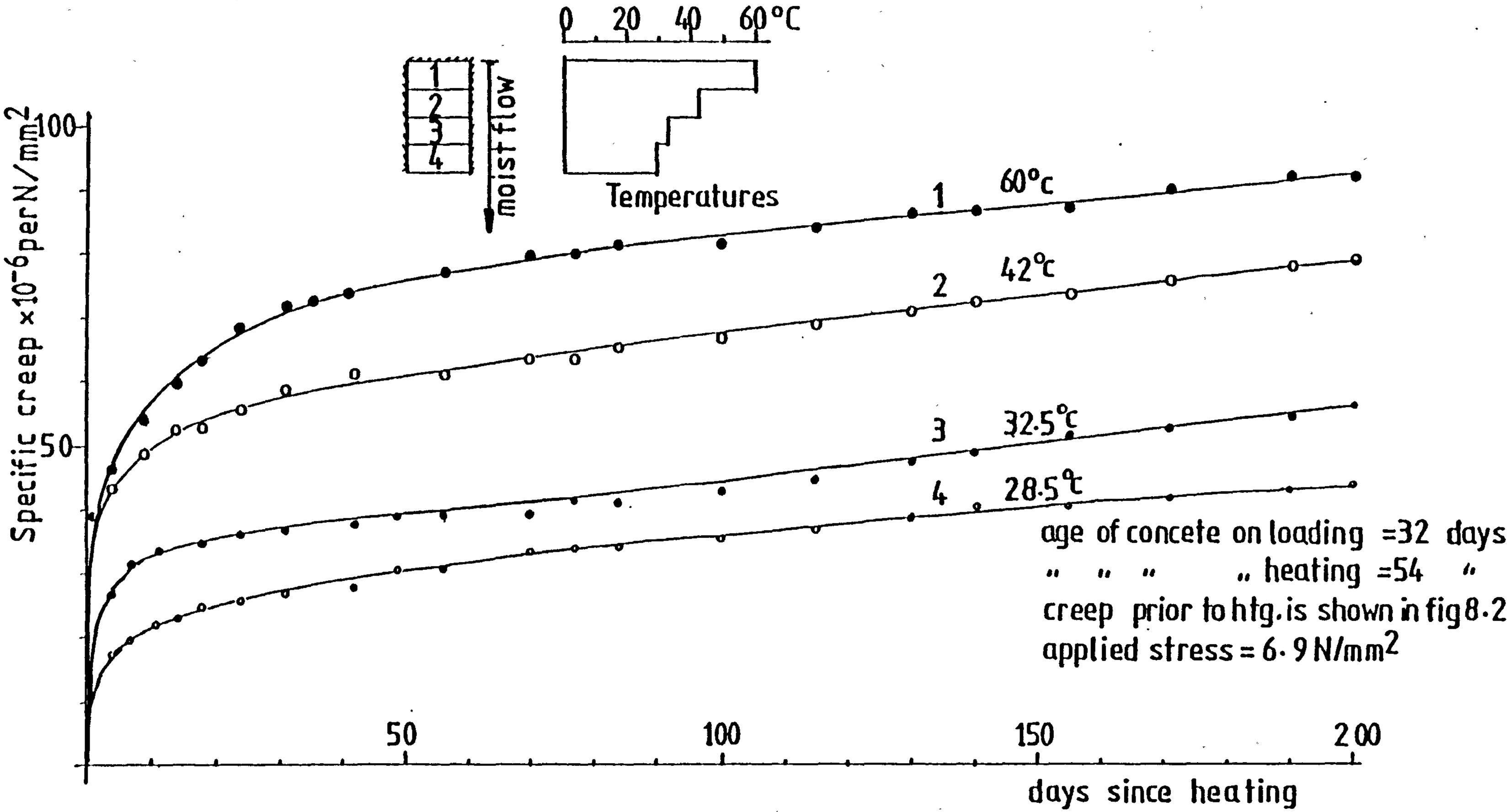

Fig.8.20 Specific creep-time relation
for specimen D2

There are some indications in the results of Fig. 8.19 that the creep rates in some parts at the cold end of C2 block were substantially reduced. After about the first two months of heating, for example, the fourth element of this block virtually ceased to creep. It may be of interest to note that the shrinkage of the corresponding elements of the comparison block C1, Fig. 8.14, was significantly reduced as a result of the continuing migration of moisture from the higher temperature zone.

In respect of the specimen block D2, it has earlier been established that, due to the shorter moisture path length, drying developed at a distinctly faster rate, thus causing minimum perturbation to the shrinkage behaviour of the elements. The results of the creep experiment, shown in Fig. 8.20, conveyed more or less the same general picture regarding the creep behaviour of these elements. It is apparent from the figure that the creep rates accelerated greatly during and shortly after the temperature rises. In comparison with the responses of the similar elements in the longer moisture path specimen C2, these were to some extent higher, as illustrated in the combined plot of the results shown in Fig. 8.21. This figure shows evidence in support of the previous argument concerning the influence of moisture concentration in the colder parts of the specimen on their creep behaviour.

Further supplementary evidence on the effects of both temperature and moisture movement on creep have been provided by the results of E2 block experiment displayed in Fig. 8.22. In discussing the results of the shrinkage block E1, it has been mentioned that, due to the severity of the temperature loading applied, the moisture seal failed at the hot front, which led to the rapid release of water from that element. Also, at a later stage, the moisture seal appeared to have failed at the cold front as well, probably as a result of higher concentration of moisture in that region. These are believed to have occurred for both E1 and E2

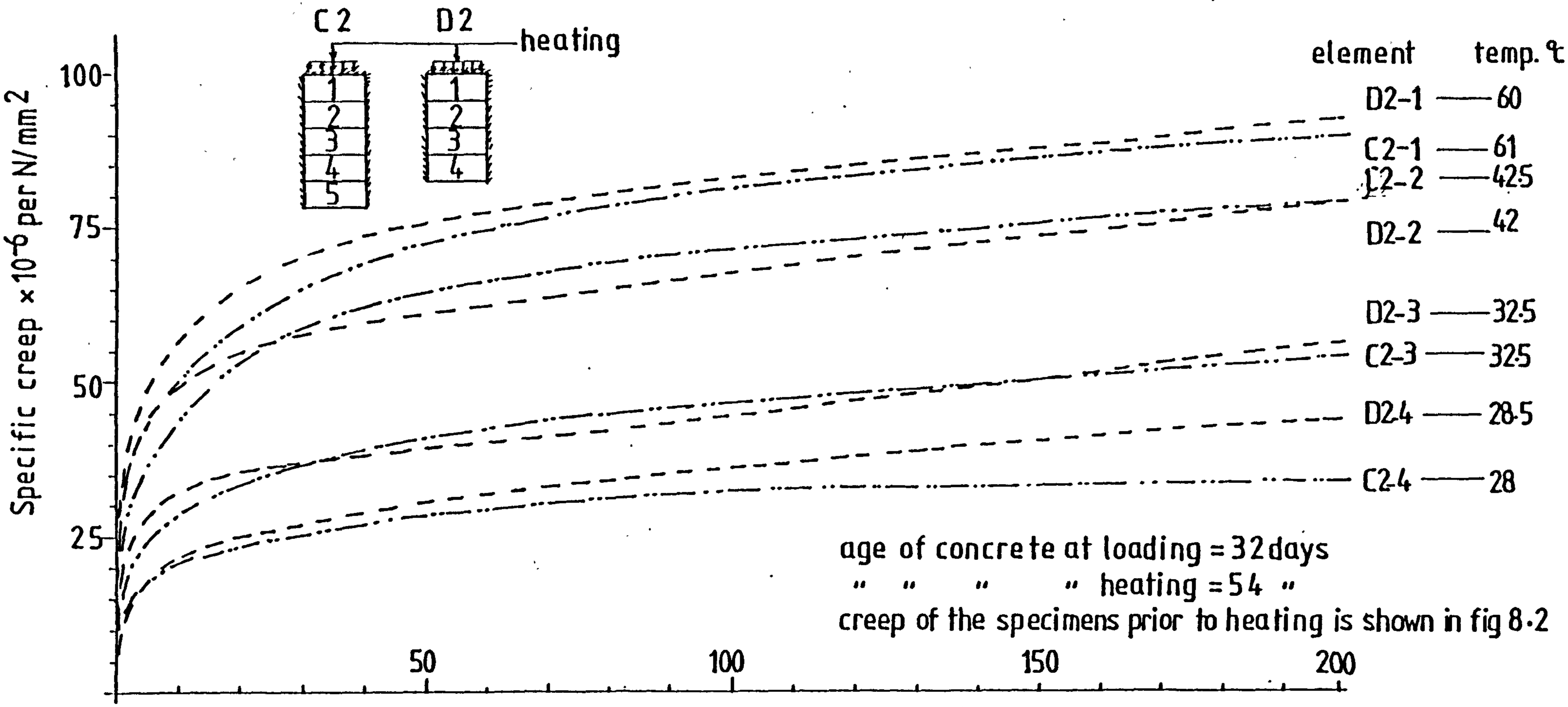

Fig.8·21 Combined plot of the specific creep profiles of the four elements of block-D2 previously shown in fig.8·20 and those of their opposite numbers of block C2 shown in fig.8·19

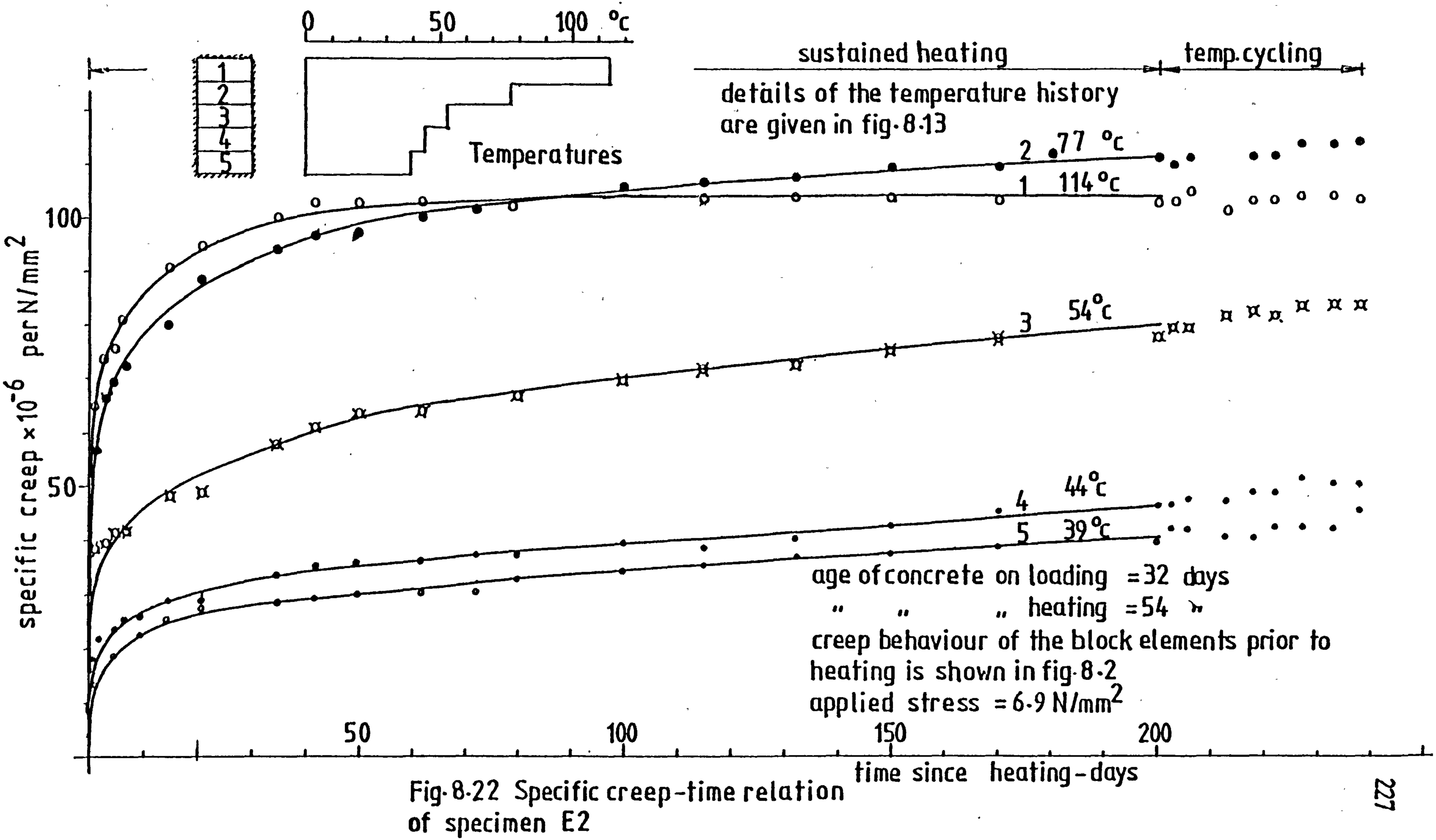

Fig·8·22 Specific creep-time relation of specimen E2

specimens, as was confirmed by the total weight losses recorded at the end of the test. In response to the applied temperature crossfall, all the elements developed large increases in the creep and creep rates, in particular elements No. 1 and 2 of the set. At 114°C, the hot front element exhibited a very sharp creep response, which reached a maximum of about 104×10^{-6} per N/mm^2 after about the first six weeks of heating. Nearly 63% of this amount was attained after the first 24 hours. The response of the second element was very similar, although the creep continued to increase with time with no apparent limit. At 200 days, it reached a value of about 112×10^{-6} per N/mm^2, of which over 50% was reached after the first 24 hours of heating. It is clearly obvious from these results that the rate of moisture movement greatly affected the creep behaviour of the specimens. The creep virtually ceased to develop in the hot front element, apparently after the complete withdrawal of the free water content. This was remarkably similar to its effect on the development of shrinkage strains discussed earlier.

With respect to the other three elements of the group, there are some indications that their creep rates were reduced considerably, sometimes over the period during which concentrations of moisture and swelling were caused in these parts of the specimen. However, as heating continued, some increase in the creep rate of the intermediate element developed, apparently when drying dominated the flow of moisture from the higher temperature zone of the specimen, whereas the creep behaviour of the other two elements was observed to continue in the same general pattern, with no significant changes over the duration of the test. To some extent, the behaviour displayed by these elements was consistent with that observed in C2 block experiment. The influence on behaviour in either case may be attributed by and large to the moisture movement potentials.

To elucidate the above argument, 200 days' creep data obtained for the three elements concerned are compared to data recorded at the same age in some elements of group C2 and D2 experiments, in Table 8.3. The latter two group elements were, by comparison to those of group E2, subjected to considerably less severe migration because of their comparatively low operating temperature gradients. Nevertheless, the data show that in spite of their temperatures being below those of E2 group elements, their creep strains were comparatively higher. The most significantly affected element, however, was here again No. 4.

Table 8.3

Specimen group	Element no.	Temp. °C.	Sp. creep $\times 10^{-6}$ per N/mm^2
E2	3	54.0	73
C2	2	42.5	79
D2	2	42.0	78
E2	4	44.0	39
C2	3	32.5	54
D2	3	32.5	56
E2	5	39.0	34
C2	4	28.0	36
D2	4	28.5	43

Effects of change and/or cycles of temperature gradients

The curves of Fig. 8.19 show that the creep of all five elements of C2 block accelerated considerably with the first increase in the applied temperature gradient. In comparison with the response of the sealed elements of B2 block, these were significantly greater, as was observed on first heating.

It should be mentioned here that the temperatures of the fifth and fourth elements of the group were unexpectedly reduced, although only slightly, during the second and/or the third attempts made to step up the temperature gradients. However, elements whose temperatures were increased during either of these steps developed further increases in creep strains.

Observations made during temperature cycling over the first and third steps, as well as during gradual cooling stages, produced no evidence of recovery or sudden increases in creep. Instead, the creep continued following approximately the same general pattern as creep at constant temperatures. The behaviour of the specimen under such temperature histories was very similar to that of specimen block E2 when it was subjected to temperature cycles involving cooling and re-heating to the previous temperature levels, in which the maximum temperatures were kept at the previous constant levels.

8.4 Conclusion

A number of test results have been given with the objective of identifying the pattern of strain behaviour under variable temperature and moisture states. From a review of the previous discussions and illustrations, it was apparent that the temperature and moisture movement were the most important factors affecting creep and shrinkage within the range and accuracy of the experiment. However, it was not intended to postulate their causes or to advance another theory of creep mechanisms. Nevertheless, it is intended where practical to advance a logical explanation or to hypothesize concerning the cause of the observed behaviour.

All conclusions are limited to the actual test conditions, and the particular material and specimens included in the investigation. It is

undoubtedly a fact that the shape and size of the specimens had some influence on the relative magnitudes of the axial shrinkage and creep strains. However, based on the results of the limited tests carried out so far, the following conclusions are believed warranted.

1. For concrete loaded in compression and sealed against moisture loss, creep increases with temperature at least up to 90°C. The increase with temperature is generally higher when moisture is allowed to migrate from the concrete during heating. With further temperature increase, creep can be expected to increase reaching a maximum with the complete removal of the evaporable water content.

2. Creep continues to increase with time following a drop in temperature, although at a reduced rate. However, re-heating to the previous level of temperature and cycling produces no sudden change in creep of concrete maintained under either stable or variable moisture state.

3. The creep rate tends to increase with the increase in the migration rate of moisture from concrete, and can be expected to decrease when and where moisture concentration dominates drying. These imply that the development of creep strains across a given section of concrete is dependent on the length of the section and the applied temperature gradient. In this context, the drying creep behaviour of concrete bears a close similarity to the attendant shrinkage.

4. Non-uniform heating causes moisture to migrate towards the cooler parts of the continuum giving rise to drying and

attendant shrinkage in hot areas and may, depending on the moisture path length and the applied temperature gradient, give rise to physical saturation and swelling in the cooler regions.

5. The rate at which drying penetrates into a given specimen is a function of temperature and the distance through which the moisture must travel before reaching a zone where further movement is unimpeded. It increases with temperature crossfall and decreases with the length of the specimen.

6. The coefficient of thermal expansion of concrete tends to increase with temperature and with the continuing migration of the attendant moisture. Therefore, for the analysis of non-isothermal concrete structures, the variability of this parameter with temperature and/or changing moisture content needs to be determined.

CHAPTER IX

STEADY STATE STRESSES IN CONTINUOUS BEAM STRUCTURES SUBJECTED TO TIME-VARYING NON-LINEAR TEMPERATURE CROSSFALLS

Chapter 9 - Synopsis

The problem of calculating the elastic and long-term effects of non-linear heating of the kind produced by solar radiation in bridges is investigated with respect to a 3-span prestressed continuous beam example. The beam having a span/depth ratio of 16 is analysed for the sustained and cyclically varying influence of a non-linear temperature cross fall with a maximum surface temperature of 38 ^{o}C. An empirical formula for calculating the elastic stresses due to an arbitrary temperature distribution over the beam depth is derived. The formula is then incorporated into the steady state formulations of the problem and the solutions are compared to the rate of creep computer analysis solutions.

It is shown that considerable redistributions of stresses and moments take place and this necessitates that the solar heating effects in bridge and road structures need to be considered in design.

9.1 Introduction

Experimental evidence reported in this thesis and elsewhere indicates clearly that creep significantly influences the state of stress in non-isothermal redundant structures. The stresses undergo a process of redistribution, which reduces in rate with time. And, when temperatures are sustained and depending on the creep capacity of the concrete, a stage in time eventually comes when the redistribution ceases and the stresses reach a steady state.

When temperatures vary in periodic or cyclic manner creep may again be influential in dictating stress and displacement behaviour. And, although creep occurs partly at one temperature and partly at others, it is possible that on the long term, a quasi steady steady state is reached, in which successive temperature cycles cause stresses to alternate between repeating states (18). It is therefore essential that cognizance is taken of the long-term effects of periodic temperature differentials, of the kind caused by solar radiation and climatic temperature changes in bridges and viaducts (119,120,121) on the serviceability of such structures.

Determination of the limiting steady state stresses in structures subjected to sustained linear temperature crossfalls may be accomplished with considerable success; as has been demonstrated earlier, by the use of the analogous elastic approach of the steady state theory. This approach has been extended recently to include the effects of temperature cycling, and applied to problems having curvature restraint (18, 19).

In this chapter, the theory is adapted to deal with the combined effects of non-linear temperature crossfall and temperature cycling for the solution of a problem, in which curvatures take on non-zero values. In the sequel, an empirical formula for estimating stresses arising from

non-linear temperature crossfall is derived and incorporated into the steady state analysis. Solutions are also obtained for the cases of sustained non-linear, and cyclic and sustained linear temperature crossfalls. These are then compared to those obtained from a step-by-step computer procedure, based on the rate of creep method.

9.1.1 Illustrative problem

Fig. 9.1 shows the symmetrical half of an axially prestressed 3-span continuous beam having a conveniently chosen rectangular cross-section, and subjected to only one type of mechanical loading (a uniformly distributed load). Two arbitrarily chosen, a linear and a non-linear, temperature distributions are considered. The latter distribution is similar in shape to those often produced by the solar radiation effects referred to earlier in bridge deck structures. In such structures the temperature changes due to solar radiation are generally confined to the upper and lower zones of the cross-section, leaving the intermediate parts relatively unaffected. Numerical data for the problem including the two temperature distributions, and the cycling mode and duration in terms of pseudo time, are all given in Fig. 9.1.

9.2 Analyses of mechanical load and temperature moments on the beam

Fig. 9.2a shows the symmetrical half of the beam having at the cut section a guide rail, which permits the cut end to slide freely along its vertical axis. Thus, the statical redundancy of the beam is reduced to one, which is taken as the guided end moment in the flexibility analysis method adopted.

The redundant moment is released, Fig. 9.2b, and the resulting rotation caused at the release due to the applied transverse loading,

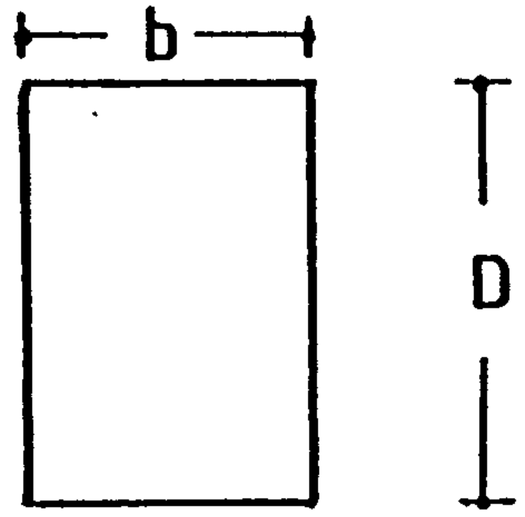

cross section

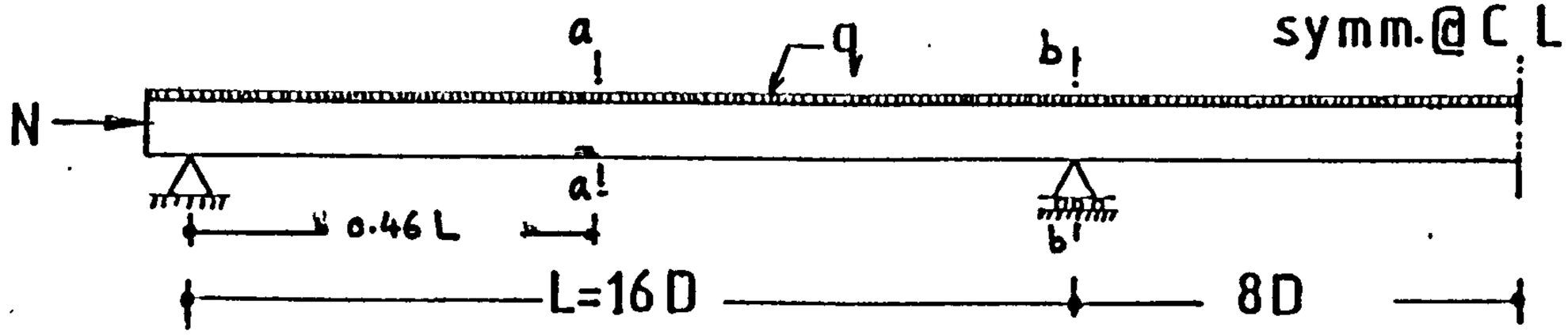

Example structure

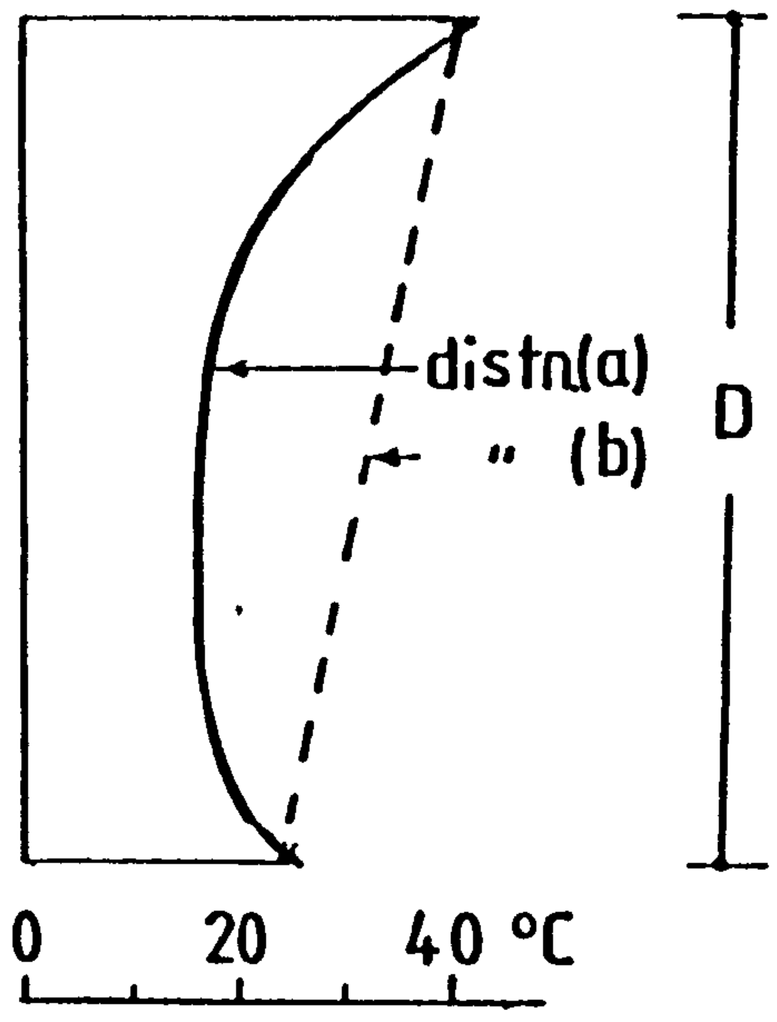

two temp.distributions

Numerical data

b=100 mm , D=150 mm
N=120 kN , q=5·2 kN/m
E=34·0 GN/m^2
$\bar{\alpha}$=13·0×10^{-6}/°c
k=1
δ_c=1·45×10^{-6} per N/mm^2 per °c

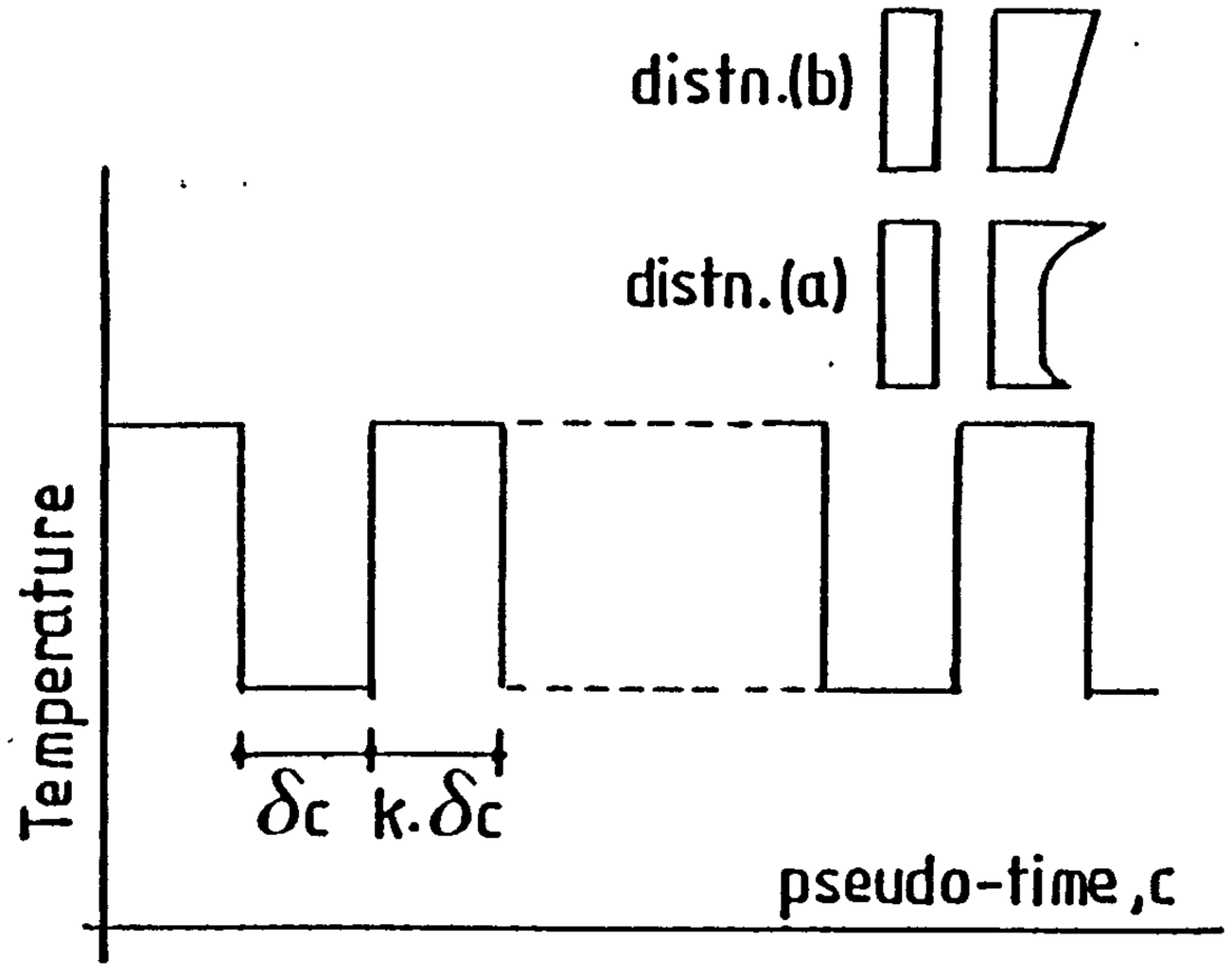

mode of temp.cycling

Fig 9.1 Illustration example and it's boundary loading

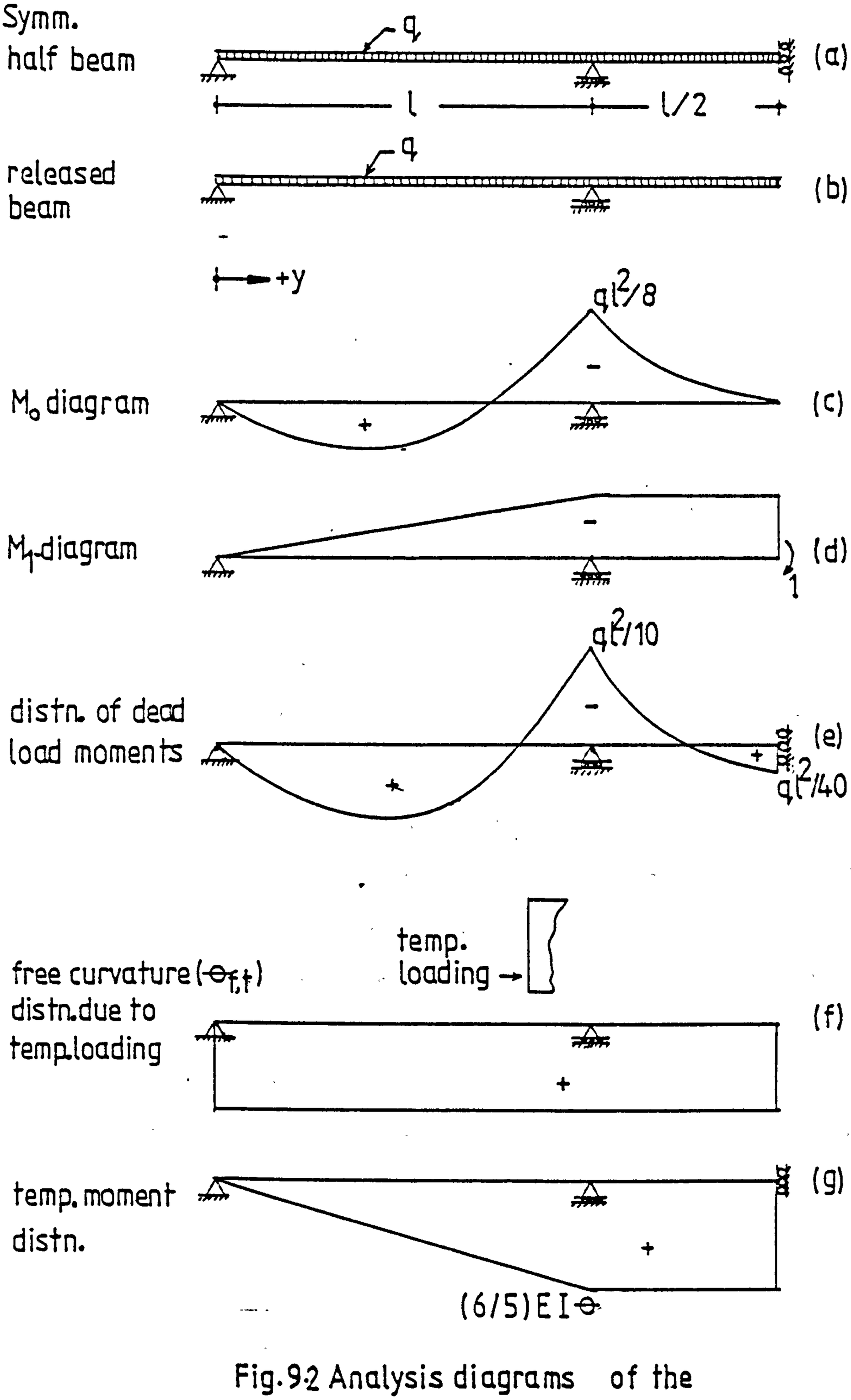

Fig. 9.2 Analysis diagrams of the external redundancy

d_{01}, and that due to the subsequently applied unit moment, d_{11}, are calculated from

$$d_{01} = \int_0^{3L/2} \frac{M_0 . M_1}{EI}\, dy = q . \frac{L^3}{48\ EI} \qquad (9.1)$$

and

$$d_{11} = \int_0^{3L/2} \frac{M_1 . M_1}{EI}\, dy = \frac{5}{6} . \frac{L}{EI} \qquad (9.2)$$

where M_0 and M_1 are the moment distributions (c) and (d).

The actual redundancy X is then calculated from the compatibility equation,

$$X = -d_{01}/d_{11}$$

$$= \frac{q.L^2}{40} \qquad (9.3)$$

Fig. 9.2e depicts the overall distribution of dead load moments on the beam calculated in the usual manner by superimposing diagram (c) to the product of diagram (d) and the redundancy X.

By the same argument, the redundant moment, X_t, produced by an arbitrary temperature loading can be calculated, when the term $\frac{M_{01}}{EI}$ in eq. 9.1 is replaced by the unrestrained temperature curvature of the beam $\theta_{f,t}$, Fig. 9.2f. Consequently, d_{01} is replaced by d_{0t}, where

$$d_{0t} = \int_0^{3L/2} \theta_{f,t} . M_1 . dy \qquad (9.4a)$$

$$= -\theta_{f,t} . L \qquad (9.4b)$$

Hence,
$$X_t = - \frac{\theta_{f,t}.L}{(5/6).L/EI} \qquad (9.5)$$

$$= \frac{6}{5} EI\theta_{f,t}$$

The distribution of thermal moment over the beam is depicted in (g), which is the product of diagram (d) and the redundancy X_t.

9.3 Approximate elastic analysis of stresses due to non-linear temperature crossfall

Detailed analysis of stresses due to non-linear temperature distributions in structures usually requires very sophisticated formulation and solution techniques, which often result in a large expenditure of time and effort. On the other hand, simple empirical formulae, while giving less accurate pictures of the stresses, can be more appreciated by engineers for solving less complicated problems and/or for use as a design check. One of such formulae, which is based on the simple elastic theory of bending is derived hereinafter.

Fig. 9.3a shows a beam element with non-linear temperature variation applied across its depth, Fig. 9.3c.

Due to the coefficient of thermal expansion $\bar{\alpha}_c$, the unrestrained thermal strains at any fibre x is given by:

$$\varepsilon_{t,x} = \bar{\alpha}_c(T_x - T_0) \qquad (9.6)$$

where $(T_x - T_0)$ = the temperature increase at fibre x.

With these strains, which are shown in (C), plane sections do not remain plane.

When compatibility is enforced, with plane sections held plane, then the locked-in stress at any fibre x would be

$$\sigma_{t,x} = E\{\varepsilon_{t,x} - (\varepsilon_a + \theta.x)\} \qquad (9.7)$$

where ε_a = axial strain, θ = the mean restrained thermal curvature of the section, and E = the modulus of elasticity of concrete (assumed constant over the section).

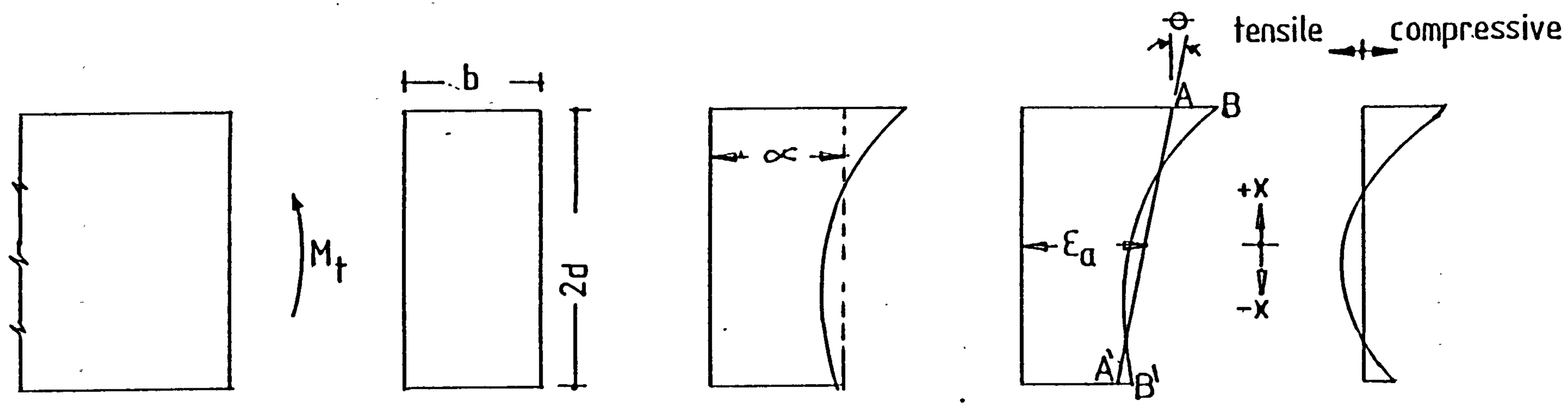

beam element (a) | cross section (b) | temperatures (c) | strains (d) | temp.stresses (e)

Fig 9.3 Strainsand stresses due to non-linear temperature crossfall

Equilibrium consideration

Due to the applied temperature stresses, the axial forces on the section should have no net resultant

$$\text{i.e.} \quad \int_{-d}^{d} b \,.\sigma_{t,x}.dx = 0 \tag{9.8}$$

$$\text{or} \quad \int_{-d}^{d} b \,\{\varepsilon_{t,x} - (\varepsilon_a + \theta.x)\} \,.dx = 0 \tag{9.9}$$

Integration of eq. 9.9 yields the following solution for the axial strain

$$\varepsilon_a = \frac{1}{A} \int_{-d}^{d} b \,.\varepsilon_{t,x}.dx$$

$$\varepsilon_a = \frac{\bar{\alpha}}{A} \int_{-d}^{d} b \,(T_x - T_0)\, dx$$

$$\varepsilon_a = \bar{\alpha}_c(\alpha - T_0) \tag{9.10}$$

where α = the overall average temperature over the section, A is the cross-section area, and T_0 = the datum temperature.

When substituting eqs. 9.6 and 9.10, equation 9.7 becomes

$$\sigma_{t,x} = E\{\bar{\alpha}(T_x - \alpha) - \theta.x\} \tag{9.11}$$

Evaluation of stresses from eq. 9.11 requires a knowledge of the mean restrained temperature curvature of the section.

From consideration of flexure, the value of θ can be related to the applied temperature moment M_t and the mean free thermal curvature $\theta_{f,t}$.

By taking moment of forces about the centroid of the section, the following equation results

$$M_t = E. \int_{-d}^{d} b \{\bar{\alpha}(T_x - \alpha) - \theta.x\} .x.dx \qquad (9.12)$$

From which $$\theta = \frac{\bar{\alpha}}{I} .b \int_{-d}^{d} T_x.x.dx - \frac{M_t}{EI} \qquad (9.13a)$$

The integral term of equation 9.13a corresponds to the unrestrained mean temperature curvature $\theta_{f,t}$ of the given section.

Hence,

$$\theta = \theta_{f,t} - \frac{M_t}{EI} \qquad (9.13b)$$

Therefore equation 9.11 becomes

$$\sigma_{t.x} = E\{\bar{\alpha}(T_x - \alpha) - [\theta_{f,t} - \frac{M_t}{EI}].x\} \qquad (9.14)$$

where

$$\theta_{f,t} = \frac{\bar{\alpha}_c}{I} b \int_{-d}^{d} T_x.x.dx$$

It is of interest to note that for a linear temperature crossfall over the section, equation 9.14 reduces to the more familiar form of

$$\sigma_{t.x} = \frac{M_t}{I} . x \qquad (9.15)$$

The difference between stresses given by equations 9.14 and 9.15 corresponds to a self-equilibrating stress system, viz.

$$\delta\sigma_{t,x} = E[\bar{\alpha}(T_x-\alpha) - \{\theta_{f,t} - \frac{M_t}{EI}\}. x] - \frac{M_t}{I} . x \qquad (9.16)$$

$$= E[\bar{\alpha}(T_x- \alpha) - \theta_{f,t} . x] \qquad (9.17)$$

It is clearly apparent that for a structure having a uniform cross-section and the same temperature distribution prevailing throughout, eq. 9.17 needs to be evaluated only once for any one section. Thus it may be more convenient to obtain crude estimates of stresses over the required sections from equation 9.15, then each distribution is adjusted by the same self-equilibrating set of stresses given by equation 9.17. The adjustment procedure for the approximate stresses, due to the applied non-linear temperatures only, is illustrated in table 9.1 for two sections of interest along the beam.

9.4 Steady state stress analyses

A. Uniform temperature cycling

For the evaluation of steady state stresses under a cyclic temperature regime of the form shown in Fig. 9.1, the following criterion is adopted. The sum of creep strains over a complete cycle constitutes a compatible strain set for the given section. When the temperature function is taken as $\phi(T) = T$, this compatibility condition can be expressed as,

$$\sigma_{sc,x}.T_{2,x}.K_2\delta c + (\sigma_{sc,x} - \sigma_{t,x}).T_{1,x}.K_1\delta c = (\bar{A}+\bar{B}.x)(K_1+K_2)\delta c \qquad (9.18)$$

where $\sigma_{sc,x}$ = the steady-state-cyclic stress at fibre x during the raised temperature portion of the cycle, $\sigma_{t,x}$ = thermo-elastic stress at fibre x,* $T_{2,x}$ and $T_{1,x}$ are the hot and cold state fibre temperatures, $K_1\delta c$ and $K_2\delta c$ are the durations of the hot and cold parts of the cycle, expressed in pseudo-time, $\bar{A}$ and $\bar{B}$ are the specific rates of change of the mean axial strain and curvature of the section respectively over a complete cycle.

---

*Due to the temperature change $(T_2 - T_1)$.

Table 9.1

Example of two-steps calculation routine of thermal stresses (elastic analysis) due to non-linear temperature crossfall

x - mm		-70	-60	-50	-40	-30	-20	-10	0	10	20	30	40	50	60	70
Temp. ^{o}C		21.00	17.50	16.25	16.00	16.00	16.00	16.00	16.00	16.50	17.25	18.75	21.00	25.00	30.50	38.00
s.e.s.	$\sigma^{(1)}$	3.40	1.42	0.44	-0.10	-0.53	-0.96	-1.39	-1.82	-2.03	-2.13	-1.89	-1.33	0.01	2.01	4.90
Sec. a-a	$\sigma^{(2)}$	-4.46	-3.82	-3.18	-2.55	-1.91	-1.27	-0.64	0.00	0.64	1.27	1.91	2.55	3.18	3.82	4.46
	$\sigma^{(3)}$	-1.06	-2.40	-2.74	-2.65	-2.44	-2.23	-2.03	-1.82	-1.39	0.86	0.02	1.22	3.19	5.83	9.36
Sec. b-b	$\sigma^{(2)}$	-3.59	-3.08	-2.56	-2.05	-1.54	-1.03	-0.51	0.00	0.51	1.03	1.54	2.05	2.56	3.08	3.59
	$\sigma^{(3)}$	0.19	-1.66	-2.12	-2.15	-2.08	-1.99	-1.90	-1.82	-1.52	-1.10	-0.35	0.72	2.55	5.10	8.49

Solutions:

$\sigma^{(1)}$ = self-equilibrating stresses (s.e.s.) as given by eq. 9.16.

$\sigma^{(2)}$ = first trial solution calculated from the elastic bending stress formula $\sigma_{t,x} = \frac{M_t}{I} .x.$

$\sigma^{(3)}$ = refined solution $= \sigma^{(1)} + \sigma^{(2)}$

sign conversion: Tensile stresses - negative

Data:

$I = 28125000\ mm^4$, $E = 34\ GN/m^2$, $\bar{\alpha}_c = 13.0 \times 10^{-6}/^{o}C$, mean Temp. $\alpha = 20.12^{o}C$

free thermal curvature, $\theta_{f,t} = 1.257244 \times 10^{-6}/mm$ (constant throughout the beam)

End-span section: $M_t = 661232$ N-mm, $\theta = 0.56576 \times 10^{-6}/mm$

Support " " : $M_t = 1.442688 \times 10^{6}$ N-mm, $\theta = 0.25145 \times 10^{-6}/mm$

Sections details are shown in fig 9.1

Re-arranging the terms of equation 9.18 yields,

$$\sigma_{sc,x} = \left[\frac{(\bar{A}+\bar{B}.x)(K_1+K_2) + \sigma_{t,x}.K_1.T_{1,x}}{(K_2.T_{2,x} + K_1.T_{1,x})}\right] \qquad (9.19a)$$

When the durations of the hot and cold parts of the temperature cycle are taken to be equal, eq. 9.18 reduces to

$$\sigma_{sc,x} = \left[\frac{2(\bar{A}+\bar{B}.x) + \sigma_{t,x}.T_{1,x}}{(T_2 + T_1)}\right] \qquad (9.19b)$$

Eq. 9.19 must satisfy the equilibrium conditions,

$$\int_{-d}^{d} b.\sigma_{sc,x}.dx = N \qquad (9.20)$$

$$\int_{-d}^{d} b.\sigma_{sc,x}.x.dx = M \qquad (9.21)$$

where N and M are the prestress and moment acting on the section at the steady state.

Substitution of the stress from eq. 9.19 into the equilibrium equations 9.20 and 9.21 yields solutions for the $\bar{A}$ and $\bar{B}$ parameters. Two solution approaches are now compared. These relate to the form of the thermal stresses which are substituted into equation 9.19. The exact and approximate representation as used in the elastic analyses of the previous section will be used.

a. Exact solution

For $\sigma_{t,x} = E[\bar{\alpha}(T_x - \alpha) - \theta.x]$, see eq. 9.11.

When the temperature stress form represented by eq. 9.11 is being used the following solution forms result,

$$\bar{A} = a_1 M + b_1 N + c_1 . E + d_1 . E . \bar{\alpha} \qquad (9.22)$$

$$\bar{B} = a_2 M + b_2 N + c_2 . E + d_2 . E . \bar{\alpha} \qquad (9.23)$$

Where the constant a, b, c and d parameters are functions of the temperature distribution and the geometry of the cross-section, and θ is the actual curvature of the section due to the applied temperature loading only, as determined in an elastic calculation for the continuous structure.

With all other parameters known, the distribution of the steady state moments over the beam remains to be determined in order that the parameters $\bar{A}$ and $\bar{B}$ can be evaluated for any required section.

9.5 Steady state moment distribution

Assuming that after a sufficiently long period of time, the statical redundancy of the beam corresponding to the value at time zero, as given by eq. 9.3, has changed by a total amount δX. As a result the distribution of moments at such time stage becomes

$$M_y = (M_{m,y} \pm \delta X \, . \, \frac{y}{L}) \quad \ldots \text{ for } y = 0 \text{ to } L$$

$$\text{and } M_y = (M_{m,y} \pm \delta X . \frac{y}{L}) \quad \ldots \text{ for } y = L \text{ to } \frac{3L}{2} \qquad (9.24)$$

where M_y and $M_{m,y}$ are the steady state and mechanical load moments respectively over any section, distance y from the end-support. The mechanical load moment distribution over the beam, as shown in Fig. 9.2e can be expressed

$$M_{m,y} = \frac{q}{10}(4.L.y - 5.y^2) \qquad \text{for } y = 0 \text{ to } L$$

(9.25)

$$\text{and} \qquad M_{m,y} = \frac{q}{10}(15.L.y - 5y^2 - 11.L^2) \quad \text{for } y = L \text{ to } \frac{3L}{2}$$

The moment increment or decrement, δX, may be treated as an additional redundancy, which can be determined from consideration of the boundary conditions prevailing at the steady state. By using the same release system used for the elastic analysis, Fig. 9.2c, the total displacement (rotation) at the release is given by

$$\delta_0 = \int_0^{3L/2} \theta.M_1.dy \tag{9.26}$$

The rate of change of the displacement w.r.t. pseudo-time 'c'

$$\dot{\delta}_0 = \int_0^{3L/2} \dot{\theta} \,.\, M_1.dy \tag{9.27}$$

By definition, $\dot{\theta} = \overline{B}$, and for $\dot{\delta}_0 = 0$ at the steady state eq. 9.27 becomes,

$$0 = \int_0^{3L/2} \overline{B}.M_1.dy \tag{9.28}$$

On substituting for the steady state moments from eqs. 9.24 into eq. 9.23, the integration of eq. 9.28 yields the following solution for the redundancy, viz.

$$\delta X = \frac{6}{5} \cdot \left\{ \frac{b_2 . N + d_2}{a_2} \right\} \tag{9.29}$$

Substitution for δX into eqs. 9.24 gives the distribution of steady state moments along the beam, which leads to the evaluation of the parameters $\overline{A}$ and $\overline{B}$ from eqs. 9.22 and 9.23, and therefore the stresses at the required sections.

b. Approximate solution

$$\text{For } \sigma_{t,x} = \frac{M_t}{I} . x$$

$$= \mu . x, \text{ say}$$

Substitution of this approximate representation of the temperature stress into equation 9.19 and subsequently into the equilibrium eqs. 9.20 and 9.21 results in the following expressions,

$$\overline{A} = a_1 . M + b_1 . N + c_1 . \mu \tag{9.30}$$

$$\overline{B} = a_2 M + b_2 . N + c_2 . \mu \tag{9.31}$$

Then by following the same routine of the exact solution procedure the following approximate solution for the redundancy results,

$$\delta X' = \left\{ \frac{(6/5) . b_2 . N + c_2 . \mu}{a_2} \right\} \tag{9.32}$$

(μ, here $= \frac{M_t}{I}$ at the interior support)

When $\delta X'$ is substituted for δX in eq. 9.24 the s.s. moment needed to evaluate $\overline{A}$ and $\overline{B}$ of eqs. 9.30 and 9.23 for any section is determined. These are then used to calculate the relevant stresses from eq. 9.19.

By the same argument of Sec. 9.3, the degree of approximation in this solution would become larger as the temperature distribution deviates

from linearity. In any event, the approximate solution of stresses can be adjusted to yield almost the same results obtained directly from procedure (a). This can easily be achieved by adding to the approximate solution the distribution, $\delta\sigma_{sc,x}$, which is incidentally the same for every section along the beam, since the temperature distribution and the beam cross-section are the same throughout. The distribution $\delta\sigma_{sc,x}$ is in fact a modified form of the self-equilibrating stress system, $\delta\sigma_{t,x}$, expressed by equation 9.17, viz.,

$$\delta\sigma_{sc,x} = \delta\sigma_{t,x} \cdot K_x \qquad (9.33)$$

where K_x is a quantity, which varies over the depth of the cross-section and according to equation 9.19b, it is given by, the ratio of the temperature at the cold part of the cycle, T_1, to the sum of the temperatures over the cold and hot part of the cycle.

i.e. $$K_x = [T_1/(T_1 + T_2)]_x \qquad (9.33a)$$

B-Sustained temperature

The steady state stress distribution under a sustained temperature regime takes the same form expressed earlier in Chapter 4 by eq. 4.22. It then follows that the solutions for the parameters A and B take the same forms expressed by equations 4.25 and 4.26. Therefore, by introducing B of eq. 4.26 instead of $\overline{B}$ into the integral equation 4.27, and following the above described routine, the total change in the redundant moment due to creep can be determined. Accordingly, the following solution is obtained

$$\delta X = \frac{6}{5} \cdot \frac{b_2}{a_2} \cdot N \qquad (9.34)$$

The steady state moments are then determined from eq. 9.24, the parameters A and B from eqs. 4.25 and 4.26, and the stresses from eq. 4.22.

9.6 Step-by-step solutions

The iterative computer procedure developed for the analysis of the experimental beam in Chapter 4, is being utilised here to check the steady state theory predictions, and to provide intermediate solutions.

In the process, the symmetrical half of the beam is divided into 72 longitudinal elements and the cross-section into 15 sub-elements. The period of investigation is divided into 400 equal pseudo-time steps, each being 1.45×10^{-8} units of strain per N/mm^2 per ^{o}C long.

9.7 Results and discussion

Fig. 9.4 shows the variations in the internal support reaction with time for the sustained and cyclic temperature regimes. The trends of behaviour indicated by the results, both short-term and time-dependent, are generally similar to those described earlier in relation to the experimental beam. However, from a comparison of the reaction changes with time, it can be concluded that the redistribution of stresses under the conditions of temperature cycling is less severe than under the sustained temperature situation. The analyses indicate also that the reaction changes, under both temperature regimes, tend, at large times, towards the directly calculated limiting steady state values. However, because stresses redistribute more rapidly under sustained temperatures, the reaction reaches its limiting state sooner than those under temperature cycling.

Fig. 9.5 depicts the total changes in the beam moments, due to creep occurring under both temperature states. The results show that the span

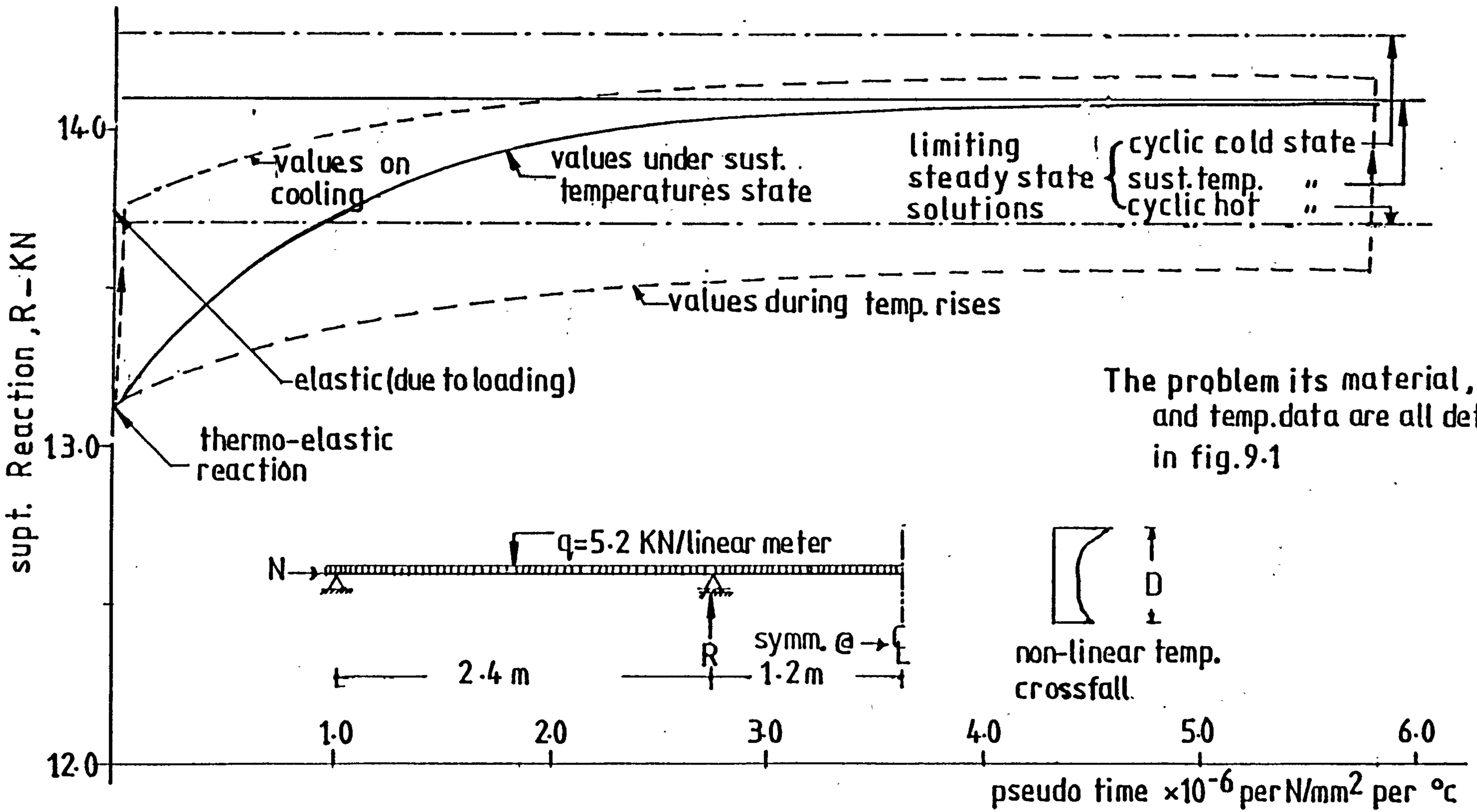

The problem its material, loading and temp. data are all detailed in fig. 9·1

Fig. 9·4 Variation of the interior support reaction with pseudo time under sustained and cyclically varying non-linear temperature crossfall.

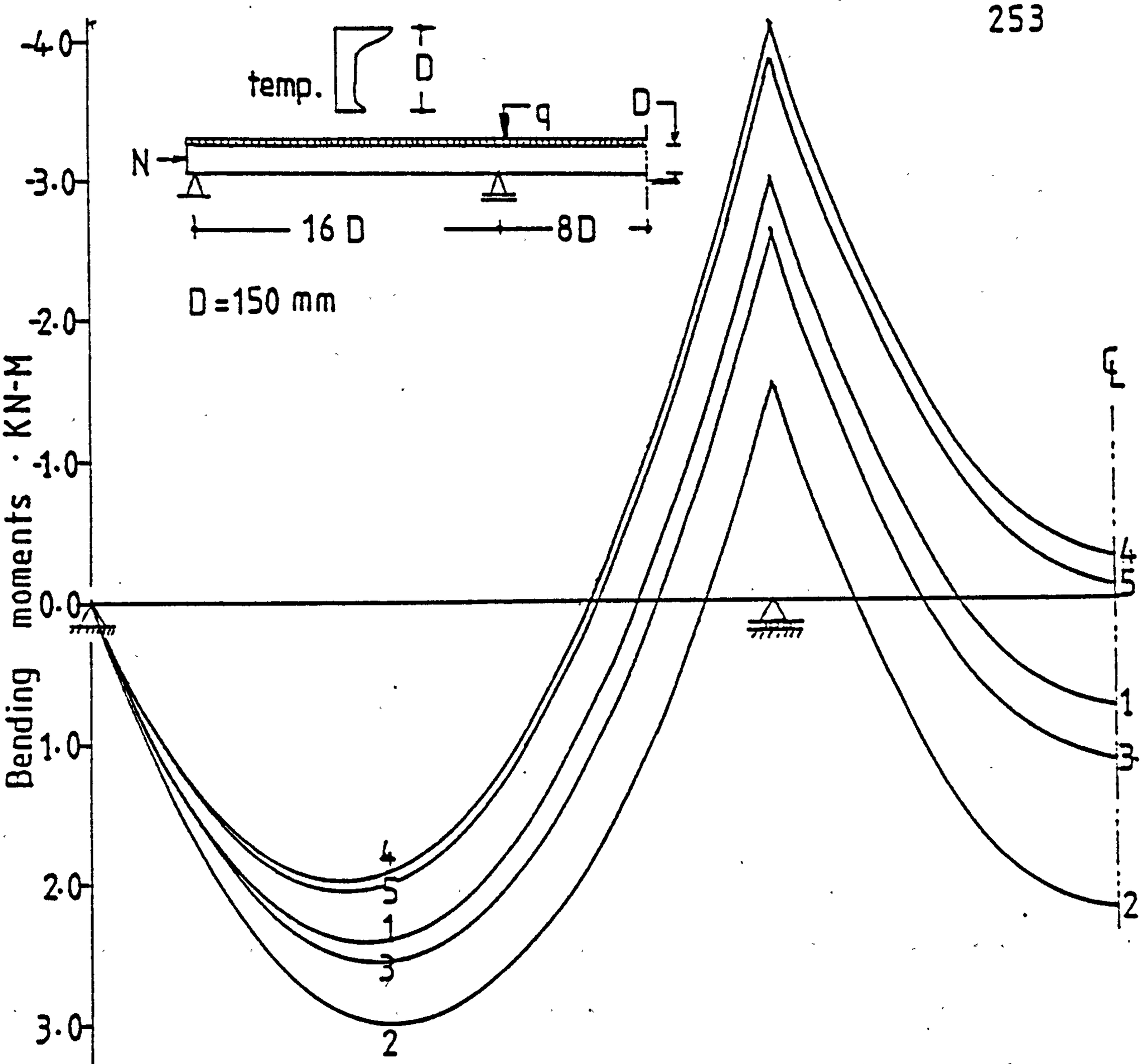

Fig. 9.5 initial & steady state moment distributions over the beam

Key

curve (1) moments due to ext. loading

" (2) " " " " &non-linear temp. distn.

" (3) steady state moments (cyclic hot state) } step-by-step solutions

" (4) " " " (" cold ") } step-by-step solutions

" (5) " " " (sust. temp. ") } step-by-step solutions

moments increase due to first heating but tend thereafter to decrease with time, while the negative support moment takes on an opposite trend. The long-term state is thus more critical than the initial conditions with superimposed temperature. The results show also that creep causes the positions of zero bending moments to move towards the centres of the spans. Such redistribution of moments is shown to produce negative moments over the entire central span, in both the 'hot' state of the sustained temperature loading, and the 'cold' state of the temperature cycling regime.

Table 9.2 lists the thermo-elastic and steady state stresses corresponding to the non-linear temperature crossfall for the two sections of interest. The long-term solutions derived from the direct calculations are compared to those of the numerical step-by-step procedure. These include the sustained temperature stresses, and the 'hot' and 'cold' state stresses of the temperature cycling. A similar set of results, which correspond to the case of linear temperature distribution for the same sections is listed in Table 9.3.

In the two sets of results, it is readily apparent that the stresses derived from the direct method of analysis for the sustained temperature state, are almost identical to the exact values given by the iterative procedure. Generally, good agreement between the two types of solutions holds also for the steady state cyclic stresses, except those of the outermost fibres of the sections. The reason for this emanates from the fact that the basic strain compatibility criterion adopted is being based on the mean values for the parameters A and B over the hot and cold parts of the temperature cycle. Such an assumption is not strictly accurate for problems of this kind, in which curvatures take non-zero values. For problems in which the curvatures are restrained, however, the degree of accuracy in the solution is expected to be significantly larger. The stresses calculated from the iterative method, listed in

Table 9.2 Thermo-elastic and steady state (cyclic and sustained) stresses over two sections of the beam - Case of non-linear temperature crossfall shown in Fig. 9.1.

Sect.	x - mm		-70	-60	-50	-40	-30	-20	-10	0	10	20	30	40	50	60	70
	Temp. °C		21.00	17.50	16.25	16.00	16.00	16.00	16.00	16.00	16.50	17.25	18.75	21.00	25.00	30.50	38.00
End-span	Th. elastic		3.88	2.98	3.07	3.60	4.25	4.89	5.54	6.18	7.05	8.02	9.33	10.97	13.38	16.46	20.42
	Sust. Temp.	a	0.70	2.05	3.49	4.86	6.19	7.51	8.84	10.17	11.18	11.96	12.20	11.96	10.93	9.66	8.30
		b	0.65	2.00	3.48	4.88	6.22	7.56	8.91	10.25	11.24	12.00	12.18	11.90	10.86	9.60	8.27
	Cyclic Temp. Hot	a	2.07	2.53	3.38	4.38	5.41	6.44	7.47	8.51	9.50	10.44	11.25	11.88	12.22	12.32	12.20
		b	2.24	2.41	3.20	4.17	5.16	6.16	7.15	8.15	9.10	10.00	10.97	11.50	12.19	13.13	14.68
	Cyclic Temp. Cold	a	0.32	2.53	4.12	5.23	6.65	7.88	9.10	10.33	11.29	12.09	12.43	12.27	11.03	8.89	5.65
		b	0.50	2.42	3.95	5.22	6.41	7.59	8.78	9.97	10.89	11.65	11.97	11.88	11.00	9.70	8.07
Support	Th. elastic		15.27	12.74	11.21	10.11	9.13	8.15	7.16	6.18	5.42	4.77	4.45	4.46	5.24	6.69	9.02
	Sust. Temp.	a	14.81	16.33	16.04	14.71	13.14	11.56	9.99	8.42	6.64	4.89	3.15	1.62	-0.35	-0.54	-1.09
		b	14.89	16.32	15.96	14.63	13.07	11.51	9.96	8.40	6.65	4.93	3.22	1.68	-0.40	-0.52	-1.09
	Cyclic Temp. Hot	a	15.43	15.05	14.06	12.81	11.50	10.19	8.88	7.57	6.28	5.03	3.92	2.98	2.35	2.01	1.94
		b	15.02	14.50	13.53	12.30	11.01	9.73	8.44	7.15	5.37	4.65	3.59	2.82	2.71	3.42	5.26
	Cyclic Temp. Cold	a	15.64	16.72	16.20	14.97	13.58	12.18	10.79	9.39	7.79	6.13	4.26	2.24	-0.23	-3.09	-6.57
		b	15.23	16.17	15.67	14.46	13.09	11.72	10.35	8.98	7.39	5.75	3.95	2.09	0.12	-1.70	-3.28

Note: end-span section is 1100 mm from the end-support, sign convention: Tensile stress = negative
Solutions: a = exact calculations b = numerical step-by-step calculations

Table 9.3 Thermo-elastic and steady state (cyclic and sustained) stresses over the same two sections defined in Table 9.2 - Case of the linear temperature crossfall shown in Fig. 9.1

Sect.	x - mm		-70	-60	-50	-40	-30	-20	-10	0	10	20	30	40	50	60	70
	Temp. ^{o}C		29.6 + 0.12.x														
End-span	Th. elastic		0.12	1.25	2.37	3.50	4.62	5.75	6.87	8.00	9.13	10.25	11.38	12.50	13.63	14.75	15.88
	Sust. Temp.	a	2.45	3.59	4.62	5.54	6.38	7.15	7.85	8.50	9.09	9.64	10.15	10.62	11.07	11.48	11.87
		b	2.45	3.57	4.62	5.54	6.38	7.15	7.85	8.50	9.10	9.68	10.16	10.63	11.08	11.49	11.88
	Cyclic Temp. Hot	a	1.50	2.67	3.77	4.81	5.78	6.71	7.58	8.41	9.19	9.93	10.64	11.32	11.96	12.58	13.16
		b	1.06	2.23	3.35	4.43	5.46	6.44	7.39	8.31	9.19	10.04	10.87	11.67	12.49	13.19	13.93
	Cyclic Temp. Cold	a	3.54	4.42	5.23	5.97	6.66	7.29	7.87	8.40	8.90	9.35	9.77	10.15	10.50	10.80	11.12
		b	3.11	3.99	4.82	5.60	6.33	7.03	7.68	8.30	8.90	9.46	9.99	10.50	10.98	11.44	11.88
Support	Th. elastic		11.00	10.57	10.14	9.71	9.29	8.86	8.43	8.00	7.57	7.14	6.71	6.29	5.86	5.43	5.00
	Sust. Temp.	a	20.45	17.89	15.59	13.51	11.63	9.91	8.33	6.89	5.56	4.32	3.18	2.11	1.12	0.19	-0.68
		b	20.35	17.84	15.57	13.51	11.64	9.92	8.35	6.91	5.57	4.34	3.19	2.13	1.14	0.21	-0.66
	Cyclic Temp. Hot	a	16.67	15.11	13.64	12.26	10.96	9.73	8.56	7.46	6.41	5.42	4.47	3.57	2.72	1.90	1.11
		b	15.68	14.15	12.74	11.45	10.26	9.17	8.17	7.26	6.42	5.66	4.96	4.33	3.76	3.24	2.77
	Cyclic Temp. Cold	a	21.13	18.93	16.82	14.80	12.87	11.00	9.20	7.46	5.78	4.15	2.57	1.03	-0.47	-1.92	-3.34
		b	20.14	17.97	15.93	14.00	12.12	10.45	8.81	7.26	5.79	4.38	3.05	1.78	0.57	-0.59	-1.70

Notes: Solution a = exact calculations
" b = step-by-step calculations

tables 9.2 and 9.3, are shown diagrammatically in Figures 9.6 and 9.7, which include stresses (not listed) for a third section of the beam. The extents of creep effects on the state of stresses in the three sections of interest are clearly defined in these plots. Indications are that creep causes significant variation of stresses near the two modes of operation and types of temperature crossfalls considered. When temperatures vary in time the stress changes are less severe than when temperatures are long sustained. In either case, cooling always produces the worst effects on stresses. Creep is thus seen to be detrimental to long-term serviceability in this example.

In continuous span bridge structures, periodic temperature changes are therefore likely to introduce effects similar to those shown in Fig. 9.6. Even more severe effects can result when due account is taken of the live load stresses, which have been discounted in this example. There is therefore a need for these eventualities to be taken into consideration at an early stage in design.

9.8 Conclusion

Although attention has been focussed on a simple problem for the purpose of gaining some insight into the magnitude of creep effects in relation to only a few temperature parameters, the methods of analyses used are equally applicable to real and more complex situations, such as bridge structures.

In the foregoing sections it has been demonstrated that by the use of a simple empirical formula, the short-term stresses arising from non-linear temperature variation, of the kind experienced by bridges, over any symmetrical section of uncracked continuous structure can be easily calculated. By incorporating this formula into an analogous elastic formulation, it has been possible to derive long-term solutions

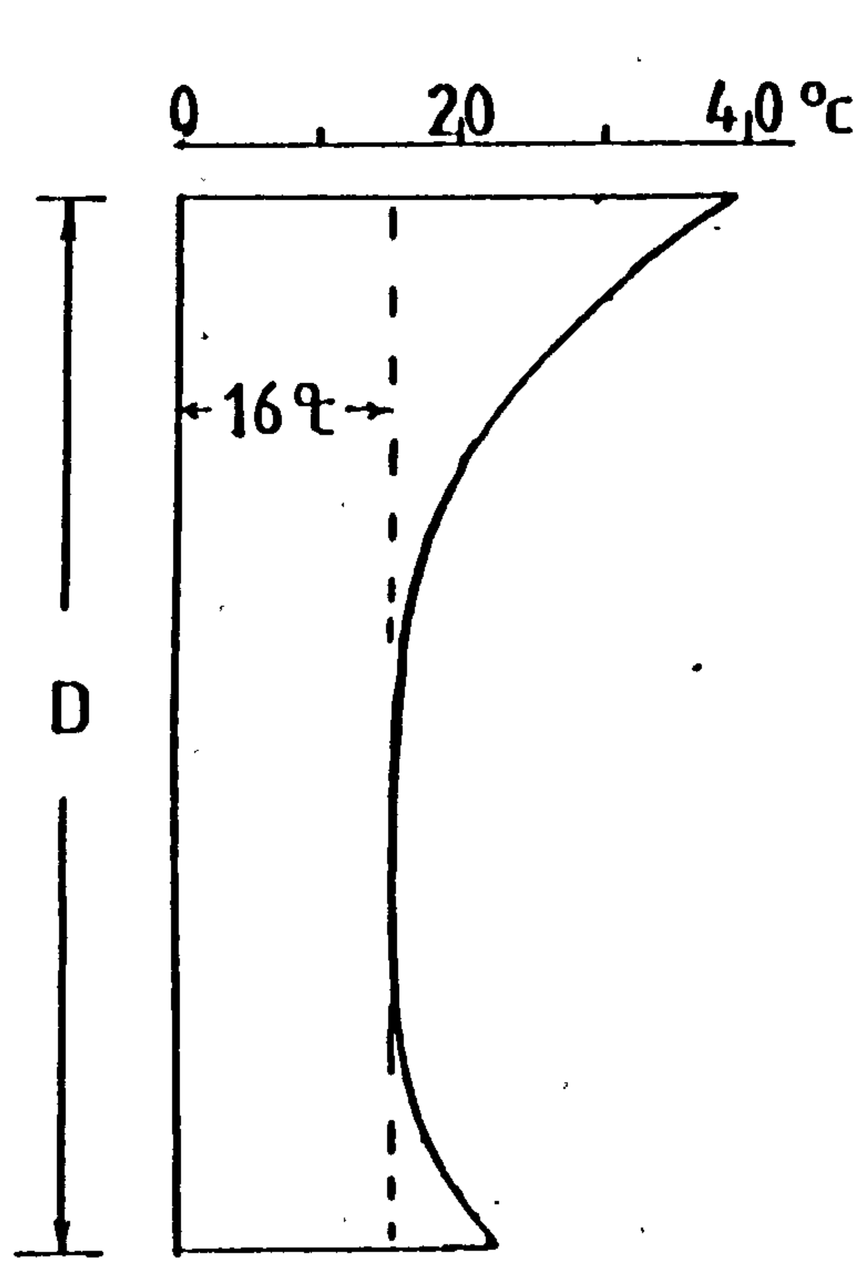

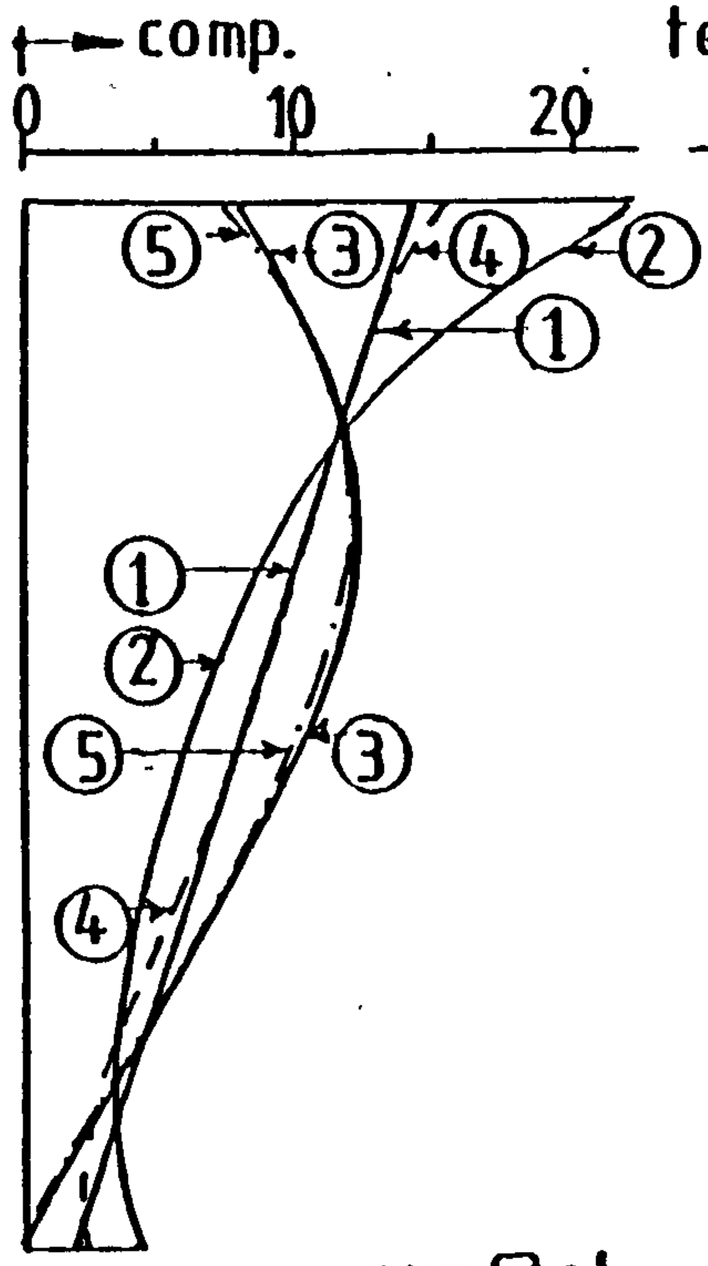

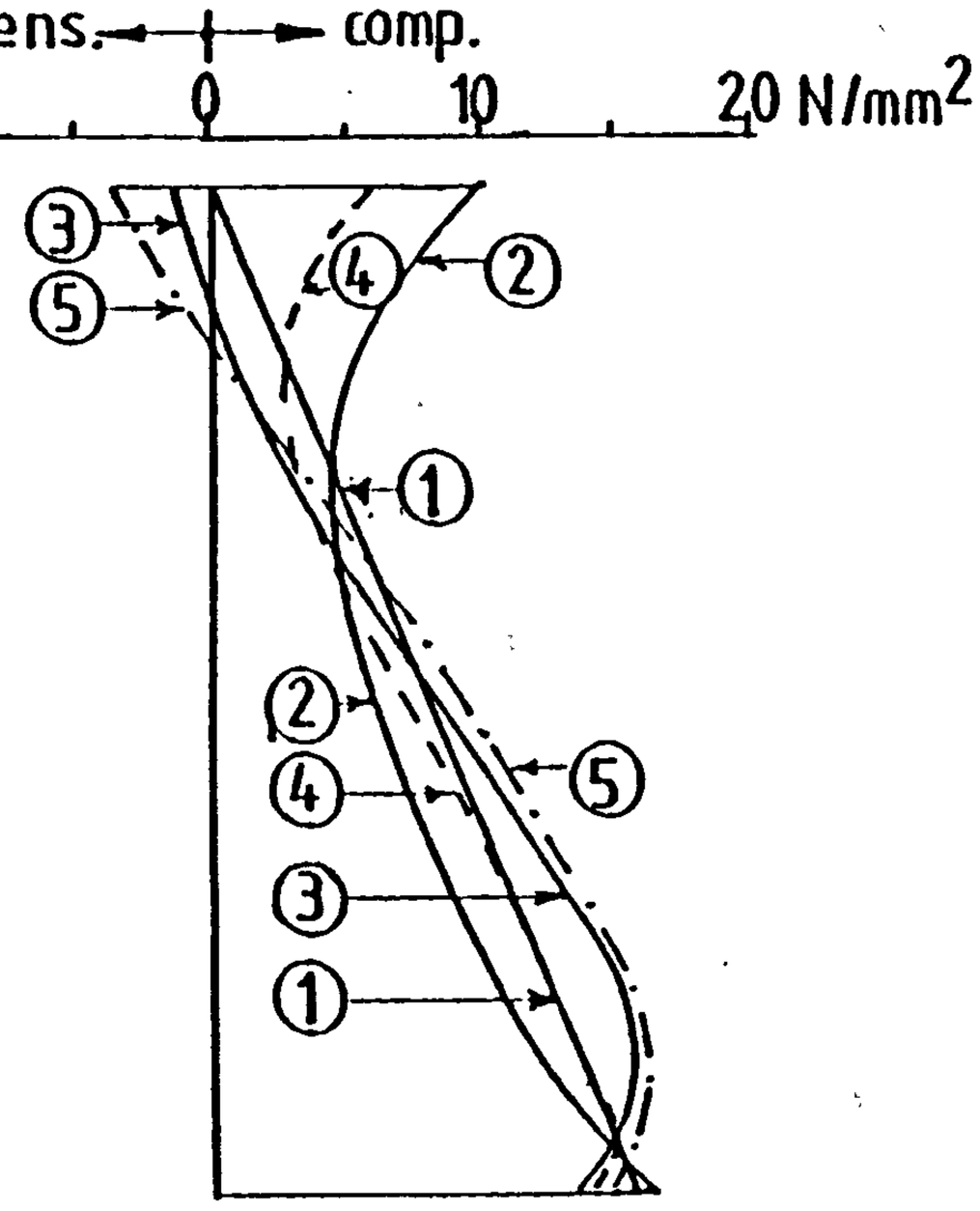

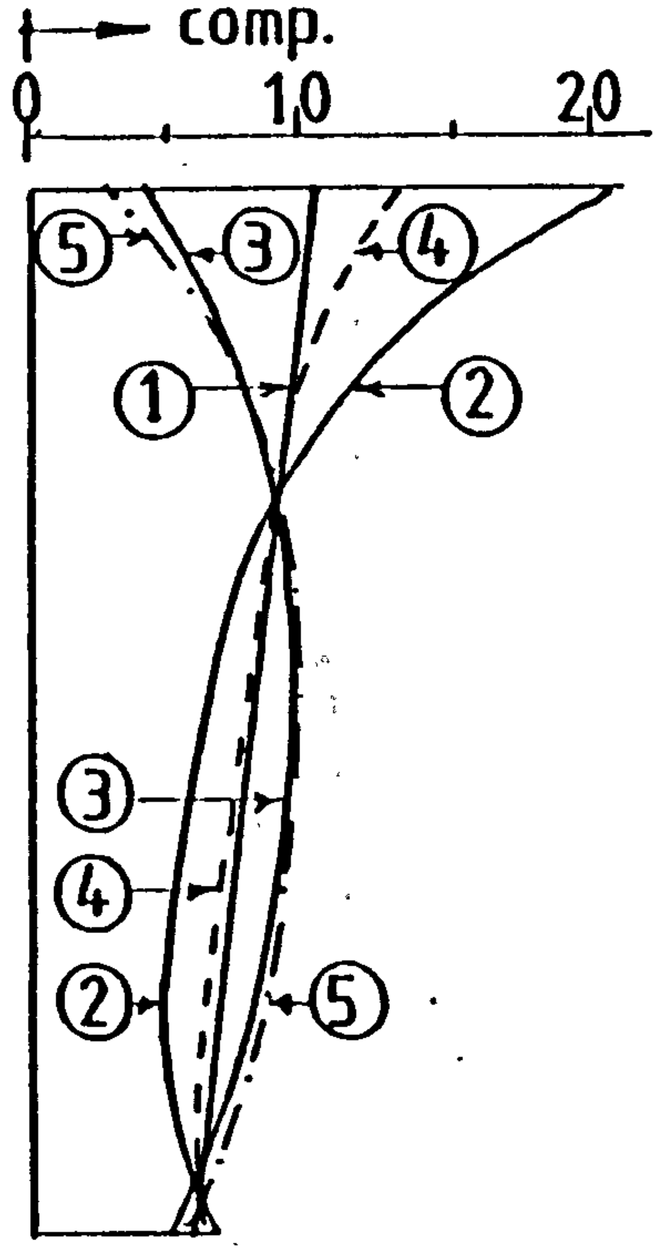

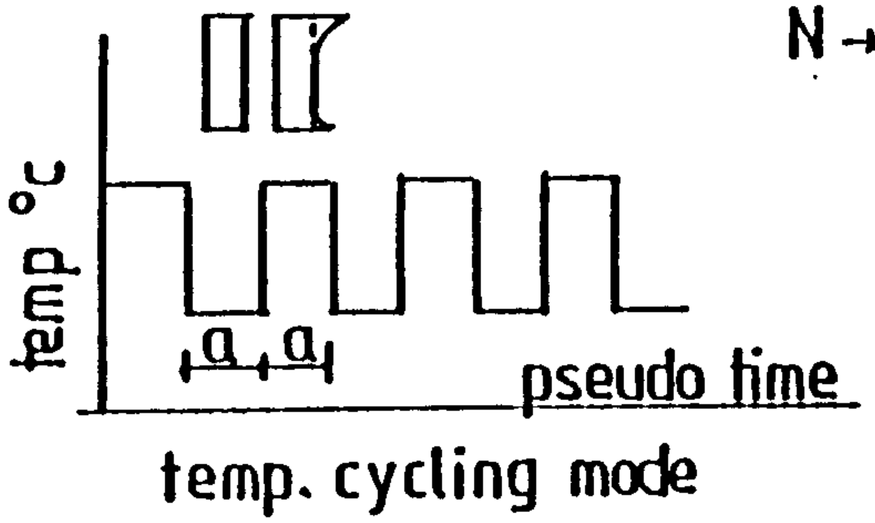

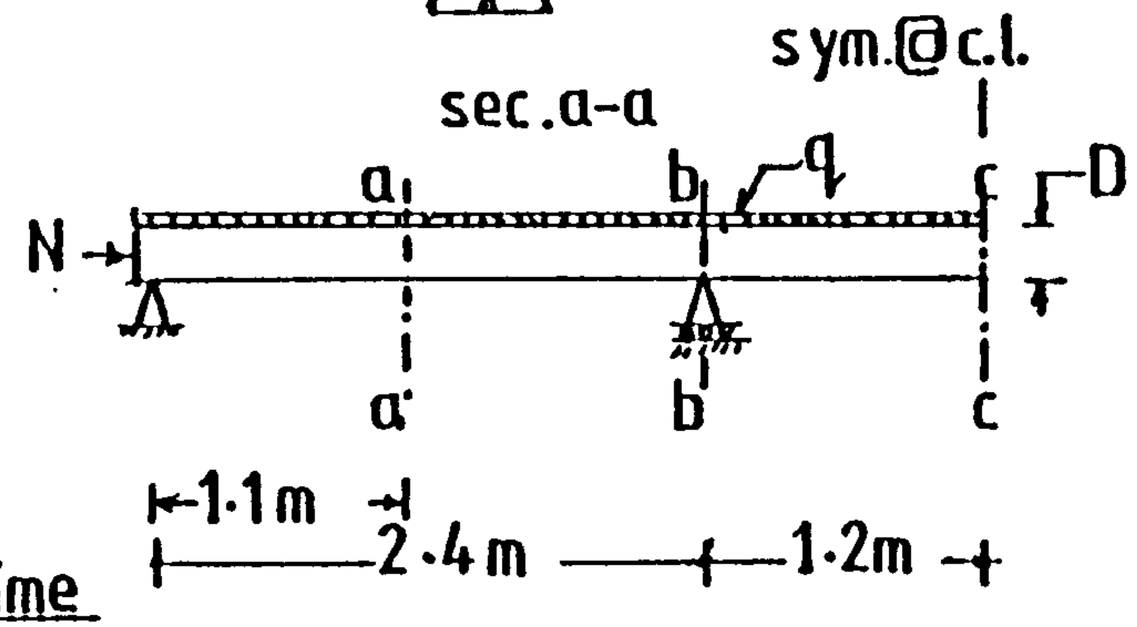

Key to the various stress distributions:
1-due to applied mechanical loading.
2-" " " " " +temperatures.
3-st.state(sustained temp.) stresses.
4-" " (cyclic ") " -hot state
5-" " (" ") " -cold state

Fig 9.6 initial and steady state(cyclic & sustained) stresses over three sections of interest along the beam. Case a: non-linear temp.crossfall

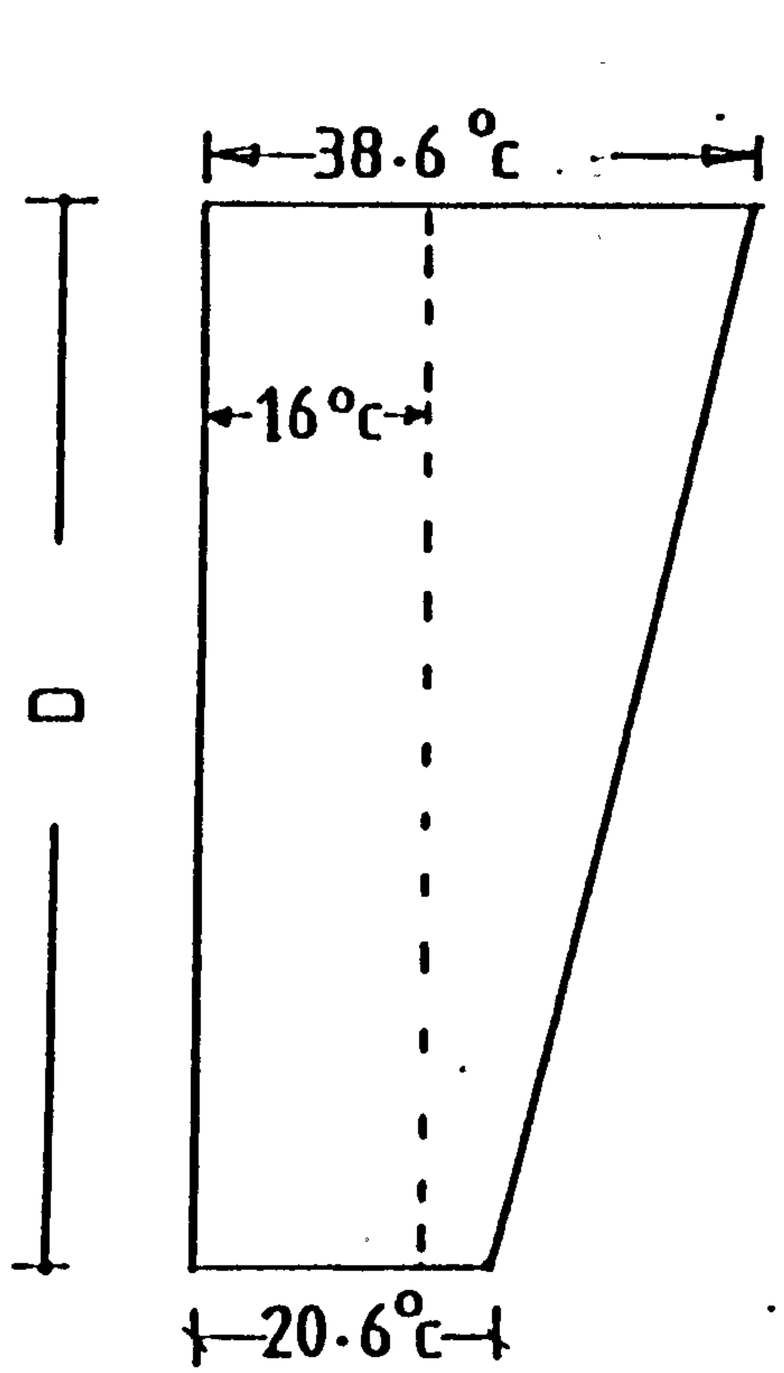

Temperatures

cyclic temp. regime

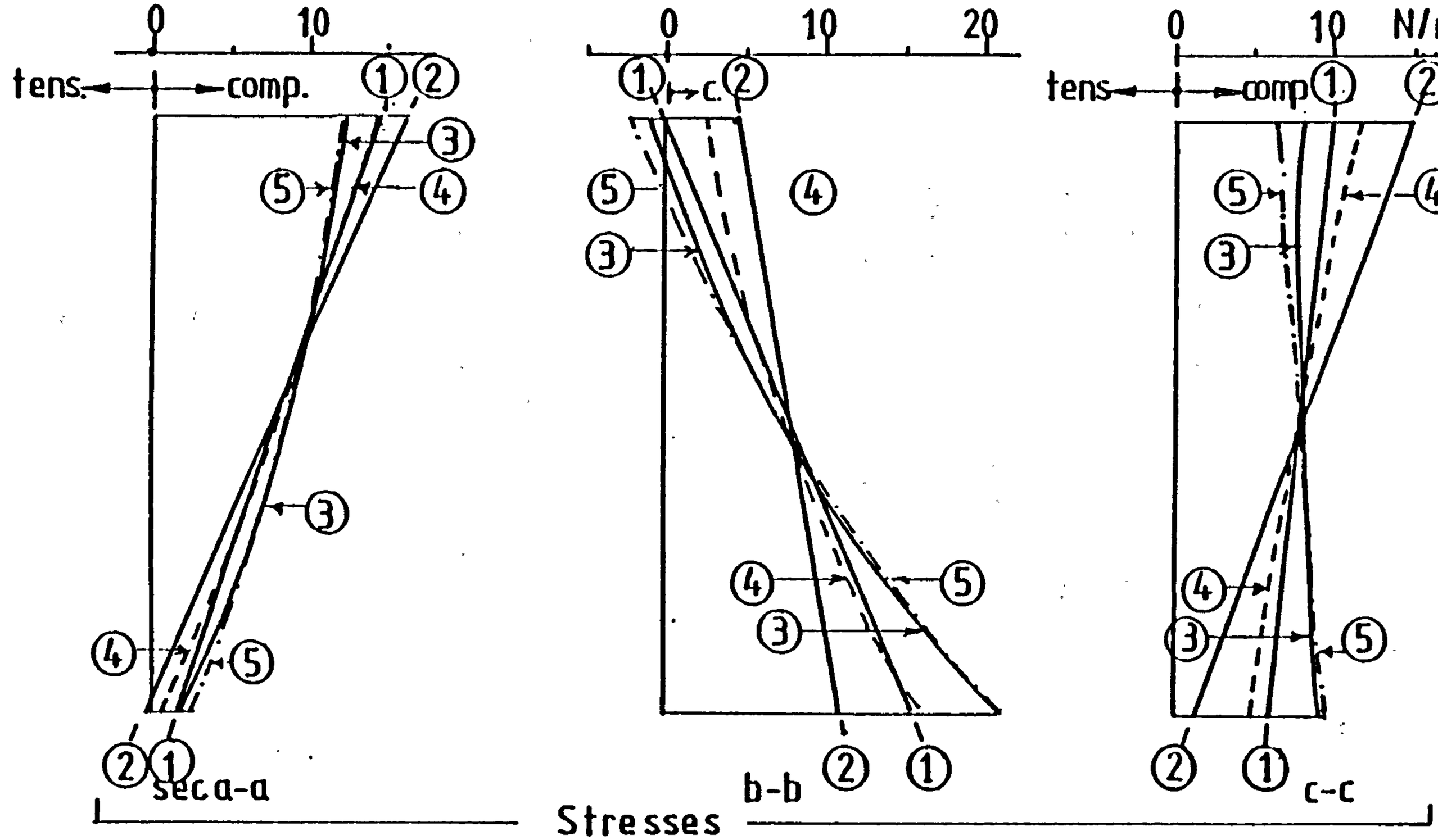

Stresses

Note: key to the distributions and sections' locations are given in fig 9·6

Fig 9·7 initial and steady state (cyc. & sust.) stresses over three sections of the beam.
Case b: linear temp. crossfall

of stresses for the conditions of cyclically varying temperatures, which simulate to a degree the climatic temperature changes on structures. Similar calculations are also performed for a linear-type temperature crossfall linking the upper and lower surface temperatures of the other case. And to provide bases for comparison, solutions are also obtained for the sustained effects of temperature.

Analyses reveal that creep significantly affects the state of stress in any non-uniformly heated structure, whether the temperatures be long sustained or vary in time.

Cyclically varying temperatures of the kind caused by solar heating and climatic temperature changes in bridges result in less severe variation of stresses than a sustained temperature situation. The accumulative effects of creep, however, can still cause a long-term drift of moments and stresses, which render the structure less serviceable than would be indicated by an elastic calculation.

Indications are that solar heating effects on bridges and similar structures should be taken into consideration at an early stage in design. The 'mean' bridge temperature concept adopted in current design practice neglects, in the first place, the bending stresses caused when the exterior parts of the bridge expand more than the interior. This situation can result in even more severe stressing conditions than when the interior parts of the cross-section are heated linearly with the exterior surfaces' temperatures. The fact that creep is influential in dictating the stress changes with time in heated situations of this kind, necessitates steady-state-cyclic stress calculations to be made if long-term serviceability of the bridge is to be guaranteed.

CHAPTER X

IMPLICATIONS, CONCLUSIONS AND SUGGESTIONS FOR FURTHER RESEARCH

10.1 Practical implications

The practical implications of this work have been mainly concerned with the behaviour of prestressed and plain concrete under the sustained influence of external loading, and temperature crossfalls, with some considerations given to temperature cycling. Previous studies in the thermal creep behaviour of some prestressed concrete structures have shown that the state of stress in these structures is greatly influenced by creep. Such findings have largely been based on the integrated response of all internal stresses observed at the supports, and from results of data analyses using some forms of creep laws relating stresses to creep strains. That is to say, the stresses have not actually been ascertained in these studies by direct means, but through analyses.

Here, an experiment was designed and successfully staged, in which it was possible to monitor the development of stresses in a given section of a prestressed continuous beam directly by employing a technique which had only been applied previously in short-term tests at normal room temperatures. The results of this experiment, besides allowing an insight to be gained into the influence of creep on stresses, provided a firm basis on which to assess the usefulness of some of the direct and iterative methods of analysis which have been based on the specific thermal creep concept.

The influence of temperature gradient on the concrete behaviour has been the subject of a separate investigation undertaken in this work. This concerned its influence on the uniaxial creep and shrinkage behaviour of the concrete from the standpoint of moisture movement.

Water, held in various degrees of fixation, constitutes an integral part of the structure of concrete. The presence of temperature gradient is known to cause the moisture to migrate, hence influencing

the properties most sensitive to the water content, and consequently the material behaviour. The aspect of moisture movement and its influence on creep has not been sufficiently understood. To promote clearer understanding of this aspect however, uniaxial creep experiments were staged in specially designed rigs; whereby moisture was caused to flow by temperature gradients across concrete blocks each consisting of a number of closely held laminations loaded independently and free from interface stresses.

The results obtained from these experiments show clear evidence on the significant role played by the moisture movement in the development of both creep and shrinkage in concrete, and call for due consideration to be given to its effects on structural behaviour.

The creep experiments also allowed some insight into the aspects of the temperature increase and cycling, effects on creep; this seemingly an under investigated subject is of considerable importance in many structural situations.

The importance of temperature cycling effects on the structural behaviour are being highlighted in an example of a prestressed continuous beam; analysed for the effects of sustained loading and cyclically varying temperature crossfalls. One form of the temperature variations considered in the analyses bears close similarity to that produced by solar radiation across bridge deck structures. The example illustrates the need for the solar heating effects to be taken more seriously in the design of exposed structures, particularly those in the tropical region countries.

10.2 Conclusions

Based upon the laboratory tests and analytical work presented, and pursuant to the limitations cited, the following conclusions are believed warranted.

10.2.1 Moment and stress redistributions due to non-homogeneous creep

Non-uniform heating across structural members gives rise to differential creep and shrinkage, which in the presence of constraints to free deformations, cause stresses, together with the applied moments to redistribute with time. With regard to the continuous beam tested, the results reported herein confirmed this kind of behaviour indisputably, and revealed the main features of this process, which can be summarized as follows:

1. The redistributions occur fairly rapidly, but slow down with age, and tend to become stationary after a sufficiently long period of time.

2. The extent of effects of the redistributions may first be noted in the complete disappearance of the elastic thermal stresses, and provided the temperatures are sustained, the moments at some sections may change sense, after a relatively short period of time.

3. While curvatures and displacements may continue to develop with time the stresses always seem to tend to limiting values, even after being perturbed by differential support displacements.

4. From limited evidence, indications are that cooling after a long sustained period of heating causes the most severe stressing conditions, which may result in cracking at sections

which experienced the greatest stress redistribution. Also, that subsequent heating and cooling result in lesser stress variations, this supports the view that temperature cyclings cause less severe redistribution than when temperatures are long sustained.

5. The elastic theory is totally inadequate to predict the time-dependent stress and moment changes due to non-homogeneous creep, and other theories accounting for such effects must therefore be considered.

6. Some of the creep methods of analysis, namely the 'variational power' and the iterative 'rate of creep' are quite successful in predicting the transient creep effects, and together with the 'steady state' theory will predict the limiting long-term stresses in structures.

10.2.2 Effects of solar type heating on exposed structures

1. Non-linear temperature variation within the depth of a structural member may cause even more severe stressing conditions than when temperatures vary in a linear manner.

2. In road and bridge structures creep can cause a long-term drift of moments and stresses as a result of periodic exposure to solar radiations and the ambient air temperatures.

3. The use of a uniform temperature change in the design of bridges and viaducts may underestimate the elastic bending stresses resulting from non-linear solar heating, and the subsequent time-dependent effects.

10.2.3 Influence of temperature and moisture movement on creep

1. For concrete sealed against moisture loss, creep increases with temperature at least up to 90°C, and the increase is generally higher when moisture is allowed to migrate from the concrete during heating.

2. Creep can be expected to increase with temperature until the complete removal of the evaporable water content.

3. Following a temperature drop, creep continues to develop with time apparently unaffected, and equally so on reheating to the previous level and on subsequent cooling.

4. Creep tends to increase with the increase in the migration rate of moisture from concrete, and can be expected to decrease when and where moisture concentration dominates drying.

5. Non-uniform heating causes moisture to migrate towards the cooler regions of the continuum giving rise to drying and attendant shrinkage in hot areas and possibly swelling in the cooler parts.

6. The drying penetration rate increases with the temperature crossfall and decreases with the moisture path length.

7. The coefficient of linear expansion of concrete tends to increase with temperature and with the migration of the attendant moisture.

10.3 Suggestions for further research

The present understanding of the long-term effects of temperature cycling on the state of stresses in structures has been based largely on the results of theoretical studies, using existing creep laws in conjunction with cyclic temperatures creep data. There is therefore a need for systematic experimental investigations to further our knowledge of this aspect of material behaviour.

It is suggested here that the direct stress correlation technique employed in the beam experiment may be extended to investigate the behaviour of similar beams subjected to temperature variations in both time and space. Conditions simulating the environmental temperature changes in road and bridge structures need to be included among the test variables.

The creep-stress relationship at elevated temperatures is another topic in need of further investigation and for which the laminated creep rigs developed and used herein seem quite appropriate. The freedom of independent loading of the separate units permits stress gradients to be established across the test groups, and a single heat source or more can provide the required temperature variation. Emphasis should be placed on the measurement of very early creep and creep recovery to help resolve some of the existing controversies. A temperature cycling programme applied to some specimens soon after loading would be a useful extension to the investigation.

In the tests carried out to investigate the influence of moisture movement on the creep of concrete, there was no effective control over the moisture exchanges between the various laminations of the test blocks. Perhaps more revealing evidence on the role of moisture movement would emerge from tests in which the timing of the moisture transfer from

one lamina to the next is in the hands of the operator. This would probably require the introduction of a moisture release system at the joint interfaces, which needs careful investigation.

APPENDICES

APPENDIX I

Mix and the hardened properties of the concrete

a. Mix Constituents

All concretes used in the experimental work reported herein were of the same mix proportions. The coarse aggregates were air dried Thames Valley river gravel of two nominal sizes 10.0 to 5.0 mm. The sand was air dried of size ranging between B.S.25 and B.S.100 sieves. Cement was ordinary Portland type mixed with the other constituents in the following proportions:

Ordinary Portland cement	10.0 Kg.
Coarse aggregates (10.0 mm)	14.4 Kg.
" " " (5.0 mm)	14.4 Kg.
Fine sand (B.S.25 - B.S.100)	18.2 Kg.
Water	4.5 Kg.

Accordingly the A/C ratio worked out to be 4.7 of which 39% sand, and the overall W/C ratio was 0.45.

b. Cold Strength

The strength properties of the hardened concrete are summarized in Table A.1.1.

Table A.1.1

Test	No. of Specimen	Age at test days	Strength N/mm^2
Compressive strength			
100 mm cubes	24	28	46.2
100 " "	12	56	53.3
Cylinder splitting test			
108.0 mm dia × 305 mm	6	28	3.3
" " " " "	4	56	4.3

c. Modulus of elasticity

The secant modulus of elasticity of the concrete used was determined at room temperatures from load-deformation tests of 108 mm dia × 305 mm cylinders, and from the axial strains of the beam on prestressing, as well as from the axial strains on loading of the creep rigs laminations. These are summarized in Table A.1.2.

Table A.1.2

Specimen	No. of tests	Age at test days	Modulus value GN/m^2
Cylinders	6	28	34.5
	2	56	38.3
Creep laminations	25	32	36.0
From axial prestressing strains			35.0

Before the beam experiment was due to be terminated a force-displacement test was performed on the interior supports of the beam. The mean value of the modulus was then determined from the V.W. principle equation:

$$f = -\delta_0/\delta_{11} \qquad (A.1)$$

where f and δ_0 are the applied force and the corresponding displacement,

δ_{11} = displacement caused by a unit force at the support

$$\delta_{11} = \frac{L_1^2}{6.E_c.I_c} [2.L_1 + 3.L_2 + 3.L_a (\phi - 1)] \qquad (A.2)$$

where L_1 and L_2 are the end and interior spans

L_a = the length of the aluminium segment

and $$\phi = \frac{E_c.I_c}{E_a.I_a} \quad . \qquad (A,3)$$

Table A.1.3 lists the modulus values calculated from the mean of three readings.

Table A.1.3

displ. mm	force KN	Young's modulus GN/M^2
0.122	0.140	31.2
0.147	0.166	30.3
0.246	0.277	30.2
0.363	0.411	30.5

By comparison with the mean value determined on application of the prestress a reduction ranging between 11 and 14% is indicated. This, however, does not rule out the probability that the reduction could have been greater at some stage during heating, but was partly recovered after cooling.

Numerical data used in the above calculations

$L_1 = 914.4$ mm, $L_2 = 1219.20$ mm, $L_a = 254.0$ mm

$I_c = 29968662.64$ mm^4, $I_a = 10544515.61$ mm^4,

$E_a = 66.6$ GN/M^2.

Appendix II

Mechanical properties of the aluminium dynamometers

The dynamometrical tube and I-sections used in the creep rigs and the beam experiment were made from hard drawn aluminium alloy of which about 98% was pure aluminium.

The load-deformation characteristics were determined for each of the eight I-sections and for a sample of 15 tube sections. The cross-section areas of the I-sections were determined by volume-displacement method in order to conclude their Young's moduli. These were subsequently determined from the slopes of the straight lines fitted to the load-deformation data by the least squares method. A summary of the results including the coefficient of linear expansion, also determined experimentally, is given in Table A.2.1.

Table A.2.1

Section	No. of sect.	Area sq. mm	Force N/ microstrain	Young's modulus GN/M^2	Coeff. of linear expansion $\times 10^{-6}/^{o}C$
I	8	687.2	45.75	66.60	23.0
Tube	15		62.5		22.7

Appendix III

Thermo-elastic and steady state analyses of the beam

a. Thermo-elastic analysis

Due to the symmetries of the structure and its boundary loading the statical redundancy of the beam is reduced to one. Then by adopting the same release system and flexibility analysis procedure described for the illustrative problem of Chapter 9, a solution for the redundancy (mid-centre span moment) is obtained, vix.,

$$X = -H^{-1}.\ D_O \tag{A.4}$$

where $H = \delta_{11}$ is the flexibility matrix for a unit action applied at the release, which is given by:

$$\delta_{11} = \int_0^{(L_2-L_a)/2} \frac{M_1.M_1}{E_c.I_c}\ .dy + \int_{(L_2-L_a)/2}^{L_{2/2}} \frac{M_1.M_1}{E_a.I_a}\ .dy \tag{A.5a}$$

$$= \left[\frac{2.L_1 + 3.L_2 + 3.L_a(\phi-1)}{6.E_c.I_c}\right] \tag{A.5b}$$

here, $\phi = \dfrac{E_c.I_c}{E_a.I_a}$

$$D_O = d_{O1} + d_{Ot} \tag{A.6}$$

where d_{O1} and d_{Ot} are the discontinuities (rotations) caused at the release by the applied transverse loading and the temperature gradient respectively. These are calculated as follows:

$$d_{01} = \int_0^{L_1} \frac{M_0 . M_1}{E_c . I_c} \, .dy \qquad \text{(A.7a)}$$

$$= - \frac{P . L_1^{\,2}}{16 . E_c . I_c} \qquad \text{(A.7b)}$$

$$d_{0t} = \int_0^{L_{2/2}} \cdot \bar{\alpha}_y . \beta_y . M_1 \, dy \qquad \text{(A.8)}$$

in which $\bar{\alpha}_y$ and β_y are the coefficient of thermal expansion and the applied temperature gradient as functions of space. M_1 is the distribution of moments due to unit action applied at the release. The integration of eq. A.8 has been carried out numerically for the temperature state of Fig. A.1 and the results are given in the following summary.

Numerical data

$E_c = 34.5 \text{ GN/M}^2$ $\qquad I_c = 29968662.64 \text{ mm}^4$

$E_a = 66.6 \text{ GN/M}^2$ $\qquad I_a = 10544515.61 \text{ mm}^4$

Hence $\phi = 1.472$ $\qquad \bar{\alpha}_c = 12.5 \times 10^{-6}/^{\circ}C$

$\bar{\alpha}_a = 23.0 \quad 10^{-6}/^{\circ}C$ $\qquad P = 8.0 \text{ KN}$

$\delta_{01} = -404.35 \times 10^{-6}$, $\qquad \delta_{0t} = 2981.5 \, \beta \, 10^{-6}$ and

$\delta_{11} = 943 \times 10^{-12}$

These give a thermo-elastic value for the redundancy of

$$X = 2.733 \text{ KN.m}$$

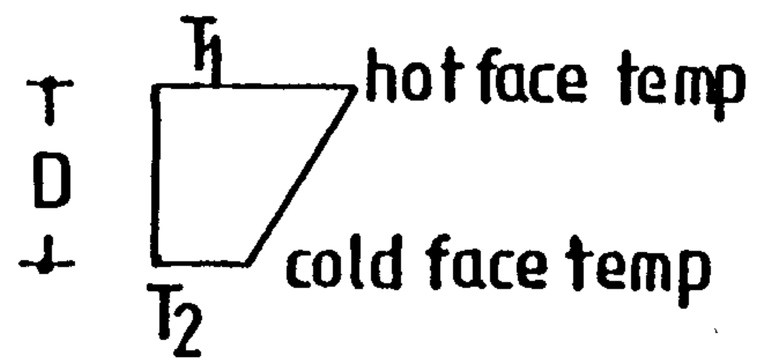

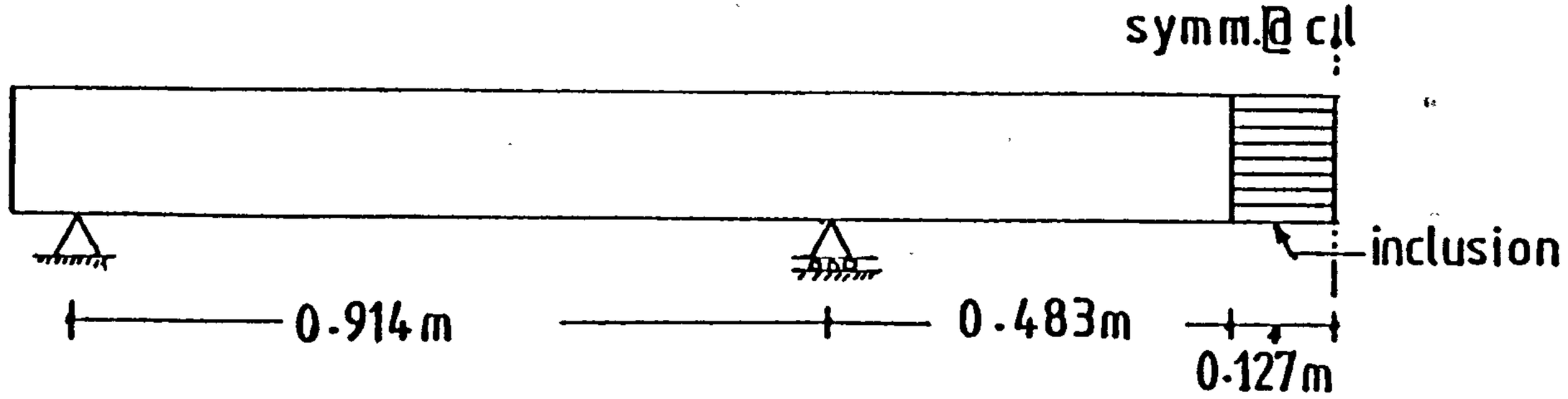

$$\beta = \frac{T_1 - T_2}{D}$$

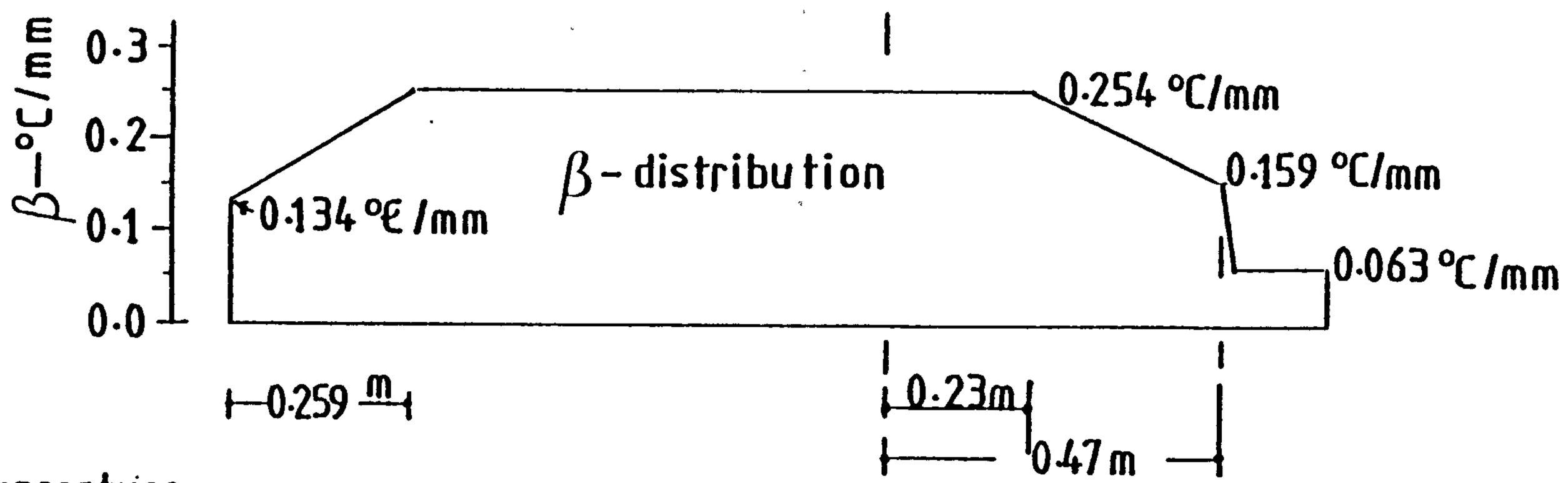

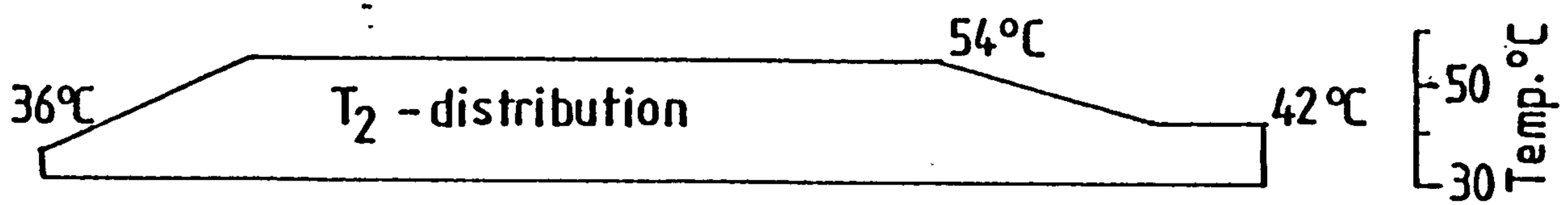

Fig A.1 Distributions of temperature gradient, β, and cold face temperature, T_2, assumed in the thermo-elastic and creep analyses of the test beam.

Note: the β and T_2 distns. given are approximated from the measured values shown in fig.6.2

b. Steady state solution

The general procedure of calculating the limiting state moments and stresses in the beam has been described in detail in Section 4.3. The solution expressed by Eq. 4.33 for the steady state reaction moment at the support holds good for such a state, when the applied temperature gradient is the same throughout the beam. For other conditions, as experienced by the beam tested, direct solution of Eq. 4.32 becomes intractable, since under these conditions the 'a' and 'b' parameters of Eqs. 4.25 and 4.26 are space variables. Nevertheless, a satisfactory solution has been reached after carrying out the integration process numerically, viz.,

$$M_s = 1.167\, M_p + 0.00855\, N \qquad (A,9)$$

The steady state support reaction can then be evaluated from

$$R_{ss} = M_s/L_1$$

Substitution of $M_p = \frac{P.L_1}{2} = 3.6576$ KN.m,

and $N = 94.0$ KN

gives $R_{ss} = 5.55$ KN

The limiting state stress over the inside end-planes of the concrete segments of the beam have been calculated using the following temperature data:

$\alpha = 46.8^{o}C$ $\beta = 0.063^{o}C/mm$

Accordingly,

$a_1 = 4.068758 \times 10^{-6}$ $a_2 = 1.562955 \times 10^{-6}$

$b_1 = 3022.506045 \times 10^{-6}$ $b_2 = a_1$

With reference to Fig. 4.2, the steady state moment over the section is

$$M_{s.s} = M_p - M_s$$
$$= -(0.167\ M_p + 0.00855\ N)$$
$$= -\ 1.4145.92 \times 10^6\ N.mm$$

Substitution of the above constants in Eq. 4.25 and 4.26 gives the following values for the specific rates of change of axial strain and curvature of the section:

$$A = 278.36$$

$$B = -1.828367$$

Substitution of the above parameters in Eq. 4.22 gives the following distribution of stresses at the steady state:

$\frac{8.x}{d}$	-7	-5	-3	-1	1	3	5	7
Stress, N/mm^2	9.40	8.34	7.35	6.40	5.50	4.65	3.84	3.07

These are the stresses plotted in Fig. 6.16 (curve c).

Appendix IV

Numerical solution procedure of the exponential matrix equation

The general procedure adopted for the numerical solution of Eq. 4.40 is described as follows:

From Eq. 4.39

$$A^{-1}.B = E \cdot \begin{bmatrix} \alpha & \frac{\beta}{6\psi} & 0 \\ -9\psi\beta & \frac{9}{2}\alpha & -\beta \\ 0 & \beta & \alpha \end{bmatrix}$$

$$= X \quad \text{say} \qquad (A.10)$$

$$\text{and} \quad B^{-1}.C = \begin{bmatrix} -\frac{9}{16} - \frac{49}{4} \cdot \frac{f\beta}{\psi\alpha} \cdot \frac{(\alpha^2-3\beta^2)}{\xi} \\ -\frac{49}{4}.\frac{f\beta}{\xi} \\ \frac{49}{4} \quad \frac{\beta^2}{\alpha} \quad \frac{(2f\beta-3P\psi\alpha)}{\xi} \end{bmatrix}$$

$$= Y \quad \text{say} \qquad (A.11)$$

in which $\xi = (21\alpha^2 - 11\beta^2)$.

Equation 4.40 then reduces to

$$R = e^{-X.c} \cdot K - Y \qquad (A.12)$$

Evaluation of the exponential matrix $e^{-X.c}$ can then be made by expanding it in series form, viz.,

$$e^{-X.c} = [I] - [X].c + \frac{[X]^2.c^2}{2!} - \frac{[X]^3.c^3}{3!} + \ldots \frac{[X]^n.c^n}{n!} \qquad (A.13)$$

By carefully selecting a value of the pseudo-time, c, the series can be made to converge at small values of the exponent 'n'.

Let us assume that the truncated sum of the series for a particular value of pseudo-time is

$$e^{-X.c} = [S_c] \qquad (A.14)$$

Then, the sum for other values, such as 2.c, becomes

$$[S_{2.c}] = [S_c]^2$$

In general, the sum for 'r' multiples of 'c' can be obtained by squaring and re-squaring the truncated sum corresponding to r = 1

$$\text{i.e.} \quad [S_{r.c}] = [S_c]^r \qquad (A.15)$$

For the illustrative example considered in Section 4.3 the following constants have been used to evaluate the elements of the matrices

$\alpha = 68^{o}C$ $\qquad$ $\beta = 0.236^{o}C/mm$

$f = 6.2\ N/mm^2$ $\qquad$ $P = 8.0\ KN$

$\psi = 1.1625 \times 10^{-3}/mm^2$ $\qquad$ $Ec = 34.5\ GN/m^2$

$c = 1.45 \times 10^{-6}$ per N/mm^2 per ^{o}C

Appendix V

Specific thermal creep relationship for the concrete

The specific thermal creep-time relationship adopted in the beam analysis has been derived from a normalization procedure to the creep curves that were obtained from the laminated block B2 experiment previously shown in Fig. 8.17. These are re-plotted here on a semi-logarithmic scale in Fig. A.2.

On the basis of the assumption that the creep-temperature normalization function $\phi(T) = T$, the creep curves of Fig. A.2. have been found to fit approximately into a single curve, depicted in Fig. A.3, according to the relationship

$$c = Q + R.\log_e(t + 1) \qquad (A.16)$$

where c is the pseudo-time, or the specific thermal creep in microstrains per N/mm^2 per degree Celsius, t is the real time in days and R and Q represent the slopes and the intercepts of the straight line segments, These are shown to vary with the age of heating.

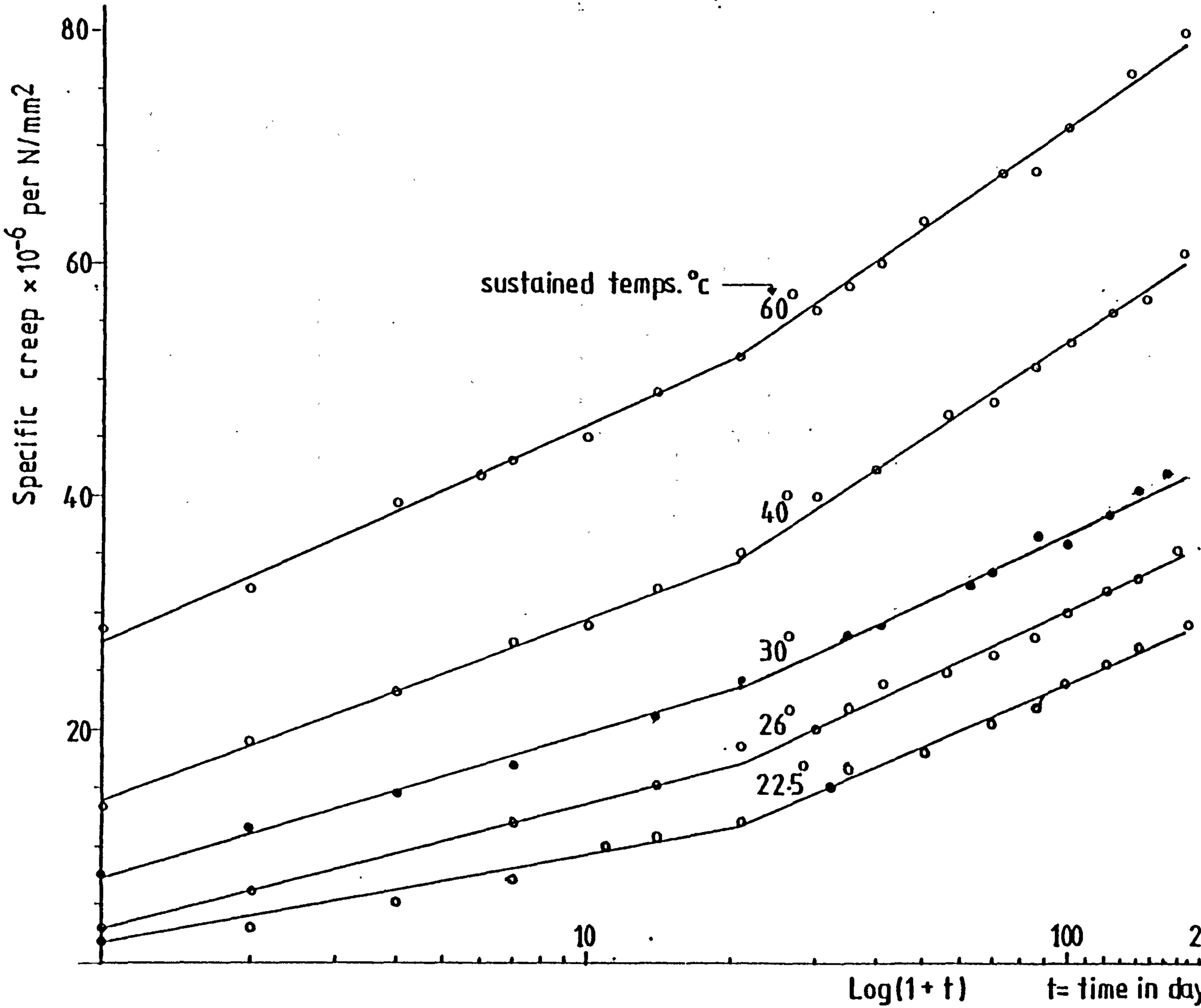

Fig.A·2 Semi-logarithmic plot of the sp.creep curves of the sealed block B2 shown in fig.8·17

$\times 10^{-6}$ per N/mm^2 per °C

$$c = R \cdot \log_e(t+1) + Q$$

	R	Q
$t \leqslant 21$ days	0·175	0·32
$21 \leqslant t \leqslant 100$ "	0·25	0·033
$t \geqslant 100$ "	0·43	-0·80

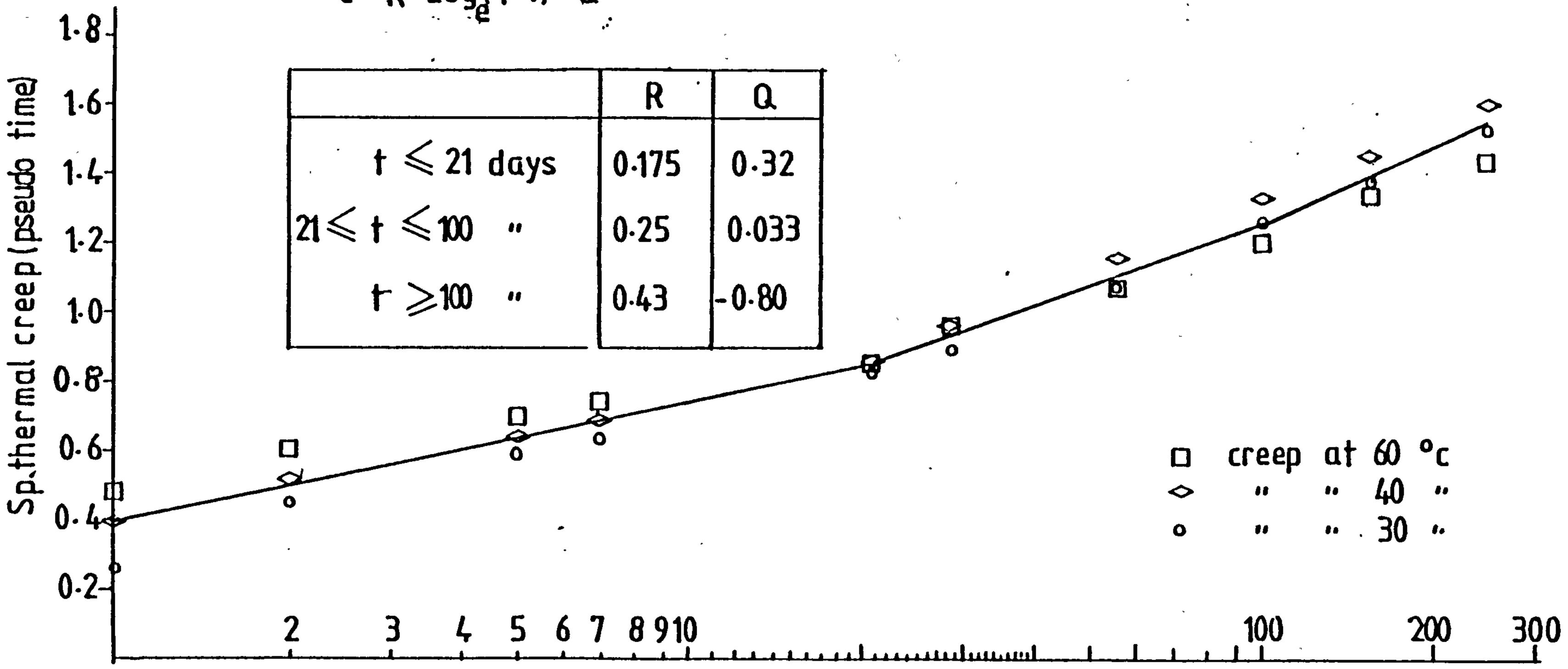

Fig A·3 Specific thermal creep - real time relationship

References

1. Diver, M. Design of reinforced concrete chimneys. A.C.I. Journal, Proc. Vol. 67 No. 10, Oct. 1970.

2. England, G.L., Phillips, E.A. Effect of Shrinkage and Creep on the Short - and Long - term state of Stresses in r.c. Chimneys. Chimney Design Symposium. Univ. of Edinburgh April 1973.

3. Clark, J.L. Thermal stress problems in offshore structures. Oceanology International 78 Brighton I.C.E. pp. 19-24.

4. Lankard, D.R., Birkimer, D.L., Fondriest, F.F., and Snyder, M.J. Effect of moisture content on the structural properties of Portland cement concrete exposed to temperatures up to 500°F. Temperature and concrete. A.C.I. special publication Sp. 25 1971.

5. Hendry, A.W. Thermal stress problems in concrete structures in hot countries. Materials and Structures, Vol. 9 - No. 49 Jan. - Feb. 1976.

6. Concrete Society Technical Paper No. 101 - The Creep of Structural Concrete. Report of a Working Party of the Materials Technology Divisional Committee. Jan. 1973.

7. Emerson, M. Temperatures in bridges during the hot summer of 1976. Transport and Road Research Laboratory. T.R.R.L. Laboratory Report 783. 1977.

8. Browne, R.D. Properties of concrete in Reactor Vessels. Proc. of Conference on Prestressed Concrete Pressure Vessels, I.C.E., London, 1967.

9. Blundell, R., Browne, R.D. Large Pours in Pressure Vessels. Int. Conf. on Experience in Design, Construction and Operation of PCPV and Containment for Nuclear Reactors. University of York, 1975.

10. Hansen, T.C. Theories of Multiphase Materials applied to Concrete, Cement Mortar and Cement Paste. Proc. of Int. Conf. on "The Structure of Concrete". London, Sept. 1965.

11. Newman, K. The Structure and Properties of Concrete - an introductory review. Proc. of Int. Conf. on "The Structure of Concrete". London, Sept. 1965.

12. Browne, R.D., Burrow, R.E.D. An example of the utilization of Complex Multiphase Material Behaviour in Engineering Design. The Proceedings of the Southampton 1969 Civil Engineering Materials Conference. Part 2, 1971.

13. Ishai, O. The time-dependent deformational behaviour of cement paste, mortar and concrete. Proc. of Int. Conf. on "The Structure of Concrete". London, Sept. 1965.

14. Ross, A.D., Illston, J.M., and England, G.L. Short- and long-term deformations of concrete as influenced by its physical structure and state. Proc. of Int. Conf. on "The Structure of Concrete". London, Sept. 1965.

15. Ross, A.D. The effects of creep on instability and indeterminancy investigated by plastic models. The Structural Engineer. Vol. 24. 1946.

16. Ross, A.D., England G.L., and Suan, R.H. Prestressed concrete beams under a sustained temperature crossfall. Mag. of Concrete Research. Vol. 17, No. 52: Sept. 1965.

17. Krishnamoorty, S. Thermal creep behaviour of concrete portal frames. Ph.D. Thesis. Imperial College, University of London, 1969.

18. England, G.L. Steady state stresses in concrete structures subjected to sustained and cyclically varying temperatures. Nuclear Engineering and Design 44 (1977). pp. 97-107.

19. England, G.L., Macleod, J.S. and Moharram, A. Designing for creep and temperature in concrete off-shore structures. Oceanology International 78.

20. Elvery, R.H. Problems associated with field measurement of stresses in concrete structures. Proc. Conf. Stresses in Service. I.C.E. 1967.

21. Czaika, N. Assessment of instrumentation for use in PCPV. ACI special publication SP-34 1972.

22. Browne, R.D. and McCurrich. Measurement of strain in concrete pressure vessels. Proc. of Conf. on PCPV. Group I paper 52. London 1967.

23. Hornby, I.W. Instrumentation techniques for strain measurements in concrete pressure vessels and similar structures. 'STRAIN' July 1972.

24. Cullington, D.W. and Hoar, M.C.P. Correcting for the effects of temperature on strain gauges - use of computer-logger on Milford Haven Bridge project. 'STRAIN', July 1975.

25. McKillen, R.R., Brading, K.F., Williams, A. Measurement of internal strain in concrete. 'STRAIN' Vol. 4 No. 1, Jan. 1968.

26. Tyler, R.G. Developments in the measurement of strain and stress in Concrete Bridge Structures. Ministry of Transport R.R.L. Report LR 189, Road Research Laboratory, Crowthorne, 1968.

27. Bertero, V.V., Bresler, B. and Polivka, M. Instrumentation and Techniques for Study of concrete properties at elevated Temperatures. AGI special publication SP-34 1972, pp. 1377-1419.

28. Morice, P.B. and Base, G.D. The design and use of a demountable mechanical strain gauge for concrete structures. Mag. of Concrete Research Vol. 5, No. 13, Aug. 1953, pp. 37-42.

29. Irving, J., Smith, J.R., Eadie, D.Mc.D., Hornby, I.W. Experience of in-service surveillance and monitoring of Prestressed Concrete Pressure Vessels for Nuclear Reactors. Int. Conf. on Experience in Design, Construction and Operation of PCPV and Containment for Nuclear Reactor. Univ. of York 1975.

30. Potocki, F.P. Vibrating-Wire Strain Gauge for Long-Term Internal Measurements in Concrete. The Engineer, London, (206) Dec. 1958.

31. Loh, Y.C. Internal stress gauges for cementitious Materials. Proc. Soc. exp. Stress Analysis Vol. II No. 2, 1954.

32. Carlson, R.W. and Pirtz, D. Development of a device for the Direct Measurement of Compressive Stress. A.C.I. Journal proc. V. 49 Nov. 1952 pp. 201-215 Disc. V. 25 No. 4, Dec.1953, Part 2, Proc. V. 49.

33. Piritz, D. and Carlson, R.W. Tests of Strain meters and Stress meters under Simulated field conditions. Proc. Symp. Mass Concrete. A.C.I. special publication SP-6, 1963.

34. Glözel, F. Unmittelbare Spannungsmessung in Beton und Baugrund. Der Bauingenieur 33 (1958), Heft 5.

35. Kidd, R.A., Stott, P. The Construction of an Experimental Prestressed Concrete Road at Winthorpe, Nottinghamshire. Paper No. 6991 proc. of I.C.E. Vol. 36 March 1967, pp. 473-498.

36. Roberts, A., Hawkes, I., Williams, F.T. and Dhir, R.K. A laboratory study of the Photoelastic Stress Meter. Int. J. Rock Mech. Mining Sci. Vol. 1, 1964, pp. 441-457.

37. Roberts, A., Hawkes, I., Williams, F.T. Some field applications of the Photo-elastic Stressmeter. Int. J. Rock Mech. Sci. Vol. 2, 1965, pp. 93-103.

38. Hawkes, I., Fellers, G.E. Theory of the determination of the greatest principal stress in a biaxial stress field using Photoelastic hollow cylinder inclusions. Int. J. Rock Mech. Min. Sci. Vol. 6, 1969, pp. 143-188.

39. Hornby, I.W., Wilson, J.M. Instrumentation techniques in large scale concrete models. Conf. Model Techniques for PCPV. London 1969.

40. Stanculescu, G., Ionescu, M. Behaviour to bending of plain concrete. Revue Roumaine des Sciences Techniques, Mec. Appl., Tome 13, No. 1, Bucarest, 1968, pp. 161-177.

41. Neville, A.M. Properties of Concrete. Pitman Publishing 1975.

42. Hannant, D.J. Effects on the strength of various concretes of sustained temperatures near 100°C. Civil Engineering and P.W. Review, June 1967, pp. 665-667.

43. Harada, T., Takeda, J., Yamane, S., Furmura, F. Strength, elasticity and thermal properties of concrete subjected to elevated temperatures. ACI special publication SP-34, 1972, Vol. 1, pp. 337-432.

44. Nishizawa, N., Ojamura, H. Strength and inelastic properties of concrete at elevated temperatures. ACI special publication, SP-34, 1972, Vol. 1, pp.407-421.

45. Bertero, V.V., Polivka, M. Influence of thermal exposures on mechanical characteristics of concrete. ACI special publication, SP-34, 1972, Vol. 1, pp. 505-531.

46. Zoldners, N.G. Thermal properties of concrete under sustained elevated temperatures. Temperature and Concrete, ACI special publication, SP-25, 1971, pp. 1-31.

47. Abrams, M.S. Compressive strength of concrete at temperatures to 1600°F. Temperature and Concrete, ACI special publication, SP-25, 1971, pp. 33-57.

48. Sullivan, P.J., Poucher, M.P. The influence of temperature on the physical properties of concrete and mortar in the range 20 to 400°C. ACI special publication, SP-25, 1971, pp.103-135.

49. Mears, A.P. Long term tests on the effect of moderate heating on the compressive strength and dynamic modulus of elasticity of concrete. ACI special publication, SP-34, 1972, Vol. 2, pp. 355-375.

50. Kaplan, M.F., Roux, F.J.P. Effects of elevated temperature on the properties of concrete for the containment and shielding of Nuclear Reactors. ACI special publication, SP-34, 1972, Vol. 1, pp. 437-441.

51. Marechal, J.C. Variations in the modulus of elasticity and Poisson's ratio with temperature. ACI special publication, SP-34, 1972, Vol. 1, pp. 495-503.

52. Crispino, E. Studies on the technology of concrete under thermal conditions. ACI special publication, SP-34, 1972, Vol. 1, pp. 443-479.

53. Cruz, C.R. Elastic properties of concrete at high temperature. Journal of the PCA, Research Development Laboratories, Vol. 8, Jan. 1966, pp. 37-45.

54. Irving, J. The effect of elevated temperatures on concrete and concrete structures. A review of literature. F.I.P./3/1. Sept. 1975.

55. Weigler, H., Fischer, R. Influence of high temperature on strength and deformations of concrete. ACI special publication, SP-34, 1972, Vol. 1, pp. 481-493.

56. Browne, R.D., Bamforth, P.B. The long term creep of Wylfa P.V. concrete for loading ages up to 12½ years. 3rd SMIRT conference, London, Sept. 1975, paper No. H 1/8.

57. Campbell-Allen, D., Thorne, C.P. The thermal conductivity of concrete. Mag. of Concrete Research, Vol. 15, No. 43, March 1963, pp. 39-48.

58. Marechal, J.C. Thermal Conductivity and thermal expansion ∞ coefficients of concrete as a function of temperature and humidity. ACI special publication, SP-34, 1972, Vol. 2, pp. 47-57.

59. Meyers, S.L. Thermal expansion characteristics of hardened cement paste and of concrete. Proc. Highway Research Board, V. 30, 1950, pp. 193-203.

60. Chapman, D.A., England, G.L. Effects of moisture migration on shrinkage, pore pressure and other concrete properties. Conf. on SMIRT, San Francisco, Aug. 1977, paper No. H 4/d.

61. A.C.I. Committee 209 (chaired by John R. Keeton). Effects of concrete constituents, environment, and stress on creep and shrinkage of concrete. Designing for effects of creep, shrinkage and temperature in concrete structures. ACI special publication, SP-27, 1971, pp. 1-42.

62. England, S.L., Ross, A.D. Shrinkage, moisture, and pore pressures in heated concrete. ACI special publication, SP-34, 1972, Vol. 2, pp. 883-907.

63. Chapman,D.A. A Study of the movement of Moisture in and from concrete at elevated and non-uniform temperatures. Ph.D. Thesis, University of London, 1976.

64. Ross, A.D., Parkinson, J.D. Shrinkage in concrete pressure vessels. Nuclear Engineering and Design, Vol. 5, 1967, pp. 150-160.

65. Poitevin, P. Water migration in concrete under a sustained temperature gradient. ACI special publication, SP-34, 1972, Vol. 2, pp. 909-929.

66. Mcdonald, J.E. An experimental study of moisture migration in concrete. ACI special publication SP-34, 1972, Vol. 2, pp. 957-929.

67. Pihlajavaara, S.E., Tiusanen, K. A preliminary study on thermal moisture transfer in concrete. ACI special publication, SP-34, 1972, Vol. 2, pp. 1019-1033.

68. Browne, R.D., Blundell, R. The behaviour of concrete in prestressed concrete pressure vessels. 1st Int. Conf. on SMIRT, Berlin, Sept. 1971, paper H1/1. Also Nuclear engineering and design, Vol. 20, 1972, pp. 429-475.

69. Ross, A.D. Shape, size and shrinkage. Concrete and Constructional Engineering, Vol. 39, No. 8, Aug. 1944, pp. 193-199.

70. Hansen, T.C. and Matlock, A.H. Influence of size and shape of member on the shrinkage and creep of concrete. ACI Journal, proc. Vol. 63, No. 2, Feb. 1966, pp. 267-290.

71. Hobbs, D.W. Influence of specimen geometry upon weight change and shrinkage of air-dried concrete specimens. Mag. of Concrete Research, Vol. 29, No. 99, June 1977, pp. 70-80.

72. Campbell-Allen, D., Rogers, D.F. Shrinkage of concrete as affected by size. Materials and Structures, Research and Testing, Vol. 8, No. 45, 1975, pp. 193-202.

73. Becker, N.K., Macinnis, C. A theoretical method for predicting the shrinkage of concrete. ACI Journal, Vol. 70, No. 9, Sept. 1973, pp. 652-657.

74. Hughes, B.P., Lowe, I.R.E., Walker, J. The diffusion of water in concrete at temperatures between 50° and 95°C. Brit. J. Appl. Phys., Vol. 17, 1966, pp. 1545-1552.

75. Yuan, R.L., Hilsdorf, H.K., and Kesler, C.E. The effect of temperature on the drying of concrete. ACI special publications, SP-34, 1972, Vol. 2, pp. 991-1017.

76. Lowe, I.R.G., Hughes, B.P., and Walker,J. The diffusion of water in concrete at 30°C. Cement and Concrete Research, Vol. 1, 1971, pp. 547-557.

77. Bozant, Z.P. and Nojjar, L.J. Drying of concrete as a non-linear diffusion problem. Cement and Concrete Research, Vol. 1, 1971, pp. 461-473.

78. England, G.L., Sharp, T.J. Migration of moisture and pore pressures in heated concrete. Proc. of the 1st Int. Conf. on SMIRT, Berlin, Sept. 1972. Vol. 4 - Part H.

79. Illston, J.M., Sanders, P.D. The effect of temperature change upon the creep of mortar under torsional loading. Mag. of Concrete Research, Vol. 25, No. 84, Sept. 1973, pp. 136-144.

80. Nasser, K.W., Neville, A.M. Creep of concrete at elevated temperatures. ACI Journal, Proc. Vol. 62, Dec. 1965, pp. 1567-1579.

81. Arthanari, S., Yu, C.W. Creep of concrete under uniaxial and biaxial stresses at elevated temperatures. Mag. of Concrete Research, Vol. 19, No. 60, Sept. 1967, pp. 149-156.

82. Nasser, K.W. Creep of concrete at low Stress - Strength ratios and elevated temperatures. Temperature and Concrete. ACI special publication, SP-25, 1971, pp. 137-147.

83. Hannant, D.J. The strain behaviour of concrete up to 95°C under compressive stress. Proc. Conf. on PCPV, Group C, paper 17, London 1967.

84. Geymayer, H.G. Effect of temperature on creep of concrete: a literature review. ACI special publication, SP-34, 1972, Vol. 1, pp. 565-539.

85. Mukaddam, M.A., Bresler, B. Behaviour of concrete under variable temperature and loading. ACI special publication, SP-34, 1972, Vol. 2, pp. 771-797.

86. Hornby, I.W. The behaviour of the Oldbury model vessel with time under thermal and pressure loadings. Proc. of Conference on Model Techniques for Prestressed Concrete Pressure Vessels, British Nuclear Energy Society, London, 1969.

87. Barret, N.T., Murray, J.T. Creep in pressure vessels at elevated temperatures. I.C.E. Conf. on Prestressed Concrete Pressure Vessels, London, March 1967, pp. 153-166.

88. Fahmi, H.M., Polivka, M., Bresler, B. Effect of sustained and cyclic elevated temperature on creep of concrete. Cement and Concrete Research, Vol. 2, Sept. 1972, pp. 591-606.

89. Carmichael, G.D.T., Hornby, I.W. The strain behaviour of concrete in PCPV. Mag. of Concrete Research, Vol. 25, no. 82, March, 1973, pp. 5-16.

90. Illston, J.M., Sanders, P.D. Characteristics and prediction of creep of a saturated mortar under variable temperature. Mag. of Concrete Research, Vol. 26, No. 88, Sept. 1974, pp. 169-179.

91. Wang, H. Creep of Concrete at elevated temperatures. Designing for effects of creep shrinkage temperature in concrete structures. ACI special publication SP-27, 1971, pp. 387-400.

92. Gross, H. Computer aided thermal creep analysis of concrete continua. Ph.D. Thesis, Imperial College, University of London, 1973.

93. Ruetz, W. A hypothesis for the creep of hardened cement paste and the influence of simultaneous shrinkage. Int. Conf. on the Structure of Concrete, London Sept., 1965.

94. Gopala Krishnan, K.S., Neville, A.M., Ghali, A. A hypothesis on mechanism of creep of concrete with reference to multiaxial compression. ACI Journal, Proc. Vol. 67, No. 1, Jan. 1970.

95. Illston, J.M. The creep of concrete in terms of its developing structure and moisture condition. Proc. of the Southampton 1969 Civil Engineering Materials Conference. 1971, pp. 1287-1297.

96. Gamble, B.R., Parrott, L.J. Creep of concrete in compression during drying and wetting. Mag. of Concrete Research, Vol. 30, No. 104, Sept. 1978, pp. 129-138.

97. Zielinski, A., Sadowski, A. The influence of moisture content on the creep of concrete at elevated temperatures. 2nd Int. Conf. on SMIRT, Berlin, Sept. 1973, paper H 6/3, pp. 1-3.

98. Fahmi, H.M., Bresler, B., Polivka, M. Prediction of creep of concrete at variable temperatures. ACI Journal Proc. Vol. 70, No. 10, Oct. 1973.

99. Marechal, J.C. Creep of concrete as a function of temperature. ACI special publication SP-34, 1972, Part I, pp. 547-564.

100. Ross, A.D. Creep of concrete under variable stress. ACI Journal, Proc. Vol. 29, No. 9, March 1958, pp. 739-759.

101. England, G.L., Illston, J.M. Methods of computing stress in concrete from a history of measured strain. Civil Engineering and P.W. Review, Vol. 60, Parts 1, 2 and 3, April, May, June 1965.

102. Neville, A.M. Creep of concrete: plain, reinforced, and prestressed. North Holland Publishing, Amsterdam, 1970.

103. Rashid, Y.R., Ople, F.S., Chang, T.Y. Comparison of experimental results with response analysis for a model of a pressure vessel. Proc. of Conf. on Model Techniques for PCPV. London, 1969.

104. Dilger, W., Ghali, A., Kountouris, C. Time-dependent forces induced by settlement in continuous prestressed concrete structures. Symposium on Design of concrete structures for creep, shrinkage and temperature changes. Int. Association for Bridge and Structural Engineering, Madrid, 1970, pp. 89-98.

105. Gamble, B.R. A constitutive relationship for maturing concrete. Symposium on Design of concrete structures for creep, shrinkage and temperature changes. Int. Ass. for Bridge and Structural Engineering, Madrid 1970, pp. 99-106.

106. Irving, J., Carmichael, G.D.T. The influence of Creep on the behaviour of concrete structures subjected to cyclic heating. Proc. of Southampton 1969 Civil Engineering Conf. (Structure, Solid mechanics and Engineering Design). Wiley-Interscience, 1971, pp. 1299-1311.

107. Goodall, I.W., Irving, J. On the approximate analysis of structures composed of non-homogeneous linear visco-elastic material. Nuclear Engineering and Design 22, (1972), pp. 63-64.

108. Gamble, B.R., Jordaan, I.J. A direct method of visco-elastic analysis for ageing concrete. Materials and Structures, Vol. 7, No. 37, 1974, pp. 37-43.

109. Tadros, M.K., Ghali, A., Dilger, W.H. Time-dependent analysis of composite frames. Journal of the Structural Division, ASCE, Vol. 103, No. S.T.4, April 1977, pp. 871-884.

110. England, G.L. Numerical creep analysis applied to concrete structures. ACI Journal, Proc. June 1967, pp. 301-310.

111. Bozant, Z.P., Wu, S.T. Creep and Shrinkage law for concrete at variable humidity. Journal of the Engineering Mechanics Division, Proc. of the ASGE, Vol. 100, No. EM6, Dec. 1974, pp. 1183-1209.

112. England, G.L. Steady state stresses in concrete structures subjected to sustained temperatures and loads. Part 1 Cases of Uniaxial Stress. Nuclear Engineering and Design Vol. 3, (1966), pp. 54-65.

113. Jordaan, I.J., A note on concrete creep analysis under static temperature fields. Materials and Structures, Vol. 7, No. 41, Sept.-Oct. 1974, pp. 329-333.

114. England, G.L. Time-dependent stresses in creep-elastic materials a general method of calculation. Conf. on recent advances in stress analysis: New concepts and techniques and their practical application. Royal Aeronautical Society, London, March 1968.

115. Jordaan, I.J., England, G.L., Kalifa, M.M.A. Creep of concrete: a Consistent Engineering Approach. Journal of the Structural Division, Proc. ASGE, Vol. 103, No. ST3, March 1977, pp. 475-491.

116. England, G.L., Jordaan, I.J. Time-dependent and steady state stresses in concrete structures with steel reinforcement, at normal and raised temperatures. Mag. of Concrete Research: Vol. 27, No. 92: Sept. 1975, pp. 131-142.

117. England, G.L., Macleod, J.S. A direct method of structural analysis for creep in heated concrete structures. Conf. on SMIRT, San Francisco, Aug. 1977.

118. England, G.L., Ross, A.D. Reinforced concrete under thermal gradients. Mag. of Concrete Research: Vol. 14, No. 40: March 1962, pp. 5-12.

119. Hambly, E.C. Temperature distribution and stresses in concrete bridges: The Structural Engineer: May 1978, No. 5, Vol. 56A, pp. 143-148.

120. Reynolds, J.C., Emanuel, J.H. Thermal Stresses and movements in bridges; Journal of the Structural Division. Proc. of the A.S.C.E., Vol. 100, No. S.T.1., January 1974, pp. 63-78.

121. Hunt, B., Cooke, N. Thermal Calculations for bridge design. Journal of the Structural Division. Proc. of the A.S.C.E., Vol. 101, No. ST9, Sept. 1975, pp. 1763-1780.

Literature not referred to in the text

1. Samelson, H., Tor, A. Stresses in reinforced concrete sections subjected to transient temperature gradients. Journal of the A.C.I. V.30, No. 3, Sept. 1958, pp. 377-385.

2. Bazant, Z. Analysis of shrinkage and creep of composite beams on redundant supports. Designing for effects of Creep Shrinkage Temperature in concrete structures. A.C.I. publication SP-27, Mitch. 1971, pp. 373-385.

3. Aoyagi, Y., Ohnuma, H., and Kawasaki, N. Behaviour of flexurally restrained prestressed concrete beams under temperature gradient. Concrete for nuclear reactors. Proc. of Int. Seminar on concrete for nuclear reactors, Mitch. 1972, A.C.I. SP-34, Vol. II, pp.799-821.

4. Branson, D.E. Deformation of concrete structures. McGraw-Hill International Book Company. 1977.

5. Arutyunyan, N.Kh. Some problems in the theory of creep in concrete Structures. Int. series of Monographs in Civil Engineering. Vol. 1, Pergamon Press, 1966.

6. Brooks, J.J., Neville, A.M. Relaxation of stress in Concrete and its Relation to Creep. Journal of the A.C.I. Proc. Vol. 73, No. 4, April 1976, pp. 227-232.

7. Gupta, B.K., Edwards, A.D. Moment-curvature characteristics of prestressed concrete sections. Mag. of Concrete Research. Vol. 24, No. 81, Dec. 1972. pp. 219-230.

8. Powers, T.C. Mechanisms of shrinkage and creep of hardened cement paste. Proc. of Int. Conference on 'The Structure of Concrete'. London, Sept. 1965.

9. Illston, J.M. The delayed elastic deformation of concrete as a composite material. Proc. of International Conf. on 'The Structure of Concrete'. London, Sept. 1965.

10. Illston, J.M. The creep of concrete in terms of its developing structure and moisture condition. Proc. of Southampton 1969 Civil Engineering Conference (Structure, Solid mechanics and Engineering Design). Wiley-Interscience, 1971, pp. 1287-1297.

11. Tyler, R.G. Determining stress in concrete structures. Site method used in precast unit for Western Avenue Extension. Civil Engineering and P.W. Review, part 1, and part 2, June-July, 1969.

12. Tyler, R.G. Determining stress in concrete structures, further notes on the method of identical strains. Civil Engineering and P.W.R., part 1 and part 2, June-July 1971.

13. Cook, H.K., Coutinho, A., Peattie, K.R., Sparrow, R.W., Raphael, J.M., Steele, B.W., and authors. Discussion of a paper by Carlson R.W. and Piritz D. (Development of a Device for the Direct Measurement of Compressive Stress). Journal of the A.C.I., Proc. Vol. 25, No. 4, Dec. 1953.

14. Newman, K., Lachance, L., Loveday, R.W. Strain measurements on saturated concrete specimens. Mag. of Conc. Research, Vol. 15, No. 45, Nov. 1963, pp.143-150.

15. Holister, G.S. The determination of in situ stresses in rock and concrete. Applied Materials Research. Jan. 1966, pp.46-49.

16. British Society for strain measurement. Monograph - Methods and practice for stress and strain measurement. Part 1: Measurement of strain, load and temperature. April, 1977.

17. Czaika, N., Mayer, N., Amber, C. and Magiera, G. Instrumentation for Use in Prestressed-concrete Reactor Pressure Vessels. Experimental Mechanics, February 1974. pp.82-88.

18. Illston, J.M. and Pomeroy, C.D. Recommendations for a standard creep test. Concrete, Dec. 1975, pp.24-25.

19. Parrott, L.J. Moisture state for a standard creep test. Concrete 1975, pp.25-26.

20. Gamble, B.R. Criteria and designs for creep apparatus. Concrete, 1975, pp.26-28 and 37.

21. Cridland, L., Bakoss, S.L., and Burfitt, A.J. A low-cost creep rig for concrete. Mag. of Concrete Research, Vol. 29, No.100, September 1977, pp.147-150.

22. England, G.L., Labib, G.A., Moharram, A. The influence of time and temperature on the working stresses in concrete structures. Project report. Research Seminar - Cement and Concrete Association Training Center, 5th to 9th Sept. 1977.

23. Mozer, J.D., Gerstle, K.H., and Tulin, L.G. Time-dependent behaviour of concrete beams. Journal of the Structural Division, Proc. of the A.S.C.E., Vol. 96, No.ST3, March 1970,pp.597-612.

24. Moncrieff, M.L.A., Waggott, J.G. Time, temperature, creep and shrinkage in concrete. Proc. of Conf. on P.C.P.V., I.C.E., London, 1967. Group C paper 12, pp.123-130.

25. Brooks and Neville, A.M. A comparison of creep, elasticity and strength of concrete in tension and in compression. Mag. of Conc. Research. Vol. 29, No. 100, Sept. 1977, pp.131-141.

26. Smith, J.R. Problems in assessing the correlation between the observed and predicted behaviour of models. Conf. Model Techniques for P.C.P.V. London 1969, pp.81-89.

27. Browne, R.D., Smith, J.R., Bamforth, P. The performance of Wylfa nuclear P.V. during commissioning in relation to design analysis. 2nd Int. Conf. on Structural Mechanics in Reactor Technology. Berlin, Sept. 1973.

28. Irving, J., Carmichael, G.D.T. The assessment of bounds on stresses and strains in P.C.R.P.V. Mag. of Conc. Research, Vol. 25, No. 85, Dec. 1973, pp.189-196.

29. Lewis, D.J., Irving, J. Operational stresses in nuclear prestressed concrete pressure vessels. Civil Eng. & P.W. Review, Part I, June 1968, pp.673-676.

30. Emanuel, J.H., Hulsey, J.L. Prediction of the Coefficient of Expansion of Concrete. Journal of the A.C.I. Proc. Vol. No. April 1977, pp.149-155.

31. Grouni, H.N. Loss of Prestress Due to Relaxation After Transfer Journal of the A.C.I., Proc. Vol. No. Feb. 1978, pp.64-66.

32. Bresler, B., Helmich, D., Ramakrishna, L.V. Non-uniform drying shrinkage in reinforced concrete. Symposium on Design of concrete structures for creep, shrinkage and temperature changes. Int. Association for Bridge and Structural Engineering, Madrid 1970, pp.171-179.

33. Bazant, Z.P., Domingo, J. Carreira, Walser, A. Creep and Shrinkage in Reactor Containment Shells. Journal of the Structural Division. Proc. of the A.S.C.E., Vol.101, No. ST10, October 1975, pp.2117-2131.

34. Brooks, J.J., Neville, A.M. Estimating long-term creep and shrinkage from short-term tests. Mag. of Concrete Research, Vol.27, No. 90, March 1975, pp.3-12.

35. Mukaddam, M. Creep Analysis of Concrete at Elevated Temperatures. Journal of the A.C.I. Proc. Vol. No. Feb. 1974, pp.72-78.

36. Campbell-Allen, D., Aust, F.I.E., Holford, J.G., Aust, S.I. Stress and Cracking in Concrete Due to Shrinkage. The Institution of Engineers, Australia, Civil Engineering Transactions, April 1970, pp.33-39.

37. England, G.L. Long-term thermal stresses in prestressed concrete structures. Proc. of Conference on Prestressed Concrete P.V., I.C.E., London, 1967, Group F, paper 34,pp.51-57.

38. Wittmann, F.H., Lukas, J. The application of rate theory to time-dependent deformation of concrete. Mag. of Concrete Research, Vol. 26, No. 89, Dec. 1974, pp.191-197.

39. Constantinescu, D.R., Illston, J.M. Direct solutions to problems of time-dependent induced stresses in restrained concrete. Materials and Structures: Research and Testing, Vol. 8, No. 43, 1975, pp.11-17.

40. Illston, J.M., England, G.L. Creep and shrinkage of concrete and their influence on structural behaviour - a review of methods of analysis. The Structural Engineer, July 1970, No. 7, Vol.48, pp.283-291.

41. Arthanary, S., Yu, C.W. An analysis of the creep and shrinkage effects upon prestressed concrete members under temperature gradient and its application. Magazine of Concrete Research, Vol. 19, No.60. Sept. 1967, pp.157-164.

42. Cederwall, K., Elfgren, L., Losberg, A. Prestressed Concrete Columns under Long-time loading. Symposium on Design of concrete structures for creep, shrinkage and temperature changes. Int. Association for Bridge and Structural Engineering, Madrid, 1970, pp.181-189.

43. Bazant, Z.P. Numerical determination of long-range stress history from strain history in concrete. Material and Structures: Research and Testing, Vol. 5, No. 27, 1972, pp.135-141.

44. Bazant, Z.P., Osman, E., Thonguthai, W. Practical formulation of shrinkage and creep of concrete. Material and Structures (Rilem), Vol. 9, No. 54, Nov-Dec, 1976, pp.395-405.

45. Sullivan, P.J.E. Time-temperature extrapolation techniques as applied to concrete creep strains. 1st Int. Conf. on Structural mechanics in reactor technology (SMIRT), Berlin 1971.

46. Chiou-Horng Chen, Krokosky, E.M. Steady and non-steady solar heat transmission through roofs. Material and Structures (Rilem), Vol.9, No. 49, Jan.-Feb. 1976, pp.19-32.

47. Emerson, M. The calculation of the distribution of temperature in bridges. Transport and Road Research Laboratory, TRRl Report LR 561, 1973.

48. Jones, M.R. Bridge temperatures calculated by a computer program. Transport and Road Research Laboratory, TRRl Laboratory Report 702, 1976.

49. Maher, D.R.H. The effects of Differential Temperature on Continuous Prestressed Concrete Bridges. The Institution of Engineers, Australia. Civil Engineering Transactions, April, 1970, pp.29-32.